



**UNIWERSYTET MARII CURIE-SKŁODOWSKIEJ
W LUBLINIE**

**Wydział Chemiczny
Instytut Nauk Chemicznych**

mgr Sebastian Dudek

**Usuwanie jonów arsenianowych(V) na
wymieniaczach jonowych na bazie tlenków żelaza
modyfikowanych jonami wybranych
lantanowców**

Rozprawa doktorska
wykonana w Katedrze Chemii Nieorganicznej
pod kierunkiem prof. dr hab. Doroty Kołodyńskiej

Lublin 2022

*Pragnę serdecznie podziękować Pani promotor
Prof. dr hab. Dorocie Kołodyńskiej
za nieocenioną pomoc w trakcie powstawania tej pracy,
owocną współpracę, cierpliwość i mobilizację do działania*

*Pracę dedykuję
mojej żonie Dagmarze oraz moim Rodzicom Elżbiecie i Jarosławowi.
Dziękuję za Wasze nieustanne wsparcie i wiarę we mnie.
Bez Was nie byłbym w tym miejscu, w którym jestem*

Spis treści

1.	Lista publikacji wchodzących w skład rozprawy doktorskiej.....	4
2.	Wprowadzenie.....	5
3.	Cel rozprawy doktorskiej.....	7
4.	Metody badawcze.....	8
4.1.	Modyfikacja i charakterystyka sorbentu.....	8
4.2.	Badania adsorpcji metodą statyczną.....	9
5.	Omówienie wyników.....	13
5.1.	Charakterystyka jonitów.....	13
5.2.	Wpływ pH.....	17
5.3.	Badania kinetyczne.....	18
5.4.	Badania równowagowe i termodynamiczne.....	21
5.5.	Regeneracja jonitów.....	22
6.	Główne osiągnięcia rozprawy doktorskiej.....	23
	Literatura.....	26
	Streszczenie w języku polskim.....	31
	Streszczenie w języku angielskim.....	33
	Życiorys naukowy.....	35
	Dorobek naukowy.....	37
	Teksty publikacji z oświadczeniami współautorów.....	40

1. Lista publikacji wchodzących w skład rozprawy doktorskiej

W skład rozprawy doktorskiej wchodzą cztery publikacje w czasopismach umieszczonych na liście JCR (ang. *Journal Citation Reports*):

- D1 S. Dudek, D. Kołodyńska, Enhanced arsenic(V) removal on an iron-based sorbent modified by lanthanum(III), Materials 13 (2020) 2553.**

IF: 3,623

Punkty MEiN: 140

- D2 S. Dudek, D. Kołodyńska, Arsenic(V) removal on the lanthanum-modified ion exchanger with quaternary ammonium groups based on iron oxide, J. Mol. Liq. 347 (2021) 117985.**

IF: 6,165

Punkty MEiN: 100

- D3 S. Dudek, D. Kołodyńska, Arsenate removal on the iron oxide ion exchanger modified with neodymium(III) ions, J. Environ. Manage. 307 (2022) 114551.**

IF: 6,789

Punkty MEiN: 100

- D4 S. Dudek, D. Kołodyńska, Arsenate removal on the ion exchanger modified with cerium(III) ions, Physicochem. Probl. Miner. Process. 58 (2022) 147412.**

IF: 1,213

Punkty MEiN: 70

Sumaryczny IF: 17,79

Sumaryczna liczba punktów MEiN: 410

2. Wprowadzenie

Bezpieczeństwo związane z zaopatrzeniem obszarów w wodę pitną pozbawioną zanieczyszczeń jest jednym z najważniejszym problemów dzisiejszego świata. Okazuje się, że w wielu miejscach na świecie wody gruntowe są jedynym źródłem wody użytkowej i pitnej [1]. Niestety, w wodach naturalnych w wielu krajach, m.in. Bangladeszu, Chinach, Indiach, Meksyku czy USA, występuje zwiększyony poziom zanieczyszczeń, wśród których pojawiają się związki arsenu [2,3]. Główną przyczyną tego zjawiska jest działalność ludzi, np. górnictwo, spalanie paliw kopalnych, stosowanie pestycydów i herbicydów. Innymi powodami są naturalne zjawiska takie jak wietrzenie skał, reakcje geochemiczne, czy aktywność wulkaniczna [4]. Wśród lokalnych populacji w krajach słabo rozwiniętych lub rozwijających się zanieczyszczone arsenem wody gruntowe były wykorzystywane bez uzdatniania, co prowadziło do różnych negatywnych skutków zdrowotnych, w tym nowotworów płuc, chorób skóry i układu krażenia [5]. W związku z tym, Światowa Organizacja Zdrowia WHO (ang. *World Health Organization*) ustaliła dopuszczalną zawartość arsenu w wodzie pitnej na poziomie $10 \mu\text{g}/\text{dm}^3$ [6]. Biorąc pod uwagę powyższe, potrzebne są wysokowydajne i opłacalne technologie do uzdatniania wody ze szczególnym uwzględnieniem usuwania arsenu.

W tym celu wykorzystuje się dobrze opracowane techniki, do których należą m.in. nanofiltracja, strącanie, koagulacja, elektrodializa, odwrócona osmoza, czy adsorpcja [7]. Niestety, wiele z tych metod ma pewne istotne wady. Koagulacja i strącanie prowadzą do utworzenia toksycznych osadów, nanofiltracja jest kosztowna i wymaga wstępnego kondycjonowania, odwrócona osmoza wymaga zaawansowanej technologicznie obsługi i konserwacji, a elektrodializa prowadzi do powstawania toksycznych ścieków [8,9]. Z kolei, adsorpcja uważana jest za jedną z najbardziej wydajnych i opłacalnych procedur, które można stosować w przypadku zróżnicowanych warunków [10–12].

Arsen w związkach jest spotykany najczęściej na -III, +III oraz +V stopniu utlenienia [13]. Warto zwrócić uwagę, że jego nieorganiczne związki są bardziej toksyczne niż organiczne. Najbardziej rozpowszechnionymi nieorganicznymi formami arsenu są te na +III i +V stopniu utlenienia, których ilość w środowisku zależy od pH i potencjału utleniania i redukcji. Biorąc pod uwagę stopień utlenienia, związki As(III) są zwykle bardziej toksyczne niż As(V). W najczęściej spotykanym zakresie pH wód gruntowych dominującymi formami As(V) są obdarzone ujemnym ładunkiem jony diwodoroarsenianowe(V) H_2AsO_4^- i wodoroarsenianowe(V) HAsO_4^{2-} , natomiast As(III)

występuje w postaci niezdysocjowanej H_3AsO_3 [14]. W związku z tym, na dodatnio naładowanej powierzchni adsorbentów adsorpcja As(V) jest łatwiejsza. Proces usuwania jonów arsenu powinien być związany z ich utlenieniem do +V stopnia utlenienia.

Powszechnie znanimi adsorbentami przeznaczonymi do usuwania arsenu są te na bazie tlenków żelaza [15], a także materiałów hybrydowych łączących związki żelaza i innych metali, w tym tytanu [16], cyrkonu [17], glinu [18] i miedzi [19]. W ostatnim czasie opublikowano również prace naukowe odnoszące się do materiałów zawierających pierwiastki ziem rzadkich REE (ang. *rare earth elements*) [20–24]. Można do nich zaliczyć adsorbenty modyfikowane tlenkiem/wodorotlenkiem metalu z grupy REE oraz adsorbenty impregnowane jonami REE. Uważa się, że takie materiały hybrydowe charakteryzują się większymi pojemnościami sorpcyjnymi względem jonów arsenu oraz większą stabilnością i są tańsze w porównaniu z czystymi materiałami na bazie REE [25]. Poprzez wymianę ligandów, tworzenie kompleksów i oddziaływanie elektrostatyczne, różne grupy funkcyjne na powierzchni adsorbentu mogą odgrywać znaczącą rolę w procesie adsorpcji [26]. Łączenie pierwiastków ziem rzadkich z powszechnie dostępnymi i tańszymi metalami (np. glinem, żelazem, manganem) w celu stworzenia nowej serii materiałów kompozytowych jako adsorbentów prowadzi do zachowania korzystnych właściwości REE przy jednoczesnym obniżeniu kosztów [27,28].

3. Cel rozprawy doktorskiej

Celem rozprawy doktorskiej było opracowanie metody modyfikacji wymieniaczy jonowych na bazie tlenków żelaza jonami lantanu(III), neodymu(III) i ceru(III) oraz wykazanie, że modyfikowane w ten sposób materiały posiadają lepsze właściwości sorpcyjne względem jonów As(V) niż te niemodyfikowane. Założono, że dzięki opisanej procedurze proces usuwania jonów arsenu stanie się bardziej wydajny i mniej kosztowny, co w przyszłości doprowadzi do polepszenia stanu wód gruntowych w wielu miejscach na świecie. Główne założenia badawcze obejmowały:

- modyfikację wymieniaczy jonowych na bazie tlenków żelaza jonami lantanu(III), neodymu(III) oraz ceru(III),
- charakterystykę nowo otrzymanych materiałów z wykorzystaniem różnych technik badawczych,
- opis procesu adsorpcji jonów arsenianowych(V) z roztworów wodnych na modyfikowanych wymieniaczach jonowych z uwzględnieniem wpływu pH, kinetyki, równowagi chemicznej, temperatury oraz możliwości regeneracji,
- porównanie właściwości sorpcyjnych materiałów przed i po modyfikacji oraz ocena ich przydatności w kontekście usuwania jonów arsenianowych(V) z roztworów wodnych.

W pierwszej kolejności sprawdzono możliwość modyfikacji handlowo dostępnego sorbentu Arsen X^{np} (Purolite, USA), zawierającego grupy sulfonowe, jonami lantanu(III) jako tymi, które pełniły rolę jonów modelowych w stosunku do pozostałych jonów lantanowców (**D1**). Kolejno stosując identyczne parametry modyfikacji, przeprowadzono modyfikację wymieniacza jonowego Ferrix A33E (Purolite, USA) zawierającego czwartorzędowe grupy amoniowe (**D2**). W następnym etapie sprawdzono, czy wprowadzenie jonów neodymu(III) i ceru(III) będzie prowadziło do podobnych rezultatów (**D3, D4**). Na każdym etapie zastosowano jednakowe parametry procesu modyfikacji i adsorpcji jonów arsenianowych(V) na jonicie Ferrix A33E. Dla modyfikowanego jonami lantanu(III) jonitu Arsen X^{np} zastosowano skrót X^{np}-La(III), natomiast dla modyfikowanego jonami lantanu(III), neodymu(III) i ceru(III) wymieniacza jonowego Ferrix A33E wprowadzono skróty A33E-La(III), A33E-Nd(III) oraz A33E-Ce(III). Skrót dla zmodyfikowanego Ferrix A33E bez wskazywania konkretnego jonu lantanowca(III) to A33E-Ln(III).

4. Metody badawcze

4.1. Modyfikacja i charakterystyka sorbentu

Do wstępnej oceny możliwości przeprowadzenia modyfikacji jonami lantanu(III) zastosowano dostępny w handlu silnie kwasowy kationit Arsen X^{np} (Purolite, USA). W celu potwierdzenia, że procedurę można zastosować w przypadku innych jonów, wybrano silnie zasadowy anionit Ferrix A33E (Purolite, USA). Ten sam materiał zastosowano w przypadku kolejnych modyfikacji jonami Nd(III) i Ce(III). Proces modyfikacji obejmował dwa etapy: (1) adsorpcja jonów lantanowców(III) Ln(III) (czas wytrząsania 6 h, stężenie początkowe 100 mg/dm³, pH 4), (2) dekantacja roztworu znad sorbentu, przemycie wodą destylowaną, a następnie suszenie w temperaturze 333 K przez 24 godziny. Roztwór La(III) o stężeniu 100 mg/dm³ przygotowano przez rozтворzenie tlenku lantanu(III) La₂O₃ (Specpure JMC, Anglia) najpierw w rozcieńczonym, a następnie w stężonym kwasie azotowym HNO₃ (Chempur, Polska). Analogicznie postępowano w przypadku roztworu Nd(III), do którego przygotowania użyto tlenku neodiumu(III) Nd₂O₃. Z kolei roztwór Ce(III) otrzymano poprzez rozpuszczenie odpowiedniej ilości heksahydrytu azotanu(V) ceru(III) Ce(NO₃)₃·6H₂O (Sigma Aldrich, USA) w wodzie destylowanej. pH roztworów lantanowców(III) doprowadzono za pomocą wodorotlenku sodu NaOH (Chempur, Polska) lub kwasu chlorowodorowego HCl (Chempur, Polska) do wartości 4. W celu przeprowadzenia adsorpcji jonów lantanowców(III) próbki jonitów o masie 0,5 g umieszczano w kolbach stożkowych o pojemności 500 cm³ i do każdej z nich dodawano 100 cm³ uprzednio przygotowanego roztworu Ln(III) o stężeniu 100 mg/dm³, a następnie wytrzązano przez 6 h. Stężenie jonów Ln(III) mierzono za pomocą atomowego spektrometru emisyjnego z indukcyjnie sprzężoną plazmą ICP-OES (ang. *inductively coupled plasma optical emission spectrometry*) (720 ES, Varian, USA).

Morfologia powierzchni niezmodyfikowanych i zmodyfikowanych jonitów została opisana za pomocą skaningowej mikroskopii elektronowej SEM (ang. *scanning electron microscopy*) (Tescan, Czechy) z funkcją rozszerzonej głębi ostrości EDF (ang. *extended depth of field*). Wykonano również zdjęcia powierzchni po sorpcji jonów As(V).

Punkt zerowego ładunku pH_{PZC} (ang. *point of zero charge*) jonitów wyznaczono metodą dryftu pH [29]. W kolbach stożkowych o pojemności 100 cm³ przygotowano po 20 cm³ 0,1 M roztworów NaCl o pH od 2 do 11 (pH₀). Do każdej kolby dodano 0,1 g jonitu, następnie wytrzązano przez 6 godzin i zmierzono pH (pH₁). Punkt zerowego

ładunku wyznaczono z zależności pH_1-pH_0 vs. pH_0 . pH_{PZC} to punkt, w którym pH_1-pH_0 jest równe 0.

Parametry charakteryzujące strukturę materiałów porowatych wyznaczono za pomocą analizy izoterm adsorpcji i desorpcji azotu w temperaturze 77 K (ASAP 2405, Micromeritics, USA) po wstępny odgazowaniu próbek w ścisłe kontrolowanej temperaturze. Powierzchnię właściwą wyznaczono metodą Brunauera, Emmetta i Tellera (BET). Ponadto wyznaczono całkowite objętości porów i średnie średnice porów według modelu Barreta-Joynera-Halenda.

Modyfikowane i niemodyfikowane materiały przed i po adsorpcji jonów arsenianowych(V) badano metodą spektroskopii w podczerwieni z transformataً Fouriera z systemem osłabionego całkowitego odbicia ATR-FTIR (ang. *Attenuated Total Reflectance Fourier transformed infrared spectroscopy*). Otrzymane widma umożliwiły identyfikację określonych wiązań chemicznych (spektrometr Cary 630 FTIR, Agilent Technologies, USA oraz Nicolet 8700A, Thermo Scientific, USA).

W celu określenia składu i stopni utlenienia pierwiastków po modyfikacji i sorpcji jonów As(V) wykorzystano rentgenowską spektroskopię fotoelektronów XPS (ang. *X-ray photoelectron spectroscopy*) (Prevac, Polska).

4.2. Badania adsorpcji metodą statyczną

Badania adsorpcji metodą statyczną przeprowadzono w kolbach o pojemności 100 cm³. W celu zbadania wpływu pH na efektywność adsorpcji jonów arsenianowych(V) próbki jonitu o masie 0,1 g dodawano do kolb zawierających 20 cm³ roztworu o stężeniu As(V) wynoszącym 100 mg/dm³ i innych wartościach pH. Wartości pH od 4 do 11 dostosowywano poprzez dodanie odpowiednich ilości 0,01 M NaOH (Chempur, Polska) lub 0,01 M HCl (Chempur, Polska). Kolby wytrząsano na wytrząsarce laboratoryjnej Elpin+ typ 357 (Elpin Plus, Polska) przez 6 godzin. Adsorbent oddzielono od roztworu przez filtrację. W kolejnym etapie metodą spektrofotometryczną (Cary 60, Agilent Technologies, USA) przy długości fali 870 nm analizowano stężenie jonów As(V) w postaci kompleksów z molibdenianem amonu. Pojemności sorpcyjne q_t oraz procent sorpcji %S obliczono za pomocą równań przedstawionych poniżej:

$$q_t = (c_0 - c_t) \times \frac{V}{m} \quad (1)$$

$$\%S = \frac{(c_0 - c_t)}{c_0} \times 100\% \quad (2)$$

gdzie: q_t to pojemność sorpcyjna po czasie t (mg/g), c_0 to początkowe stężenie As(V) w roztworze (mg/dm³), c_t to stężenie As(V) w roztworze po czasie t (mg/dm³), V to objętość roztworu (dm³), m to masa jonitu (g).

W celu zbadania kinetyki sorpcji odważki jonitu o masie 0,1 g dodawano do kolb stożkowych o pojemności 100 cm³ zawierających 20 cm³ roztworu o stężeniach początkowych As(V) 25, 50 i 100 mg/dm³ i pH 6. Próbki wytrząsano przez 1, 3, 5, 7, 10, 20, 30, 60, 120, 240 i 360 min (temperatura 295 K, szybkość wytrząsania 180 obr./min). Ponadto do określenia oddziaływań adsorbent-adsorbat wykorzystano modele pseudo-pierwszego rzędu PFO (ang. *pseudo-first order*), pseudo-drugiego rzędu PSO (ang. *pseudo-second order*), Elovicha i dyfuzji wewnętrzczastkowej IPD (ang. *intraparticle diffusion*). Użyteczność modeli oceniono na podstawie analizy błędów – współczynnika korelacji (R^2) oraz sumy kwadratów błędów SSE (ang. *sum of squared errors*). Porównano również właściwości sorpcyjne względem As(V) modyfikowanych jonitów z niemodyfikowanymi. Równania form liniowych i nieliniowych dla różnych modeli kinetycznych zebrane w Tabeli 1.

Tabela 1. Formy nieliniowe i liniowe modeli kinetycznych [18,30–34].

Model kinetyczny	Forma nieliniowa	Forma liniowa	Wykres dla formy liniowej	Publikacja
PFO	$\frac{dq_t}{dt} = k_1(q_e - q_t)$	$\ln(q_e - q_t) = \ln q_e - k_1 t$	$\ln(q_e - q_t)$ vs t	D1-D4
PSO	$\frac{dq_t}{dt} = k_2(q_e - q_t)^2$	$\frac{t}{q_t} = \frac{1}{k_2 q_e^2} + \frac{t}{q_e}$	t/q_t vs t	D1-D4
Elovich	$\frac{dq_t}{dt} = \alpha \exp^{-\beta q_t}$	$q_t = \frac{1}{\beta} \ln(\alpha\beta) + \frac{1}{\beta} \ln t$	q_t vs $\ln t$	D2-D4
IPD	-	$q_t = k_i \sqrt{t} + C$	q_t vs $t^{1/2}$	D2-D4

gdzie: q_t jest to pojemność sorpcyjna po czasie t (mg/g), q_e to pojemność sorpcyjna w stanie równowagi (mg/g), k_1 to stała szybkości PFO (1/min), k_2 to stała szybkości PSO (g/(mg·min)), α to początkowa szybkość adsorpcji (mg/(g·min)), β jest związane z pokryciem powierzchni i energią aktywacji dla chemisorpcji (g/mg), k_i to stała szybkości IPD, C to stała wprost proporcjonalna do grubości warstwy granicznej.

W przypadku badań równowagowych adsorpcji przygotowano roztwory As(V) o stężeniach 25–1000 mg/dm³ i pH 6. Wytrząsanie próbek jonitów z tak przygotowanymi roztworami prowadzono przy ustalonych parametrach, tj. masa jonitu 0,1 g, objętość

roztworu 20 cm³, czas 6 godzin, szybkość 180 obr./min). Ocenę dopasowania danych do modeli teoretycznych izoterm Langmuira, Freundlicha, Dubinina-Radushkevicha, Halseya i Redlich-Petersona przeprowadzono za pomocą analizy regresji liniowej, sumy błędów kwadratów SSE i testu F. Równania przedstawiające zastosowane modele izoterm zestawiono w Tabeli 2.

Tabela 2. Formy nieliniowe i liniowe modeli izoterm [35–40].

Model izotermy	Forma nieliniowa	Forma liniowa	Wykres dla formy liniowej	Publikacja
Langmuira	$q_e = \frac{q_m K_L c_e}{1 + K_L c_e}$ $R_L = \frac{1}{1 + K_L c_0}$	$\frac{c_e}{q_e} = \frac{1}{q_m K_L} + \frac{c_e}{q_m}$	c_e/q_e vs c_e	D1-D4
Freundlicha	$q_e = K_F c_e^n$	$\log q_e = \log K_F + \frac{1}{n} \log c_e$	$\log q_e$ vs $\log c_e$	D1-D4
Dubinina-Radushkevicha	$q_e = q_{DR} e^{-K_{DR}\varepsilon^2}$ $\varepsilon = RT \ln \left(1 + \frac{1}{c_e} \right)$ $E = \frac{1}{\sqrt{2\beta}}$	$\ln q_e = \ln q_{DR} - \beta \varepsilon^2$	$\ln q_e$ vs ε^2	D2-D4
Halseya	$q_e = \frac{1}{n_H} \ln K_H - \frac{1}{n_H} \ln c_e$	$\ln q_e = \frac{1}{n_H} \ln K_H - \frac{1}{n_H} \ln \frac{1}{c_e}$	$\ln q_e$ vs $\ln c_e$	D2,D3
Redlich-Petersona	$q_e = \frac{K_{RP} c_e}{1 + a_{RP} c_e^g}$	$\ln \left(\frac{c_e}{q_e} \right) = g \ln c_e - \ln K_{RP}$	$\ln(c_e/q_e)$ vs $\ln c_e$	D4

gdzie: q_e jest to pojemność sorpcyjna w stanie równowagi (mg/g), c_e to stężenie adsorbatu w stanie równowagi (mg/g), q_m (g/mg), K_L (dm³/mg), R_L (-) to stałe Langmuira związane odpowiednio z maksymalną pojemnością sorpcyjną i energią sorpcji, K_F (mg/g) i n (-) to stałe Freundlicha, q_{DR} oznacza maksymalną pojemność sorpcyjną wg Dubinina-Radushkevicha (mol/g), β to stała związana z energią adsorpcji (mol²/J²), ε odpowiada potencjałowi Polanyi'ego, R to stała gazowa (8,314 J/K/mol), T to temperatura (K), E to energia adsorpcji (J/mol), K_H and n_H są stałymi Halseya, K_{RP} (dm³/g) i a_{RP} (dm³/mg)^g są stałymi Redlich-Petersona; g jest wykładnikiem, którego wartość musi zawierać się w przedziale od 0 do 1.

Zbadano również wpływ temperatury na wydajność adsorpcji jonów As(V), a główne parametry termodynamiczne obliczono za pomocą poniższych równań [41]:

$$K_d = \frac{q_e}{c_e} \quad (3)$$

$$\Delta G^0 = -RT \ln K_d \quad (4)$$

$$\ln K_d = -\frac{\Delta H^0}{RT} + \frac{\Delta S^0}{R} \quad (5)$$

gdzie: K_d jest to współczynnik podziału (dm^3/g), ΔG^0 to zmiana entalpii swobodnej Gibbsa (kJ/mol), ΔH^0 to zmiana entalpii (kJ/mol), ΔS^0 to zmiana entropii ($\text{kJ/mol}\cdot\text{K}$).

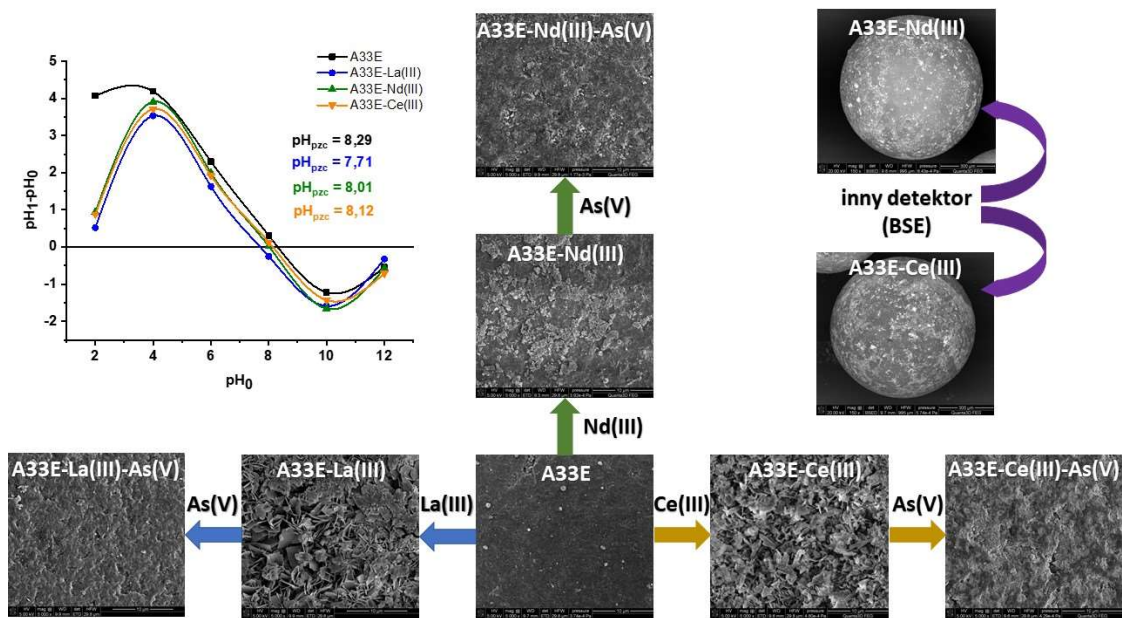
Badania przeprowadzono identycznie w stosunku do badań równowagowych, prowadząc proces w trzech różnych temperaturach 295, 313 i 333 K.

W celu oceny możliwości ponownego użycia modyfikowanych materiałów w trzech kolbach o pojemności 100 cm^3 umieszczono $0,1 \text{ g}$ jonitu i do każdej z nich dodano 20 cm^3 roztworu As(V) o stężeniu $100 \text{ mg}/\text{dm}^3$ i pH 6. Próbki wytrząsano przez 6 godzin w temperaturze 295 K i przy szybkości 180 obr./min. W kolejnym etapie sorbent oddzielono od roztworu metodą filtracji i suszono w temperaturze 333 K przez 24 godziny. Suche próbki ponownie umieszczono w kolbach o pojemności 100 cm^3 i dodano do nich 20 cm^3 roztworu NaOH o stężeniach 0,05, 0,2 i 1 M. Próbki wytrząsano przez 6 godzin (temperatura 295 K, szybkość wytrząsania 180 obr/min). Po tym czasie jonit usunięto z roztworu poprzez filtrację i suszono w 333 K przez 24 godziny. Doświadczenie przeprowadzono jeszcze dwukrotnie z 1 M NaOH. Stężenie jonów As(V) w roztworze mierzono po każdym etapie adsorpcji i desorpcji.

5. Omówienie wyników

5.1. Charakterystyka jonitów

Zastosowanie skaningowej mikroskopii elektronowej SEM pozwoliło na wizualną ocenę struktury powierzchni badanych jonitów. Na podstawie przeprowadzonych badań można przypuszczać, że po sorpcji jonów lantanowców zachodzą zmiany w morfologii powierzchni materiałów, która staje się bardziej niejednorodna. Na heterogenicznych powierzchniach X^{np} -La(III) [D1] i A33E-La(III) [D2] stwierdzono obecność płatkowatych nanocząstek (wodoro)tlenku lantanu(III), natomiast powierzchnie jonitu przed modyfikacją były gładkie i jednorodne. Rozmiary nanopłatków wahały się w przedziale 100–2300 nm, przy czym ich średnia średnica wynosiła około 800 nm. W przypadku modyfikacji A33E jonami neodiumu(III) zauważono osadzanie się cząstek w postaci aglomeratów [D3]. Cząstki te wydawały się mieć strukturę bąbelkową, płytową oraz ziarnistą. Analogiczne rezultaty dotyczące materiałów na bazie związków neodiumu(III) uzyskano w pracach Khana i wsp. oraz Ahmadiego i wsp. [42,43]. W przypadku modyfikacji Ce(III) Zhang i wsp. [44] przedstawili trzy typy morfologii tlenku ceru(III), tj. nanopręty Ce-R, nanocząstki Ce-P i nanopłatki Ce-F, co wynika z odmiennego sposobu przygotowania sorbentu. Wykazano, że modyfikacja jonami Ce(III) spowodowała wzrost heterogeniczności i utworzenie nanopłatków Ce-F na powierzchni A33E [D4]. Ponadto w przypadku materiałów A33E-Nd(III) i A33E-Ce(III) zastosowano obrazowanie elektronów wstecznie rozproszonych BSE (ang. *backscattered electron*) do wykrywania układów zawierających pierwiastki o stosunkowo wysokich masach atomowych takich jak pierwiastków ziem rzadkich REE [45]. Jaśniejsze punkty na obrazach SEM-BSE są związane z zaadsorbowanymi jonami neodiumu(III) i ceru(III), co wskazuje na to, że A33E został pomyślnie zmodyfikowany. Warto zwrócić uwagę, że po adsorpcji As(V) na wszystkich zmodyfikowanych jonitach nastąpiło zmniejszenie niejednorodności powierzchni w wyniku wypełnienia porów jonami As(V). Obrazy SEM po modyfikacji A33E jonami La(III), Nd(III) i Ce(III) oraz po adsorpcji jonów As(V) zostały przedstawione na Rysunku 1.



Rysunek 1. Obrazy SEM po modyfikacji A33E jonami La(III), Nd(III) i Ce(III) oraz po adsorpcji jonów As(V) (powiększenie 5000 x) oraz dodatkowe zdjęcia A33E-Nd(III) i A33E-Ce(III) wykonane przy pomocy detektora BSE (powiększenie 150 x). Lewa strona rysunku przedstawia wartości punktu ładunku zerowego pH_{PZC} zmodyfikowanych A33E w porównaniu z niemodyfikowanym jonitem.

Powszechnie wiadomo, że pH roztworu wpływa m.in. na ładunek powierzchniowy adsorbentów, dysocjację obecnych na powierzchni materiału grup funkcyjnych oraz stopień dysocjacji jonów w roztworze [46]. W związku z tym, wyznaczono punkt ładunku zerowego pH_{PZC} jonitów przed i po modyfikacji. W wyniku adsorpcji jonów La(III) obniżył się on z 8,38 do 7,21 w przypadku X^{np}. Podobny trend zauważono po modyfikacji A33E jonami La(III), Nd(III) i Ce(III) (Rysunek 1), jednak w tej sytuacji nie zaobserwowano tak wyraźnego spadku. Największą różnicę zauważono w przypadku adsorpcji jonów La(III), która spowodowała obniżenie pH_{PZC} z 8,29 do 7,71. Przy wartościach pH wyższych niż pH_{PZC} powierzchnia materiału staje się naładowana ujemnie, natomiast jeżeli pH jest niższe niż pH_{PZC} powierzchnia jest obdarzona ładunkiem dodatnim. Biorąc pod uwagę diagram specjacji jonów arsenu przedstawiony przez Issę i wsp. [47], główną formą As(V) w zakresie pH od 4 do 11 są aniony diwodoarsenianowe(V) H₂AsO₄⁻ i wodoarsenianowe(V) HAsO₄²⁻. W rezultacie adsorpcja anionów arsenianowych(V) na powierzchni badanych jonitów jest uprzywilejowana dla wartości pH roztworu poniżej pH_{PZC}, ponieważ ma miejsce przyciąganie elektrostatyczne [48].

Kolejnym badaniem, które przeprowadzono była szeroko stosowana do wyznaczania rozkładu objętości porów i powierzchni właściwej metoda niskotemperaturowej adsorpcji azotu. Stwierdzono, że w przypadku wszystkich zmodyfikowanych jonitów otrzymane izotermy adsorpcji/desorpcji N₂ należą do typu IV zgodnie z klasyfikacją IUPAC. Sugeruje to, że materiały charakteryzowały się mezoporową strukturą [49]. Na wszystkich izotermach widoczne są pętle histerezy typu H3, których kształt świadczy o szczelinowej budowie porów i obecności płytкоподобnych cząsteczek na powierzchni jonitów [12]. Ponadto wyznaczono powierzchnie właściwe, całkowite objętości porów oraz średnie średnice porów. Powierzchnia właściwa X^{np} wynosiła 55,3 m²/g i po modyfikacji jonami La(III) nieznacznie obniżyła się do 52,8 m²/g. Całkowita objętość porów i średnia średnica porów przed adsorcją jonów lantanu(III) miały wartości 0,19 cm³/g i 13,7 nm, a po adsorpcji osiągnęły odpowiednio 0,17 cm³/g i 12,8 nm. Zauważono, że różnice w omawianych parametrach materiałów przed i po modyfikacji były niewielkie, tak samo jak w przypadku modyfikacji A33E jonami La(III), Nd(III) i Ce(III) (Tabela 3).

Tabela 3. Parametry charakteryzujące strukturę porowatą A33E przed i po modyfikacji jonami La(III), Nd(III) i Ce(III).

Parametr	Powierzchnia właściwa S_{BET} (m ² /g)	Calkowita objętość porów V_t (cm ³ /g)	Średnia średnica porów D_p (nm)	Publikacja
A33E	53,1	0,12	9,2	D2-D4
A33E-La(III)	59,4	0,13	8,5	D2
A33E-La(III)-As(V)	56,0	0,12	8,9	
A33E-Nd(III)	54,7	0,13	9,4	D3
A33E-Nd(III)-As(V)	60,4	0,14	9,5	
A33E-Ce(III)	56,7	0,13	8,8	D4
A33E-Ce(III)-As(V)	60,7	0,14	9,2	

Podczas badania adsorpcji z roztworów wodnych należy zwrócić uwagę nie tylko na strukturę porowatą adsorbentu, ale również na występowanie na jego powierzchni określonych grup funkcyjnych. Mogą do nich należeć zarówno grupy naturalnie występujące na powierzchni materiału, jak również takie, które zostały wprowadzone w wyniku modyfikacji chemicznej. Powszechnie wykorzystywana do tego celu metodą jest spektroskopia w podczerwieni umożliwiająca identyfikację ugrupowań powierzchniowych, a nawet badanie mechanizmu adsorpcji. W związku z tym widma

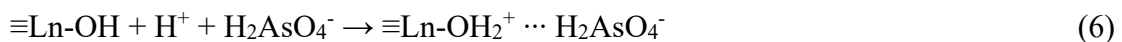
ATR-FTIR niemodyfikowanych i modyfikowanych jonitów zebrano przed i po sorpcji jonów As(V). W przypadku badań dotyczących X^{np} [D1] pasma przy 3600-3200 cm⁻¹ wskazują na drgania rozciągające O-H pochodzące od grup wodorotlenowych na powierzchni tlenku żelaza oraz zaadsorbowanych cząsteczek wody, które były również odpowiedzialne za drgania deformacyjne (1638 cm⁻¹). Pasma znajdujące się w obszarze 1200-900 cm⁻¹ przypisano grupie sulfonowej, w której można wyróżnić symetryczne i asymetryczne drgania rozciągające S=O oraz rozciągające S-OH. Wzrost intensywności pasma przy 827 cm⁻¹ dotyczy utworzenia wiązania As-O-La, sugerując, że wprowadzone jony lantanu(III) uczestniczyły w procesie adsorpcji jonów arsenianowych(V) tworzących kompleksy powierzchniowe [50]. W przypadku badań dotyczących A33E [D2-D4] występowały istotne różnice w zebranych widmach w porównaniu do X^{np}. Przy długości fali ok. 1480 cm⁻¹ [D2-D4] pojawiły się pasma pochodzące od czwartorzędowych grup amoniowych. Na widmie A33E-La(III) przy 920 cm⁻¹ zaobserwowano nachylenie pasma zidentyfikowane jako wiązanie La-O [D2], które było również obecne na widmie pochodzący od impregnowanej lantanem mezoporowej krzemionki SBA-15 [51]. Porównując widma A33E-La(III) i A33E po adsorpcji jonów As(V) zauważono, że pasmo pochodzące od drgań rozciągających As-O (825 cm⁻¹) ma mniejszą intensywność. Sugeruje to odmienny mechanizm adsorpcji jonów arsenianowych(V) na jonicie modyfikowanym. W przypadku A33E-Nd(III) i A33E-Ce(III) po adsorpcji jonów As(V) pojawiły się nowe pasma przy długościach fali odpowiednio 445 cm⁻¹ i 448 cm⁻¹ [D3,D4]. Przypisano je do drgań pochodzących od wiązań Nd-O-As oraz Ce-O-As [22], które zostały utworzone w wyniku utworzenia wiązania koordynacyjnego między miejscami aktywnymi REE a atomami tlenu w jonach arsenianowych(V). Wskazują one na tworzenie się powierzchniowych kompleksów wewnętrzferowych.

Dokonując identyfikacji określonych grup funkcyjnych oraz utworzonych wiązań na powierzchni materiału porowatego warto przeprowadzić jego analizę składu powierzchniowego. Stosując rentgenowską spektroskopię fotoelektronów XPS określono skład i stopnie utlenienia pierwiastków po modyfikacji i sorpcji jonów As(V) na jonicie A33E [D2-D4]. Analiza widm wykazała obecność Fe, O, N i C we wszystkich próbkach. Żelazo i tlen występują jako tlenki żelaza(II,III) Fe_xO_y. Azot występuje w czwartorzędowych grupach amoniowych, natomiast węgiel zidentyfikowano w alifatycznych C-H i C-C oraz aromatycznych C=C wiązaniach obecnych w polistyrenie usieciowanym diwinylobenzenem PS-DVB. Na wszystkich widmach modyfikowanych

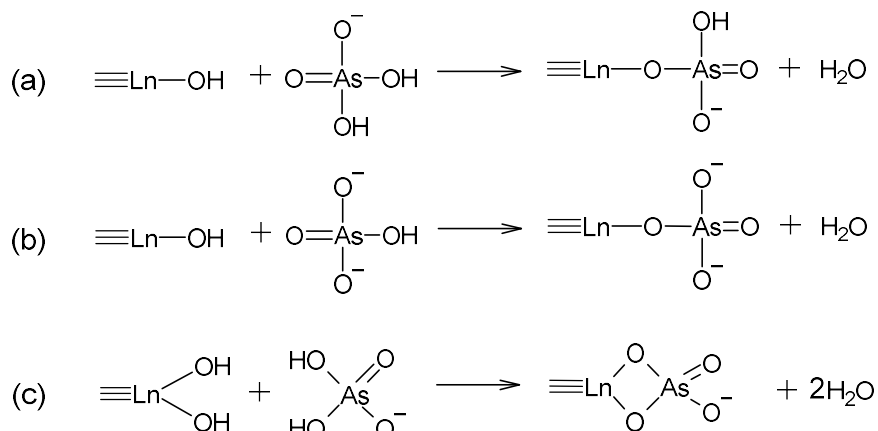
jonitów widoczne są piki pochodzące od REE, co świadczy o udanej adsorpcji jonów La(III), Nd(III) i Ce(III). Ponadto, piki w regionie As3d (48-42 eV) wskazują, że adsorpcja jonów arsenianowych(V) może przebiegać zarówno na zmodyfikowanych, jak i niezmodyfikowanych wymieniaczach jonowych. W przypadku A33E-Ln(III) piki As są przesunięte i mają różne intensywności w porównaniu z A33E. Sugeruje to różne mechanizmy adsorpcji As(V) na zmodyfikowanych materiałach w porównaniu z niemodyfikowanymi. W przypadku regionów La3d, Nd3d oraz Ce3d obecne w nich piki również uległy przesunięciu, a ich intensywności zmieniły się po adsorpcji As(V). Sugerowało to, że wprowadzone jony REE były zaangażowane w proces adsorpcji arsenianów(V). Dodatkowo stwierdzono, że w regionie As3d pojawiają się piki pochodzące od As(III). Można to wytlumaczyć podatnością jonów As(V) na redukcję wywołaną promieniowaniem rentgenowskim podczas analizy XPS [52].

5.2. Wpływ pH

Analizując wpływ pH na wydajność adsorpcji jonów arsenianowych(V) na jonicie X^{np} -La(III) stwierdzono, że jest ona największa przy pH 6 [D1]. Analogiczne wyniki uzyskano dla modyfikowanego A33E jonami La(III), Nd(III) i Ce(III) [D2-D4]. Przy pH 6 arsen(V) występuje w formie anionów $HAsO_4^{2-}$ i $H_2AsO_4^-$ w stosunku molowym około 1:9 [47]. Oddziaływanie elektrostatyczne między centrami aktywnymi jonitu a jonami arsenianowymi(V) mogą mieć istotne znaczenie w procesie adsorpcji. Z uwagi na fakt, że wyznaczona optymalna wartość pH jest niższa od wartości punktu ładunku zerowego pH_{PZC} zachodzi silniejsze protonowanie grup funkcyjnych na jego powierzchni. Skutkuje to zwiększym przyciąganiem elektrostatycznym pomiędzy dodatnio naładowanymi miejscami aktywnymi jonitu a ujemnie naładowanymi jonami As(V) [53]:



Ponadto, analiza FTIR ujawniła utworzenie nowych wiązań Ln-O-As [D3,D4] wynikających z obecności monodentnych i bidentnych kompleksów powierzchniowych (Rysunek 2).



Rysunek 2. Schemat tworzenia kompleksów monodentnych (a,b) i bidentnych (c) przez jony As(V).

Wykazano, że w roztworze o zasadowym odczynie adsorcja As(V) była nadal możliwa, wydajność sorpcji była znacznie mniejsza. Gdy pH roztworu przekracza wartość pH_{PZC}, zjawisko odpychania elektrostatycznego znacznie ogranicza adsorcję arsenianów(V) [54].

5.3. Badania kinetyczne

W metodach adsorpcyjnych czas potrzebny do osiągnięcia stanu równowagi jest bardzo istotnym problemem. W związku z tym zbadano wpływ stężenia i czasu kontaktu faz na wydajność procesu adsorpcji w celu określenia szybkości jego przebiegu. W przypadku jonitu X^{np} okazało się, że jego modyfikacja spowodowała wzrost wydajności usuwania As(V) [D1]. X^{np}-La(III) był zdolny do stu procentowej adsorpcji jonów arsenianowych(V) z roztworu o stężeniu 50 mg/dm³ w czasie 60 minut. Warto zwrócić uwagę na to, że przed modyfikacją nie udało się całkowicie usunąć jonów As(V) z roztworu o stężeniu 25 mg/dm³. Przy bardzo wysokiej zawartości arsenu w roztworze (100 mg/dm³) wydajność jego usuwania była o prawie 20% wyższa w przypadku X^{np}-La(III). Dodatkowo, po modyfikacji czas potrzebny do osiągnięcia stanu równowagi nie pogorszył się przy żadnym z początkowych stężeń As(V). Analogiczne wyniki uzyskano w przypadku modyfikowanego lantanem(III), neodymem(III) oraz cerem(III) jonitu A33E [D2-D4]. Zostały one zestawione w Tabeli 4.

Tabela 4. Zestawienie procentu sorpcji oraz czasu potrzebnego do osiągnięcia równowagi przez A33E i A33E-Ln(III) w zależności od stężenia początkowego As(V).

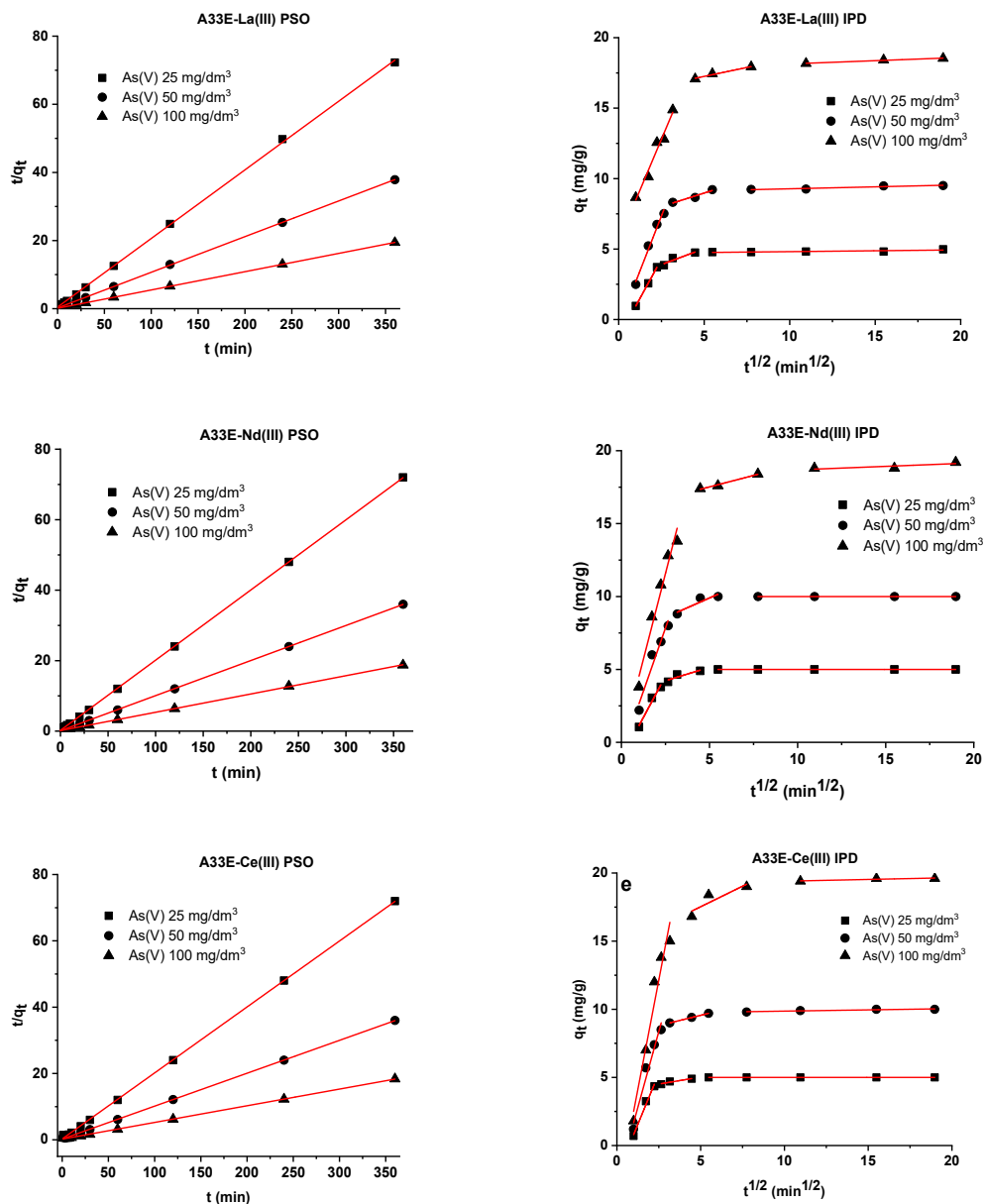
Wymieniacz jonowy		A33E	A33E-La(III)	A33E-Nd(III)	A33E-Ce(III)
As(V) 25 mg/dm ³	%S	97,0%	99,6%	100,0%	100,0%
	czas potrzebny do osiągnięcia równowagi (min)	60	60	30	30
As(V) 50 mg/dm ³	%S	88,0%	95,1%	100,0%	100,0%
	czas potrzebny do osiągnięcia równowagi (min)	60	60	30	60
As(V) 100 mg/dm ³	%S	86%	92,7%	96%	98%
	czas potrzebny do osiągnięcia równowagi (min)	120	60	120	120
Publikacja		D2-D4	D2	D3	D4

A33E-Nd(III) i A33E-Ce(III), podobnie jak X^{np}-La(III), były w stanie usunąć całkowicie jony As(V) z roztworu o stężeniu 50 mg/dm³, przy czym czas potrzebny do osiągnięcia stanu równowagi przez pierwszy z nich wynosił jedynie 30 minut. Warto zauważyć, że w każdym przypadku proces modyfikacji jonitu A33E jonami REE spowodował wzrost efektywności usuwania arsenianów(V), nie wydłużając czasu potrzebnego do osiągnięcia stanu równowagi.

W badaniach zastosowano modele kinetyczne pseudo-pierwszego rzędu PFO [D1-D4], pseudo-drugiego rzędu PSO [D1-D4], Elovicha [D2-D4] i dyfuzji wewnętrzcząstkowej IPD [D2-D4]. Najczęściej wykorzystywany modelami są PFO i PSO [55]. Porównując uzyskane dane stwierdzono, że model PSO zdecydowanie lepiej dopasowuje się do danych eksperymentalnych dotyczących adsorpcji As(V) na X^{np}-La(III), co zostało potwierdzone przez analizę błędu [D1]. Ponadto, obliczone na podstawie modelu PSO równowagowe pojemności sorpcyjne są bardzo zbliżone do tych otrzymanych doświadczalnie. Identyczny wniosek wyciągnięto w przypadku modyfikowanych jonitów A33E (Rysunek 3) [D2-D4]. Świadczy to o tym, że proces usuwania As(V) związany jest z chemisorpcją [11]. Porównano również model Elovicha z modelem PSO w kontekście stosowności w opisanych przypadkach. Zauważono, że

nie był on dobrze dopasowany do danych eksperymentalnych ze względu na niskie wartości R^2 i stosunkowo wysokie wartości SSE.

Do określenia etapów limitujących szybkość procesu wykorzystano model IPD. Wieloliniowe wykresy IPD q_t vs $t^{1/2}$ (Rysunek 3) wskazują, że w proces adsorpcji As(V) na modyfikowanych jonitach A33E zaangażowane są trzy etapy dyfuzji [56].



Rysunek 3. Liniowe wykresy modeli kinetycznych PSO i IPD dla jonitów A33E-La(III), A33E-Nd(III) oraz A33E-Ce(III).

Pierwszy etap obejmuje dyfuzję jonów arsenianowych(V) przez roztwór do zewnętrznej powierzchni materiału. Proces ten jest szybki. W drugim etapie dyfuzja wewnętrzczastkowa limituje szybkość adsorpcji. W wyniku osiągnięcia równowagi i spadku stężenia jonów arsenianowych(V) w roztworze następuje zahamowanie procesu

dyfuzji (etap trzeci). Na podstawie otrzymanych wartości stałych szybkości IPD można wywnioskować, że parametry te maleją w szeregu $k_{i1} > k_{i2} > k_{i3}$. Powierzchnia jonitów ulega wysyceniu, a szybkość adsorpcji spada po wypełnieniu zewnętrznej powierzchni jonami arsenianowymi(V).

5.4. Badania równowagowe i termodynamiczne

Istotnym problemem podczas opisu procesu adsorpcji w układach ciało stałe-ciecz jest wyjaśnienie oddziaływań pomiędzy adsorbatem i adsorbentem w stanie równowagi. Analiza wyników w stanie równowagi może prowadzić do uzyskania informacji na temat powinowactwa jonitu do usuwanych jonów, właściwości jego powierzchni, czy mechanizmu adsorpcji. W tym celu dane eksperymentalne przeanalizowano z wykorzystaniem modeli izoterm Langmuira [D1-D4], Freundlicha [D1-D4], Dubinina-Radushkevicha [D2-D4], Halseya [D2,D3] oraz Redlicha-Petersona [D4].

W przypadku X^{np} -La(III) [D1] obliczone bezwymiarowe współczynniki R_L z modelu Langmuira i $1/n$ z modelu Freundlicha były zawarte w przedziale $<0;1>$, co wskazuje, że adsorpcja jonów arsenianowych(V) na badanym materiale jest procesem korzystnym i wydajnym [18]. Maksymalna pojemność sorpcyjna modyfikowanego jonami lantanu(III) jonitu X^{np} obliczona na podstawie równania izotermy Langmuira wyniosła 61,97 mg/g. Należy zauważyć, że po modyfikacji wzrosła ona prawie trzykrotnie, podobnie jak po modyfikacji jonitu A33E jonami La(III), Nd(III) oraz Ce(III) [D2-D4] (Tabela 5). Największy wzrost maksymalnej pojemności sorpcyjnej względem As(V), o ponad 75%, odnotowano w przypadku jonitu A33E-Ce(III).

Równanie izotermy Dubinina-Radushkevicha zostało wykorzystane do określenia, czy proces adsorpcji na niejednorodnej powierzchni jest fizyczny czy chemiczny. Zgodnie z założeniem tego modelu, jeśli wartość energii E jest mniejsza niż 8 kJ/mol, charakter procesu adsorpcji jest fizyczny, natomiast adsorpcja chemiczna występuje, gdy wartości E przekraczają 8 kJ/mol [57]. W prezentowanych badaniach [D2-D4] wartość E znacznie przekraczała 8 kJ/mol, co sugeruje, że adsorpcja jonów As(V) na powierzchni modyfikowanych jonitów miała głównie charakter chemiczny.

Ze względu na wysokie współczynniki regresji R^2 w przypadku każdego zastosowanego modelu izotermy, dokonano dalszej analizy błędu. Suma kwadratów błędów SSE oraz F-Test ujawniły, że modele Freundlicha i Halseya [D2,D3] oraz Redlicha-Petersona [D4] są najlepiej dopasowane do danych eksperymentalnych. W związku z tym stwierdzono możliwość wielowarstwowej adsorpcji na niejednorodnej

powierzchni jonitu (Freundlich i Halsey) oraz fakt, że proces usuwania jonów As(V) nie przebiegał zgodnie z założeniami idealnej adsorpcji monowarstwowej (Redlich-Peterson) [39,58].

Tabela 5. Maksymalne pojemności sorpcyjne niemodyfikowanego oraz modyfikowanego jonami REE jonitu A33E.

Jonit	Maksymalna pojemność sorpcyjna q_e (mg/g)	Model izotermy	Uwagi	Publikacja
A33E	34,41	-	-	D2-D4
A33E-La(III)	54,64	Freundlich, Halsey	$E = 13,97 \text{ kJ/mol}$ $\Delta H^0 < 0$ $\Delta G^0 < 0$	D2
A33E-Nd(III)	56,01	Freundlich, Halsey	$E = 18,50 \text{ kJ/mol}$ $\Delta H^0 < 0$ $\Delta G^0 < 0$	D3
A33E-Ce(III)	60,41	Redlich-Peterson	$E = 18,12 \text{ kJ/mol}$ $\Delta H^0 < 0$ $\Delta G^0 < 0$	D4

W przypadku jonitów modyfikowanych dodatkowo przedstawiono modele izotermy z najlepszym dopasowaniem, wartości energii adsorpcji oraz parametrów termodynamicznych.

Wyznaczono również parametry termodynamiczne w celu zbadania wpływu temperatury na zdolność adsorpcji jonów As(V) na A33E-La(III), A33E-Nd(III) i A33E-Ce(III). Ujemne wartości ΔG^0 i ΔH^0 wskazują, że proces był spontaniczny i egzotermiczny [59]. Wartość współczynnika separacji R_L potwierdziła spontaniczność sorpcji. Jednak, wraz ze wzrostem temperatury pojemności sorpcyjne jonitów względem jonów As(V) zmniejszały się. W związku z tym, nie jest zalecana wysoka temperatura prowadzenia adsorpcji jonów arsenianowych(V) na omawianych materiałach.

5.5. Regeneracja jonitów

Po ustaleniu się stanu równowagi adsorpcji jonów As(V) jonity nie nadają się do ponownego użytku i konieczna jest ich regeneracja. W celu przeprowadzenia desorpcji zużyty jonit należy oddzielić od roztworu i potraktować roztworem odpowiedniej substancji desorbującej. Powszechnie uważa się, że proces ten najlepiej zachodzi w środowisku zasadowym [60–62]. Przeprowadzono trzy cykle sorpcji i desorpcji oraz oceniono możliwość ponownego wykorzystania badanych materiałów. Sorpcję

проводжено в розчині As(V) о концентрації 100 mg/dm³, а десорбцію в 1 M зasadі sodової NaOH.

W przypadku jonitu X^{np}-La(III) po 3 cyklach sorpcji/desorpcji nie odnotowano istotnego spadku pojemności sorpcyjnej [D1]. Procent desorpcji wyniósł 90,02%, co oznacza, że adsorpcję jonów As(V) można przeprowadzić wielokrotnie na tym samym materiale. Z kolei pojemności sorpcyjne modyfikowanych materiałów A33E-Ln(III) zmniejszały się stopniowo wraz z kolejnym cyklem regeneracji [D2-D4]. Spadek ten nie był znaczący i po trzech desorpcjach w każdym przypadku utrzymywało się ponad 92% początkowej pojemności sorpcyjnej (Tabela 6). Wyniki te pokazują, że proces adsorpcji jonów arsenianowych(V) na modyfikowanych jonitach jest odwracalny i że wymieniacz jonowy można z powodzeniem regenerować za pomocą NaOH. Warto również zauważyć, że po trzeciej desorpcji badane materiały nadal wykazują większą pojemność sorpcyjną niż niemodyfikowany A33E przed pierwszą adsorpcją jonów As(V).

Tabela 6. Porównanie pojemności sorpcyjnych modyfikowanych jonitów A33E-Ln(III) po 3 cyklach sorpcji/desorpcji z niemodyfikowanym A33E po jednej sorpcji jonów As(V) (początkowe stężenie As(V) 100 mg/dm³, czas sorpcji 360 min, czas desorpcji 360 minut).

Jonit	A33E	A33E-La(III) po 3 cyklach sorpcji/desorpcji	A33E-Nd(III) po 3 cyklach sorpcji/desorpcji	A33E-Ce(III) po 3 cyklach sorpcji/desorpcji
Procent desorpcji po 3 cyklach sorpcji/desorpcji	-	94,54%	94,00%	92,47%
Pojemność sorpcyjna (mg/g)	17,17	17,50	18,05	18,12
Publikacja	D2-D4	D2	D3	D4

6. Główne osiągnięcia rozprawy doktorskiej

Uzyskane w ramach rozprawy doktorskiej pt. „Usuwanie jonów arsenianowych(V) na wymieniaczach jonowych na bazie tlenków żelaza modyfikowanych jonami wybranych lantanowców” wyniki można podsumować w formie następujących wniosków:

1. Po sorpcji jonów lantanowców(III) zachodzą zmiany w morfologii powierzchni materiałów, która staje się bardziej niejednorodna. Modyfikacja jonami La(III) prowadzi do powstania płatkowatych nanocząstek na powierzchni materiału, podczas gdy jony Nd(III) powodują formowanie aglomeratów o strukturze bąbelkowej, płytkowej oraz ziarnistej. Adsorpcaja jonów Ce(III), podobnie do jonów La(III), spowodowała utworzenie nanopłatków. Taka morfologia przyczyniła się do ułatwienia adsorpcji jonów arsenianowych(V), w wyniku której nastąpiło ponowne zmniejszenie heterogeniczności powierzchni.
2. Badania rentgenowskiej spektroskopii fotoelektronów XPS oraz spektroskopii w podczerwieni z transformatą Fouriera ATR-FTIR potwierdziły skuteczną modyfikację jonitów jonami lantanowców(III) oraz adsorpcję jonów As(V) na takich materiałach.
3. Optymalna wartość pH usuwania jonów As(V) na badanych materiałach równa 6, tj. poniżej punktu ładunku zerowego pH_{PZC}, skutkuje zwiększym przyciąganiem elektrostatycznym pomiędzy dodatnio naładowanymi miejscami aktywnymi jonitów a ujemnie naładowanymi jonami diwodoarsenianowymi(V) i wodoroarsenianowymi(V). Stwierdzono również tworzenie powierzchniowych kompleksów monodentnych i bidentnych.
4. Proces modyfikacji jonitów A33E i X^{np} jonami REE spowodował wzrost efektywności usuwania arsenianów(V). Stosując jonity X^{np}-La(III), A33E-Nd(III) i A33E-Ce(III) można całkowicie usunąć jony As(V) z roztworów o stosunkowo wysokim stężeniu (50 mg/dm³) w czasie 60 minut. W przypadku jonitów przed modyfikacją nie było to możliwe nawet przy początkowym stężeniu As(V) wynoszącym 25 mg/dm³.
5. Po modyfikacji pojemności sorpcyjne wszystkich badanych jonitów znacznie wzrosły. Największy wzrost zanotowano w przypadku jonitu X^{np} (o 177%), natomiast w przypadku modyfikowanych jonitów A33E – modyfikacja jonami Ce(III) spowodowała wzrost o ponad 75%.
6. Chemisorpcja jonów As(V) na modyfikowanych jonitach była procesem spontanicznym i egzotermicznym. Nie jest zalecana wysoka temperatura prowadzenia procesu adsorpcji jonów arsenianowych(V) na omawianych materiałach.

7. Usuwanie jonów arsenianowych(V) na materiałach modyfikowanych jonami REE nie przebiegało zgodnie z założeniami idealnej adsorpcji monowarstwowej. Stwierdzono możliwość wielowarstwowej adsorpcji na niejednorodnej powierzchni jonitu.

8. Proces adsorpcji jonów arsenianowych(V) na modyfikowanych jonitach jest odwracalny. Zużyty wymieniacz jonowy można z powodzeniem regenerować za pomocą 1 M NaOH. Po trzech cyklach sorpcji/desorpcji wymieniacze jonowe zawierające REE nadal wykazują większą pojemność sorpcyjną niż materiały niemodyfikowane przed pierwszą adsorpcją jonów As(V).

Wymieniacze jonowe modyfikowane jonami REE posiadają lepsze właściwości sorpcyjne niż te niemodyfikowane. Są one obiecującymi materiałami w kontekście usuwania jonów arsenu. Sam proces modyfikacji stwarza możliwości poprawy właściwości sorpcyjnych jonitów zawierających tlenki żelaza oraz obniżenie zawartości jonów As(V) w roztworze do limitu WHO dotyczącego zawartości arsenu w wodzie pitnej. Dzięki wprowadzeniu stosunkowo niewielkiej ilości jonów REE usuwanie arsenu z roztworów wodnych znacznie poprawia skuteczność oczyszczania wody przy jednoczesnym obniżeniu kosztów całej operacji.

Literatura

- [1] Z.A. Alothman, A.H. Bahkali, M.A. Khiyami, S.M. Alfadul, S.M. Wabaidur, M. Alam, B.Z. Alfarhan, Low cost biosorbents from fungi for heavy metals removal from wastewater, *Sep. Sci. Technol.* 55 (2020) 1766–1775.
<https://doi.org/10.1080/01496395.2019.1608242>.
- [2] S.B. Adeloju, S. Khan, A.F. Patti, Arsenic contamination of groundwater and its implications for drinking water quality and human health in under - developed countries and remote communities - a review, *Appl. Sci.* 11 (2021) 1–25.
<https://doi.org/10.3390/app11041926>.
- [3] E. Shaji, M. Santosh, K. V. Sarath, P. Prakash, V. Deepchand, B. V. Divya, Arsenic contamination of groundwater: A global synopsis with focus on the Indian Peninsula, *Geosci. Front.* 12 (2021) 101079.
<https://doi.org/10.1016/j.gsf.2020.08.015>.
- [4] M.R.I. Chowdhury, C.N. Mulligan, Biosorption of arsenic from contaminated water by anaerobic biomass, *J. Hazard. Mater.* 190 (2011) 486–492.
<https://doi.org/10.1016/j.jhazmat.2011.03.070>.
- [5] J.E. Podgorski, S. Eqani, T. Khanam, R. Ullah, H. Shen, M. Berg, Extensive arsenic contamination in high-pH unconfined aquifers in the Indus Valley, *Sci. Adv.* 3 (2017).
<https://doi.org/10.1126/sciadv.1700935>.
- [6] G. Ungureanu, S. Santos, R. Boaventura, C. Botelho, Arsenic and antimony in water and wastewater: Overview of removal techniques with special reference to latest advances in adsorption, *J. Environ. Manage.* 151 (2015) 326–342.
<https://doi.org/10.1016/j.jenvman.2014.12.051>.
- [7] E.R. Kenawy, A.A. Ghfar, S.M. Wabaidur, M.A. Khan, M.R. Siddiqui, Z.A. Alothman, A.A. Alqadami, M. Hamid, Cetyltrimethylammonium bromide intercalated and branched polyhydroxystyrene functionalized montmorillonite clay to sequester cationic dyes, *J. Environ. Manage.* 219 (2018) 285–293.
<https://doi.org/10.1016/j.jenvman.2018.04.121>.
- [8] R. Zakhar, J. Dercó, F. Cacho, An overview of main arsenic removal technologies, *Acta Chim. Slovaca.* 11 (2018) 107–113.
<https://doi.org/10.2478/acs-2018-0016>.
- [9] S. Alka, S. Shahir, N. Ibrahim, M.J. Ndejiko, D.V.N. Vo, F.A. Manan, Arsenic removal technologies and future trends: A mini review, *J. Clean. Prod.* 278 (2021).
<https://doi.org/10.1016/j.jclepro.2020.123805>.
- [10] A. Mittal, M. Naushad, G. Sharma, Z.A. Alothman, S.M. Wabaidur, M. Alam, Fabrication of MWCNTs/ThO₂ nanocomposite and its adsorption behavior for the removal of Pb(II) metal from aqueous medium, *Desalin. Water Treat.* 57 (2016) 21863–21869. <https://doi.org/10.1080/19443994.2015.1125805>.
- [11] M.A. Khan, A.A. Alqadami, S.M. Wabaidur, M.R. Siddiqui, B.H. Jeon, S.A. Alshareef, Z.A. Alothman, A.E. Hamedelniel, Oil industry waste based non-magnetic and magnetic hydrochar to sequester potentially toxic post-transition metal ions from water, *J. Hazard. Mater.* 400 (2020) 123247.
<https://doi.org/10.1016/j.jhazmat.2020.123247>.
- [12] Z.A. Alothman, A review: Fundamental aspects of silicate mesoporous materials, *Materials,* 5 (2012) 2874–2902.
<https://doi.org/10.3390/ma5122874>.

- [13] S.M. Prasad, V.P. Singh, S. Singh, P. Parihar, R. Singh, Arsenic contamination, consequences and remediation techniques: A review, *Ecotoxicol. Environ. Saf.* 112 (2014) 247–270.
<https://doi.org/10.1016/j.ecoenv.2014.10.009>.
- [14] R. Ozola, A. Bhatnagar, L. Ansone-Bertina, I. Vircava, M. Leitietis, J. Burlakovs, M. Klavins, A. Krauklis, FeOOH-modified clay sorbents for arsenic removal from aqueous solutions, *Environ. Technol. Innov.* 13 (2016) 364–372.
<https://doi.org/10.1016/j.eti.2016.06.003>.
- [15] S.I. Siddiqui, S.A. Chaudhry, Iron oxide and its modified forms as an adsorbent for arsenic removal: A comprehensive recent advancement, *Process Saf. Environ. Prot.* 111 (2017) 592–626.
<https://doi.org/10.1016/j.psep.2017.08.009>.
- [16] K. Gupta, U.C. Ghosh, Arsenic removal using hydrous nanostructure iron(III)–titanium(IV) binary mixed oxide from aqueous solution, *J. Hazard. Mater.* 161 (2009) 884–892.
<https://doi.org/10.1016/j.jhazmat.2008.04.034>.
- [17] S.A. Chaudhry, Z. Zaidi, S.I. Siddiqui, Isotherm, kinetic and thermodynamics of arsenic adsorption onto iron-zirconium binary oxide-coated sand (IZBOCS): modelling and process optimization, *J. Mol. Liq.* 229 (2017) 230–240.
<https://doi.org/10.1016/j.molliq.2016.12.048>.
- [18] S. Maji, A. Ghosh, K. Gupta, A. Ghosh, U. Ghorai, A. Santra, P. Sasikumar, U.C. Ghosh, Efficiency evaluation of arsenic(III) adsorption of novel graphene oxide@iron-aluminium oxide composite for the contaminated water purification, *Sep. Purif. Technol.* 197 (2018) 388–400.
<https://doi.org/10.1016/j.seppur.2018.01.021>.
- [19] G. Zhang, Z. Ren, X. Zhang, J. Chen, Nanostructured iron(III)-copper(II) binary oxide: A novel adsorbent for enhanced arsenic removal from aqueous solutions, *Water Res.* 47 (2013) 4022–4031.
- [20] Q. Shi, L. Yan, T. Chan, C. Jing, Arsenic adsorption on lanthanum-impregnated activated alumina: spectroscopic and DFT study, *ACS Appl. Mater. Interfaces.* 7 (2015) 26735–26741.
<https://doi.org/10.1021/acsami.5b08730>.
- [21] L.P. Lingamdinne, J.R. Koduru, Y.Y. Chang, S.H. Kang, J.K. Yang, Facile synthesis of flowered mesoporous graphene oxide-lanthanum fluoride nanocomposite for adsorptive removal of arsenic, *J. Mol. Liq.* 279 (2019) 32–42.
<https://doi.org/10.1016/j.molliq.2019.01.103>.
- [22] Y. Wang, Y. Liu, T. Guo, H. Liu, J. Li, S. Wang, X. Li, X. Wang, Y. Jia, Lanthanum hydroxide: a highly efficient and selective adsorbent for arsenate removal from aqueous solution, *Environ. Sci. Pollut. Res.* 27 (2020) 42868–42880.
<https://doi.org/10.1007/s11356-020-10240-1>.
- [23] Y. Yu, C. Zhang, L. Yang, J. Paul Chen, Cerium oxide modified activated carbon as an efficient and effective adsorbent for rapid uptake of arsenate and arsenite: Material development and study of performance and mechanisms, *Chem. Eng. J.* 315 (2017) 630–638.
<https://doi.org/10.1016/j.cej.2016.09.068>.
- [24] T. Liang, L. Li, C. Zhu, X. Liu, H. Li, Q. Su, J. Ye, B. Geng, Y. Tian, M.F. Sardar, X. Huang, F. Li, Adsorption of As(V) by the novel and efficient adsorbent cerium-manganese modified biochar, *Water.* 12 (2020) 2720.
<https://doi.org/10.3390/w12102720>.

- [25] Y. Yu, L. Yu, K.Y. Koh, C. Wang, J.P. Chen, Rare-earth metal based adsorbents for effective removal of arsenic from water: A critical review, *Crit. Rev. Environ. Sci. Technol.* 48 (2018) 1127–1164.
<https://doi.org/10.1080/10643389.2018.1514930>.
- [26] S. Muthu Prabhu, C. Chuaicham, K. Sasaki, A mechanistic approach for the synthesis of carboxylate-rich carbonaceous biomass-doped lanthanum-oxalate nanocomplex for arsenate adsorption, *ACS Sustain. Chem. Eng.* 6 (2018) 6052–6063.
<https://doi.org/10.1021/acssuschemeng.7b04678>.
- [27] M. Muthuselvi, K. Jeyasubramanian, G.S. Hikku, M. Muthuselvan, M. Eswaran, N. Senthil Kumar, V.K. Ponnusamy, Rare earth metal oxide-doped reduced graphene-oxide nanocomposite as binder-free hybrid electrode material for supercapacitor application, *Int. J. Energy Res.* 45 (2021) 8255–8266.
<https://doi.org/10.1002/er.6441>.
- [28] S. Liang, H. Wang, Y. Li, H. Qin, Z. Luo, B. Huang, X. Zhao, C. Zhao, L. Chen, Rare-earth based nanomaterials and their composites as electrode materials for high performance supercapacitors: a review, *Sustain. Energy Fuels.* 4 (2020) 3825–3847.
<https://doi.org/10.1039/d0se00669f>.
- [29] N. Le My Linh, D. Hoang Van, T. Duong, M.X. Tinh, D. Quang Khieu, Adsorption of arsenate from aqueous solution onto modified vietnamese bentonite, *Adv. Mater. Sci. Eng.* 2019 (2019) 1–13.
<https://doi.org/10.1155/2019/2710926>.
- [30] Q. Hu, Q. Wang, C. Feng, Z. Zhang, Z. Lei, K. Shimizu, Insights into mathematical characteristics of adsorption models and physical meaning of corresponding parameters, *J. Mol. Liq.* 254 (2018) 20–25.
<https://doi.org/10.1016/j.molliq.2018.01.073>.
- [31] W. Plazinski, W. Rudzinski, A. Plazinska, Theoretical models of sorption kinetics including a surface reaction mechanism: a review, *Adv. Colloid Interface Sci.* 152 (2009) 2–13.
<https://doi.org/10.1016/j.cis.2009.07.009>.
- [32] Y.-S. Ho, Review of second-order models for adsorption systems, *J. Hazard. Mater.* 136 (2006) 681–689.
<https://doi.org/https://doi.org/10.1016/j.jhazmat.2005.12.043>.
- [33] D. Balarak, F. Mostafapour, A. Khatibi, Nonlinear isotherms and kinetics and application error functions for adsorption of tetracycline on Lemma Minor, *J. Pharm. Res. Int.* 23 (2018) 1–11.
<https://doi.org/10.9734/jpri/2018/42583>.
- [34] N.S. Randhawa, D. Dwivedi, S. Prajapati, R.K. Jana, Application of manganese nodules leaching residue for adsorption of nickel(II) ions from aqueous solution, *Int. J. Environ. Sci. Technol.* 12 (2015) 857–864.
<https://doi.org/10.1007/s13762-013-0460-4>.
- [35] W.-H. Kim, H.-K. Chung, J. Park, P.-K. Park, J. Cho, T.-Y. Jeong, Application of Langmuir and Freundlich isotherms to predict adsorbate removal efficiency or required amount of adsorbent, *J. Ind. Eng. Chem.* 28 (2015) 241–246.
<https://doi.org/10.1016/j.jiec.2015.02.021>.
- [36] V. Fierro, V. Torné-Fernández, D. Montané, A. Celzard, Adsorption of phenol onto activated carbons having different textural and surface properties, *Microporous Mesoporous Mater.* 111 (2008) 276–284.
<https://doi.org/10.1016/j.micromeso.2007.08.002>.

- [37] M. Thakkar, V. Randhawa, S. Mitra, L. Wei, Synthesis of diatom- FeO_x composite for removing trace arsenic to meet drinking water standards, *J. Colloid Interface Sci.* 457 (2015) 169–173.
<https://doi.org/10.1016/j.jcis.2015.07.003>.
- [38] A. Iriel, M.G. Lagorio, A. Fernández Cirelli, Biosorption of arsenic from groundwater using *Vallisneria gigantea* plants. Kinetics, equilibrium and photophysical considerations, *Chemosphere*. 138 (2015) 383–389.
<https://doi.org/10.1016/j.chemosphere.2015.06.053>.
- [39] J. Liu, X. Wang, Novel silica-based hybrid adsorbents: Lead(II) adsorption isotherms, *Sci. World J.* 2013 (2013) 897159.
<https://doi.org/10.1155/2013/897159>.
- [40] R. Zhang, T. Leiviskä, Surface modification of pine bark with quaternary ammonium groups and its use for vanadium removal, *Chem. Eng. J.* 385 (2020) 123967.
<https://doi.org/10.1016/j.cej.2019.123967>.
- [41] M. Pan, X. Lin, J. Xie, X. Huang, Kinetic, equilibrium and thermodynamic studies for phosphate adsorption on aluminum hydroxide modified palygorskite nano-composites, *RSC Adv.* 7 (2017) 4492–4500.
<https://doi.org/10.1039/C6RA26802A>.
- [42] M.U. Khan, R.A. Rather, Z.N. Siddiqui, Design, characterization and catalytic evaluation of halometallic ionic liquid incorporated Nd_2O_3 nanoparticles ($[\text{smim}][\text{FeCl}_4]^- @ \text{Nd}_2\text{O}_3$) for the synthesis of: N-aryl indeno pyrrole derivatives, *RSC Adv.* 10 (2020) 44892–44902.
<https://doi.org/10.1039/d0ra08812a>.
- [43] S. Ahmadi, L. Mohammadi, A. Rahdar, S. Rahdar, R. Dehghani, C.A. Igwegbe, G.Z. Kyzas, Acid dye removal from aqueous solution by using neodymium(III) oxide nanoadsorbents, *Nanomaterials*. 10 (2020) 1–26.
<https://doi.org/10.3390/nano10030556>.
- [44] W. Zhang, X. Niu, L. Chen, F. Yuan, Y. Zhu, Soot combustion over nanostructured ceria with different morphologies, *Sci. Rep.* 6 (2016) 1–10.
<https://doi.org/10.1038/srep29062>.
- [45] N. Xu, A.W. Rate, B. Morgan, M. Saunders, Micro- and nanoscale identification of rare earth element-mineral associations in an acidified dredge spoil and adjacent reduced sediments, *ACS Earth Sp. Chem.* 3 (2019) 51–61.
<https://doi.org/10.1021/acsearthspacechem.8b00134>.
- [46] M.N. Pervez, D. Fu, X. Wang, Q. Bao, T. Yu, V. Naddeo, H. Tian, C. Cao, Y. Zhao, A bifunctional $\alpha\text{-FeOOH}@GCA$ nanocomposite for enhanced adsorption of arsenic and photo Fenton-like catalytic conversion of As(III), *Environ. Technol. Innov.* 22 (2021) 101437.
<https://doi.org/10.1016/j.eti.2021.101437>.
- [47] K. Komnitsas, D. Zaharaki, G. Bartzas, G. Alevizos, Adsorption of scandium and neodymium on biochar derived after low-temperature pyrolysis of sawdust, *Minerals*. 7 (2017) 1–18.
<https://doi.org/10.3390/min7100200>.
- [48] N. Ben Issa, V.N. Rajaković-Ognjanović, A.D. Marinković, L. V. Rajaković, Separation and determination of arsenic species in water by selective exchange and hybrid resins, *Anal. Chim. Acta*. 706 (2011) 191–198.
<https://doi.org/10.1016/j.aca.2011.08.015>.

- [49] P.K. Dutta, A.K. Ray, V.K. Sharma, F.J. Millero, Adsorption of arsenate and arsenite on titanium dioxide suspensions, *J. Colloid Interface Sci.* 278 (2004) 270–275.
<https://doi.org/10.1016/j.jcis.2004.06.015>.
- [50] F.M. Jais, S. Ibrahim, Y. Yoon, M. Jang, Enhanced arsenate removal by lanthanum and nano-magnetite composite incorporated palm shell waste-based activated carbon, *Sep. Purif. Technol.* 169 (2016) 93–102.
<https://doi.org/10.1016/j.seppur.2016.05.034>.
- [51] M. Jang, J.K. Park, E.W. Shin, Lanthanum functionalized highly ordered mesoporous media: Implications of arsenate removal, *Microporous Mesoporous Mater.* 75 (2004) 159–168.
<https://doi.org/10.1016/j.micromeso.2004.05.018>.
- [52] H. Viltres, O.F. Odio, L. Lartundo-Rojas, E. Reguera, Degradation study of arsenic oxides under XPS measurements, *Appl. Surf. Sci.* 511 (2020) 145606.
<https://doi.org/10.1016/j.apsusc.2020.145606>.
- [53] Z. Li, J. Qu, H. Li, T.C. Lim, C. Liu, Effect of cerium valence on As(V) adsorption by cerium-doped titanium dioxide adsorbents, *Chem. Eng. J.* 175 (2011) 207–212.
<https://doi.org/10.1016/j.cej.2011.09.096>.
- [54] D. Nabi, I. Aslam, I.A. Qazi, Evaluation of the adsorption potential of titanium dioxide nanoparticles for arsenic removal, *J. Environ. Sci.* 21 (2009) 402–408.
[https://doi.org/10.1016/S1001-0742\(08\)62283-4](https://doi.org/10.1016/S1001-0742(08)62283-4).
- [55] X. Guo, J. Wang, A general kinetic model for adsorption: Theoretical analysis and modeling, *J. Mol. Liq.* 288 (2019) 111100.
<https://doi.org/10.1016/j.molliq.2019.111100>.
- [56] M. Sharma, J. Singh, S. Hazra, S. Basu, Adsorption of heavy metal ions by mesoporous ZnO and TiO₂@ZnO monoliths: Adsorption and kinetic studies, 145 (2019) 105–112.
<https://doi.org/10.1016/j.microc.2018.10.026>.
- [57] M.T. Amin, A.A. Alazba, M. Shafiq, Adsorptive removal of reactive black 5 from wastewater using bentonite clay: isotherms, kinetics and thermodynamics, *Sustain.* 7 (2015) 15302–15318.
<https://doi.org/10.3390/su71115302>.
- [58] N. Ayawei, A.N. Ebelegi, D. Wankasi, Modelling and interpretation of adsorption isotherms, *J. Chem.* 2017 (2017) 3039817.
<https://doi.org/10.1155/2017/3039817>.
- [59] U.A. Edet, A.O. Ifelebuegu, Wastewater using recycled brick waste, *Processes.* 8 (2020) 665.
<https://doi.org/10.3390/pr8060665>
- [60] A.Z.M. Badruddoza, Z.B.Z. Shawon, M.T. Rahman, K.W. Hao, K. Hidajat, M.S. Uddin, Ionically modified magnetic nanomaterials for arsenic and chromium removal from water, *Chem. Eng. J.* 225 (2013) 607–615.
<https://doi.org/10.1016/j.cej.2013.03.114>.
- [61] S. Zhang, H. Niu, Y. Cai, X. Zhao, Y. Shi, Arsenite and arsenate adsorption on coprecipitated bimetal oxide magnetic nanomaterials: MnFe₂O₄ and CoFe₂O₄, *Chem. Eng. J.* 158 (2010) 599–607.
<https://doi.org/10.1016/j.cej.2010.02.013>.
- [62] S. Lin, D. Lu, Z. Liu, with magnetic γ-Fe₂O₃ nanoparticles, *Chem. Eng. J.* 211–212 (2012) 46–52.
<https://doi.org/10.1016/j.cej.2012.09.018>.

Streszczenie w języku polskim

W wielu krajach na całym świecie w naturalnych wodach występuje zwiększyony poziom zanieczyszczeń zawierających związki arsenu. Wśród głównych przyczyn tego zjawiska należy wymienić spalanie paliw kopalnych, stosowanie pestycydów i herbicydów, wietrzenie skał, reakcje geochemiczne, czy aktywność wulkaniczną. Spożywanie wody pitnej zawierającej znaczne ilości arsenu prowadzi do negatywnych skutków zdrowotnych m.in. nowotworów płuc, chorób skóry i układu krążenia. W następstwie tego, Światowa Organizacja Zdrowia WHO ustaliła poziom $10 \mu\text{g}/\text{dm}^3$ jako dopuszczalne stężenie arsenu w wodzie pitnej.

W przedstawionej rozprawie doktorskiej zaprezentowano metodę modyfikacji wymieniaczy jonowych na bazie tlenków żelaza jonami lantanu(III), neodymu(III) i ceru(III) oraz udowodniono ich przewagę w stosunku do niemodyfikowanych materiałów w kontekście usuwania jonów arsenianowych(V). Stwierdzono, że po sorpcji jonów lantanowców(III) powierzchnie jonitów stają się bardziej niejednorodne, co było efektem tworzenia obiektów o różnych kształtach m.in. płatkowatym, bąbelkowym, płytowym czy ziarnistym. Taka morfologia przyczyniła się do ułatwienia adsorpcji jonów arsenianowych(V), w wyniku której nastąpiło ponowne zmniejszenie heterogeniczności powierzchni. Skuteczna modyfikacja jonami REE oraz adsorpcja jonów As(V) została potwierdzona za pomocą badań metodami rentgenowskiej spektroskopii fotoelektronów XPS oraz spektroskopii w podczerwieni z transformatą Fouriera FTIR. Wykazano, że przy optymalnym pH 6 głównymi mechanizmami sorpcji jonów wodoroarsenianowych(V) i diwodoroarsenianowych(V) są przyciągające oddziaływanie elektrostatyczne i tworzenie powierzchniowych kompleksów mono- i bidentnych. W każdym przypadku proces modyfikacji jonitów spowodował znaczący wzrost maksymalnych pojemności sorpcyjnych oraz efektywności usuwania arsenianów(V). Czas potrzebny do osiągnięcia równowagi nie wydłużył się, a modyfikowane wymieniacze jonowe były w stanie całkowicie usunąć jony As(V) z roztworów o stężeniu nawet $50 \text{ mg}/\text{dm}^3$. Wykorzystanie niemodyfikowanych materiałów nie mogło tego zagwarantować przy dwukrotnie niższym stężeniu As(V). Ustalono, że proces adsorpcji jonów arsenianowych(V) jest spontaniczną i egzotermiczną chemisorpcją. W związku z tym, nie ma potrzeby prowadzenia procesu w podwyższonej temperaturze. Ponadto, proces adsorpcji jonów arsenianowych(V) na modyfikowanych jonitach jest odwracalny. Zużyty wymieniacz jonowy wystarczy regenerować za pomocą

1 M NaOH. Po trzech cyklach sorpcji/desorpcji wymieniacze jonowe zawierające REE wciąż wykazują większą pojemność sorpcyjną niż materiały niemodyfikowane przed pierwszym użyciem.

Materiały na bazie tlenków żelaza modyfikowane jonami lantanowców(III) są bardzo interesującą propozycją w kontekście usuwania arsenu z zanieczyszczonych zbiorników wodnych. Proces modyfikacji z wykorzystaniem REE stwarza nowe perspektywy poprawy właściwości jonitów zawierających tlenki żelaza, w tym spełnienia restrykcyjnego limitu WHO dotyczącego zawartości arsenu w wodzie pitnej. Wprowadzenie stosunkowo niewielkiej ilości jonów REE zdecydowanie poprawia skuteczność oczyszczania wody ze związków arsenu(V).

Streszczenie w języku angielskim

In many countries around the world, natural waters contain increased amounts of contaminants including arsenic compounds. The main causes of this phenomenon comprise burning of fossil fuels, use of pesticides and herbicides, weathering of rocks, geochemical reactions or volcanic activity. Consuming water that contains significant amounts of arsenic leads to negative health effects such as lung cancer, skin and cardiovascular diseases. Consequently, the World Health Organization, WHO, established a level of $10 \mu\text{g}/\text{dm}^3$ as the permissible concentration of arsenic in drinking water.

In the presented doctoral thesis, the method of modifying ion exchangers based on iron oxides with lanthanum(III), neodymium(III) and cerium(III) ions was applied, and their advantage over the unmodified materials in terms of removing arsenate(V) ions was proved. It was found that after sorption of lanthanide(III) ions, the ion exchanger surfaces become more heterogeneous as a result of forming objects of various shapes, e.g. flaky, bubble-like, lamellar or grainy. This morphology facilitates the adsorption of arsenate(V) ions, leading to a further reduction in the surface heterogeneity. The effective modification with REE ions and adsorption of As(V) ions were confirmed by photoelectron spectroscopy (XPS) and Fourier transform infrared spectroscopy (FTIR). It has been shown that at the optimum pH of 6, the main mechanisms of sorption of hydrogen arsenate(V) and dihydrogen arsenate(V) ions are attractive electrostatic interactions as well as mono- and bidentate surface complexes are formed. In each case, the ion exchange modification process increases the maximum sorption capacity and the arsenate(V) removal efficiency significantly. The time needed to achieve equilibrium did not lengthen, and the modified ion exchangers were able to remove As(V) ions completely from the solutions with a concentration of even up to $50 \text{ mg}/\text{dm}^3$. The use of the unmodified materials could not guarantee the above at the twice lower concentration of As(V). It was established that the arsenate(V) ions adsorption process is spontaneous and exothermic chemisorption. Therefore, there is no need to run the process at the elevated temperature. Moreover, the process of arsenate(V) ions adsorption on the modified ion exchangers is reversible. 1 M NaOH is sufficient for the spent ion exchanger regeneration. After three sorption/desorption cycles, the REE-containing ion exchangers are still characterized by a higher sorption capacity than the unmodified materials before their first use.

The iron oxides based materials modified with lanthanide(III) ions are a very interesting proposal in terms of removing arsenic from the contaminated water reservoirs. The modification process with the use of REEs provides new prospects for improving the properties of ion exchangers containing iron oxides, including observing the restrictive WHO requirements concerning the arsenic content in drinking water. The addition of a relatively small amount of REE ions improves the effectiveness of water purification from arsenic(V) compounds significantly.

Życiorys naukowy

W 2013 r. ukończył I Liceum Ogólnokształcące im. Stanisława Staszica w Lublinie. W tym samym roku rozpoczęłem studia I stopnia na kierunku Chemia specjalność Chemia podstawowa i stosowana na Wydziale Chemii Uniwersytetu Marii Curie-Skłodowskiej w Lublinie. W lipcu 2016 r. z wynikiem bardzo dobrym obroniłem pracę licencjacką pt. „Usuwanie arsenu na sorbentach różnego typu” napisaną pod kierunkiem prof. dr. hab. Zbigniewa Hubickiego. W październiku 2016 r. rozpoczęłem studia II stopnia na Wydziale Chemii Uniwersytetu Marii Curie-Skłodowskiej w Lublinie na kierunku Chemia specjalność Chemia analityczna. W lipcu 2018 r. uzyskałem tytuł magistra chemii na podstawie pracy pt. „Usuwanie jonów As na jonitach i sorbentach różnego typu” uzyskując wynik bardzo dobry (promotor prof. dr hab. Zbigniew Hubicki). W tym samym roku ukończył studia podyplomowe dotyczące przygotowania do nauczania chemii w szkole (Uniwersytet Marii Curie-Skłodowskiej, Wydział Chemii). W latach akademickich 2014/2015, 2015/2016 i 2016/2017 otrzymywałem stypendium Rektora dla najlepszych studentów Uniwersytetu Marii Curie-Skłodowskiej. W trakcie studiów I stopnia otrzymywałem również stypendium motywacyjne w ramach projektu „Od studenta do eksperta – ochrona środowiska w praktyce”.

W październiku 2018 r. rozpoczęłem Międzynarodowe Studia Doktoranckie z Chemii na Wydziale Chemii UMCS. Badania do rozprawy doktorskiej pt. „Usuwanie jonów arsenianowych(V) na wymieniaczach jonowych na bazie tlenków żelaza modyfikowanych jonami wybranych lantanowców” realizowałem w Katedrze Chemii Nieorganicznej pod kierunkiem prof. dr hab. Doroty Kołodyńskiej. Mój dorobek naukowy to 4 publikacje w czasopismach z listy JCR, 2 rozdziały w monografii oraz 8 komunikatów na konferencjach międzynarodowych i 4 na konferencjach krajowych. Jeden z komunikatów został wyróżniony nagrodą za najlepszy poster w sekcji „Chemia analityczna, chemia środowiskowa, technologia chemiczna” na XVII Scientific Conference „Lviv Chemical Readings – 2019” (Lwów, 2-5 czerwca 2019 r.). Ponadto, odbyłem półroczny staż naukowy na Wydziale Chemii Lwowskiego Narodowego Uniwersytetu Iwana Franki (Ukraina, czerwiec – grudzień 2021). Uczestniczyłem również w realizacji projektu „Nowe związki kompleksowe lantanowców dla technologii światłowodów do laserów włóknowych i wzmacniaczy optycznych” - akronim projektu REEPHOT, Nr POIR.04.01.01-00-0040/17-00 (marzec – październik 2019). W trakcie studiów doktoranckich ukończył szkołę letnią „2nd PhD Summer School and

Executive Training on Solid Waste Management (Heraklion, Grecja, czerwiec 2019). W latach akademickich 2018/2019 i 2019/2020 otrzymywałem zwiększone stypendium doktoranckie z dotacji projakościowej.

Od października 2019 r. jestem zatrudniony na stanowisku wykładowcy na Wydziale Chemii Uniwersytetu Marii Curie-Skłodowskiej w Lublinie, gdzie m.in. pełnię funkcję opiekuna praktyk studenckich w ramach modułu nauczycielskiego. Dodatkowo jestem nauczycielem chemii w Liceum Ogólnokształcącym im. Kazimierza Wielkiego w Lublinie. W październiku 2021 r. podjąłem studia podyplomowe w zakresie zarządzania oświatą w Akademii Nauk Stosowanych Wincentego Pola w Lublinie.

Dorobek naukowy

a) Publikacje

- **S. Dudek**, D. Kołodyńska, Enhanced arsenic(V) removal on an iron-based sorbent modified by lanthanum(III), *Materials* 13 (2020) 2553.
- **S. Dudek**, D. Kołodyńska, Arsenic(V) removal on the lanthanum-modified ion exchanger with quaternary ammonium groups based on iron oxide, *J. Mol. Liq.*, 347 (2021) 117985.
- **S. Dudek**, D. Kołodyńska, Arsenate removal on the iron oxide ion exchanger modified with neodymium(III) ions, *J. Environ. Manage.*, 307 (2022) 114551.
- **S. Dudek**, D. Kołodyńska, Arsenate removal on the ion exchanger modified with cerium(III) ions, *Physicochem. Probl. Miner. Process.* 58 (2022) 147412.

b) Rozdziały w monografiach

- **S. Dudek**, Właściwości fotokatalityczne i adsorpcyjne tlenku tytanu(IV) względem jonów arsenu, w: Etyka Biznesu i Zrównoważony Rozwój. Interdyscyplinarne studia teoretyczno-empiryczne (red. H. Kretek), Zabrze 2018, ISSN 2451-456X, str. 11-24.
- **S. Dudek**, Czy adsorbenty zawierające lantanowce mogą okazać się pomocne w procesie usuwania arsenu?, w: Implementacja idei europejskiego zielonego ładu na bazie społecznej gospodarki rynkowej determinantą zarządzania w realizacji założeń zrównoważonego rozwoju (red. H. Kretek), Racibórz 2020, ISBN 978-83-951494-7-4, str. 199-210.

c) Projekty badawcze

- Udział w realizacji projektu „Nowe związki kompleksowe lantanowców dla technologii światłowodów do laserów włóknowych i wzmacniaczy optycznych” - akronim projektu REEPHOT, Nr POIR.04.01.01-00-0040/17-00 (marzec – październik 2019)

d) Staże zagraniczne

- Lwowski Narodowy Uniwersytet Iwana Franki (Ukraina, czerwiec – grudzień 2021)

e) Szkoły letnie

- 2nd PhD Summer School and Executive Training on Solid Waste Management (Heraklion, Grecja, czerwiec 2019)

f) Konferencje

- **S. Dudek**, D. Kołodyńska, Usuwanie jonów arsenu z roztworów wodnych na sorbencie zawierającym tlenek żelaza z zaadsorbowanymi wcześniej jonami wybranych lantanowców, Ogólnopolska konferencja naukowa *Innowacje w praktyce*, 4-5 kwietnia 2019, Lublin (poster)
- **S. Dudek**, D. Kołodyńska, As500 jako adsorbent na bazie tlenku tytanu(IV) umożliwiający usuwanie arsenu i adsorpcję lantanowców, Ogólnopolska konferencja naukowa *Innowacje w praktyce*, 4-5 kwietnia 2019, Lublin (poster)
- **S. Dudek**, D. Kołodyńska, Właściwości fotokatalityczne i adsorpcyjne tlenku tytanu(IV) względem jonów arsenu, Międzynarodowa Konferencja Naukowa *Zrównoważony rozwój – sustainable development– Debiut Naukowy 2018*, Zabrze, 10 maja 2019 (wystąpienie ustne)
- **S. Dudek**, D. Kołodyńska, Właściwości adsorpcyjne tlenku tytanu(IV) względem jonów arsenu i wybranych lantanowców na przykładzie handlowo dostępnego sorbentu, Ogólnopolska Konferencja Naukowa *Ochrona środowiska – rozwiązań i perspektywy*, 17 maja 2019, Lublin (wystąpienie ustne)
- **S. Dudek**, D. Kołodyńska, Badanie zdolności sorpcyjnych sorbentu Ferrix A33E względem jonów As(V) i lantanowców(III), Ogólnopolska Konferencja Naukowa *Ochrona środowiska – rozwiązań i perspektywy*, 17 maja 2019, Lublin (poster)
- **S. Dudek**, D. Kołodyńska, Adsorption of arsenic and lanthanides on sorbent containing titanium dioxide, *XVII Scientific Conference Lviv Chemical Readings-2019*, Lwów (Ukraina), 2-5 czerwca 2019 (wystąpienie ustne)
- **S. Dudek**, D. Kołodyńska, Arsen X^{np} modified with lanthanide ions in the context of arsenic ions removal, *XVII Scientific Conference Lviv Chemical Readings-2019*, Lwów (Ukraina), 2-5 czerwca 2019 (poster)
- **S. Dudek**, D. Kołodyńska, Removal of arsenic on sorbents containing iron oxide and titanium oxide modified with lanthanide ions, *7th International Conference on Sustainable Solid Waste Management*, Heraklion (Grecja), 26-29 czerwca 2019 (wystąpienie ustne)

- **S. Dudek**, D. Kołodyńska, Can adsorbents containing lanthanides be helpful in the arsenic removal?, Międzynarodowa konferencja naukowa *Zrównoważony rozwój – Debiut naukowy 2019*, Wydział Organizacji i Zarządzania Politechniki Śląskiej w Zabrzu, 16 września 2020 (wystąpienie ustne)
- **S. Dudek**, D. Kołodyńska, Adsorption of As(V) ions on La(III)-modified sorbent containing iron oxide, *XVIII Scientific Conference Lviv Chemical Readings – 2021*, Lwów (Ukraina), 31 maja - 2 czerwca 2021 (wystąpienie ustne)
- **S. Dudek**, D. Kołodyńska, Enhanced arsenic(V) removal by commercially available ion exchanger modified with lanthanum(III) ions, *XVIII Scientific Conference Lviv Chemical Readings – 2021*, Lwów (Ukraina), 31 maja – 2 czerwca 2021 (poster)
- **S. Dudek**, D. Kołodyńska, The iron oxide sorbent modified with lanthanum(III) ions in the context of arsenic removal, *8th International Conference on Sustainable Solid Waste Management*, Saloniki (Grecja), 23-26 czerwca 2021 (wystąpienie ustne)

Teksty publikacji z oświadczeniami współautorów

D1

S. Dudek, D. Kołodyńska

Enhanced arsenic(V) removal on an iron-based sorbent modified by lanthanum(III), Materials, 13 (2020) 2553

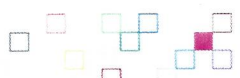
IF: 3,623 Punkty MEiN: 140

Oświadczenie

Oświadczam, że mój udział w pracy:

S. Dudek, D. Kołodyńska, Enhanced arsenic(V) removal on an iron-based sorbent modified by lanthanum(III), Materials 13 (2020) 2553

polegał na współtworzeniu jej ogólnej koncepcji, wykonaniu wszystkich eksperymentów, opracowaniu wyników, współudziale w stworzeniu oryginalnego manuskryptu, pełnieniu roli autora korespondencyjnego, współudziale w przygotowywaniu odpowiedzi do recenzentów. Udział ten szacuję na 50%.



OŚWIADCZENIE

Oświadczam, że w pracy:

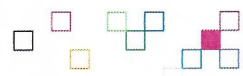
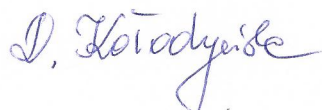
Sebastian Dudek, Dorota Kołodyńska, Enhanced arsenic(V) removal on iron based sorbent modified by lanthanum(III), Materials 13 (2020) 2553, IF₂₀₂₀ 3,057, pkt MNiE₂₀₂₀ 140

mój wkład merytoryczny w przygotowanie, przeprowadzenie i opracowanie badań oraz przedstawienie pracy w formie publikacji to:

opracowanie koncepcji i założeń, analiza i dyskusja uzyskanych wyników, opracowanie manuskryptu – krytyczna analiza pod kątem istotnej zawartości i poprawności merytorycznej, współdziałał w redagowaniu odpowiedzi na uwagi recenzentów.

Swój wkład szacuję na 50%.

Jednocześnie wyrażam zgodę na przedłożenie wyżej wymienionej pracy przez Pana mgr Sebastiana Dudka jako część rozprawy doktorskiej w formie spójnego tematycznie cyklu prac opublikowanych w czasopismach naukowych.



Article

Enhanced Arsenic(V) Removal on an Iron-Based Sorbent Modified by Lanthanum(III)

Sebastian Dudek *  and Dorota Kołodyńska 

Department of Inorganic Chemistry, Institute of Chemical Sciences, Faculty of Chemistry, Maria Curie-Skłodowska University, pl. Marii Curie-Skłodowskiej 2, 20-031 Lublin, Poland; d.kolodynska@poczta.umcs.lublin.pl

* Correspondence: sebastian.dudek@poczta.umcs.lublin.pl; Tel.: +48-81-5375770

Received: 24 April 2020; Accepted: 29 May 2020; Published: 3 June 2020



Abstract: Modification of a commercial iron oxide ion exchanger (Arsen X^{NP}) was carried out to enhance the removal of arsenic(V) ions. The modification consisted of the adsorption of lanthanum(III) ions on the Arsen X^{NP} surface. After adsorption, the material was dried at 313 K to obtain the modified ion exchanger Arsen X^{NP}-La(III). The modification process itself was tested for optimal pH, kinetics, and equilibrium adsorption isotherm study. Accurate sorbent characteristics were made using, among others, SEM, FTIR, and nitrogen adsorption/desorption isotherms. Then, various tests were carried out to compare the adsorption properties of the modified and unmodified material. It turned out that the tested material was able to completely remove arsenic from an aqueous solution with an initial concentration of up to 50 mg/dm³. Without modification, it was not possible to reach the WHO recommended 10 µg/dm³ arsenic limit even at an initial concentration of 25 mg/dm³. Moreover, the maximum sorption capacity increased from 22.37 to 61.97 mg/g after modification (3 times greater than before modification). It is worth noting that the process of removing arsenic on Arsen X^{NP}-La(III) is fast—equilibrium is reached after about 120 min. Under almost neutral conditions, precipitation and adsorption can be the main mechanisms of As(V) removal. After modification, the removal capacity was enhanced by the co-precipitation and adsorption by exchange of the OH⁻ group with arsenic ions. Such La(III) based adsorbent can be successfully applied in wastewater purification and displays superior performance for removing arsenic.

Keywords: arsenic removal; lanthanum; iron oxides; adsorption; Arsen X^{NP}

1. Introduction

Arsenic is an element known for its toxicity. It is found in South and North America, Europe, Australia and Africa, but the largest problem occurs in the areas of southern and south-east Asia where the maximum permissible level of arsenic is largely exceeded [1,2]. Arsenic penetrates into water systems as a result of natural weathering processes, volcanic emissions, geochemical reactions or anthropogenic activities, e.g., fossil fuel combustion, the use of arsenic pesticides and herbicides, and mining activities [3,4].

According to the World Health Organization (WHO) guidelines, the admissible content of arsenic in drinking water is 10 µg/dm³. Therefore, more than 100 million people around the world are at risk of its exposure. However, 45 million people from developing Asian countries are still exposed to arsenic concentration greater than 50 µg/dm³. Long-term consumption of arsenic contaminated water can lead to neurological disorders, skin pigment changes, vomiting and also kidney, lung or bladder cancer [5]. Therefore high-efficiency and cost-effective technologies have been needed to treat and remove arsenic from drinking water.

In numerous available studies, adsorption has been chosen as the most appropriate method for solving the problem of water systems contaminated by arsenic(V). Adsorbents which combine the best advantages, i.e., low cost, great strength, and the ability to be used in changing environmental conditions, are desirable. Many authors decide to exploit ion exchangers based on iron oxides [6–8]. However, these adsorbents often have low adsorption capacity towards arsenic ions. Consequently, a lot of authors try to modify them in order to obtain greater adsorption. Moreover, to enhance sorption capacity and selectivity, immobilization of ligands with multi-coordinating active sites, ligands which are biomimetically relevant, complexes with low molecular weight and immobilizing of ethers, calixarenes, impregnation of metal ions, and preparation of reactive ion exchangers are proposed. In the paper by Jiang et al. [9], adsorption of arsenic(V) onto polystyrene-iron oxide PS- Fe_3O_4 sorbent was tested depending on the pH of the solution, arsenic concentration, and phase contact time. Additionally, the effect of accompanying anions on the efficiency of the process was checked. PS- Fe_3O_4 was able to reach equilibrium faster and exhibited higher sorption capacity for arsenates(V) than the unmodified Fe_3O_4 (139.3 mg/g—77.7% higher than pure Fe_3O_4). Chloride and nitrate(V) anions, unlike PO_4^{3-} and SiO_3^{2-} ions, did not have a major impact on the sorption process. The discussed hybrid material was effectively separated from the water in the presence of a weak magnetic field (<0.035 T). In addition, it could be reused after regenerating the sorbent with NaOH solution.

This type of adsorbent containing inbuilt iron nanooxide molecules of the goethite structure—Purolite Arsen X^{NP}—is produced on a commercial scale. In the production process, iron oxide was distributed in the pores of the above-mentioned ion exchanger as a layer of a few nanometers thickness. However, in order to increase the surface effectiveness of such adsorbents, other modification methods can be applied. One of them could be modification of the R-N(CH₃)₃(OH)/FeO(OH) structure by trivalent or tetravalent ions. In the study by He et al. [10], an iron-cerium bimetal oxide adsorbent was applied for As(V) removal sorption capacity (149.84 mg/g) more successfully than many reported adsorbents. The bimetal oxide adsorbents were prepared by a co-precipitation method. Based on the XPS results, it was proved that the obtained sorbent was composed of hydroxyl (30.8%) and CeO₂ and Fe₃O₄ (12.6% and 19.6%). Therefore, both the integral area of the As-O band and the As(V) adsorption capacity increased almost linearly with the decrease in the integral area of M-OH bands, proving that the adsorption of As(V) is mainly realized through the mechanism of quantitative ligand exchange. Analogous results were obtained using Fourier transform infrared spectra where it was revealed that in As(V) adsorption M-OH groups play an important role.

In this study, attempts have been made to enhance the removal of arsenate ions onto Arsen X^{NP} modified by La(III) in order to reduce their amount in the environment. The sorbent was prepared by adsorption of lanthanum(III) ions under specific conditions and then for arsenic(V) removal. Lanthanum is one of the cheapest rare-earth elements. Comparison of the sorption properties of the raw Arsen X^{NP} and the modified sorbent Arsen X^{NP}-La(III) was made. There are studies in which various sorbents have been modified with lanthanum. Jang et al. [11] synthesized the highly ordered mesoporous silica, SBA-15, and incorporated various amounts of lanthanum oxide into it. Then, they applied the material for arsenate removal in the adsorption process. Tan et al. [12] fabricated a novel adsorbent CSN-La of lanthanum immobilized on electrospun chitosan nanofiber (CSN). The saturated adsorption capacity of CSN-La reached up to 83.6 mg As(V)/g, which was significantly higher than that of CSN. The exhausted CSN-La could be repeatedly used after being eluted by sodium hydroxide solution. In the paper by Lingamdinne et al. [13], the surface of graphene oxide was functionalized with lanthanum to produce porous flowered graphene oxide-lanthanumfluoride (GO-LaF) nanocomposite. The adsorption results obtained under different conditions suggest that As(V) adsorption onto GO-LaF occurs through mixed processes such as electrostatic, ion-exchange, and surface complexation. However, a study, in which a commercially available sorbent based on iron oxide was modified with lanthanum, does not exist. A successful modification can help supply safe arsenic-free drinking water. Moreover, the multiple use of the same material can reduce significantly the costs of the groundwater treatment process.

2. Materials and Methods

2.1. Modification of the Adsorbent

In order to increase As(V) sorption capacity, the modification of the sorbent consisted in adsorption of lanthanum(III) ions from aqueous solution ($t = 6$ h, $c_0 = 100$ mg/dm 3) and then drying the sorbent at 313 K. In that way, Arsen X^{nP} modified with La(III) ions was obtained. To learn more about the sorbent modification process, the effects of pH and sorption kinetics of lanthanum were studied. Moreover, Langmuir and Freundlich isotherms were determined for this process. The abbreviation X^{nP} will be used for the pure Arsen X^{nP} sorbent, while X^{nP}-La(III) for Arsen X^{nP} with adsorbed lanthanum(III) ions.

2.2. Materials and Chemicals

Purolite Arsen X^{nP} (Purolite, Philadelphia, PA, USA) is a macroporous, selective resin based on polystyrene crosslinked with divinylbenzene skeleton with sulfonic groups and a unique structure of hydrated iron nanoparticles (designed to remove arsenic(V) and arsenic(III) ions). This ion exchanger is characterized by high durability and selectivity towards Cu(II), Zn(II), Cr(VI), Cd(II), and Pb(II) ions [14,15]. It is available on a commercial scale due to the finding of SenGupta and Cumbal (U.S. Patent US7291578B2 [16]) and used to impregnate strongly basic anion exchange resins with iron hydroxide nanoparticles. Next, the technology was further modified and commercialized by SolmeteX, Layne Christensen Company (The Woodlands, TX, USA), and Purolite International Ltd. Its physicochemical properties are collected in Table 1.

Table 1. Properties of Purolite Arsen X^{nP}.

Polymer Structure	Divinylbenzene Crosslinked with Polystyrene
Matrix structure	Macroporous
Physical form and appearance	Reddish-brown spherical particles
Particle size range	0.300–1.200 mm
Maximum working temperature	80 °C
Working pH range	4–9

The point of zero charge (pH_{pzc}) before and after the lanthanum(III) sorption of the sorbents was determined using the drift method [17]. The determination of pH_{pzc} was conducted by adjusting the pH of 20 mL 0.01 M NaCl solution to a value between 2 and 11 (pH_i). 0.1 g of the sorbent was added and the final pH (pH_f) was measured after 6 h under agitation. The pH_{pzc} is the point where pH_i–pH_f = 0. The initial and final pHs were measured using the Radiometer PHM 84 pH meter (Copenhagen, Denmark) with the glass REF 451 and calomel pHG 201-8 electrodes.

The morphology of the sorbent before and after the lanthanum(III) sorption was determined using scanning electron microscopy (SEM) (Tescan, Brno, Czech Republic) with an extended depth of field (EDF) function.

Using an ASAP 2405 analyzer (Micromeritics, Norcross, GA, USA), porous structure parameters of the sorbents were evaluated. These tests were aimed at determining nitrogen adsorption-desorption isotherms of the analyzed materials. The specific surface area was determined by the Brunauer-Emmett-Teller method as well as the total volume and pore size distribution according to the Barret-Joyner-Halenda model.

Infrared spectroscopy analysis with Fourier transformation was used to record the spectra of the analyzed adsorbents. X^{nP} and X^{nP}-La(III) before and after the As(V) sorption were tested by the attenuated total reflection method using the Agilent Cary 630 FTIR spectrometer. Thanks to this, it was possible to define the characteristic functional groups located on the surface of the material used. In the FTIR analyses, infrared radiation covered the wavenumber range of 4000–650 cm $^{-1}$.

The solutions in the model wastewater were prepared for experiments by dissolving La(NO₃)₃·6H₂O and Na₂HAsO₄·7H₂O in water. The specific pH of the solutions was achieved

by adding appropriate amounts of 1 M hydrochloric acid and 1 M sodium hydroxide. All chemicals applied were used at analytical purity and purchased from POCh (Gliwice, Poland).

2.3. Batch Experiments

2.3.1. Sorbent Modification

To examine lanthanum(III) adsorption depending on pH values, solutions containing 10 mg/dm³ of lanthanum(III) at pH in the range from 2 to 6 were prepared. 0.1 g of X^{NP} and 20 cm³ of lanthanum(III) solution at different pH values were added separately to 100 cm³ conical flasks. After that, the samples were shaken for 24 h ($c = 10 \text{ mg/dm}^3$, pH = 2–6, shaking speed 180 rpm, temperature 295 K). The ELPIN+ type 358A shaker (Lubawa, Poland) was used. After shaking, the solutions were separated from the sorbent by filtration on filter paper. After the experiment, the lanthanum(III) concentrations of the analyzed ions were determined using inductively coupled plasma optical emission spectrometry (ICP-OES) (720 ES, Varian, Palo Alto, CA, USA). The wavelength used for the analysis of La(III) was 333.749 nm. The ICP-OES instrument was calibrated using the appropriate standards. To prepare all standards and blank samples, ultrapure nitric acid was used in order to avoid any matrix interference.

The sorption kinetics of lanthanum(III) was investigated using the static method. The solutions of lanthanum(III) were prepared at concentrations of 10, 50, and 100 mg/dm³ (and at the previously determined optimal pH value). 0.1 g of X^{NP} was added to Erlenmeyer flasks. 20 cm³ of the above-mentioned solutions was added to each flask and shaken for 1, 3, 5, 7, 10, 20, 30, 60, 120, 240, and 360 min. After shaking, the samples were filtered on filter paper and the solutions were separated from the sorbent. Then, the concentrations of lanthanum(III) were determined using ICP-OES.

The amount of adsorbed lanthanum(III) ions (q_t) was estimated from the following equation:

$$q_t = (c_0 - c_t) \times \frac{V}{m} \quad (1)$$

where: q_t is the amount of lanthanum(III) adsorbed at time t (mg/g), c_0 is the initial concentration of lanthanum(III) in the solution (mg/dm³), c_t is the concentration of lanthanum(III) in the solution after time t (mg/dm³), V is the volume of the solution containing lanthanum(III) ions (dm³), m is the mass of sorbent (g).

The percentage of adsorption (%S) is that of lanthanum(III) adsorbed on the adsorbent beads calculated from the following equation:

$$\%S = \frac{(c_0 - c_t)}{c_0} \times 100\% \quad (2)$$

The kinetic parameters of metal ions sorption onto the sorbent were determined using the pseudo-first order kinetic equation (PFO) and pseudo-second order equation (PSO) [18–20]:

$$\log(q_e - q_t) = \log(q_e) - \frac{k_1}{2.303} \times t \quad (3)$$

$$\frac{t}{q_t} = \frac{1}{k_2 \times q_e^2} + \frac{t}{q_e} \quad (4)$$

where: q_e is the amount of lanthanum(III) adsorbed at equilibrium (mg/g), q_t is the amount of lanthanum(III) adsorbed at time t (mg/g), k_1 and k_2 are the reaction rate constants of the pseudo-first order (1/min) and pseudo-second order (g/mg min).

The adsorption capacity of X^{NP} towards lanthanum(III) ions was determined by the equilibrium adsorption isotherm study. The initial concentrations of La(III) ions were equal to 10, 50, 100, 150, 300 and 500 mg/dm³ ($t = 6 \text{ h}$, shaking speed 180 rpm, temperature 295 K).

2.3.2. Influence of pH

The solutions of 25 mg/dm³ As(V) ions were prepared to examine arsenic(V) adsorption depending on the pH values. The same parameters were used as when testing the effect of pH on lanthanum(III) sorption, as described in Section 2.3.1. After the experiment, the concentrations of the analyzed ions and the sorption capacities were determined using the spectrophotometric method (Cary 60, Agilent Technologies) at a wavelength 870 nm by obtaining coloured As(V) complex compounds with ammonium molybdate. The UV-Vis instrument was calibrated using the appropriate standards.

2.3.3. Kinetic Studies

The arsenic(V) sorption kinetics was investigated using the static method. The solutions of arsenate(V) at concentrations of 25, 50, and 100 mg/dm³ (pH 6). 0.1 g of X^{NP} were added to Erlenmeyer flasks. 20 cm³ of the above-mentioned solutions was added to each flask and shaken for 1, 3, 5, 7, 10, 20, 30, 60, 120, 240 and 360 min (shaking speed 180 rpm). The experiment was repeated for the X^{NP}-La(III) sorbent and the results on the modified and unmodified X^{NP} were compared. The laboratory water bath shaker Elpin+ type 357 (Elpin Plus, Lubawa, Poland) was used for the experiments. After shaking, the samples were filtered on filter paper and the solutions were separated from the sorbent. Then, the concentrations of arsenic(V) ions were determined using the UV-Vis method (Cary 60, Agilent Technologies, Santa Clara, CA, USA), as described below.

The amount of adsorbed arsenic ions was estimated from Equation (1). The experimental data of As(V) kinetic studies was fitted to the PFO (Equation (3) and the PSO (Equation (4)) models.

2.3.4. Equilibrium Adsorption Isotherm Study

The adsorption capacity of X^{NP} towards arsenic(V) ions was determined by the equilibrium adsorption isotherm study. The same study was carried out for X^{NP}-La(III). The initial concentrations of As(V) ions were equal to 25, 50, 100, 150, 300, 500, 750, and 1000 mg/dm³ (t = 6 h, shaking speed 180 rpm, temperature 295 K). The adsorption data was fitted into both the Langmuir isotherm and the Freundlich isotherm, whose equations are presented below [18–20]:

$$q_e = \frac{q_0 K_L c_e}{1 + K_L c_e} \quad (5)$$

$$q_e = K_F c_e^{1/n} \quad (6)$$

where: q_0 is the maximum monolayer adsorption capacity (mg/g); K_L is the Langmuir constant (dm³/mg); c_e is the adsorbate concentration in the solution at equilibrium (mg/dm³); K_F is the Freundlich isotherm constant (mg/g); n is the Freundlich exponent (degrees of sorption favourability and intensity) (-).

The two parameters (K_L and q_e) can be obtained using the slope and the intercept to characterize the adsorption process. The R_L parameter is determined from the equation:

$$R_L = \frac{1}{1 + K_L c_0} \quad (7)$$

2.3.5. Desorption

Three cycles of sorption and desorption of arsenate(V) ions were carried out on 0.1 g of the modified and unmodified sorbent. Sorption was conducted from a solution with an initial arsenic concentration of 100 mg/dm³, volume 20 cm³, temperature 295 K, pH 6, and shaking time 6 h (180 rpm). The desorption conditions were identical, and the desorbing agent was 1 M NaOH. One sorption and desorption cycle were also carried out for NaOH concentrations 0.05 and 0.2 M. After each sorption and desorption, the sorbent was separated from the solution and dried at a temperature of 313 K. Then, the ion exchanger reusability was evaluated.

3. Results and Discussion

3.1. Sorbent Characterization

The point of zero charge pH_{pzc} of X^{np} is equal to 8.38. After adsorption of lanthanum (III) ions, the pH_{pzc} decreased to 7.21 (Figure 1). The pH_{pzc} value of a given substance depends on the nature of the surface [17,18]. It means that X^{np} and $X^{\text{np}}\text{-La(III)}$ are able to exchange anions at a pH below 8.38 and 7.21, respectively. Analysing the adsorption data at different pH values in connection with the speciation distribution of the As(V) forms dependent on the pH_a values as well as pH_{ZPC} will provide useful information about sorption mechanism. At $\text{pH} > \text{pH}_{\text{ZPC}}$ or $\text{pH} < \text{pK}_a$ the electrostatic repulsion reduces the adsorption when pH increases (at $\text{pH} > \text{pH}_{\text{ZPC}}$) or decrease (when $\text{pH} < \text{pK}_a$). However, at $\text{pK}_a < \text{pH} < \text{pH}_{\text{ZPC}}$ the electrostatic attraction is an important interaction. The solution pH affected largely the behaviour of the functional groups. If the number of negative groups decreases with the decreasing solution pH, the surface becomes positively charged. Additionally, due to the high electrostatic repulsive forces involved in the adsorbent-adsorbate and adsorbate-adsorbate interactions, the adsorption capacity of $X^{\text{np}}\text{-La(III)}$ towards As(V) can be lower than when the solute is in its molecular form or if the solution pH is below pH_{ZPC} . Therefore, the maximum removal of arsenic oxyanions can be observed in the acidic systems. pH_{ZPC} of $X^{\text{np}}\text{-La(III)}$ was 7.21 therefore at pH lower than this value protonation proceeds thus negatively charged arsenic species can be attracted electrostatically. As was mentioned during the discussion the mechanism of As(V) removal is more complicated. For As(V), this indicates that the attractive interaction between the positively charged surface of adsorbents and anionic As(V) species can be a major factor for arsenic removal. Similar results were obtained by Yoon et al. [19] who investigated magnetite-graphene oxide and magnetite-reduced graphene oxide composite for As(III) and As(V) removal.

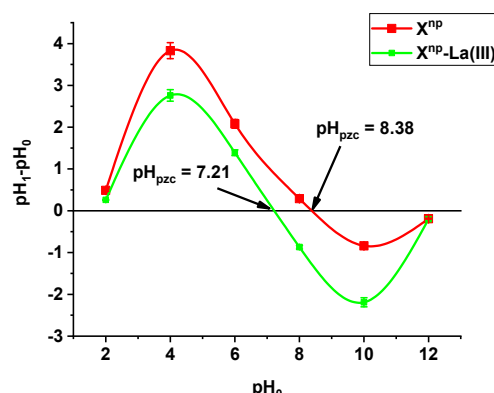


Figure 1. pH_{pzc} measured by the drift method for X^{np} before and after La(III) adsorption.

The SEM images of the raw and lanthanum-modified sorbent are presented in Figure 2.

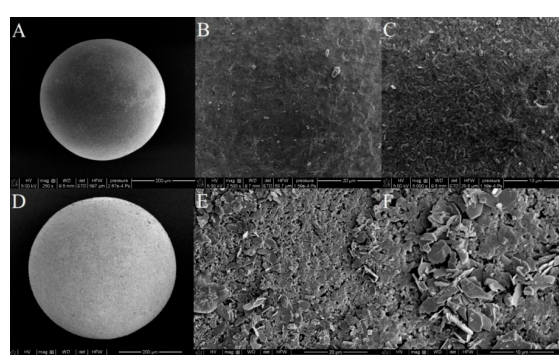


Figure 2. SEM images of X^{np} before (A–C) and after the modification with La(III) ions (D–F) at various magnifications (250 \times ; 2500 \times and 5000 \times).

The use of SEM scanning electron microscopy allowed a visual assessment of the surface structure of the tested sorbents. On the basis of the conducted tests, it can be assumed that after the sorption of lanthanum changes occur in the morphology of the sorbent surface, which becomes more heterogeneous. La (hydr)oxide nanoparticles and nanoflakes of several hundred nanometers spread over the surface. After the adsorption of As(V) process, morphology of X^{np} -La(III) changes to be more “fluffy” similarly to the results presented in the paper by Vijaykumar et al. [21]. When the particle structure presents zero or low porosity, the specific surface area of the particle is a function of these attributes. Specific surface area, particle size as well as the presence of the functional groups are three of the most important parameters for sorptive materials of different types because they are related to the adsorption capacity and rate of the sorption processes. The smaller the size of the material, the higher is the surface area obtained. However, after aggregation of the particles during the La (hydr)oxide formation the surface area decreases.

The adsorption isotherms of N_2 on the carbon adsorbers were used to determine surface characteristics, including the BET surface area and the micropore and mesopore volumes. In the case of the modified and unmodified sorbent, the N_2 adsorption and desorption isotherm is type IV according to the International Union of Pure and Applied Chemistry (IUPAC) classification. For type IV there appears a hysteresis loop, which is associated with capillary condensation in the pores. The sorbent is characterized by the presence of micro- and mesopores. The initial part of the isotherm is associated with single and multilayer adsorption of N_2 because it resembles the beginning of the type II isotherm. The adsorption hystereses (type IV and V) are classified and it is widely accepted that there is a correlation between the shape of the hysteresis loop and the texture (e.g., pore geometry, pore size distribution and connectivity) of a mesoporous material. An empirical classification of hysteresis loops was given by IUPAC, which is based on an earlier classification of hysteresis by de Boer. The tested materials demonstrate H3 hysteresis due to the slit-shaped pores [22]. The hysteresis loop shapes of X^{np} and X^{np} -La(III) are presented in Figure 3.

The specific surface area (S_{BET}) was evaluated based on the BET multilayer adsorption. The total pore volume (V_t) was determined from the adsorbed nitrogen volume at $p/p_0 = 0.99$. The average pore diameter (D_p) is estimated from the pore volume, assuming a cylindrical pore geometry and using the equation $4V_t/S_{BET}$. The mesopore distribution curve was obtained from the adsorption branch of the N_2 isotherm by the Barrett–Joyner–Halenda (BJH) method. The specific surface area of X^{np} is equal to $55.27 \text{ m}^2/\text{g}$ and its total pore volume is $0.189 \text{ cm}^3/\text{g}$. Due to lanthanum(III) adsorption and the formation of nanoflakes, X^{np} -La(III) demonstrates slightly lower values of the specific surface area and total pore volume, equal to $52.75 \text{ m}^2/\text{g}$ and $0.169 \text{ cm}^3/\text{g}$, respectively. There was also a slight difference in the average pore diameter of the unmodified sorbent (13.70 nm) and the modified one (12.79 nm). The data are presented in Table 2.

Table 2. Physical properties of X^{np} and X^{np} -La(III).

Ion Exchanger	X^{np}	X^{np} -La(III)
Specific surface area (S_{BET}) (m^2/g)	55.27	52.75
Total pore volume (V_t) (cm^3/g)	0.189	0.169
Average pore diameter (D_p) (nm)	13.70	12.79

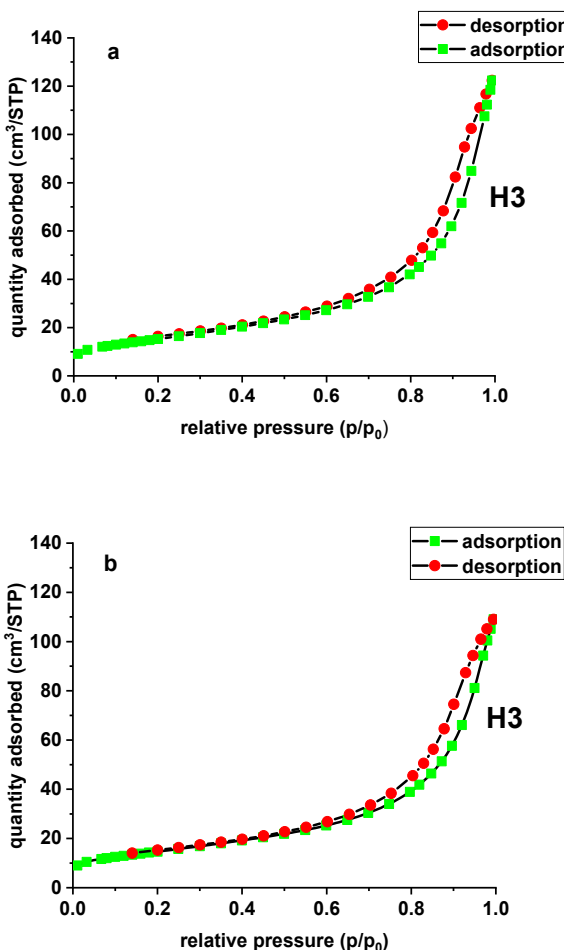


Figure 3. N_2 adsorption/desorption isotherms of X^{NP} (a) and $\text{X}^{\text{NP}}\text{-La(III)}$ (b).

FTIR spectra of X^{NP} and $\text{X}^{\text{NP}}\text{-La(III)}$ were collected before and after sorption of As(V) ions (Figures 4 and 5). The bands at $3600\text{--}3200\text{ cm}^{-1}$ indicate an O-H stretching group on the surface of iron oxide. The peak at 1638 cm^{-1} is observed to be the deformation vibration of water molecules physisorbed on the adsorbent. In comparison to the pure sorbent, the intensity of the above-mentioned peaks decreased after sorption of lanthanum and/or arsenic. Moreover, the absorption bands in the $1200\text{--}900\text{ cm}^{-1}$ region are attributed to the S=O stretching vibrations in the $-\text{SO}_3-$ groups, i.e., asymmetric and symmetric, as well as stretching of single S-OH. The increase of the peak intensity at 827 cm^{-1} was assigned to As-O-La bonding after the As(V) sorption onto $\text{X}^{\text{NP}}\text{-La(III)}$. In their paper, Jais et al. demonstrated two peaks at 808 and 839 cm^{-1} derived from the As-O-La group [23]. These can indicate that arsenate(V) ions were primarily bound as a surface complex. Additionally, based on paper [24], it was found that with the increasing sorption time, the intensity of the band corresponding to the vibrations of As-O bond was progressively increased which is correlated with the fact that the amount of adsorbed As(V) also changed over the pH values. What is more, the peak position is shifted from 839 cm^{-1} to 819 cm^{-1} with the pH change from 5 to 9. In the case of the sorption of As(V) on silica derived sorbent [11] the peak around 960 cm^{-1} is connected with the La(III) modification. The Author found that in the case of the increase in lanthanum impregnation degree the absorbance intensities at 960 cm^{-1} decreased due to formation of Si-O-La bonds. It can be suggested that the monolayer phase of lanthanum oxide may be dominant at below lower lanthanum impregnation, while the multilayer phase of lanthanum oxide may be dominant at the higher lanthanum impregnation. However, the peak at 790 cm^{-1} is connected with the PS-DVB ion exchanger structure.

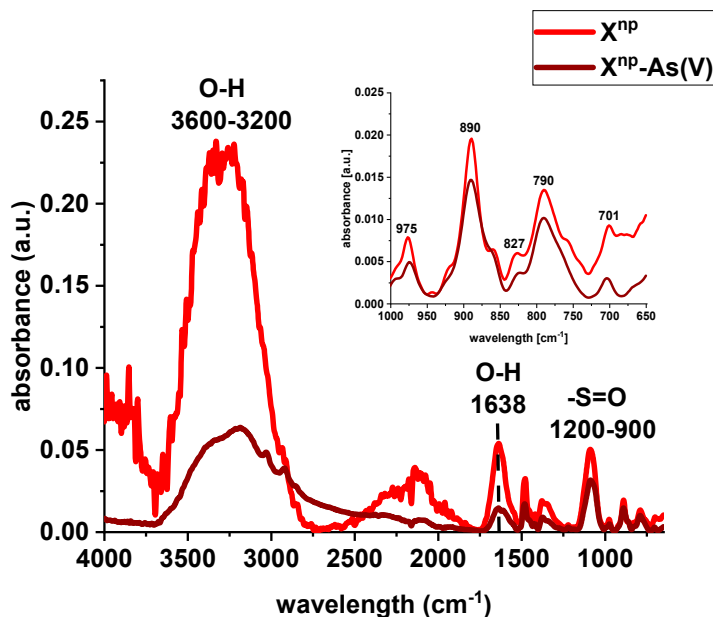


Figure 4. FTIR spectra of X^{np} before and after sorption of As(V) ions.

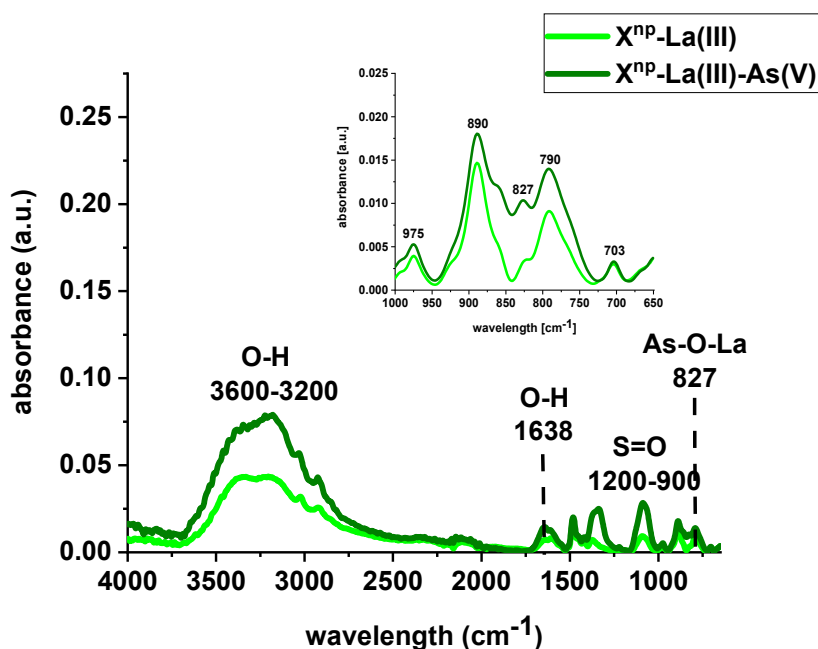


Figure 5. FTIR spectra of X^{np} -La(III) before and after sorption of As(V) ions.

3.2. Sorbent Modification

Studying the effect of pH on La(III) sorption on X^{np} , it was found that the maximum sorption capacity was obtained at pH 4 (Figure 6). At pH > 6, the precipitation of La(OH)_3 occurred and therefore lanthanum(III) adsorption became impossible to proceed.

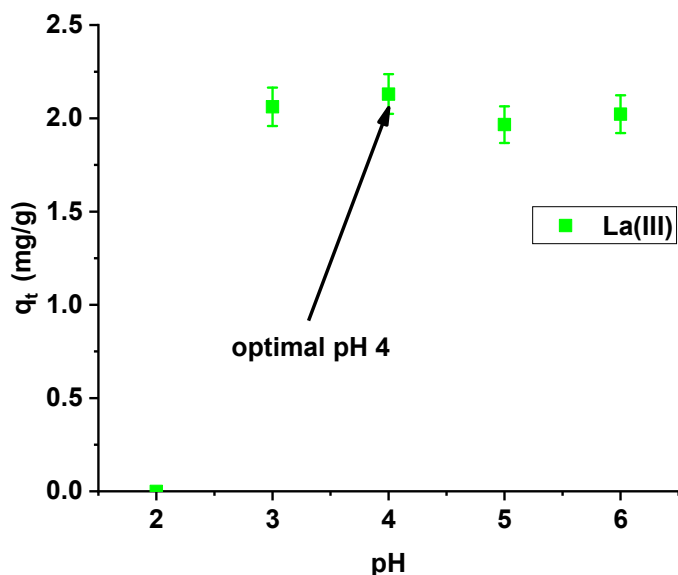


Figure 6. Effect of pH on lanthanum(III) adsorption on X^{np} ($c_0 = 10 \text{ mg/dm}^3$; $m = 0.1 \text{ g}$; $t = 24 \text{ h}$).

Sorption capacities at the pH range from 3 to 6 are similar, but slightly higher at pH 4, so this value was selected for further studies.

Kinetic studies show that the La(III) adsorption processes are quite fast. It is observed that sorption efficiency is greater for solutions with lower initial concentrations (Figure 7).

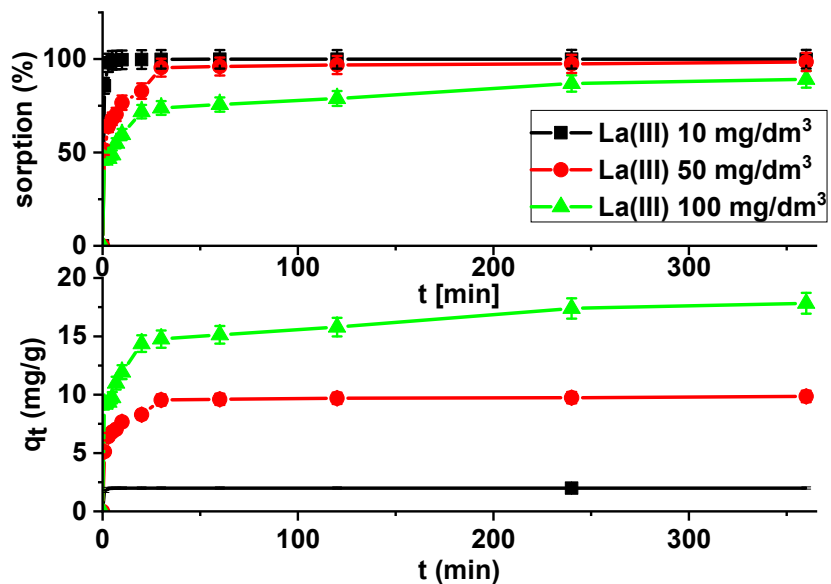


Figure 7. Lanthanum(III) sorption efficiency and sorption capacities as a function of time on X^{np} ($c_0 = 10, 50$ and 100 mg/dm^3 , $\text{pH} = 4$, shaking speed 180 rpm , temperature 295 K).

It was found that the linear regression coefficient based on the pseudo-second order (PSO) model ($R^2 > 0.99$) gave the best fitting (Table 3, Figure 8). Based on the PSO model, the calculated adsorption capacities (1.99, 9.84, 17.82) were nearly the same as the experimental ones. The adsorption rate constants decreased with the increase in La(III) initial concentration.

Table 3. Kinetic parameters of lanthanum(III) adsorption on X^{NP}.

Kinetic Parameters	X ^{NP} -La(III)		
	10 (mg/dm ³)	50 (mg/dm ³)	100 (mg/dm ³)
PFO			
$q_{1,cal}$	0.01	2.06	6.71
k_1	0.025	0.016	0.011
R^2	0.6537	0.6786	0.9105
PSO			
$q_{2,cal}$	2.00	9.89	17.87
k_2	8.968	0.045	0.010
h	35.843	4.406	3.131
R^2	1.0000	0.9999	0.9986

Where: $q_{1,cal}$ and $q_{2,cal}$ —the calculated amount of arsenic adsorbed at equilibrium for the PFO and PSO models; k_1 and k_2 are the reaction rate constants of the pseudo-first order (1/min) and pseudo-second order (g/mg min); R^2 —the correlation coefficient; h —the initial rate of adsorption for the PSO model (mg/g min).

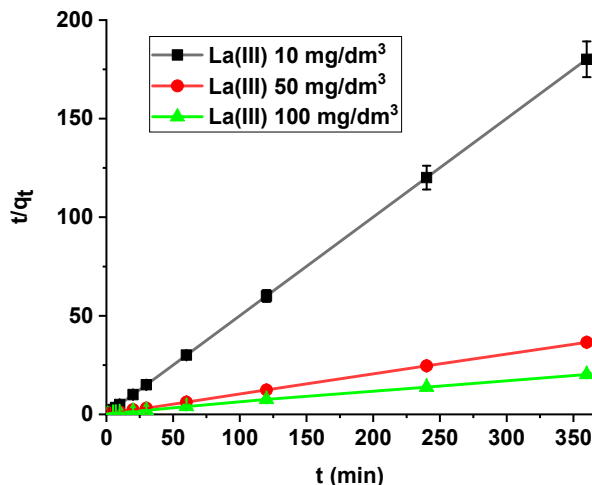


Figure 8. PSO plots of lanthanum(III) adsorption on X^{NP} ($c_0 = 10, 50, 100 \text{ mg/dm}^3$, pH = 4, shaking speed 180 rpm, temperature 295 K).

The isotherm data were analysed using the Langmuir and Freundlich models (Figure 9).

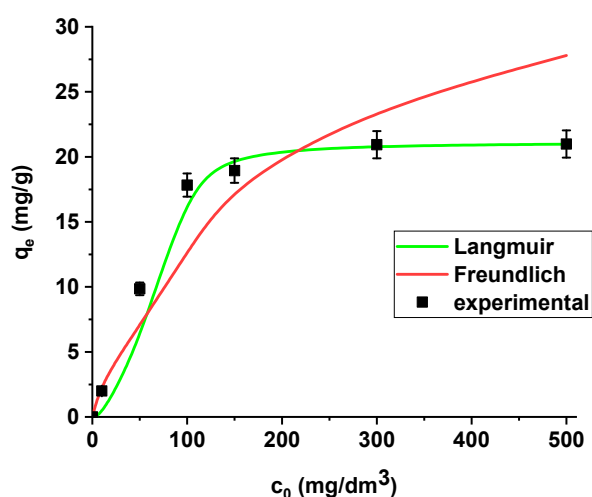


Figure 9. The Langmuir and Freundlich sorption isotherms of La(III) on X^{NP} (pH 4, shaking speed 180 rpm, temperature 295 K).

La(III) adsorption was described better by the Langmuir model ($R^2 = 0.9998$) than the Freundlich model ($R^2 = 0.8996$). X^{np} demonstrates the maximum sorption capacity towards lanthanum(III) equal to 21.08 mg/g. It is worth mentioning that the coefficient R_L lies in the range 0–1 (0.171), which indicates that the process is favourable.

3.3. Influence of pH on As(V) Adsorption on X^{np} -La(III)

Arsenic is present in compounds at various oxidation states, but the most common ones are -3, 0, +3, and +5 [25]. Arsenic(V) is more readily adsorbed on solid surfaces than arsenic(III), so in order to remove arsenic effectively, all forms of arsenic should be oxidized to the +5 oxidation state. Moreover, inorganic arsenic compounds are more toxic than organic ones, and as for the oxidation state, arsenic(III) is usually more toxic than arsenic(V). The most common inorganic forms of arsenic are arsenic(III) and arsenic(V), the amount of which depends on the pH and redox potential. At pH 3–9, arsenic(III) dominates as undissociated H_3AsO_3 , while arsenic(V) exists as the anions $HAsO_4^{2-}$ and $H_2AsO_4^-$ ($pK_1 = 2.2$, $pK_2 = 7.1$, $pK_3 = 11.5$) [26]. At pH 6, arsenic(V) exists as the anions $HAsO_4^{2-}$ and $H_2AsO_4^-$.

On the basis of the presented results of dependence of sorption capacities of the tested hybrid material on the initial pH of the arsenic(V) solution, the sorption capacities of X^{np} -La(III) were observed to be almost equal. The highest efficiency of arsenic(V) sorption was achieved at pH 6 (Figure 10). At pH 6, arsenic(V) exists as the anions $HAsO_4^{2-}$ and $H_2AsO_4^-$. As follows from the speciation distribution the ratio of $HAsO_4^{2-}$ and $H_2AsO_4^-$ are about 10%: 90% [27]. Consequently, they can be more readily adsorbed on an electrically charged surface. Additionally, as follows from the paper by Sarkar et al. [28] it is worth noting that the chronic toxicity caused by the presence of low concentration of arsenic (well below 1 mg/L) is not influenced by the relative distribution of As(III) and As(V). At such low concentration, As(V) gets instantaneously converted to As(III). That is why the World Health Organization (WHO), the United States Environmental Protection Agency (USEPA), and the European Union (EU), specify only the total amount of arsenic for the maximum contamination level (MCL) in drinking water.

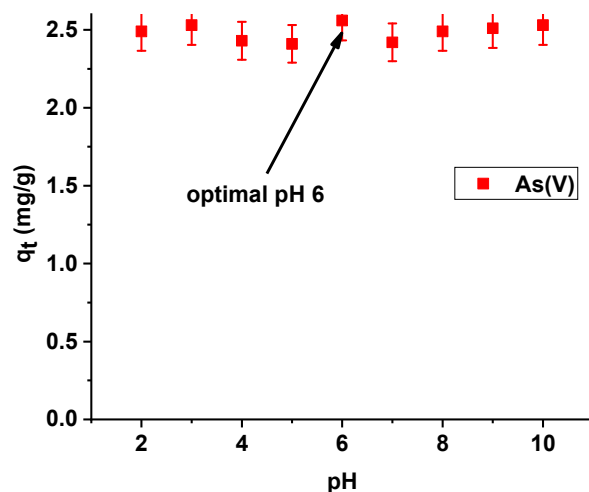


Figure 10. Effect of pH on adsorption of arsenic(V) on X^{np} -La(III) ($c_0 = 10 \text{ mg/L}$; $m = 0.1 \text{ g}$; $t = 24 \text{ h}$, $T = 295 \text{ K}$, shaking speed 180 rpm).

Thus, the pH value of 6, which is slightly lower than the pH of municipal water, was selected for further studies for both X^{np} and X^{np} -La(III) to ensure uniform conditions of arsenic (V) ions. In addition, a pH of 6 is a value below the pH_{pzc} of X^{np} and X^{np} -La(III). The positively charged surfaces of the modified and unmodified sorbent should attract hydrogen arsenate(V) and dihydrogen arsenate(V) anions.

3.4. Kinetic Studies of As(V) on X^{np} -La(III)

In the case of a static method, for all practical purposes the choice of experimental variables usually narrows down to two: the concentration and amount of sorbent. In the presented results, for comparison the adsorption studies were carried out for X^{np} before and after modification. Figures 11 and 12 show that all the presented adsorption processes are quite fast. It is observed that sorption efficiency (%) is greater for the solutions with lower initial concentrations. For example, in the case of X^{np} at the highest adsorption percentage the concentration of arsenic(V) was reduced from 25 mg/dm^3 to 0.94 mg/dm^3 . Interestingly, arsenate(V) ions were completely removed from the 25 and 50 mg/dm^3 solutions in the case of X^{np} -La(III) (100% sorption efficiency). The ability to remove arsenic completely at relatively low initial concentrations is very important and shows successful modification. Li et al. examined hybrid Ce-Ti sorbent in terms of arsenic removal [29]. The authors claimed that in industrial drinking water treatment, the arsenic(V) concentration usually does not exceed 0.1 mg/dm^3 and the final arsenic concentration in wastewater must be lower than the generally accepted limit of $10 \mu\text{g/dm}^3$ and therefore the sorption ability to adsorb at a low initial arsenic(V) concentration is more important than the maximum sorption capacity obtained experimentally at high arsenic(V) concentration. To predict the optimal conditions of adsorbate removal both isotherm adsorption and intraparticle kinetic parameters should be determined under different system conditions because they are dependent, among others, on the concentration, temperature and interactions between the adsorbent and the adsorbate. If the adsorbent possesses particular functional groups and active centres to adsorb the adsorbate, its effect should be evaluated from the experimental data.

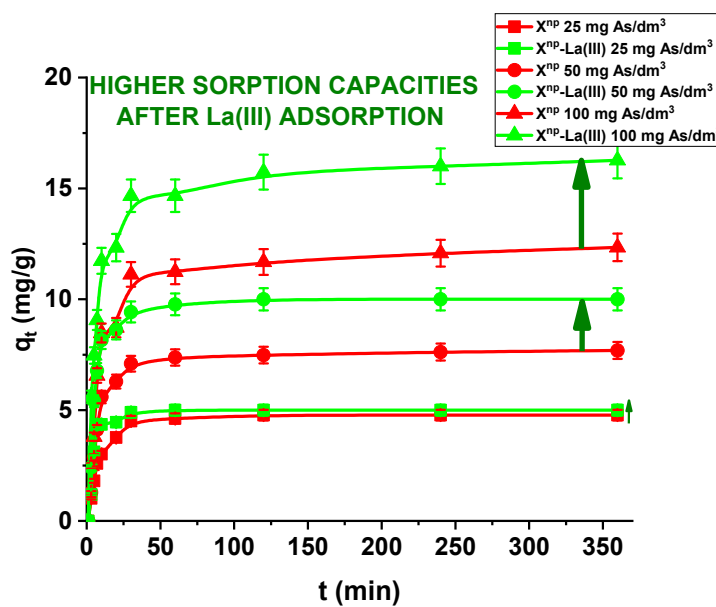


Figure 11. Sorption of arsenic(V) on X^{np} and X^{np} -La(III) as a function of time ($c_0 = 25, 50$ and 100 mg/dm^3 , pH = 6, shaking speed 180 rpm, temperature 295 K).

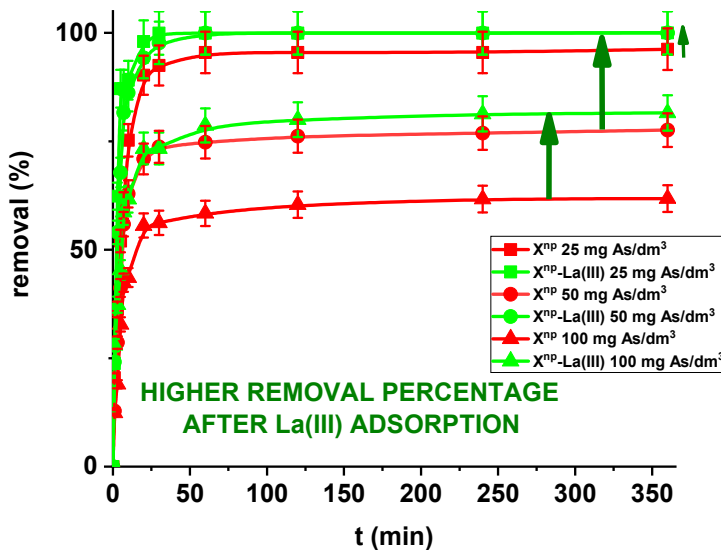


Figure 12. Arsenic(V) sorption efficiency for X^{np} and $X^{np}\text{-La(III)}$ ($c_0 = 25, 50$ and 100 mg/dm^3 , $\text{pH} = 6$, shaking 180 rpm, temperature 295 K).

Moreover, in our studies arsenic(V) ions sorption increases very sharply within the first 15 min of the phase contact time and the equilibrium appears to be reached after 120 min with the adsorption capacities equal to 4.81, 7.76, and 12.36 mg/g for X^{np} as well as 5.00, 10.00 and 16.31 mg/g for $X^{np}\text{-La(III)}$ at initial concentrations of 25, 50 and 100 mg/dm^3 , respectively. These results demonstrate that the 120-min phase contact time selected for adsorption studies is adequate for adsorption on both sorbents. The adsorption is the fastest at the beginning of the process at short time intervals and then gradually declines throughout the studied period. This indicates that as the adsorption sites on X^{np} and $X^{np}\text{-La(III)}$ surface were occupied, the rate of adsorption decreased.

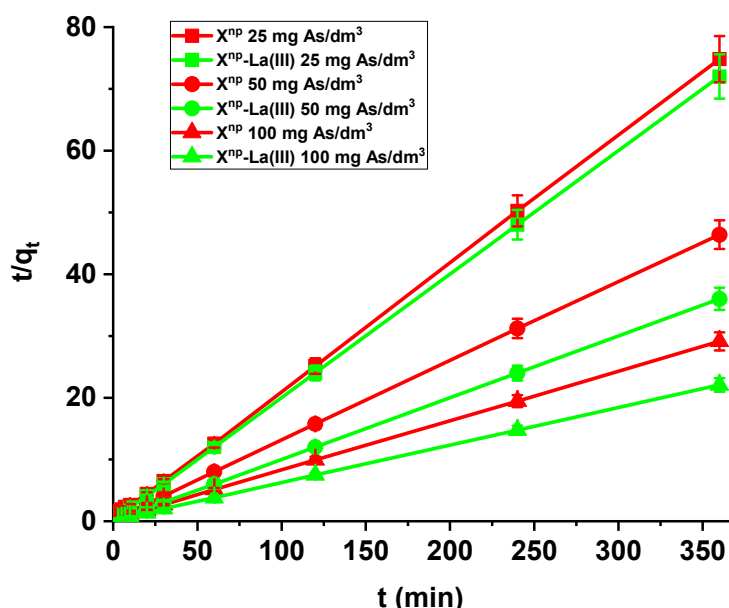
Comparing the kinetic studies of arsenic(V), it was found that the linear regression coefficient based on the pseudo-second order (PSO) model ($R^2 > 0.99$) gave the best fitting (Tables 4 and 5, Figure 13) for both X^{np} and $X^{np}\text{-La(III)}$. The As(V) adsorption rate constants determined using the PSO model are 0.030, 0.018 and 0.009 1/min, while the adsorption capacities are 3.14, 5.07, and 8.64 mg/g for X^{np} . For $X^{np}\text{-La(III)}$, they are higher and equal to 0.178, 0.057, 0.020 1/min, whereas the adsorption capacities are 5.02, 10.07, and 16.46 mg/g. It is worth mentioning that the $q_{e,exp}$ values are well comparable with these calculated $q_{e,cal}$ (Tables 4 and 5). What is more, an increase in the initial arsenic(V) concentration leads to an increase in the adsorption capacity.

Table 4. Kinetic parameters of arsenic(V) adsorption on X^{np} .

Kinetic Parameters	$X^{np}\text{-As(V)}$		
	25 (mg/dm^3)	50 (mg/dm^3)	100 (mg/dm^3)
PFO			
$q_{1,cal}$	0.83	1.70	4.55
k_1	0.032	0.031	0.032
R^2	0.4355	0.5807	0.7847
PSO			
$q_{2,cal}$	3.14	5.07	8.64
k_2	0.030	0.018	0.009
h	0.292	0.460	0.702
R^2	0.9999	0.9999	0.9999

Table 5. Kinetic parameters of arsenic(V) adsorption on X^{np}-La(III).

Kinetic Parameters	X ^{np} -As(V)-La(III)		
	25 (mg/dm ³)	50 (mg/dm ³)	100 (mg/dm ³)
PFO			
$q_{1,cal}$	0.29	1.34	5.09
k_1	0.029	0.036	0.021
R^2	0.4854	0.6614	0.8920
PSO			
$q_{2,cal}$	5.02	10.07	16.46
k_2	0.178	0.057	0.020
h	4.488	5.825	5.306
R^2	0.9999	0.9999	1.0000

**Figure 13.** PSO plots of arsenic(V) adsorption on X^{np} (red) and X^{np}-La(III) (green) ($c_0 = 25, 50, 100 \text{ mg/dm}^3$, pH 6, shaking speed 180 rpm, temperature 295 K).

It can be noticed that the adsorption involves bulk phase transport of the metal ions to the external surface of X^{np}, transport across the boundary layer (external mass transfer), transport through/within X^{np} by surface diffusion and/or pore diffusion (intraparticle diffusion), and adsorption on the adsorbent surface. The last one can be affected by the stirring rate, volume, and initial concentration of the solution.

3.5. Equilibrium Adsorption of As(V) on X^{np}-La(III)

The isotherm data were analysed using the Langmuir and Freundlich models to provide an insight into the interactions between the adsorbent and the adsorbate. Sorption equilibrium is usually described by an isotherm equation whose parameters express the affinity and surface properties of the sorbent at a fixed temperature and pH. To optimise an adsorption system, it is important to establish the most appropriate correlations for the equilibrium. Therefore, the isotherm data were analysed using the Langmuir and Freundlich isotherm models. Therefore, the isotherm data were analysed using the Langmuir and Freundlich isotherm models. The correlation parameter (R^2) and the corresponding average relative errors were calculated according to the following equation:

$$\Delta q(\%) = \sum_{i=1}^N \left| \frac{q_{exp} - q_0}{q_{exp}} \right| \times \frac{100}{N} \quad (8)$$

where: q_{exp} —the experimental amount of arsenic adsorbed at equilibrium (mg/g); q_0 —the calculated amount of arsenic adsorbed at equilibrium and N —the number of the experimental data.

The results are summarized in Table 6. The regression coefficients (R^2) are higher for the Langmuir model in both cases, i.e., the sorption of As(V) on the unmodified and modified sorbent. What is more, the average relative errors are smaller for the Langmuir equation in both cases. The high correlation coefficients and relatively small errors suggested that the Langmuir model provides good fit of the experimental adsorption data and can be applied for description of the sorption process. The sorption capacity of X^{np} and X^{np} -La(III) increased with the increase in arsenic concentration in the solution. Based on the Langmuir model, the maximum sorption capacities towards arsenic(V) were determined as 22.37 mg/g and 61.97 mg/g on X^{np} and X^{np} -La(III), respectively. It is worth noting that the maximum sorption capacity of the modified sorbent is almost 3 times greater than the unmodified one. For the Freundlich model, the K_F values related to arsenic(V) adsorption on the unmodified and modified ion exchanger are equal to 4.64 and 14.49, respectively (Table 6). The parameters R_L ($0 < R_L < 1$) for adsorption of arsenic(V) on both sorbents indicate that the process is favourable. The Langmuir and Freundlich sorption isotherms of As(V) on X^{np} and X^{np} -La(III) are presented in Figures 14 and 15.

Table 6. The Langmuir and Freundlich parameters for adsorption of arsenic(V) on X^{np} and X^{np} -La(III) (pH 6, shaking speed 180 rpm, temperature 295 K).

Isotherm Parameters	X^{np} -As(V)	X^{np} -La(III)-As(V)
Langmuir Model		
q_0	22.37	61.97
K_L	0.047	0.017
R_L	0.462	0.696
R^2	0.9931	0.9637
error (%)	5.47	6.54
Freundlich Model		
K_F	4.64	14.49
n	3.775	5.589
R^2	0.9790	0.8611
error (%)	6.50	18.28

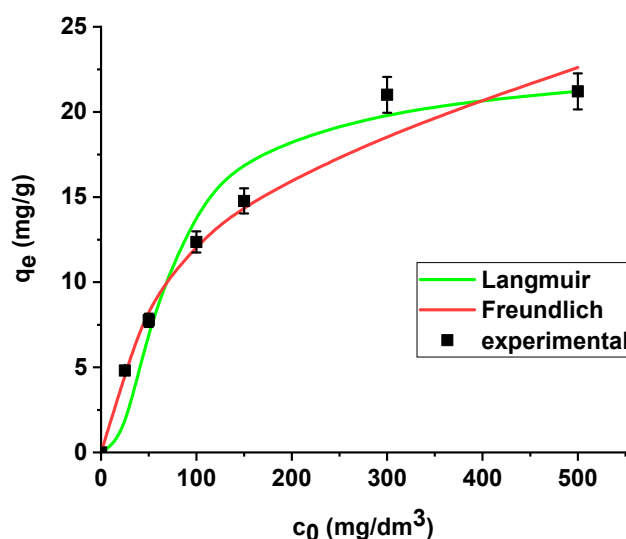


Figure 14. The Langmuir and Freundlich sorption isotherms of As(V) on X^{np} (pH 6, shaking speed 180 rpm, temperature 295 K).

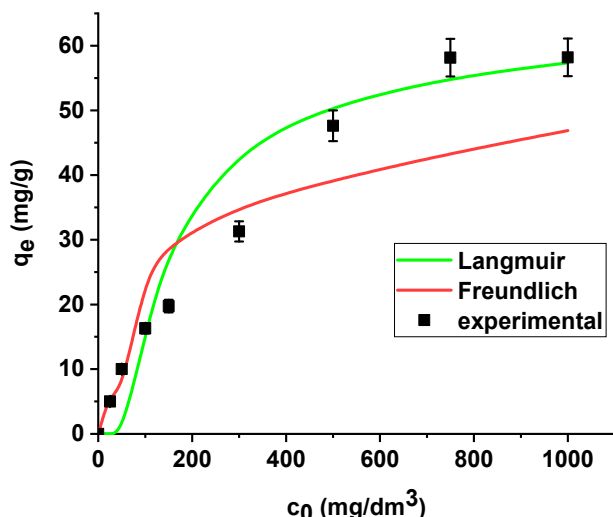
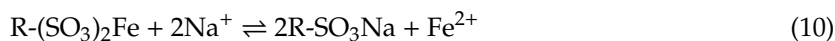


Figure 15. The Langmuir and Freundlich sorption isotherms of As(V) on X^{np} -La(III) (pH 6, shaking speed 180 rpm, temperature 295 K).

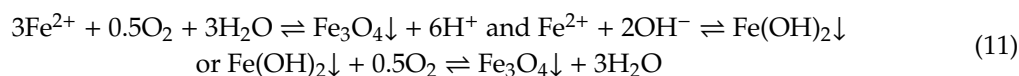
In the case of commercial hybrid ion exchangers based on nanosized iron oxides, their quality depends on the quantity, structure, crystallinity and degree of dispersion of the iron oxides introduced, the physical form of the base polymer, the type of functional groups involved in the preparation of hybrid polymers as well as their influence on the process of adsorption [7]. The process of dispersing of iron oxide can be applied to different types of polymers such as those containing sulfonic, diphosphonic/sulfonic/carboxylic, bispicolylamine or quaternary ammonium as well as iminodiacetic functional groups:



and slow oxidation of Fe(II) into Fe_3O_4 at alkaline pH, i.e.,

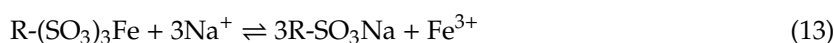


as well as

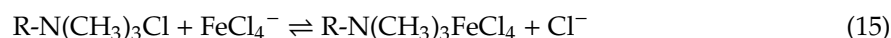


where: R is the resin matrix.

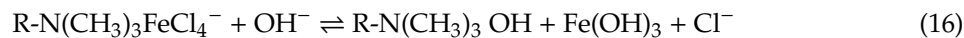
The magnetic properties of these sorbents are greatly influenced by the kind of functional groups. They were found to change in the following order: sulfonic > diphosphonic/sulfonic/carboxylic > bispicolylamine > iminodiacetic. However, in the case of introducing the hydrated Fe(III) oxide (HFO), to obtain hybrid ion exchangers (HIXs) the first step of preparation includes loading of Fe(III) onto the functional groups of the ion exchanger (for example sulfonic one), then desorption of Fe(III) and simultaneous precipitation of Fe(III) hydroxides within the gel and pore phase of the exchanger by passage of a solution containing both NaCl and NaOH:



As for anion exchanges used as a support the following reactions can be proposed:



and



The next one is alcohol washing and precipitation:

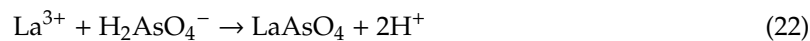


As for the mechanism, the adsorption of As(V) on the surface covered with iron oxides takes place in two stages. The first stage is characterized by a very high speed and consists in the diffusion of arsenic(V) to the adsorbent surface. The second stage, however, is much slower and involves the diffusion of the sorbed molecules into the micropores of iron oxides. Then, a structural transformation takes place on the adsorbent surface. In the case of arsenates(V), the process of complex formation is initially connected with the formation of monodentate and then bidentate mononuclear complexes, which transform into double-core binary complexes as the degree of polymer coverage with metal oxide increases. The speed and scale of these transformations are influenced by various factors, which include the number of active sites as well as the pH value of the solution in which the process takes place. As a result of a low pH value, the adsorption process may be affected by electrostatic interactions between the arsenate anions and the positive charge on the adsorbent surface. Under such conditions, proper ligand exchange can proceed by non-specific adsorption of arsenates(V) on the surface of iron oxides, which takes place through ion exchange with the previously adsorbed anions [30–35]. The mechanism reactions can be as follows:



Contrary to alkaline conditions (where only adsorption of As(V) takes place), under almost neutral conditions precipitation and adsorption can be the main mechanisms of As(V) removal.

However, in the case of $\text{X}^{\text{np}}\text{-La(III)}$, i.e., after modification, the removal capacity was enhanced by the co-precipitation and adsorption by exchange of the OH- group with arsenic ions. At pH 6.0, the arsenic H_2AsO_4^- (about 90% in the system) and HAsO_4^{2-} (10% in the system) species are present as strong electron donors and can interact with La(III); therefore, the following reaction can be proposed:



In such conditions, the insoluble lanthanum arsenate, LaAsO_4 , precipitates in the acid pH range. As for the analogous FeAsO_4 , its dissolution increases at a pH value greater than 5.0 and FeAsO_4 can decompose at a pH greater than 6.0. Moreover, the effect of the presence of the functional groups of the ion exchanger should be neglected. The high concentration of the functional groups only allowed a high and fairly uniform loading of hydrous iron oxide particles within the polymeric matrix. Similar results were described in [36] where the removal of arsenic(V) onto lanthanum(III) modified sorbents of (hydr)oxide type was described. Additionally, it was found that with an increase of lanthanum(III) content (within Fe/La ratio from 3:1, 1:1 and 1:3), the specific surface area of the obtained composites decreased, but the pore diameter, the pore volume and their grain increased gradually (which can be explained by the increase in the particle size and shape at the highest content of La) [36]. The Langmuir adsorption capacities of 3:1, 1:1, 1:3 and 0:1 Fe-La composite (hydr)oxides were 116 mg/g, 166 mg/g, 235 mg/g, and 368 mg/g at pH 7.0, respectively. Taking into account the comparison of the examined sorbents and others used for arsenic removal (Table 7), it can be concluded that the high

removal efficiency of the R-Fe-La composite (hydro)oxide makes it attractive for treatment of water contaminated with As(V).

Table 7. The comparison of other sorbents used for arsenic(V) removal.

Adsorbent Type	pH	As(V) (mg/g)	Ref.
La and Ce-loaded orange waste gels	6.0–9.5	42	[37]
La-modified ceramic material	4.0–8.0	23	[38]
Ce oxide modified activated carbon	5.0	43.6	[39]
Fe–La composite (hydr)oxide	7.0	235	[36]
Fe ₃ O ₄ @SiO ₂ @TiO ₂ nanosorbent	9.0	10.2	[40]
Mg doped α -Fe ₂ O ₃	7.0	10	[41]
Fe ₃ O ₄	8.2	12.56	[42]
Nanoscale zero-valent iron-reduce graphite oxide modified composite	7.0	29.04	[43]
Hydrated ferric hydroxide	9.0	7.0	[44]
X ^{np}	6.0	22.37	this study
X ^{np} -La(III)	6.0	61.97	this study

3.6. Reuse of X^{np} and X^{np}-La(III)

When the equilibrium of arsenic sorption is established, the adsorbent is unserviceable and regeneration is needed to use it in a cyclic manner. The loaded adsorbent should be separated from the aqueous solution in order to perform desorption and subsequent regeneration employing an external magnetic field. The most commonly used substances desorbing arsenic ions are strong bases or strong acids, e.g., NaOH and HCl.

Three sorption and desorption cycles were carried out and the possibility of reusing the tested sorbents was assessed. Sorption was conducted using an arsenic solution of 100 mg/dm³ and desorption with 1M NaOH. In the case of X^{np} during the first, second and third sorption, the percentage of sorption remained relatively constant (66.67%, 66.34%, 65.34%). No significant decrease in the sorption capacity was noted. After the third cycle, the desorption effectiveness was 93.32% (Figure 16). Similar results were obtained for X^{np}-La(III). The percentages of sorption amounted to 77.00%, 77.67%, and 75.85%. After the third cycle, the percentage of desorption was 90.02%. This desorption efficiency can be explained by the following mechanism:

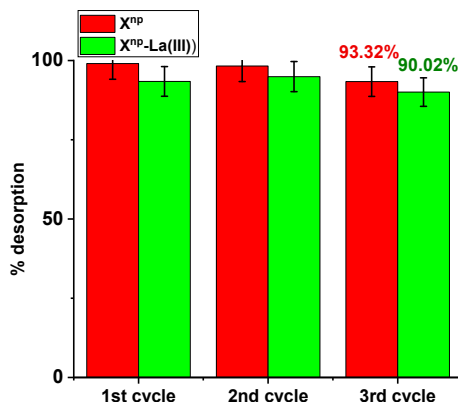
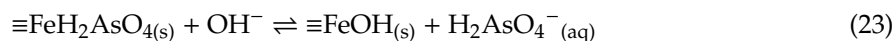


Figure 16. Desorption efficiency (%) for As(V) recovery using X^{np} and X^{np}-La(III) (As(V) concentration: 100 mg/dm³, desorbing agent: 1M NaOH, sorption/desorption time: 6 h, shaking speed 180 rpm, temperature 295 K).

The obtained results clearly indicate that the arsenic adsorption can be carried out repeatedly on the same material after NaOH regeneration. The ability to reuse the same material significantly reduces costs.

1 M NaOH was used for the regeneration of maghemite and it was found that after six cycles the adsorbent maintained over 40% of the initial sorption capacity [45]. In turn, arsenic adsorbed on granular iron and cerium hydroxide (GFC) was subjected to elution of 1 M NaOH and the recovery efficiency was equal to 89%. After that, As(V) was removed with the same efficiency [46]. Another example could be the regeneration of Fe-Cu double oxide with NaOH. After 4 cycles of adsorption and desorption, the sorption capacity decreased by only 6.2% regarding As(V) [47]. Also the spent Fe-La composite (hydr)oxide could be effectively regenerated using NaOH solution and reused several times [36].

4. Conclusions

The paper has proved that earlier adsorption of lanthanum(III) ions on the iron oxide ion exchanger contributed to an increase in the sorption efficiency of arsenic(V) ions.

- (a) The maximum sorption capacity for arsenic ions was almost 3 times greater after the modification.
- (b) X^{np} -La(III) removed arsenic entirely from the solution of 50 mg/dm^3 in a relatively short time (about 2 h).
- (c) It was found that after modification the sorbent can be successfully reused for purification of water contaminated with arsenic. After 3 cycles of adsorption and desorption, no significant decrease in the process efficiency was observed.
- (d) Under almost neutral conditions precipitation and adsorption can be the main mechanisms of As(V) removal. After modification, the removal capacity was enhanced by the co-precipitation and adsorption by exchange of the OH⁻ group with arsenic ions.

The threefold greater maximum sorption capacity after the modification together with the short duration time of the process lead to a reduction in operating costs. What is more, the arsenic removal process is very efficient at the pH of municipal waters. A lack of significant decrease in the process efficiency, even after 3 cycles of adsorption and desorption, enables the multiple use of the same material. All these factors confirmed that lanthanum-modified X^{np} achieves better results than unmodified X^{np} and is a very promising material in the context of arsenic removal from contaminated water bodies. The modification process itself is a great opportunity to improve the properties of iron oxide containing sorbents and to achieve the WHO restrictive limit for arsenic.

Author Contributions: Investigation S.D.; supervision D.K. All authors have read and agreed to the published version of the manuscript.

Funding: This research received no external funding.

Conflicts of Interest: The authors declare no conflict of interest.

References

1. Jain, C.K.; Ali, I. Arsenic: Occurrence, toxicity and speciation techniques. *Water Res.* **2000**, *34*, 4304–4312. [[CrossRef](#)]
2. Mandal, B.K.; Suzuki, K.T. Arsenic round the world: A review. *Talanta* **2002**, *58*, 201–235. [[CrossRef](#)]
3. Duker, A.A.; Carranza, E.J.M.; Hale, M. Arsenic geochemistry and health. *Environ. Int.* **2005**, *31*, 631–641. [[CrossRef](#)] [[PubMed](#)]
4. Matschullat, J. Arsenic in the geosphere—A review. *Sci. Total Environ.* **2000**, *249*, 297–312. [[CrossRef](#)]
5. Ng, J.C.; Wang, J.; Shraim, A. A global health problem caused by arsenic from natural sources. *Chemosphere* **2003**, *52*, 1353–1359. [[CrossRef](#)]
6. Ociński, D.; Jacukowicz-Sobala, I.; Raczyk, J.; Kociołek-Balawejder, E. Evaluation of hybrid polymer containing iron oxides as As(III) and As(V) sorbent for drinking water purification. *React. Funct. Polym.* **2014**, *83*, 24–32. [[CrossRef](#)]

7. Aredes, S.; Klein, B.; Pawlik, M. The removal of arsenic from water using natural iron oxide minerals. *J. Clean. Prod.* **2013**, *60*, 71–76. [[CrossRef](#)]
8. Giles, D.E.; Mohapatra, M.; Issa, T.B.; Anand, S.; Singh, P. Iron and aluminium based adsorption strategies for removing arsenic from water. *J. Environ. Manage.* **2011**, *92*, 3011–3022. [[CrossRef](#)]
9. Jiang, W.; Chen, X.; Niu, Y.; Pan, B. Spherical polystyrene—supported nano- Fe_3O_4 of high capacity and low-field separation for arsenate removal from water. *J. Hazard. Mater.* **2012**, *243*, 319–325. [[CrossRef](#)]
10. He, Z.; Tian, S.; Ning, P. Adsorption of arsenate and arsenite from aqueous solutions by cerium-loaded cation exchange resin. *J. Rare Earths* **2012**, *30*, 563–572. [[CrossRef](#)]
11. Jang, M.; Park, J.K.; Shin, E.W. Lanthanum functionalized highly ordered mesoporous media: Implications of arsenate removal. *Microporous Mesoporous Mater.* **2004**, *75*, 159–168. [[CrossRef](#)]
12. Tan, P.; Zheng, Y.; Hu, Y. Efficient removal of arsenate from water by lanthanum immobilized electrospun chitosan nanofiber. *Colloids Surfaces A Physicochem. Eng. Asp.* **2020**, *589*, 124417. [[CrossRef](#)]
13. Lingamdinne, L.P.; Koduru, J.R.; Chang, Y.Y.; Kang, S.H.; Yang, J.K. Facile synthesis of flowered mesoporous graphene oxide-lanthanum fluoride nanocomposite for adsorptive removal of arsenic. *J. Mol. Liq.* **2019**, *279*, 32–42. [[CrossRef](#)]
14. Kołodyńska, D.; Kowalczyk, M.; Hubicki, Z.; Shvets, V.; Golub, V. Effect of accompanying ions and ethylenediaminedisuccinic acid on heavy metals sorption using hybrid materials Lewatit FO 36 and Purolite Arsen X^{nP}. *Chem. Eng. J.* **2015**, *276*, 376–387. [[CrossRef](#)]
15. Kowalczyk, M.; Hubicki, Z.; Kołodyńska, D. Modern hybrid sorbents—New ways of heavy metal removal from waters. *Chem. Eng. Process. Process Intensif.* **2013**, *70*, 55–65. [[CrossRef](#)]
16. SenGupta, A.K.; Cumbal, L.H. Hybrid anion exchanger for selective removal of contaminating ligands from fluids and method of manufacture thereof. U.S. Patent 7291578B2, 6 November 2007.
17. Padilla-Rodríguez, A.; Hernández-Viezzcas, J.A.; Peralta-Videa, J.R.; Gardea-Torresdey, J.L.; Perales-Pérez, O.; Román-Velázquez, F.R. Synthesis of protonated chitosan flakes for the removal of vanadium(III, IV and V) oxyanions from aqueous solutions. *Microchem. J.* **2015**, *118*, 1–11. [[CrossRef](#)]
18. Sharma, M.; Singh, J.; Hazra, S.; Basu, S. Adsorption of heavy metal ions by mesoporous ZnO and TiO_2 @ ZnO monoliths: Adsorption and kinetic studies. *Microchem. J.* **2019**, *145*, 105–112. [[CrossRef](#)]
19. Berhane, T.M.; Levy, J.; Krekeler, M.P.S.; Danielson, N.D. Chemosphere Kinetic sorption of contaminants of emerging concern by a palygorskite-montmorillonite fi lter medium. *Chemosphere* **2017**, *176*, 231–242. [[CrossRef](#)]
20. Hu, Q.; Wang, Q.; Feng, C.; Zhang, Z.; Lei, Z.; Shimizu, K. Insights into mathematical characteristics of adsorption models and physical meaning of corresponding parameters. *J. Mol. Liq.* **2018**, *254*, 20–25. [[CrossRef](#)]
21. Marakatti, V.S.; Rao, P.V.C.; Choudary, N.V.; Ganesh, G.S.; Shah, G.; Maradur, S.P.; Halgeri, A.B.; Shanbhag, G.V.; Ravishankar, R. Influence of alkaline earth cation exchanged X-zeolites towards ortho-selectivity in alkylation of aromatics: Hard-soft-acid-base concept. *Adv. Porous Mater.* **2015**, *2*, 221–229. [[CrossRef](#)]
22. Alothman, Z.A. A review: Fundamental aspects of silicate mesoporous materials. *Materials* **2012**, *5*, 2874–2902. [[CrossRef](#)]
23. Jais, F.M.; Ibrahim, S.; Yoon, Y.; Jang, M. Enhanced arsenate removal by lanthanum and nano-magnetite composite incorporated palm shell waste-based activated carbon. *Sep. Purif. Technol.* **2016**, *169*, 93–102. [[CrossRef](#)]
24. Shi, Q.; Yan, L.; Chan, T.; Jing, C. Arsenic adsorption on lanthanum-impregnated activated alumina: Spectroscopic and DFT study. *ACS Appl. Mater. Interfaces* **2015**, *7*, 26735–26741. [[CrossRef](#)] [[PubMed](#)]
25. Prasad, S.M.; Singh, V.P.; Singh, S.; Parihar, P.; Singh, R. Arsenic contamination, consequences and remediation techniques: A review. *Ecotoxicol. Environ. Saf.* **2014**, *112*, 247–270.
26. Ozola, R.; Bhatnagar, A.; Ansone-Bertina, L.; Vircava, I.; Leitietis, M.; Burlakovs, J.; Klavins, M.; Krauklis, A. FeOOH-modified clay sorbents for arsenic removal from aqueous solutions. *Environ. Technol. Innov.* **2016**, *13*, 364–372. [[CrossRef](#)]
27. Ben Issa, N.; Rajaković-Ognjanović, V.N.; Marinković, A.D.; Rajaković, L.V. Separation and determination of arsenic species in water by selective exchange and hybrid resins. *Anal. Chim. Acta* **2011**, *706*, 191–198. [[CrossRef](#)]

28. Sarkar, S.; Blaney, L.M.; Gupta, A.; Ghosh, D.; Sengupta, A.K. Arsenic removal from groundwater and its safe containment in a rural environment: Validation of a sustainable approach. *Environ. Sci. Technol.* **2008**, *42*, 4268–4273. [[CrossRef](#)]
29. Li, Z.; Deng, S.; Yu, G.; Huang, J.; Lim, V.C. As (V) and As (III) removal from water by a Ce-Ti oxide adsorbent: Behavior and mechanism. *Chem. Eng. J.* **2010**, *161*, 106–113. [[CrossRef](#)]
30. Jain, A.; Raven, K.P.; Loepert, R.H. Arsenite and arsenate adsorption on ferrihydrite: Surface charge reduction and net OH⁻ release stoichiometry. *Environ. Sci. Technol.* **1999**, *33*, 1179–1184. [[CrossRef](#)]
31. Guo, X.; Du, Y.; Chen, F.; Park, H.S.; Xie, Y. Mechanism of removal of arsenic by bead cellulose loaded with iron oxyhydroxide (β -FeOOH): EXAFS study. *J. Colloid Interface Sci.* **2007**, *314*, 427–433. [[CrossRef](#)]
32. Grossl, P.R.; Eick, M.; Sparks, D.L.; Goldberg, S.; Ainsworth, C.C. Arsenate and chromate retention mechanisms on goethite. 2. Kinetic evaluation using a pressure-jump relaxation technique. *Environ. Sci. Technol.* **1997**, *31*, 321–326. [[CrossRef](#)]
33. Lakshmi pathiraj, P.; Narasimhan, B.R.V.; Prabhakar, S.; Raju Bhaskar, G. Adsorption of arsenate on synthetic goethite from aqueous solutions. *J. Hazard. Mater.* **2006**, *136*, 281–287. [[CrossRef](#)] [[PubMed](#)]
34. Hiemstra, T.; Van Riemsdijk, W.H. Surface structural ion adsorption modeling of competitive binding of oxyanions by metal (hydr)oxides. *J. Colloid Interface Sci.* **1999**, *210*, 182–193. [[CrossRef](#)] [[PubMed](#)]
35. Vatutina, O.M.; Soldatov, V.S.; Sokolova, V.I.; Johann, J.; Bissen, M.; Weissenbacher, A. A new hybrid (polymer/inorganic) fibrous sorbent for arsenic removal from drinking water. *React. Funct. Polym.* **2007**, *67*, 184–201. [[CrossRef](#)]
36. Zhang, W.; Fu, J.; Zhang, G.; Zhang, X. Enhanced arsenate removal by novel Fe-La composite (hydr)oxides synthesized via coprecipitation. *Chem. Eng. J.* **2014**, *251*, 69–79. [[CrossRef](#)]
37. Ohto, K.; Biswas, B.K.; Kawakita, H.; Ghimire, K.N.; Harada, H.; Inoue, K. Effective Removal of Arsenic with Lanthanum(III)- and Cerium(III)-loaded Orange Waste Gels. *Sep. Sci. Technol.* **2008**, *43*, 2144–2165.
38. Yang, H.; Wang, Y.; Bender, J.; Xu, S. Removal of arsenate and chromate by lanthanum-modified granular ceramic material: The critical role of coating temperature. *Sci. Rep.* **2019**, *9*, 1–12. [[CrossRef](#)]
39. Yu, Y.; Zhang, C.; Yang, L.; Paul Chen, J. Cerium oxide modified activated carbon as an efficient and effective adsorbent for rapid uptake of arsenate and arsenite: Material development and study of performance and mechanisms. *Chem. Eng. J.* **2017**, *315*, 630–638. [[CrossRef](#)]
40. Feng, C.; Aldrich, C.; Eksteen, J.J.; Arrigan, D.W.M. Removal of arsenic from alkaline process waters of gold cyanidation by use of γ -Fe₂O₃@ZrO₂ nanosorbents. *Hydrometallurgy* **2017**, *174*, 71–77. [[CrossRef](#)]
41. Tang, W.; Su, Y.; Li, Q.; Gao, S.; Shang, J.K. Mg-doping: A facile approach to impart enhanced arsenic adsorption performance and easy magnetic separation capability to α -Fe₂O₃ nanoadsorbents. *J. Mater. Chem. A* **2013**, *1*, 830–836. [[CrossRef](#)]
42. Akin, I.; Arslan, G.; Tor, A.; Ersoz, M.; Cengeloglu, Y. Arsenic (V) removal from underground water by magnetic nanoparticles synthesized from waste red mud. *J. Hazard. Mater.* **2012**, *235–236*, 62–68. [[CrossRef](#)] [[PubMed](#)]
43. Wang, C.; Luo, H.; Zhang, Z.; Wu, Y.; Zhang, J.; Chen, S. Removal of As (III) and As (V) from aqueous solutions using nanoscale zero valent iron-reduced graphite oxide modified composites. *J. Hazard. Mater.* **2014**, *268*, 124–131. [[CrossRef](#)] [[PubMed](#)]
44. Lenoble, V.; Bouras, O.; Deluchat, V.; Serpaud, B.; Bollinger, J.C. Arsenic adsorption onto pillared clays and iron oxides. *J. Colloid Interface Sci.* **2002**, *255*, 52–58. [[CrossRef](#)] [[PubMed](#)]
45. Lin, S.; Lu, D.; Liu, Z. Removal of arsenic contaminants with magnetic c-Fe₂O₃ nanoparticles. *Chem. Eng. J.* **2012**, *211–212*, 46–52. [[CrossRef](#)]
46. Zhang, Y.; Dou, X.; Yang, M.; He, H.; Jing, C.; Wu, Z. Removal of arsenate from water by using an Fe-Ce oxide adsorbent: Effects of coexistent fluoride and phosphate. *J. Hazard. Mater.* **2010**, *179*, 208–214. [[CrossRef](#)]
47. Zhang, G.; Ren, Z.; Zhang, X.; Chen, J. Nanostructured iron (III)-copper (II) binary oxide: A novel adsorbent for enhanced arsenic removal from aqueous solutions. *Water Res.* **2013**, *47*, 4022–4031. [[CrossRef](#)]



D2

S. Dudek, D. Kołodyńska

Arsenic(V) removal on the lanthanum-modified ion exchanger
with quaternary ammonium groups based on iron oxide, J. Mol.
Liq, 347 (2021) 117985

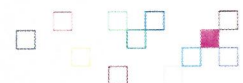
IF: 6,165 Punkty MEiN: 100

Oświadczenie

Oświadczam, że mój udział w pracy:

S. Dudek, D. Kołodyńska, Arsenic(V) removal on the lanthanum-modified ion exchanger with quaternary ammonium groups based on iron oxide, J. Mol. Liq. 347 (2021) 117985

polegał na współtworzeniu jej ogólnej koncepcji, wykonaniu wszystkich eksperymentów, opracowaniu wyników, współudziale w stworzeniu oryginalnego manuskryptu, pełnieniu roli autora korespondencyjnego, współudziale w przygotowywaniu odpowiedzi do recenzentów. Udział ten szacuję na 65%.



OŚWIADCZENIE

Oświadczam, że w pracy:

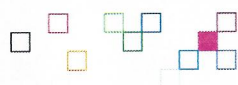
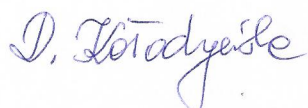
Sebastian Dudek, Dorota Kołodyńska, Arsenic(V) removal on the lanthanum-modified ion exchanger with quaternary ammonium groups based on iron oxide, Journal of Molecular Liquids, 347 (2022) 117985, IF₂₀₂₂ 5,154 pkt, MNiE₂₀₂₂ 100.

mój wkład merytoryczny w przygotowanie, przeprowadzenie i opracowanie badań oraz przedstawienie pracy w formie publikacji to:

opracowanie koncepcji i założeń, analiza i dyskusja uzyskanych wyników, sformułowanie wniosków, współudział w redagowaniu odpowiedzi na uwagi recenzentów.

Swój wkład szacuję na 35%.

Jednocześnie wyrażam zgodę na przedłożenie wyżej wymienionej pracy przez Pana mgr Sebastiana Dudka jako część rozprawy doktorskiej w formie spójnego tematycznie cyklu prac opublikowanych w czasopismach naukowych.



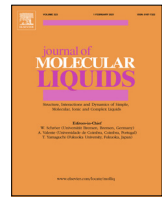


ELSEVIER

Contents lists available at ScienceDirect

Journal of Molecular Liquids

journal homepage: www.elsevier.com/locate/molliq



Arsenic(V) removal on the lanthanum-modified ion exchanger with quaternary ammonium groups based on iron oxide



Sebastian Dudek*, Dorota Kołodyńska

Department of Inorganic Chemistry, Institute of Chemical Sciences, Faculty of Chemistry, Maria Curie-Skłodowska University, Maria Curie-Skłodowska Sq. 2, 20-031 Lublin, Poland

ARTICLE INFO

Article history:

Received 12 September 2021

Revised 20 October 2021

Accepted 26 October 2021

Available online 29 October 2021

Keywords:

Arsenic

Adsorption

Lanthanum

Iron oxides

Ferrix A33E

ABSTRACT

In this study, the commercially available iron oxide sorbent with quaternary ammonium groups was modified with lanthanum(III) ions for removing arsenate(V) from water. Several analyses, such as SEM, N₂ adsorption-desorption method, FTIR and XPS, were employed to characterize the ion exchanger and explore the adsorption of As(V) ions on Ferrix A33E-La(III) (in the abbreviated form A33E-La(III)). The experimental results revealed much better sorption properties of A33E-La(III) than those of unmodified A33E. After the modification, the maximum sorption capacity of the ion exchanger increased by 55% and the percentage removal at various initial As(V) concentrations was higher. According to the results, the As(V) removal was spontaneous and of the exothermic chemisorption type which proceeded due to the formation of monodentate and bidentate inner-sphere complexes as well as lanthanum arsenate by precipitation. Even after 3 cycles of adsorption-desorption A33E-La(III) could be used for arsenic(V) removal with almost the same initial efficiency. It was found that the presence of lanthanum on the surface of the ion exchanger plays a great role in the adsorption of As(V) from the contaminated water due to changing the mechanism of the process.

© 2021 The Author(s). Published by Elsevier B.V. This is an open access article under the CC BY license (<http://creativecommons.org/licenses/by/4.0/>).

1. Introduction

Arsenic contamination of groundwater is a serious global problem. Human and anthropogenic practices are causes of As emissions and include fossil fuel combustion, mining and employing pesticides [1]. Long-term exposure to this element has been linked with skin, lung or liver cancer and may also cause a variety of other non-cancerous effects [2]. Therefore, the World Health Organization (WHO) has set a recommended limit of arsenic in drinking water at 10 µg/dm³ [3]. In order to meet the WHO requirements, a highly effective removal technique should be developed.

Several methods, such as precipitation, oxidation, coagulation, ion exchange, adsorption, and membrane filtration have been elaborated for arsenic removal from water [4]. Some of these technologies such as precipitation using iron or aluminium salts are not sufficient to meet drinking water requirements. The others are simply expensive or too complicated to handle. The adsorption process seems to be the most encouraging method among available technologies and has been widely used for arsenate(V) removal because of its convenient operation, low cost and high efficiency.

Different materials have already been designed for the sorption of arsenate(V) from wastewater. Many adsorbents employed for water treatment include iron oxides which have been one of the most often used adsorbents characterized by strong affinity for arsenic(V) species [5–7]. In recent years considerable work has been done on developing novel composite materials containing binary iron-metal oxides like iron-manganese [8], iron-titanium [9], iron-zirconium [10] or iron-cobalt [11]. These composites are very often characterized by higher adsorption capacity towards arsenic than their single components. Of great interest are the components in the form of rare earth metals that exhibit a great number of coordination sites and can offer specific affinity.

Among the rare earth elements, lanthanum is comparatively abundant and inexpensive. Therefore many papers about lanthanum-based sorbents have been written over the last decade [12–14]. However, there were few papers in the literature related to the removal of arsenic(V) by such sorbents [15–17]. In this study, the commercially available ion exchanger Ferrix A33E was modified with lanthanum(III) ions. There is no literature data dealing with the La-modification of an iron oxide sorbent with quaternary ammonium groups in the context of arsenic(V) removal. The main novelty is the description of the sorption process of arsenate(V) ions on the obtained through such a modification material A33E-La(III). The La-modified iron oxide ion exchanger, in which quaternary ammonium groups are additionally involved in the

* Corresponding author.

E-mail address: sebastian.dudek@mail.umcs.pl (S. Dudek).

process, has not been described in the literature so far. The main aims of this study were (1) modification of Ferrix A33E with La(III) ions and characterization of novel composite material with various techniques, (2) description of the As(V) ions adsorption process including sorption kinetics, equilibrium, effect of pH and temperature as well as regeneration, (3) comparison of sorption properties of the modified material with the unmodified one and evaluation of its application in the industrial process.

2. Materials and methods

2.1. Sorbent modification and characterization

In order to carry out the modification process with lanthanum(III) ions, the commercially available strong base anion exchanger Ferrix A33E (Purolite, USA) was used. The short characteristics of the sorbent is presented in Table S1. The modification process included two stages: (1) adsorption of lanthanum(III) ions (shaking time 6 h, initial concentration 100 mg/dm³, pH 4), (2) decanting the solution from above the sorbent, washing it with distilled water and then drying at 333 K for 24 h. La(III) solution at the concentration 100 mg/dm³ was prepared by dissolving lanthanum oxide La₂O₃ (Specpure JMC, England) first in the diluted (1 mol/dm³) and next in the concentrated nitric acid. The La(III) concentration was measured by means of the inductively coupled plasma optical emission spectrometer ICP-OES (720 ES, Varian, USA). In order to adjust pH a proper volume of 1 mol/dm³ NaOH solution was added and the pH was measured by the use of pH meter PHM82 (Radiometer, Copenhagen).

The surface morphology, including surface structures, was described by means of the scanning electron microscopy (SEM) (Tescan, Czech Republic) with an extended depth of field (EDF) function. The SEM images of the unmodified and modified A33E were compared. The images of A33E-La(III) surface after the sorption of As(V) ions were also taken.

The point of zero charge (pH_{PZC}) of A33E-La(III) was measured by the pH drift method [18] and the obtained value was compared to that of the unmodified ion exchanger. In 100 cm³ conical flasks 20 cm³ of 0.1 M NaCl solutions with a pH of 2 to 11 (pH₀) was prepared. 0.1 g of the sorbent was added to each flask, then shaken for 6 h and the pH of the solutions was measured (pH₁). The point of zero charge pH_{PZC} was determined from the plot pH₁-pH₀ vs. pH₀. The pH_{PZC} is the point where pH₁-pH₀ is equal to 0.

The textural properties of A33E, A33E-La(III) and A33E-La(III) after the As(V) adsorption were characterized by nitrogen adsorption/desorption isotherms at 77 K (ASAP 2405, Micromeritics, USA) after the preliminary degassing of the samples at strictly controlled temperature. The specific surface area was determined by the Brunauer, Emmett and Teller (BET) method. Moreover, the total pore volumes and the average pore diameters were found according to the Barret-Joyner-Halenda model.

The Fourier transform infrared spectroscopy (FTIR) analysis of A33E and A33E-La(III) was performed before and after the arsenate ions adsorption to detect the chemical bonds based on the studied samples (Cary 630 FTIR spectrometer, Agilent Technologies, USA). The device offered the wavelengths in the range 4000–650 cm⁻¹.

Additionally, in order to study the functional groups, composition and valence state of the elements contained in both ion exchangers after the As(V) ions sorption, the X-ray photoelectron spectroscopy XPS was employed (Prevac, Poland).

2.2. Batch experiments

All batch adsorption experiments were conducted in 100 cm³ flasks. In order to study the effect of pH on the As(V) adsorption

efficiency, the A33E-La(III) samples of 0.1 g were added into the flasks containing 20 cm³ solution with the pH values ranging from 4 to 11 and the constant arsenate(V) concentration equal to 100 mg/dm³. The pH solutions were adjusted to the eligible values by adding proper amounts of 0.01 M NaOH or 0.01 M HCl, and the flasks were shaken using the laboratory shaker Elpin + type 357 (Elpin Plus, Poland) for 6 h. The adsorbent was separated from the solution by filtration. Then the concentration of As(V) ions in the form of complexes with ammonium molybdate was analyzed by the spectrophotometric method (Cary 60, Agilent Technologies) at the wavelength 870 nm. The adsorption capacity of arsenate(V) was calculated using Equation (1):

$$q_t = (c_0 - c_t) \times \frac{V}{m} \quad (1)$$

where: q_t is the amount of arsenate(V) adsorbed at time t (mg/g), c₀ is the initial concentration of arsenate in the solution (mg/dm³), c_t is the concentration of arsenate in the solution after time t (mg/dm³), V is the volume of the solution containing arsenate ions (dm³), m is the mass of sorbent (g).

Moreover, the percentage of sorption was calculated from Equation (2):

$$\%S = \frac{(c_0 - c_t)}{c_0} \times 100\% \quad (2)$$

For kinetic experiments, the 0.1 g portions of adsorbent were added into the 100 cm³ conical flasks containing 20 cm³ solutions with the constant As(V) concentrations (25, 50 and 100 mg/dm³) and pH 6. For each concentration, the samples were shaken for 1, 3, 5, 7, 10, 20, 30, 60, 120, 240 and 360 min (pH 6, temperature 295 K, shaking speed 180 rpm). Moreover, the pseudo-first order (PFO), pseudo-second order (PSO), Elovich and intraparticle diffusion (IPD) models were employed to prefigure the adsorbent-adsorbate interactions. The suitability of the models was assessed by the error level – correlation coefficient (*R*²) and the sum of squared errors (SSE) [19]. The sorption properties of A33E-La(III) were also compared with those of the unmodified ion exchanger. The extremely popular and commonly used models are the PFO and PSO ones, whose mathematical representation is expressed by Equations (3) and (4) [20]:

$$\frac{dq_t}{dt} = k_1(q_e - q_t) \quad (3)$$

$$\frac{dq_t}{dt} = k_2(q_e - q_t)^2 \quad (4)$$

where: q_t is the amount of As(V) adsorbed onto the adsorbent at time t (mg/g), q_e is the equilibrium adsorption capacity (mg/g), k₁ is the PFO rate constant (1/min), and k₂ is the PSO rate constant (g/(mg·min)).

The above-mentioned equations can be presented in their linear forms according to Equations (5) and (6) [21,22]:

$$\ln(q_e - q_t) = \ln q_e - k_1 t \quad (5)$$

$$\frac{t}{q_t} = \frac{1}{k_2 q_e^2} + \frac{t}{q_e} \quad (6)$$

To learn more about the chemical nature of adsorption, the Elovich model, represented by non-linear and linear Equations (7) and (8), was utilized [23]:

$$\frac{dq_t}{dt} = \alpha e^{-\beta q_t} \quad (7)$$

$$q_t = \frac{1}{\beta} \ln(\alpha\beta) + \frac{1}{\beta} \ln t \quad (8)$$

where: α is the initial adsorption rate ($\text{mg}/(\text{g}\cdot\text{min})$), and β is associated with the surface coverage and activation energy of chemisorption (g/mg).

To examine the rate limiting step during adsorption the IPD model, represented by Equation (9), was applied [24]:

$$q_t = k_i \sqrt{t} + C \quad (9)$$

where: k_i is the IPD rate constant and C is the boundary layer thickness.

The utilized calculations connected with kinetic models are presented in Table S2 [25].

The adsorption capacity of A33E-La(III) towards arsenic(V) ions was evaluated by the equilibrium adsorption isotherm study. The same study was carried out for A33E to compare the results. The initial concentrations of As(V) ions were equal to 25, 50, 100, 150, 300, 500 and 1000 mg/dm^3 (time 6 h, shaking speed 180 rpm, temperature 295 K). The assessment of the data fit to the theoretical models (Langmuir, Freundlich, Dubinin-Radushkevich and Halsey) was performed using the linear regression analysis as well as the sum of squared errors (SSE) and F-Test.

The Langmuir model, which assumes monolayer adsorption on the adsorbent active sites, is expressed by non-linear Equation (10) [26]:

$$\frac{c_e}{q_e} = \frac{1}{q_m K_L} + \frac{c_e}{q_m} \quad (10)$$

where: c_e is the equilibrium concentration of adsorbate (mg/g), q_e is the amount of adsorbate at equilibrium (mg/g), q_m (g/mg) and K_L (dm^3/mg) are the Langmuir constants which were calculated from the slope and intercept of the linear plot c_e/q_e vs c_e .

For the linear form of the Freundlich isotherm it is as follows (Equation (11)) [27]:

$$\log q_e = \log K_F + \frac{1}{n} \log c_e \quad (11)$$

where: K_F (mg/g) and n (-) are the constants which were determined from the slope and intercept of the linear plot $\log q_e$ vs $\log c_e$.

The Dubinin-Radushkevich isotherm is expressed as follows (Equations 12–14) [28,29]:

$$\ln q_e = \ln q_{DR} - \beta \varepsilon^2 \quad (12)$$

$$\varepsilon = RT \ln \left(1 + \frac{1}{c_e} \right) \quad (13)$$

$$E = \frac{1}{\sqrt{2\beta}} \quad (14)$$

where: q_{DR} (mol/g) is the theoretical Dubinin-Radushkevich adsorption capacity of metal ions, β (mol^2/J^2) is the isotherm constant related to the average free energy of adsorption, ε represents the Polanyi potential, R (8.314 J/K/mol) is the universal gas constant, T (K) is the absolute temperature, E (J/mol) represents the average free energy change.

The Halsey model is presented below (Equation (15)) [30]:

$$\ln q_e = \frac{1}{n_H} \ln K_H - \frac{1}{n_H} \ln \frac{1}{c_e} \quad (15)$$

where: K_H and n_H are the Halsey constants which were calculated from the slope and intercept of the linear plot $\ln q_e$ vs $\ln c_e$.

Moreover, to determine thermodynamic parameters, the temperature effect (295, 313 and 333 K) on the As(V) adsorption capacity of A33E-La(III) was examined. That study was carried out in the same way as the equilibrium test, but additionally at the temperature of 313 and 333 K. There were used the following expressions (Equations 16–18) [31]:

$$K_d = \frac{q_e}{c_e} \quad (16)$$

$$\Delta G^0 = -RT \ln K_d \quad (17)$$

$$\ln K_d = -\frac{\Delta H^0}{RT} + \frac{\Delta S^0}{R} \quad (18)$$

where: K_d (dm^3/g) is the distribution coefficient based on the experimental data, ΔG^0 (kJ/mol) is the change of Gibbs energy, ΔH^0 (kJ/mol) is the change of enthalpy and ΔS^0 ($\text{kJ/mol}\cdot\text{K}$) represents the entropy.

Three consecutive adsorption–desorption cycles were conducted to evaluate the reusability of A33E-La(III). 0.05 M, 0.2 M and 1 M NaOH solutions were used as desorbing agents in the first cycle as the preliminary step. 1 M NaOH was chosen as the most powerful regenerant for further study. After the As(V) adsorption, the adsorbent separated by filtration was gently rinsed with deionised water, immersed again in 20 cm^3 of regenerator (1 M NaOH) and shaken for 6 h.

3. Results and discussion

3.1. Sorbent characterization

The SEM analysis revealed the surface morphology of A33E-La(III) and made it possible to compare it with the pure ion exchanger (Fig. 1). The surface of A33E-La(III) was heterogeneous, full of flake-like nanoparticles of lanthanum (hydr)oxide while the surface of the raw sorbent was smooth and homogeneous. The size of the nanoflakes varied from about one to almost twenty three hundred nanometers (Fig. 2). The average diameter of the nanoflakes was approximately 800 nm. Similar results were obtained by Wu et al. [32] in the SEM image of Mg/Fe/La hydrotalcite-like compound (Mg/Fe/La HLC). The morphology was dominated by plate-like structures with visible edges. Similar micrometer scale structures were observed on the surface of the lanthanum-modified ceramic materials obtained by Yang et al. [33]. Such a morphology could facilitate adsorption onto A33E-La(III) for As(V) ions. Therefore, the SEM analysis of A33E-La(III) after the As(V) adsorption was made. The results indicated that the arsenate(V) adsorption had an evident effect on the morphology of the modified A33E-La(III) [34]. Many slits and empty spaces were filled with the adsorbate resulting in the surface heterogeneity reduction.

The point of zero charge (pH_{PZC}) was equal to 8.29 for A33E and after the lanthanum modification this value dropped to 7.71 (Figure S1). The concentrations of As(V) species are pH-dependent: the acid dissociation constants pKa_1 , pKa_2 , and pKa_3 for arsenate (V) are 2.2, 7.08, and 11.5, respectively [35]. Consequently, at the pH of municipal water it occurs as H_2AsO_4^- and HAsO_4^{2-} anions. At the pH below 7.71 the positive surface charge of A33E-La(III) facilitates the interactions with the above mentioned arsenic ions through electrostatic attraction improving the arsenate sorption capacity. The other adsorbents based on lanthanum and iron oxides showed very similar pH_{PZC} . For instance magnetic $\text{La(OH)}_3/\text{Fe}_3\text{O}_4$ (La-to-Fe mass ratio of 4:1) had pH_{PZC} of 7.9 [14] while for the Fe-La composite (La-to-Fe molar ratio of 1:1) this was equal to 7.8 [17].

The obtained N_2 adsorption/desorption isotherms were classified as type IV according to the IUPAC classification (Fig. 3).

Those suggested that both materials were characterized by a mesoporous structure. On both N_2 adsorption/desorption isotherms of A33E and A33E-La(III) the hysteresis loops occurred. The shape of the hysteresis loop and the texture of mesoporous material are commonly accepted to be correlated. The isotherms revealed H3 type of hysteresis for both ion exchangers [36]. These

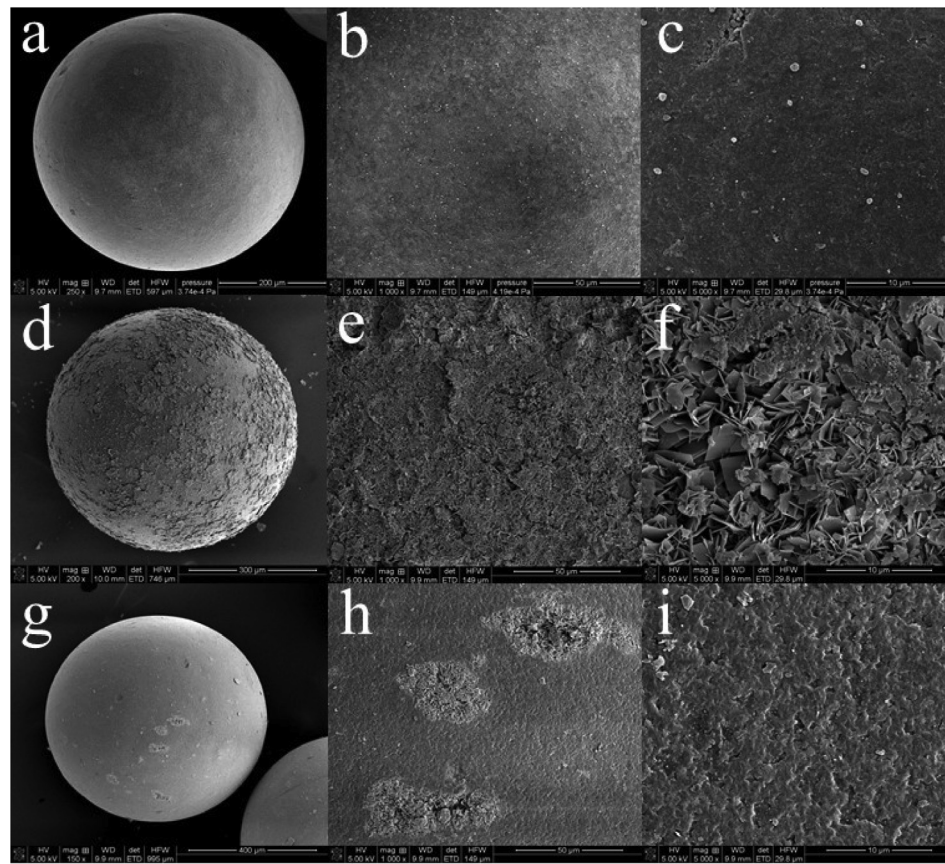


Fig. 1. SEM images of A33E (a-c) and A33E-La(III) before (d-f) and after the adsorption of As(V) ions (g-i). The magnification powers were 150 \times (g), 200 \times (d), 250 \times (a), 1000 \times (b, e, h) and 5000 \times (c, f, i).

materials have slit-shaped pores and do not show any limiting adsorption at high p/p_0 values which can be observed for the non-rigid aggregates of plate-like particles [37]. Moreover, the specific surface areas, total pore volumes and average pore diameters of the ion exchangers were determined. As shown in Table S3, the specific surface area, total pore volume and average pore diameter of A33E were 53.12 m²/g, 0.122 cm³/g and 9.18 nm while those of A33E-La(III) were 59.39 m²/g, 0.127 cm³/g and 8.53 nm, respectively. The surface area and the total pore volume increased after the La(III) modification. This was confirmed by the SEM images in which the surface of the ion exchanger became more heterogeneous. As mentioned previously, the SEM analysis revealed that the As(V) adsorption on such an ion exchanger caused decrease in heterogeneity. The N₂ adsorption/desorption analysis confirmed such a phenomenon resulting in drop of specific surface area and total pore volume. The drop of specific surface area from 59.39 to 56.04 m²/g was observed. Regarding the total pore volume its value decreased from 0.127 to 0.124 cm³/g. Type IV of all isotherms and the average pore diameters ranging from 8.53 to 9.18 nm indicated that the materials were mesoporous.

The FTIR study of A33E (Figure S2) and A33E-La(III) (Figure S3) was carried out before and after the As(V) sorption. In both spectra in the range of 3600–3200 cm⁻¹ wide bands associated with the vibrations of O-H stretching were present due to water physisorption [38]. The peaks at 1638 and 1481 cm⁻¹ were assigned to the deformation vibrations of water molecules and quaternary amine group -NR₄⁺, respectively in each spectrum. In Figure S3 at 920 cm⁻¹ deformed inclinations showing the combination bands of La-O appeared as fundamental vibrational modes which were also present in the lanthanum-impregnated mesoporous silica

SBA-15 [39]. In the A33E-As(V) spectrum the strong peak at 825 cm⁻¹ appeared which was recognized as O-As stretching vibrations of As(V) which indicated formation of the inner-sphere bonds [40,41]. As(V) ions were successfully adsorbed on the surface of A33E. In the case of A33E-La(III), the intensity of the peak was significantly smaller which suggested a slightly different As (V) sorption mechanism. As shown in Figure S3 the band of O-H connected with the stretching vibration (in the range 3600–3200 cm⁻¹) was significantly reduced due to the arsenate(V) ions adsorption. Regarding the way in which As(V) ions retained on the A33E-La(III) surface, the possible mechanism was lanthanum arsenate precipitation [15]. For the lanthanum arsenate, the authors assigned the band at 853 cm⁻¹ to the vibration band of As – O, however, the band at 445 cm⁻¹ was attributed to the La–O coordination between the lanthanum active sites and the oxygen atom of arsenate(V). These two peaks were the characteristic vibration bands of lanthanum arsenate. In this study the band at 889 cm⁻¹ overlapped that at 853 cm⁻¹ and the wavelength range offered by the device was from 4000 to 650 cm⁻¹. Therefore those peaks could not be seen in Figure S3, but there was a great probability that the mechanism was practically identical.

The XPS spectra of A33E and A33E-La(III) (Figure S4) were collected to study the valence state and composition of the elements contained in both ion exchangers after the sorption of As(V) ions. As shown in Tables S4 and S5 the main forms of carbon were C = C, C-H, C-C. C = C, C-H and C-C bonds in the polymer structure i.e. polystyrene cross-linked with divinylbenzene. There was also nitrogen bonded carbon mainly as the quaternary ammonium group [42]. The sorbent impregnation with iron oxides was confirmed by the presence of iron primarily at +3 oxidation state.

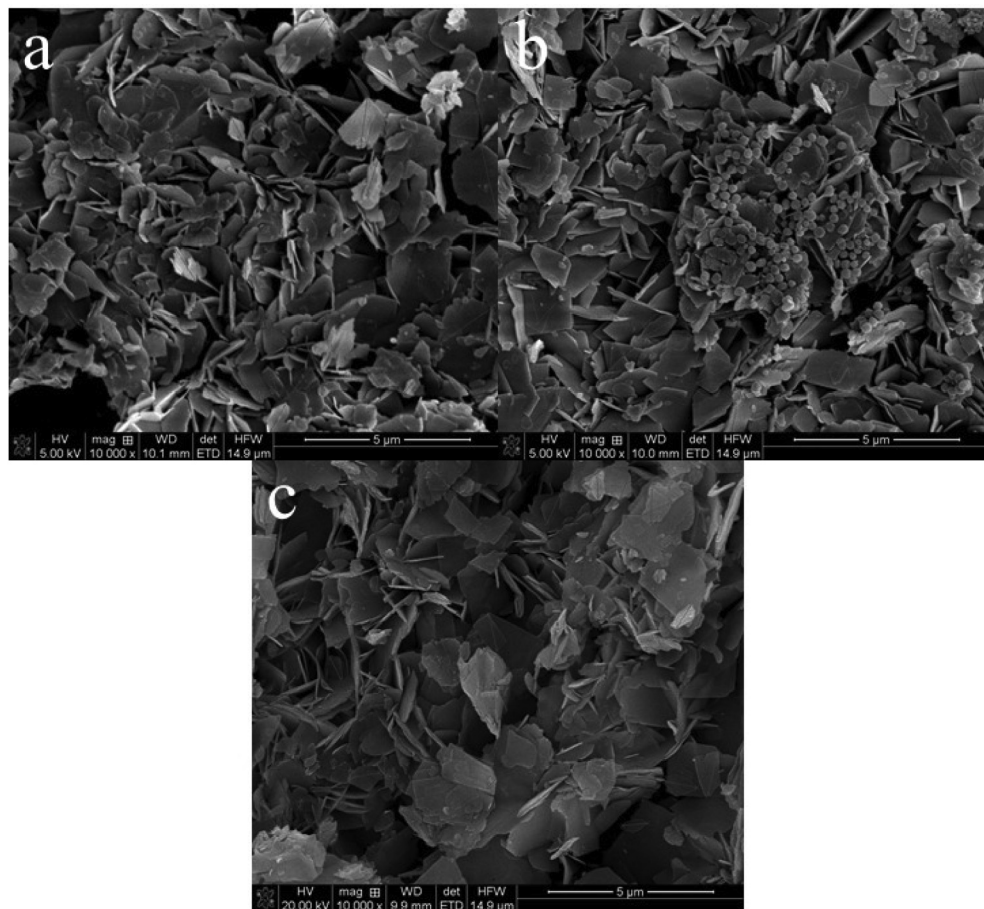


Fig. 2. The size of the nanoflates on the A33E-La(III) surface measured with the magnification power 10 000 × (a-c).

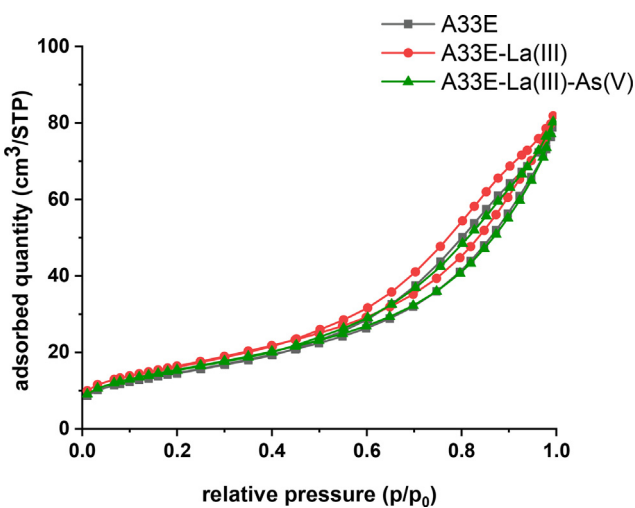


Fig. 3. N₂ adsorption/desorption isotherms of A33E (black), A33E-La(III) (red) and A33E-La(III)-As(V) (green). (For interpretation of the references to colour in this figure legend, the reader is referred to the web version of this article.)

After the modification the new peaks (835.6, 837.6 and 839.4 eV) appeared which indicated evidently the presence of lanthanum (III) on the surface of A33E-La(III). The peaks in the range of 44.4 to 46.2 eV confirm the successful adsorption of arsenate(V) ions. Most As(V) ions did not change their oxidation state, however, 45.1% and 38.8% of As(V) were reduced to As(III) on the surface of A33E and A33E-La(III), respectively. Interestingly, that was

slightly different behaviour of arsenic(V) in comparison to Fe/La composite (hydr)oxides, on the surface of which no reduction took place. As(V) still remained the same [17]. The difference in behaviour was due to the fact that in this study X-rays reduced the adsorbed arsenate(V) ions in contrast to the Zhang's paper. Han et al. observed the same phenomenon during the X-ray absorption spectroscopy (XAS) measurements of arsenic species immobilized by poorly crystallized mackinawite FeS [43]. Surface-complexed As(V) was photocatalytically reduced.

Fig. 4 shows the XPS spectra of As, N and Fe regions after the As (V) sorption on A33E (**Fig. 4 a, c, e**) and A33E-La(III) (**Fig. 4 b, d, f**). The peak shifts in these regions suggest that the arsenic sorption mechanism on A33E-La(III) was different from that on the pure ion exchanger which was also confirmed by the FTIR analysis. Of great interest was the presence of a peak derived from the nitro groups -NO₂ that did not appear on the pure sorbent after the As (V) adsorption. This was certainly due to the presence of adsorbed lanthanum(III) ions and the oxidation of part of the quaternary ammonium groups.

3.2. Effect of pH

Suitable solution pH is of crucial importance for adsorption capacity of many ion exchangers. It determines strongly the chemical speciation of adsorbates as well as the surface charge of adsorbents [44,45]. Depending on pH, four dominant forms of arsenate (V) in the aqueous solution occur. In a strongly acidic environment undissociated arsenic acid H₃AsO₄ predominates while in the strongly basic solutions AsO₄³⁻ ions are present. In the pH ranges

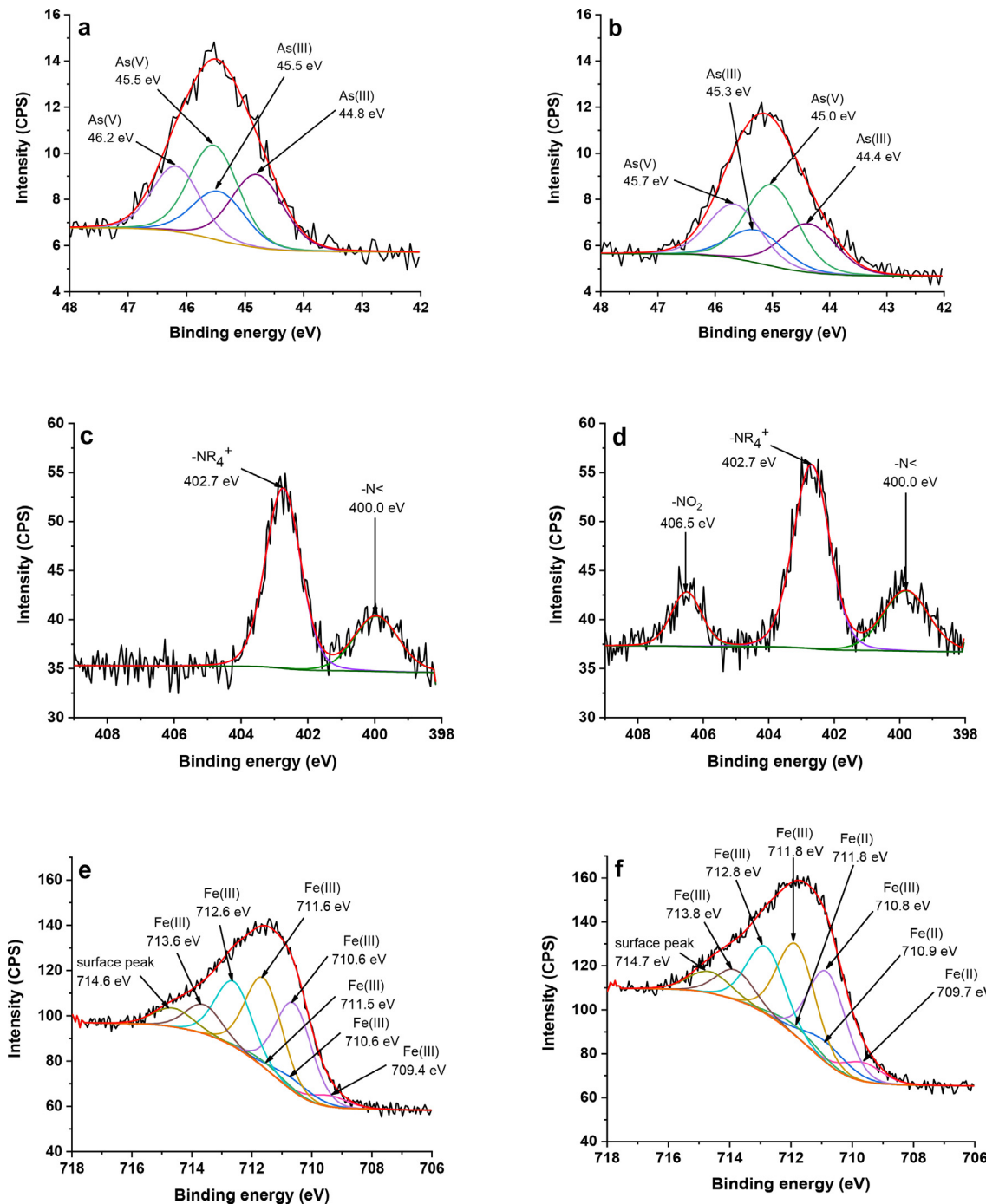


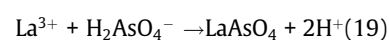
Fig. 4. A33E-As(V) high-resolution spectra of the As 3d (a), N 1 s (c), Fe 2p (e) and A33E-La(III)-As(V) high-resolution spectra of As 3d (b), N 1 s (d), Fe 2p (f).

of 2.2–6.9 and 6.9–11.5 the main arsenate species are H_2AsO_4^- and HAsO_4^{2-} , respectively [46]. For further studies on the As(V) adsorption on A33E-La(III), the process was conducted in the range of initial pH from 4 to 11. Hence, the main forms of arsenate species were H_2AsO_4^- and HAsO_4^{2-} anions at any given pH in this study.

A33E-La(III) reached the largest arsenic(V) removal (92.7%) and sorption capacity (q_e 18.54 mg/g) at pH 6 (Fig. 5).

It could be observed that the sorption capacity was increasing from pH 4 to 6. However, further rise in the pH value reduced clearly the adsorbent performance and the removal percentage dropped from 92.7% to 75.4% at pH 11.

The arsenate removal was obtained by both adsorption and precipitation [17]. At optimal pH 6 the surface of A33E-La(III) gained positive charge due to the protonation of iron oxide hydroxyl groups. Therefore, H_2AsO_4^- ions were adsorbed through the formation of inner-sphere monodentate or bidentate complexes. What is more, under such conditions lanthanum could be leached from A33E-La(III) and exist as La(III) ions in the solution. These species react readily with H_2AsO_4^- forming the lanthanum arsenate precipitate (Equation 19):



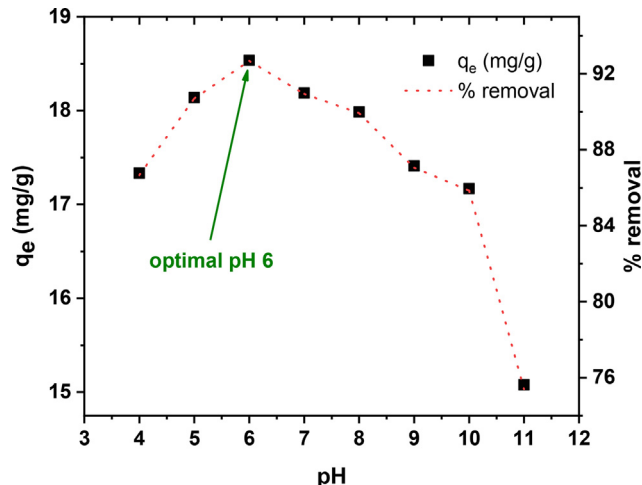


Fig. 5. Effect of pH on adsorption of As(V) ions on A33E-La(III) ($c_0 = 100 \text{ mg/dm}^3$, pH range 4–11, mass 0.1 g, time 360 min; temperature 295 K, shaking speed 180 rpm).

Moreover, positively charged quaternary ammonium groups enhanced electrostatic attractions of As(V) ions to the ion exchanger surface [47]. Above pH 7.71 (pH_{PZC}) the surface of A33E-La(III) was charged negatively, so electrostatic repulsions of the negative HAsO₄²⁻ anions occurred [48]. However, the adsorption could proceed due to the inner-sphere complexation with lanthanum hydroxide according to Equation 20 [14,16]:



Considering the above facts, pH 6 was chosen as the optimal value for further studies.

3.3. Kinetic studies

The kinetic studies of adsorption are important to explain the mechanism and gain information about the rate of adsorbate transfer from the aqueous environment to the adsorbent surface. It allows to predict the minimum time needed for the removal of impurities. Therefore the influence of initial As(V) concentration and time on adsorption capacity of A33E-La(III) was studied.

This study revealed that equilibrium was attained relatively quickly, i.e. about 60 min at all tested initial As(V) concentrations (Fig. 6). After 1 h no significant change in adsorption capacity was noticed. At the initial arsenate(V) concentrations 25, 50 and 100 mg/dm³ the sorption capacities were equal to 4.98, 9.51 and 18.54 mg/g, respectively (Table 1). Those values corresponded to 99.6, 95.1 and 92.7% of arsenic(V) removal. According to the results, a decrease in the efficiency of arsenic adsorption with an increase in its concentration was observed. Nevertheless, at such high adsorbate concentrations, the adsorption efficiency above 90% was an excellent result.

Comparing PFO and PSO kinetic models, it was found that at any given initial As(V) concentration the best fit of the experimental data was found for the latter. That was confirmed by the higher correlation coefficients R^2 and the lower values of SSE (Table 1). It is worth noting that the correlation coefficients R^2 were equal to 1. Moreover, the experimental q_e values are almost identical to the calculated ones q_2 . The PSO plots t/q_t vs t are presented in Figure S5. That suggests that the kinetic mechanism can be described by the PSO model which assumes that the sorption process is chemisorption. Ho explained that removal efficiency depends on the existing active sites on the adsorbent [22].

As the As(V) adsorption was a chemisorption process and the A33E-La(III) surface was heterogeneous, the Elovich model was

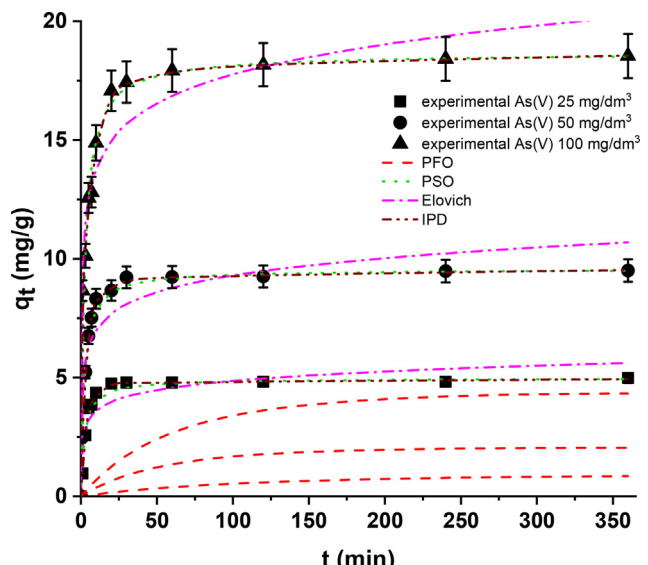


Fig. 6. Kinetics of As(V) adsorption onto A33E-La(III) with the fitted models of PFO, PSO, Elovich and IPD ($c_0 = 25, 50$ and 100 mg/dm^3 , pH = 6, shaking speed 180 rpm, temperature 295 K).

used [31]. It was found that the parameter α was increasing with the growing arsenate(V) initial concentration. This indicates that the initial adsorption rate was also increasing. Hence, it could be stated that the increasing initial concentration will lead to a decrease in the accessible adsorption surface. Indeed, the β constant decreased inversely proportional to the initial concentration. The Elovich plots q_t vs $\ln t$ are presented in Figure S6.

The IPD model could also help to find out the sorption mechanism. The multilinear plot q_t vs $t^{1/2}$ (Fig. 7) revealed that three diffusion steps were involved in this process.

The C_i constants are not zero, thus indicating that none of the straight lines pass through the origin. Hence, the intraparticle diffusion was not the only rate limiting step during the adsorption process but also other kinetic mechanisms could be involved [16]. The first stage was connected with the fast diffusion of As(V) ions from the bulk fluid phase to the external surface of A33E-La(III). The second one was associated with the intraparticle diffusion process which limited the reaction rate (the plot flattening) [11]. As the concentration of As(V) ions decreased significantly, the final step based on chemisorption took place [49]. The system reached equilibrium. At any given As(V) initial concentration the rate constants decreased in the series $k_{i1} > k_{i2} > k_{i3}$.

These results suggest that the chemisorption was dominant in the As(V) adsorption process, indicating the phenomena of electron sharing or exchange between the binding sites of the ion exchanger and the molecules of arsenic species. It can also be stated that adsorption variety was caused by the diffusion mechanism and rate-controlling step. As a consequence, our findings show that the larger specific surface area of A33E-La(III) than A33E makes it more conducive to diffusion, resulting in a diversity of rapid adsorption kinetics [50].

The influence of the initial concentration and the phase contact time on the sorption properties of A33E-La(III) and A33E was also compared. As can be seen in Fig. 8, in both cases the sorption capacities increased and the removal efficiency decreased with the increasing initial concentration.

The time needed to reach equilibrium on the modified and unmodified ion exchangers was almost the same – 60 min at the initial As(V) concentrations 25, 50 mg/dm³ and 120 min at 100 mg/dm³. However, it was found that the A33E-La(III) equilibrium sorption capacities q_e were higher than those of A33E. The

Table 1

Kinetic parameters calculated using the models: the pseudo-first order (PFO), the pseudo-second order (PSO), the Elovich and the intraparticle diffusion (IPD) for As(V) ions on A33E-La(III) at the concentrations 25, 50 and 100 mg/dm³. The sums of square errors were also presented for each kinetic model.

Model	Parameter	As(V) 25 mg/dm ³	As(V) 50 mg/dm ³	As(V) 100 mg/dm ³
PFO	q_e (mg/g)	4.98	9.51	18.54
	q_1 (mg/g)	0.88	2.05	4.34
	k_1 (1/min)	0.010	0.019	0.017
	R^2	0.3959	0.7830	0.7898
	SSE	165.55	551.32	2006.49
PSO	q_2 (mg/g)	4.97	9.56	18.63
	k_2 (g/mg·min)	0.085	0.049	0.023
	R^2	0.9997	1.0000	1.0000
	SSE	0.70	0.77	11.17
Elovich	α (mg/g·min)	36.58	95.89	418.05
	β (g/mg)	1.79	0.98	0.56
	R^2	0.7020	0.7560	0.8715
	SSE	4.64	11.93	16.39
IPD	k_{i1} (mg/g·min ^{-1/2})	2.223	3.104	2.881
	C_1 (mg/g)	-1.264	-0.413	5.597
	R^2	0.9999	0.9839	0.9696
	k_{i2} (mg/g·min ^{-1/2})	0.452	0.385	0.253
	C_2 (mg/g)	2.773	7.051	15.987
	R^2	0.9041	0.9583	0.9814
	k_{i3} (mg/g·min ^{-1/2})	0.012	0.028	0.046
	C_3 (mg/g)	4.694	8.996	17.678
	R^2	0.7169	0.9094	0.9867
	SSE	0.05	0.26	0.73

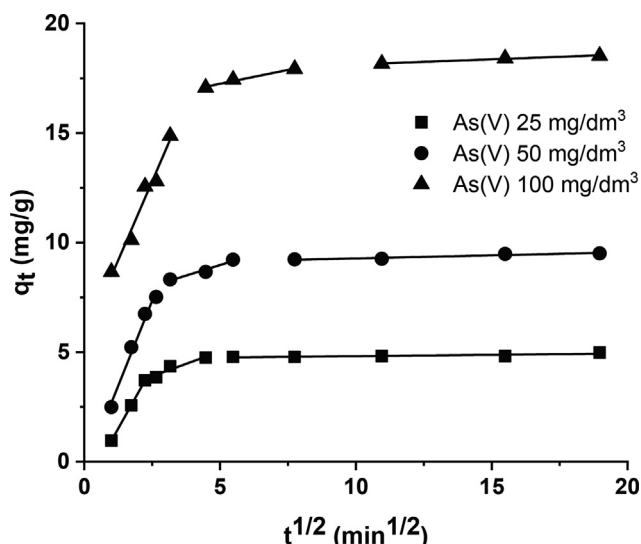


Fig. 7. IPD kinetic plots for As(V) adsorption onto A33E-La(III) (various As(V) initial concentrations).

difference was more noticeable as the initial concentration of arsenate(V) ions increased. For instance, at 100 mg As(V)/dm³ the sorption capacity of A33E was equal to 17.16 mg/g (removal efficiency 85.8%), while for A33E-La(III) that value was 18.54 mg/g (removal efficiency 92.7%). The above-mentioned information indicated that A33E-La(III) was characterized by better sorption capacities and not worse equilibrium time than A33E.

3.4. Adsorption equilibrium isotherms

The influence of the initial solution concentration on the As(V) adsorption capacity was studied. It was found that the As(V) adsorption capacity increased with an increase in the initial solution concentration. To understand the adsorption behaviour of arsenate(V) ions on A33E-La(III), the experimental data were analyzed using four isotherm models (Langmuir, Freundlich, Dubinin-Radushkevich and Halsey),

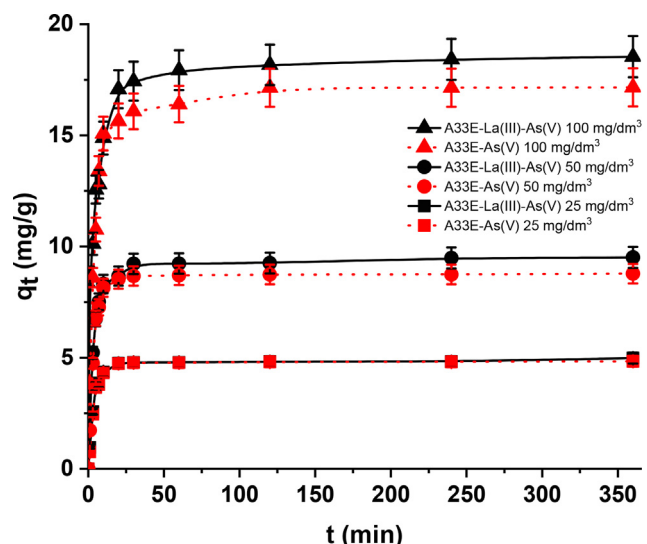


Fig. 8. Comparison of time and initial concentration effects on the As(V) adsorption onto A33E-La(III) (black) and A33E (red). (For interpretation of the references to colour in this figure legend, the reader is referred to the web version of this article.)

All linear plots of the Langmuir, Freundlich, Dubinin-Radushkevich and Halsey isotherm models are presented in Fig. 9.

As shown in Table 2, it was found that the correlation coefficient (R^2) was equal to 0.992, suggesting that the experimental data fitted the Langmuir isotherm equation well. The calculated maximum sorption capacity q_m 54.64 mg/g was very similar to the experimental one $q_{e,\text{exp}}$ 53.33 mg/g. Interestingly, the experimental maximum sorption capacity of the unmodified A33E was only 34.41 mg/g. The comparison of the maximum sorption capacities of various sorbents is presented in Table 3. The other characteristics of the Langmuir isotherm can be expressed by the dimensionless separation factor R_L (Equation (21)) [51]:

$$R_L = \frac{1}{1 + K_L C_0} \quad (21)$$

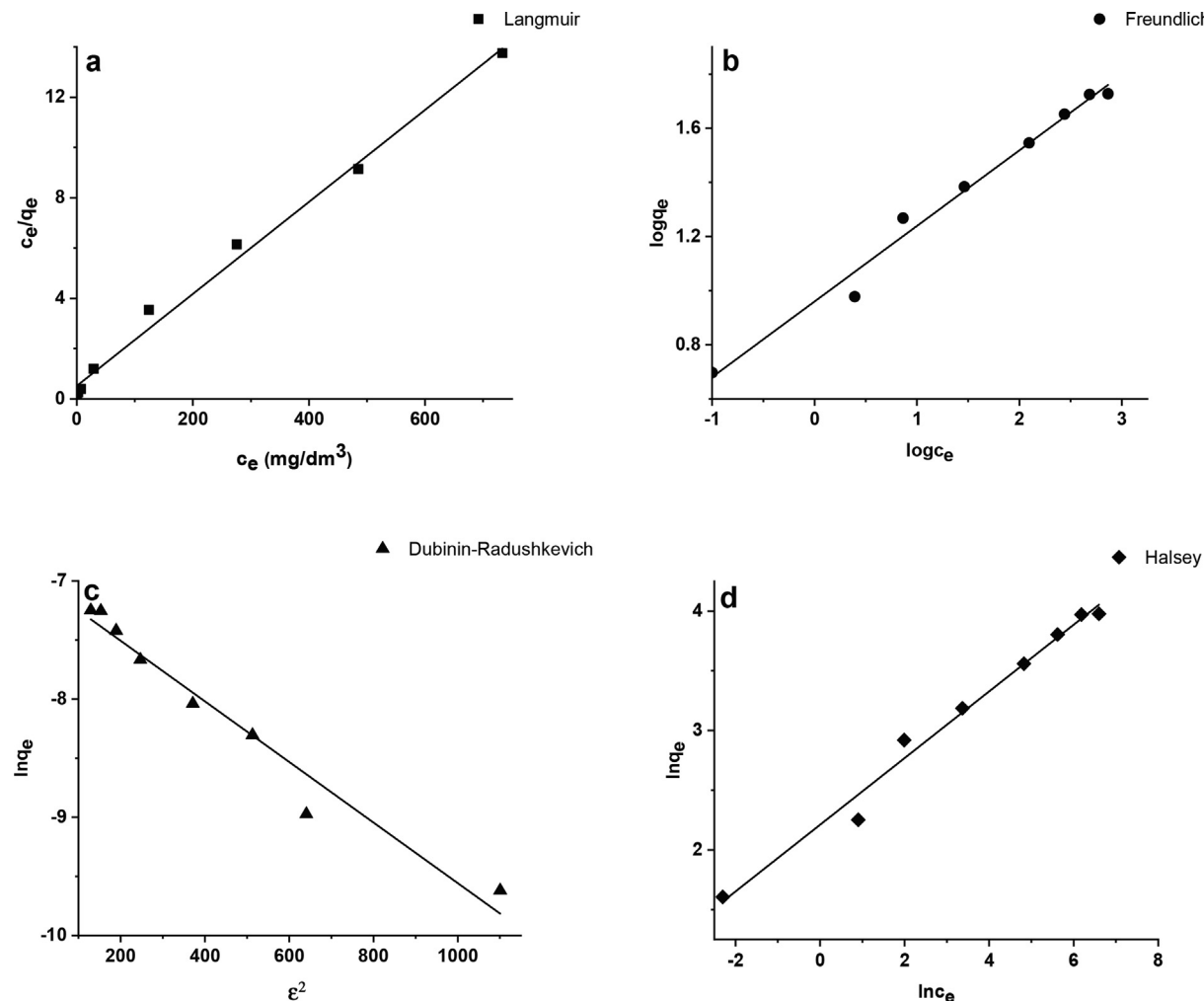


Fig. 9. Linear plots of the Langmuir (a), Freundlich (b), Dubinin-Radushkevich (c) and Halsey (d) isotherm models for As(V) adsorption onto A33E-La(III).

R_L parameter indicates the process to be irreversible when $R_L = 0$, favourable when $0 < R_L < 1$, linear when $R_L = 1$ and unfavourable when R_L greater than 1 [34]. In this study, the measured R_L value (0.530) indicated the favourable adsorption of As(V) ions onto A33E-La(III).

The value of the linear regression coefficient R^2 (0.985) was slightly smaller than that of the Langmuir equation. To find out which isotherm describes the experimental data better, the error analysis was performed using the SSE and F-Test.

The Freundlich model is applicable to the processes that occur on the heterogenous surfaces. As shown in Table 2 the smaller value of SSE and the larger one of F-Test in the case of the Freundlich model indicated that it described the experimental data better than the Langmuir isotherm. This means that the As(V) adsorption occurred mainly on the heterogeneous surface of A33E-La(III). Moreover, the n constant (3.582) was within $1 < n < 10$ which indicated feasible adsorption [30].

The Dubinin-Radushkevich isotherm was used to determine whether the adsorption process on the heterogeneous surface is physical or chemical. According to this model, if the value of E is < 8 kJ/mol, the nature of adsorption process is physical whereas chemical adsorption occurs if the E values are between 8 and 16 kJ/mol [52]. In the present study the E value was equal to 13.97 kJ/mol suggesting that the adsorption of As(V) ions on the surface of A33E-La(III) was mainly chemical in its nature.

Generally, the Halsey model describes the multilayer adsorption at a relatively large distance from the surface. The correlation coefficient R^2 0.985 indicated quite good fit of the experimental data to this model. Those results revealed that the adsorption of As(V) ions could proceed on active sites of heterogeneous distribution. The error analysis by SSE and F-Test confirmed the applicability of the Halsey model and the heteroporous nature of the adsorbent.

Comparing the values of linear regression coefficients R^2 , the best fit of all experimental data was represented by the Langmuir model but it turned out that all correlation coefficients were relatively large. Therefore, the further error analysis was conducted using SSE and F-Test. Those parameters revealed that the Freundlich and Halsey isotherms described sorption behaviour the best. To conclude, the adsorption isotherms showed that adsorption was mainly chemisorption due to the energy larger than 8 kJ/mol and that the process took place on the heteroporous material. Nevertheless, multilayer adsorption as the coexisting process could not be excluded.

3.5. Thermodynamic studies

Thermodynamic parameters were determined to examine the temperature effect on the As(V) adsorption capacity of A33E-La(III). The changes of enthalpy ΔH° and entropy ΔS° were calculated

Table 2

The Langmuir, Freundlich, Dubinin-Radushkevich and Halsey isotherm parameters with the values of error analysis for the As(V) adsorption.

Parameters and error analysis	
Langmuir model	
q_m (mg/g)	54.64
K_L (dm ³ /mg)	0.035
R_L	0.530
R^2	0.992
SSE	227.68
F-Test	0.69
Freundlich model	
K_F (mg/g)	9.119
n	3.582
R^2	0.985
SSE	34.58
F-Test	0.96
Dubinin-Radushkevich model	
q_{DR} (mol/g)	$9.177 \cdot 10^{-4}$
β (mol ² /J ²)	$2.564 \cdot 10^{-9}$
E (kJ/mol)	13.97
R^2	0.964
SSE	88.40
F-Test	0.73
Halsey model	
n_H	-3.582
K_H	$3.646 \cdot 10^{-4}$
R^2	0.985
SSE	34.58
F-Test	0.96

Table 3

The comparison of adsorption capacities of sorbents used for the arsenate(V) removal.

Adsorbent	As(V) adsorption capacity (mg/g)	pH	Reference
Lanthanum hydroxide	299.4	5.0	[15]
Graphene oxide-lanthanum fluoride	17.0	6.0	[48]
Lanthanum immobilized on electrospun chitosan nanofiber (CSN-La)	83.6	4.0–6.0	[46]
Lanthanum-modified granular ceramic material	23.0	6.8	[33]
Lanthanum-impregnated mesoporous silica SBA-15	123.7	7.2	[39]
Iron-zirconium binary oxide-coated sand (IZBOCS)	84.75	7.0	[10]
Synthetic bimetal iron(III)- titanium(IV) oxide (NHITO)	85.0	7.0	[53]
Iron-coated seaweeds	7.3	7.0	[54]
A33E-La(III)	53.33	6.0	This study

from the slope and intercept of the linear plot $\ln K_d$ vs $1/T$. The negative values of ΔG° and ΔH° showed that the process was spontaneous and exothermic. As it was previously mentioned, the value of the dimensionless separation factor R_L confirmed the sorption spontaneity. However, high temperature diminished the adsorption efficiency. The preferred temperature for this process was predicted to be at the lower values as it was exothermic. The negative values of entropy ΔS° revealed the decreased randomness in the temperature range 295–333 K. All thermodynamic parameters are presented in Table S6.

3.6. Reusability of A33E-La(III)

The important issue is determining the possibility of the ion exchanger reuse. This enables significant reduction of the water purification costs. For this purpose, three consecutive arsenate(V) sorption/desorption cycles were performed to assess the reusabil-

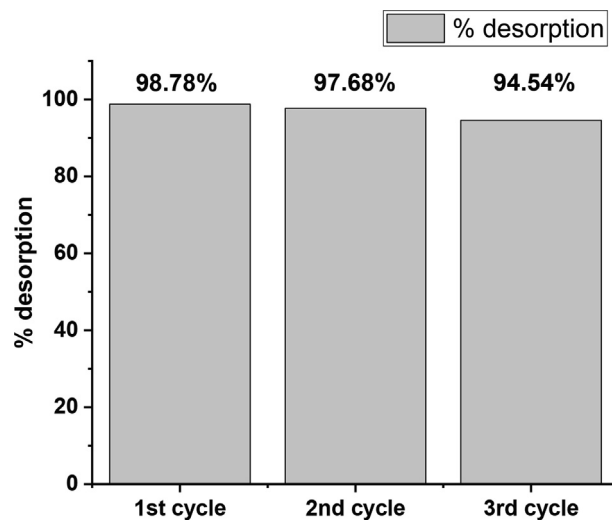


Fig. 10. Desorption efficiency in the three consecutive sorption-desorption cycles. Initial arsenate(V) concentration 100 mg/dm³, desorption solution 1 M NaOH, sorption/desorption time 6 h, temperature 295 K, shaking speed 180 rpm.

ity of A33E-La(III). It was agreed in many papers that the desorption of arsenic(V) from the sorbents based on iron oxides takes place in an alkaline environment [11,55,56]. Therefore, there were used the 0.05 M, 0.2 M and 1 M NaOH solutions as desorbing agents in the first cycle. For those concentrations the desorption efficiency was 40.95%, 83.03%, 98.78%, respectively. Consequently, 1 M NaOH, as the most powerful agent, was used for the next cycles. After 3 cycles desorption efficiency dropped from 98.78% to 94.54% (Fig. 10).

With regard to the sorption capacity, its value decreased from 18.51 to 17.40 which indicated A33E-La(III) could be employed several times with no significant decline in arsenic(V) removal efficiency. Moreover, after three cycles it still had a higher sorption capacity compared to the unmodified A33E (17.17 mg/g). Thus A33E-La(III) could be a great, recoverable material that would enable cheap removal of arsenic(V).

4. Conclusions

To conclude, the lanthanum-modified iron oxide adsorbent was successfully obtained by adsorption of lanthanum(III) ions on FerrixA33E and used for the arsenic(V) removal. This was confirmed by the SEM, FTIR and XPS analyses. After the La(III) modification the surface area and the total pore volume increased. Moreover, the maximum sorption capacity towards As(V) ions increased from 34.41 to 53.33 mg/g. A33E-La(III) was characterized by better sorption capacities at the initial As(V) concentration 25, 50 and 100 mg/dm³. The time needed to reach equilibrium was practically identical. The Freundlich and Halsey isotherms described arsenic(V) sorption behaviour the best and this process was mainly chemisorption due to the energy larger than 8 kJ/mol. Moreover, thermodynamic studies revealed spontaneous and exothermic nature of the As(V) adsorption. As for the sorption mechanism, at optimal pH 6 the arsenate(V) ions were adsorbed through the formation of inner-sphere monodentate or bidentate complexes as well as lanthanum arsenate precipitation. However, in the alkaline environment the adsorption could still proceed due to the inner-sphere complexation with lanthanum hydroxide. Moreover, even after 3 cycles of adsorption-desorption, A33E-La(III) had still larger As(V) adsorption than that of A33E. The exceptional As(V) removal capability of lanthanum-modified A33E-La(III) leads to its potential application for not expensive treatment of arsenic-contaminated water.

CRediT authorship contribution statement

Sebastian Dudek: Investigation, Writing – original draft, Visualization. **Dorota Kołodyńska:** Supervision, Writing – review & editing.

Declaration of Competing Interest

The authors declare that they have no known competing financial interests or personal relationships that could have appeared to influence the work reported in this paper.

Appendix A. Supplementary data

Supplementary data to this article can be found online at <https://doi.org/10.1016/j.molliq.2021.117985>.

References

- [1] B.K. Mandal, K.T. Suzuki, Arsenic round the world: a review, *Talanta*. 58 (2002) 201–235, [https://doi.org/10.1016/S0039-9140\(02\)00268-0](https://doi.org/10.1016/S0039-9140(02)00268-0).
- [2] A.A. Duker, E.J.M. Carranza, M. Hale, Arsenic geochemistry and health, *Environ. Int.* 31 (2005) 631–641, <https://doi.org/10.1016/j.envint.2004.10.020>.
- [3] G. Ungureanu, S. Santos, R. Boaventura, C. Botelho, Arsenic and antimony in water and wastewater: Overview of removal techniques with special reference to latest advances in adsorption, *J. Environ. Manage.* 151 (2015) 326–342, <https://doi.org/10.1016/j.jenvman.2014.12.051>.
- [4] T.S.Y. Choong, T.G. Chuah, Y. Robiah, F.L. Gregory Koay, I. Azni, Arsenic toxicity, health hazards and removal techniques from water: an overview, *Desalination*. 217 (2007) 139–166. Doi: 10.1016/j.desal.2007.01.015.
- [5] D. Ociński, I. Jacukowicz-Sobala, J. Raczyk, E. Kociołek-Baławejder, Evaluation of hybrid polymer containing iron oxides as As(III) and As(V) sorbent for drinking water purification, *React. Funct. Polym.* 83 (2014) 24–32, <https://doi.org/10.1016/j.reactfunctpolym.2014.07.005>.
- [6] I.M.M. Rahman, Z.A. Begum, H. Sawai, T. Maki, H. Hasegawa, Decontamination of spent iron-oxide coated sand from filters used in arsenic removal, *Chemosphere*. 92 (2013) 196–200, <https://doi.org/10.1016/j.chemosphere.2013.03.024>.
- [7] S. Aredes, B. Klein, M. Pawlik, The removal of arsenic from water using natural iron oxide minerals, *J. Clean. Prod.* 60 (2013) 71–76, <https://doi.org/10.1016/j.jclepro.2012.10.035>.
- [8] C. Shan, M. Tong, Efficient removal of trace arsenite through oxidation and adsorption by magnetic nanoparticles modified with Fe-Mn binary oxide, *Water Res.* 47 (2013) 3411–3421, <https://doi.org/10.1016/j.watres.2013.03.035>.
- [9] C. Feng, C. Aldrich, J.J. Eksteen, D.W.M. Arrigan, Removal of arsenic from alkaline process waters of gold cyanidation by use of γ -Fe₂O₃@ZrO₂ nanosorbents, *Hydrometallurgy*. 174 (2017) 71–77, <https://doi.org/10.1016/j.hydromet.2017.09.007>.
- [10] S.A. Chaudhry, Z. Zaidi, S.I. Siddiqui, Isotherm, kinetic and thermodynamics of arsenic adsorption onto Iron-Zirconium Binary Oxide-Coated Sand (IZBOCS): Modelling and process optimization, *J. Mol. Liq.* 229 (2017) 230–240, <https://doi.org/10.1016/j.molliq.2016.12.048>.
- [11] S. Zhang, H. Niu, Y. Cai, X. Zhao, Y. Shi, Arsenite and arsenate adsorption on coprecipitated bimetal oxide magnetic nanomaterials: MnFe₂O₄ and CoFe₂O₄, *Chem. Eng. J.* 158 (2010) 599–607, <https://doi.org/10.1016/j.cej.2010.02.013>.
- [12] J. Goscianska, M. Ptaszowska-Koniarz, M. Frankowski, M. Franus, R. Panek, W. Franus, Removal of phosphate from water by lanthanum-modified zeolites obtained from fly ash, *J. Colloid Interface Sci.* 513 (2018) 72–81, <https://doi.org/10.1016/j.jcis.2017.11.003>.
- [13] A. Teutli-Sequeira, V. Martínez-Miranda, M. Solache-Ríos, I. Linares-Hernández, Aluminum and lanthanum effects in natural materials on the adsorption of fluoride ions, *J. Fluor. Chem.* 148 (2013) 6–13, <https://doi.org/10.1016/j.jfluchem.2013.01.015>.
- [14] B. Wu, L. Fang, J.D. Fortner, X. Guan, I.M.C. Lo, Highly efficient and selective phosphate removal from wastewater by magnetically recoverable La(OH)₃/Fe₃O₄ nanocomposites, *Water Res.* 126 (2017) 179–188, <https://doi.org/10.1016/j.watres.2017.09.034>.
- [15] Y. Wang, Y. Liu, T. Guo, H. Liu, J. Li, S. Wang, X. Li, X. Wang, Y. Jia, Lanthanum hydroxide: a highly efficient and selective adsorbent for arsenate removal from aqueous solution, *Environ. Sci. Pollut. Res.* (2020), <https://doi.org/10.1007/s11356-020-10240-1>.
- [16] F.M. Jais, S. Ibrahim, Y. Yoon, M. Jang, Enhanced arsenate removal by lanthanum and nano – magnetite composite incorporated palm shell waste – based activated carbon, *Sep. Purif. Technol.* 169 (2016) 93–102, <https://doi.org/10.1016/j.seppur.2016.05.034>.
- [17] W. Zhang, J. Fu, G. Zhang, X. Zhang, Enhanced arsenate removal by novel Fe-La composite (hydr)oxides synthesized via coprecipitation, *Chem. Eng. J.* 251 (2014) 69–79, <https://doi.org/10.1016/j.cej.2014.04.057>.
- [18] Q. Tang, C. Shi, W. Shi, X. Huang, Y. Ye, W. Jiang, J. Kang, D. Liu, Y. Ren, D. Li, Science of the Total Environment Preferable phosphate removal by nano-La (III) hydroxides modified mesoporous rice husk biochars : Role of the host pore structure and point of zero charge, *Sci. Total Environ.* 662 (2019) 511–520. Doi: 10.1016/j.scitotenv.2019.01.159.
- [19] D.G. Kim, Y.H. Hwang, H.S. Shin, S.O. Ko, Kinetics of nitrate adsorption and reduction by nano-scale zero valent iron (NZVI): Effect of ionic strength and initial pH, *KSCF J. Civ. Eng.* 20 (2016) 175–187, <https://doi.org/10.1007/s12205-015-0464-3>.
- [20] Q. Hu, Q. Wang, C. Feng, Z. Zhang, Z. Lei, K. Shimizu, Insights into mathematical characteristics of adsorption models and physical meaning of corresponding parameters, *J. Mol. Liq.* 254 (2018) 20–25, <https://doi.org/10.1016/j.molliq.2018.01.073>.
- [21] W. Plazinski, W. Rudzinski, A. Plazinska, Theoretical models of sorption kinetics including a surface reaction mechanism: A review, *Adv. Colloid Interface Sci.* 152 (2009) 2–13, <https://doi.org/10.1016/j.cis.2009.07.009>.
- [22] Y.-S. Ho, Review of second-order models for adsorption systems, *J. Hazard. Mater.* 136 (2006) 681–689, <https://doi.org/10.1016/j.jhazmat.2005.12.043>.
- [23] D. Balarak, F. Mostafapour, A. Khatibi, Nonlinear Isotherms and Kinetics and Application Error Functions for Adsorption of Tetracycline on Lemna Minor, *J. Pharm. Res. Int.* 23 (2018) 1–11, <https://doi.org/10.9734/jpri/2018/4253>.
- [24] S. Maji, A. Ghosh, K. Gupta, A. Ghosh, U. Ghorai, A. Santra, P. Sasikumar, U.C. Ghosh, Efficiency evaluation of arsenic(III) adsorption of novel graphene oxide@iron-aluminium oxide composite for the contaminated water purification, *Sep. Purif. Technol.* 197 (2018) 388–400, <https://doi.org/10.1016/j.seppur.2018.01.021>.
- [25] N.S. Randhawa, D. Dwivedi, S. Prajapati, R.K. Jana, Application of manganese nodules leaching residue for adsorption of nickel(II) ions from aqueous solution, *Int. J. Environ. Sci. Technol.* 12 (2015) 857–864, <https://doi.org/10.1007/s13762-013-0460-4>.
- [26] W.-H. Kim, H.-K. Chung, J. Park, P.-K. Park, J. Cho, T.-Y. Jeong, Application of Langmuir and Freundlich isotherms to predict adsorbate removal efficiency or required amount of adsorbent, *J. Ind. Eng. Chem.* 28 (2015) 241–246, <https://doi.org/10.1016/j.jiec.2015.02.021>.
- [27] V. Fierro, V. Torné-Fernández, D. Montané, A. Celzard, Adsorption of phenol onto activated carbons having different textural and surface properties, *Microporous Mesoporous Mater.* 111 (2008) 276–284, <https://doi.org/10.1016/j.micromes.2007.08.002>.
- [28] M. Thakkar, V. Randhawa, S. Mitra, L. Wei, Synthesis of diatom-FeO_x composite for removing trace arsenic to meet drinking water standards, *J. Colloid Interface Sci.* 457 (2015) 169–173, <https://doi.org/10.1016/j.jccs.2015.07.003>.
- [29] A. Iriel, M.G. Lagorio, A. Fernández Cirelli, Biosorption of arsenic from groundwater using *Vallisneria gigantea* plants. Kinetics, equilibrium and photophysical considerations, *Chemosphere*. 138 (2015) 383–389, <https://doi.org/10.1016/j.chemosphere.2015.06.053>.
- [30] J. Liu, X. Wang, Novel silica-based hybrid adsorbents: Lead(II) adsorption isotherms, *Sci. World J.* 2013 (2013), <https://doi.org/10.1155/2013/897159>.
- [31] M. Pan, X. Lin, J. Xie, X. Huang, Kinetic, equilibrium and thermodynamic studies for phosphate adsorption on aluminum hydroxide modified palygorskite nano-composites, *RSC Adv.* 7 (2017) 4492–4500, <https://doi.org/10.1039/C6RA26802A>.
- [32] P. Wu, J. Wu, L. Xia, Y. Liu, L. Xu, S. Song, Adsorption of fluoride at the interface of water with calcined magnesium-ferril-lanthanum hydrocalcite-like compound, *RSC Adv.* 7 (2017) 26104–26112, <https://doi.org/10.1039/c7ra04382a>.
- [33] H. Yang, Y. Wang, J. Bender, S. Xu, Removal of Arsenate and Chromate by Lanthanum-modified Granular Ceramic Material: The Critical Role of Coating Temperature, *Sci. Rep.* 9 (2019) 1–12, <https://doi.org/10.1038/s41598-019-44165-8>.
- [34] N.L.M. Linh, D. Hoang Van, T. Duong, M.X. Tinh, D.Q. Khieu, Adsorption of Arsenate from Aqueous Solution onto Modified Vietnamese Bentonite, *Adv. Mater. Sci. Eng.* 2019 (2019), <https://doi.org/10.1155/2019/2710926>.
- [35] E.O. Kartinen, C.J. Martin, An overview of arsenic removal processes, *Desalination*. 103 (1995) 79–88, [https://doi.org/10.1016/0011-9164\(95\)00089-5](https://doi.org/10.1016/0011-9164(95)00089-5).
- [36] M.N. Pervez, D. Fu, X. Wang, Q. Bao, T. Yu, V. Naddeo, H. Tian, C. Cao, Y. Zhao, A bifunctional α -FeOOH@GCA nanocomposite for enhanced adsorption of arsenic and photo Fenton-like catalytic conversion of As(III), *Environ. Technol. Innov.* 22 (2021), <https://doi.org/10.1016/j.eti.2021.101437>.
- [37] Z.A. Alothman, A review: Fundamental aspects of silicate mesoporous materials, *Materials (Basel)*. 5 (2012) 2874–2902, <https://doi.org/10.3390/mats20122874>.
- [38] O. Valdés, A. Marican, Y. Mirabal-Gallardo, L.S. Santos, Selective and efficient arsenic recovery from water through quaternary amino-functionalized silica, *Polymers (Basel)*. 10 (2018), <https://doi.org/10.3390/polym10060626>.
- [39] M. Jang, J.K. Park, E.W. Shin, Lanthanum functionalized highly ordered mesoporous media: Implications of arsenate removal, *Microporous Mesoporous Mater.* 75 (2004) 159–168, <https://doi.org/10.1016/j.micromes.2004.05.018>.
- [40] F. Partey, D.I. Norman, S. Nduri, R. Narrey, Mechanism of arsenic sorption onto laterite iron concretions, *Colloids Surfaces A Physicochem. Eng. Asp.* 337 (2009) 164–172, <https://doi.org/10.1016/j.colsurfa.2008.12.018>.
- [41] P. Qi, T. Pichler, Competitive Adsorption of As(III) and As(V) by Ferrihydrite: Equilibrium, Kinetics, and Surface Complexation, *Water. Air. Soil Pollut.* 227 (2016), <https://doi.org/10.1007/s11270-016-3091-9>.
- [42] L.C. Staicu, N. Morin-Crini, G. Crini, Desulfurization: Critical step towards enhanced selenium removal from industrial effluents, *Chemosphere*. 172 (2017) 111–119, <https://doi.org/10.1016/j.chemosphere.2016.12.132>.

- [43] Y.-S. Han, H.Y. Jeong, S.P. Hyun, K.F. Hayes, C.-M. Chon, IUCr, Beam-induced redox transformation of arsenic during As K-edge XAS measurements: availability of reducing or oxidizing agents and As speciation, *J. Synchrotron Radiat.* 25 (2018) 763–770, <https://doi.org/10.1107/S1600577518002576>.
- [44] Y. Yu, C. Zhang, L. Yang, J. Paul Chen, Cerium oxide modified activated carbon as an efficient and effective adsorbent for rapid uptake of arsenate and arsenite: Material development and study of performance and mechanisms, *Chem. Eng. J.* 315 (2017) 630–638, <https://doi.org/10.1016/j.cej.2016.09.068>.
- [45] M.R. Awual, M.A. Shenashen, T. Yaita, H. Shiwaku, A. Jyo, Efficient arsenic(V) removal from water by ligand exchange fibrous adsorbent, *Water Res.* 46 (2012) 5541–5550, <https://doi.org/10.1016/j.watres.2012.07.038>.
- [46] P. Tan, Y. Zheng, Y. Hu, Efficient removal of arsenate from water by lanthanum immobilized electrospun chitosan nanofiber, *Colloids Surfaces A Physicochem. Eng. Asp.* 589 (2020), <https://doi.org/10.1016/j.colsurfa.2020.124417>.
- [47] J.E. Greenleaf, J.C. Lin, A.K. Sengupta, Two novel applications of ion exchange fibers: Arsenic removal and chemical-free softening of hard water, *Environ. Prog.* 25 (2006) 300–311, <https://doi.org/10.1002/ep.10163>.
- [48] L.P. Lingamdinne, J.R. Koduru, Y.Y. Chang, S.H. Kang, J.K. Yang, Facile synthesis of flowered mesoporous graphene oxide-lanthanum fluoride nanocomposite for adsorptive removal of arsenic, *J. Mol. Liq.* 279 (2019) 32–42, <https://doi.org/10.1016/j.molliq.2019.01.103>.
- [49] M. Sharma, J. Singh, S. Hazra, S. Basu, Adsorption of heavy metal ions by mesoporous ZnO and TiO₂@ZnO monoliths : Adsorption and kinetic studies, 145 (2019) 105–112. Doi: 10.1016/j.microc.2018.10.026.
- [50] M.N. Pervez, Y. Wei, P. Sun, G. Qu, V. Naddeo, Y. Zhao, α -FeOOH quantum dots impregnated graphene oxide hybrids enhanced arsenic adsorption: The mediation role of environmental organic ligands, *Sci. Total Environ.* 781 (2021), <https://doi.org/10.1016/j.scitotenv.2021.146726> 146726.
- [51] A. Padilla-Rodríguez, J.A. Hernández-Viecas, J.R. Peralta-Videa, J.L. Gardea-Torresdey, O. Perales-Pérez, F.R. Román-Velázquez, Synthesis of protonated chitosan flakes for the removal of vanadium(III, IV and V) oxyanions from aqueous solutions, *Microchem. J.* 118 (2015) 1–11, <https://doi.org/10.1016/j.microc.2014.07.011>.
- [52] M.T. Amin, A.A. Alazba, M. Shafiq, Adsorptive removal of reactive black 5 from wastewater using bentonite clay: Isotherms, kinetics and thermodynamics, *Sustain.* 7 (2015) 15302–15318, <https://doi.org/10.3390/su71115302>.
- [53] K. Gupta, U.C. Ghosh, Arsenic removal using hydrous nanostructure iron(III)-titanium (IV) binary mixed oxide from aqueous solution, *J. Hazard. Mater.* 161 (2009) 884–892, <https://doi.org/10.1016/j.jhazmat.2008.04.034>.
- [54] A.M.A. Pintor, B.R.C. Vieira, S.C.R. Santos, R.A.R. Boaventura, C.M.S. Botelho, Arsenic removal from water using iron-coated seaweeds, *J. Environ. Manage.* 192 (2017) 224–233, <https://doi.org/10.1016/j.jenvman.2017.01.054>.
- [55] A.Z.M. Badruddoza, Z.B.Z. Shawon, M.T. Rahman, K.W. Hao, K. Hidajat, M.S. Uddin, Ionically modified magnetic nanomaterials for arsenic and chromium removal from water, *Chem. Eng. J.* 225 (2013) 607–615, <https://doi.org/10.1016/j.cej.2013.03.114>.
- [56] S. Lin, D. Lu, Z. Liu, with magnetic γ -Fe₂O₃ nanoparticles, *Chem. Eng. J.* 211–212 (2012) 46–52, <https://doi.org/10.1016/j.cej.2012.09.018>.

Table S1. Brief characteristics of Ferrix A33E (Staicu et al., 2017).

Polymer Structure	Divinylbenzene cross-linked with polystyrene
Matrix structure	Macroporous
Physical form and appearance	Reddish-light spherical particles
Particle size range	0.3- 1.2 mm
Maximum working temperature	353 K
Working pH range	4.5–8.5

Table S2. Kinetic models calculations.

Kinetic model	Linear form	Plot	Slope	Intercept
PFO	$\ln(q_e - q_t) = \ln q_e - k_1 t$	$\ln(q_e - q_t)$ vs t	k_1	$\ln q_e$
PSO	$\frac{t}{q_t} = \frac{1}{k_2 q_e^2} + \frac{t}{q_e}$	$\frac{t}{q_t}$ vs $\frac{1}{t}$	$\frac{1}{q_e}$	$\frac{1}{k_2 q_e^2}$
Elovich	$q_t = \frac{1}{\beta} \ln(\alpha\beta) + \frac{1}{\beta} \ln t$	q_t vs $\ln t$	$\frac{1}{\beta}$	$\frac{1}{\beta} \ln(\alpha\beta)$
IPD	$q_t = k_i \sqrt{t} + C$	q_t vs \sqrt{t}	k_i	C

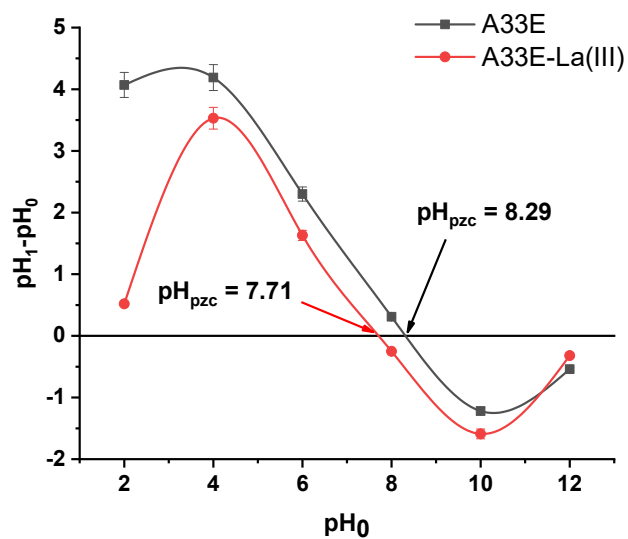


Figure S1. The points of zero charge (pH_{PZC}) of A33E (black) and A33E-La(III) (red).

Table S3. Pore structure parameters of the samples measured by the adsorption branch of N₂ adsorption–desorption isotherms.

Ion exchanger	A33E	A33E-La(III)	A33E-La(III)-As(V)
Specific surface area (S_{BET}) (m ² /g)	53.12	59.39	56.04
Total pore volume (V_t) (cm ³ /g)	0.122	0.127	0.124
Average pore diameter (D_p) (nm)	9.18	8.53	8.86

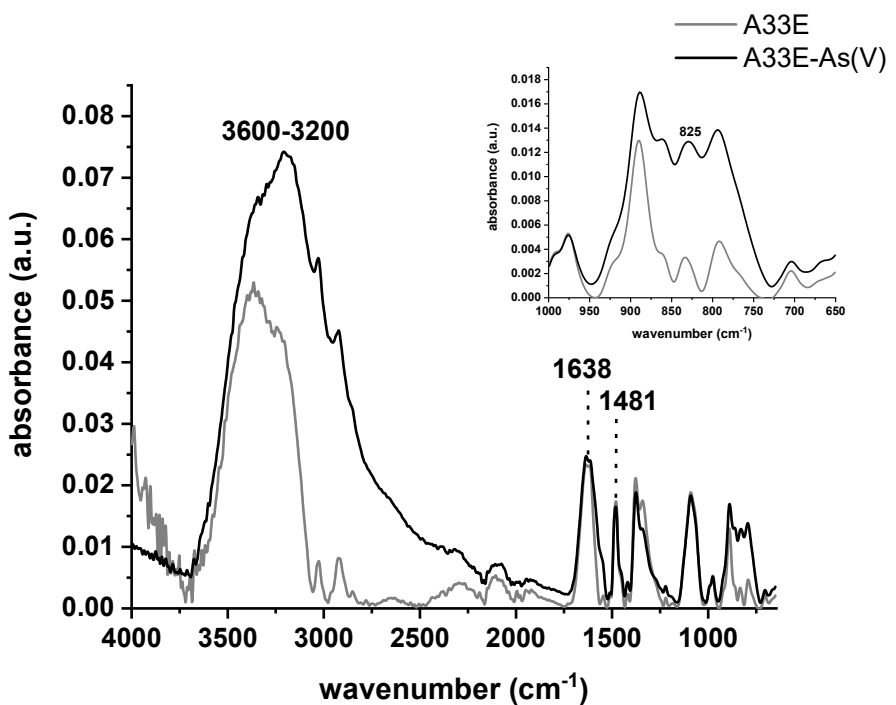


Figure S2. FTIR spectra of A33E before and after the As(V) sorption.

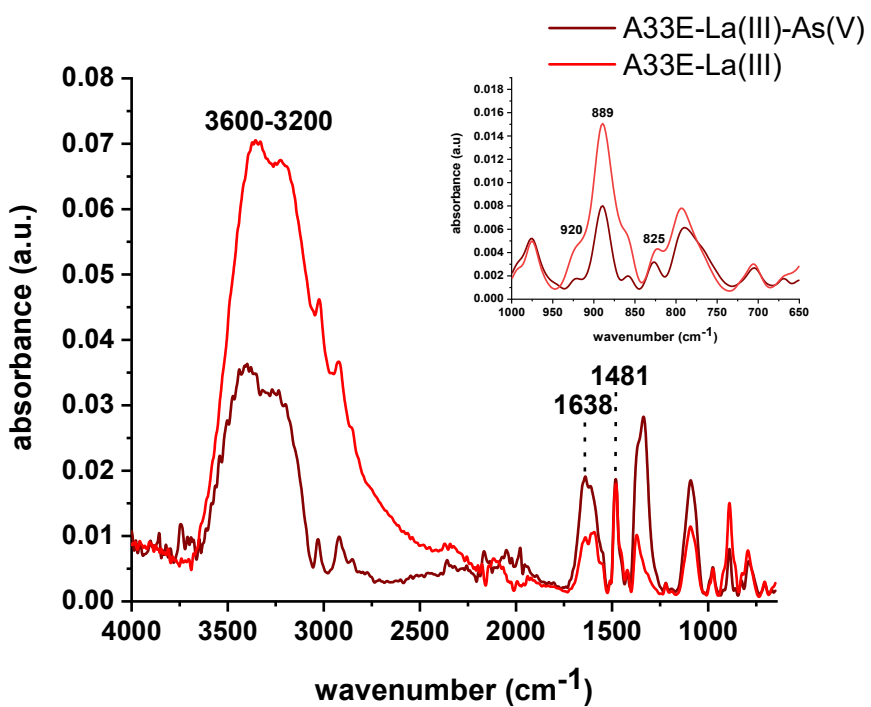


Figure S3. FTIR spectra of A33E-La(III) before and after the As(V) sorption.

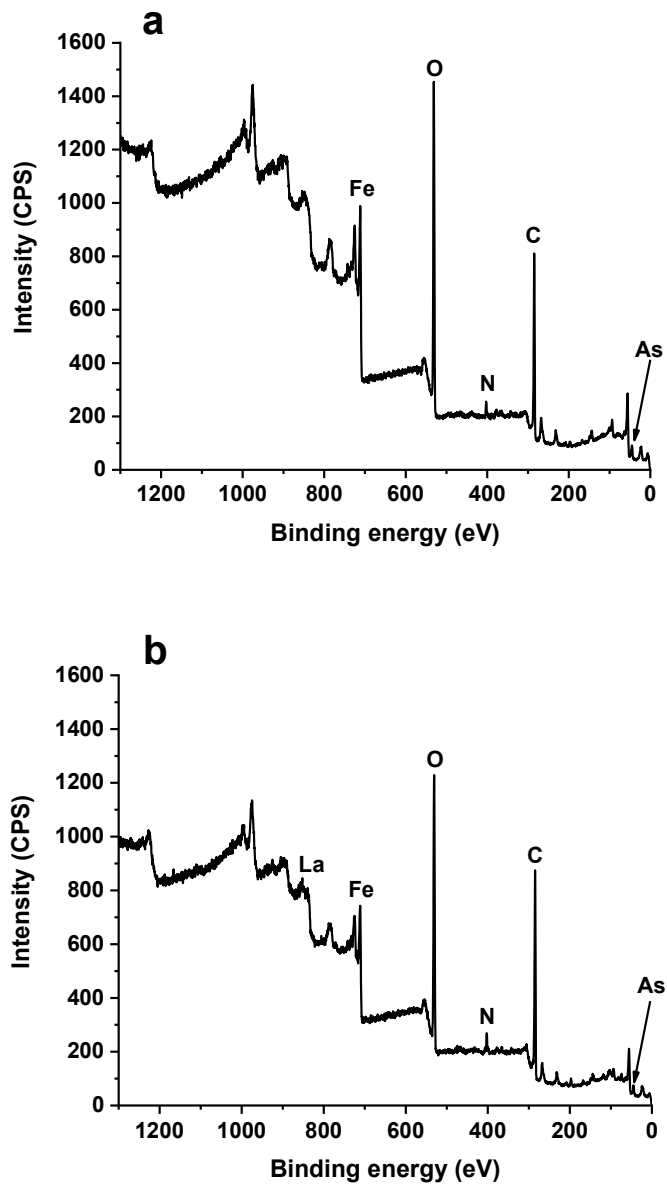


Figure S4. XPS spectra of A33E (a) and A33E-La(III) after the As(V) adsorption.

Table S4. Fitted As 3d, C 1s, N 1s and Fe 2p peak parameters deduced from the XPS analysis for A33E after the As(V) ions adsorption.

Region	Peak (eV)	Assignment	Atomic content (%)
As 3d	44.8	As(III)	45.1
	45.5	As(III)	
	45.5	As(V)	54.9
	46.2	As(V)	
C 1s	284.6	C=C aromatic carbon	26.2
	285.0	C-H aliphatic carbon	31.0
	285.4	C-C aliphatic carbon	15.9
	286.0	C-N nitrogen bonded	7.5
		carbon	
N 1s	400.0	-N< amine group	27.8
	402.7	-NR ₄ ⁺ quaternary ammonium group	72.2
Fe 2p	709.4	Fe(II)	10.7
	710.6	Fe(II)	
	711.5	Fe(II)	
	710.6	Fe(III)	89.3
	711.6	Fe(III)	
	712.6	Fe(III)	
	713.6	Fe(III)	

Table S5. Fitted As 3d, C 1s, N 1s, Fe 2p and La 3d peak parameters deduced from the XPS analysis for A33E-La(III) after the As(V) ions adsorption.

Region	Peak (eV)	Assignment	Atomic content (%)
As 3d	44.4	As(III)	38.8
	45.3	As(III)	
	45.0	As(V)	61.2
	45.7	As(V)	
C 1s	284.6	C=C aromatic carbon	30.7
	285.0	C-H aliphatic carbon	26.6
	285.5	C-C aliphatic carbon	16.1
	286.0	C-N nitrogen bonded	8.6
		carbon	
N 1s	399.8	-N< amine group	24.9
	402.7	-NR ₄ ⁺ quaternary ammonium group	60.3
	406.5	-NO ₂ nitro group	14.9
Fe 2p	709.7	Fe(II)	16.4
	710.9	Fe(II)	
	711.8	Fe(II)	
	710.8	Fe(III)	83.6
	711.8	Fe(III)	
	712.8	Fe(III)	
	713.8	Fe(III)	
La 3d	835.6	La(III)	100.0

837.6 La(III)

839.4 La(III)

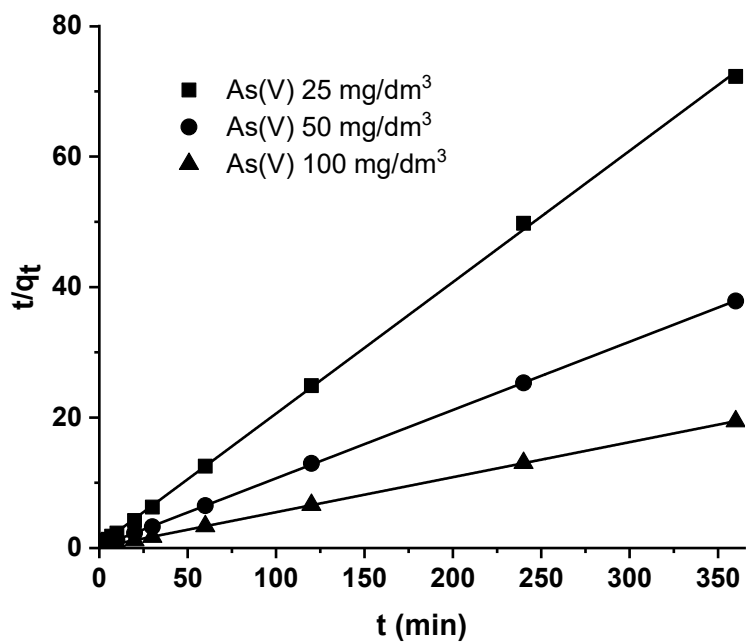


Figure S5. Pseudo-second order kinetic plots for the As(V) adsorption onto A33E-La(III) (various As(V) initial concentrations).

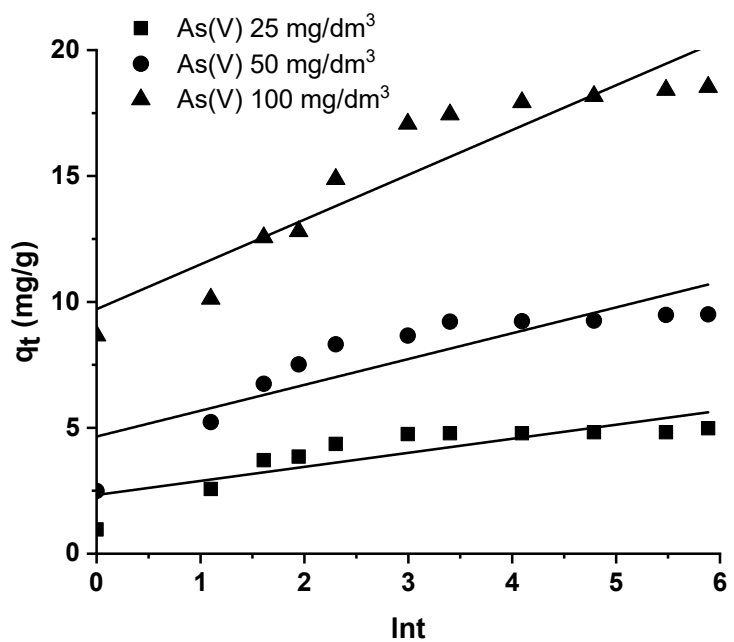


Figure S6. Elovich kinetic plots for the As(V) adsorption onto A33E-La(III) (various As(V) initial concentrations).

Table S6. Thermodynamic parameters of arsenate adsorption onto A33E-La(III).

<i>T</i> (K)	<i>q_e</i> (mg/g)	<i>c_e</i> (mg/g)	<i>K_d</i> (dm ³ /g)	<i>ΔG^θ</i> (kJ/mol)	<i>ΔH^θ</i> (kJ/mol)	<i>ΔS^θ</i> (kJ/mol·K)
295	53.33	733.33	0.073	-10.51	-12.347	-0.0064
313	40.00	800.00	0.050	-10.18		
333	34.00	830.00	0.041	-10.28		

D3

S. Dudek, D. Kołodyńska

Arsenate removal on the iron oxide ion exchanger modified
with neodymium(III) ions, J. Environ. Manage., 307 (2022)
114551

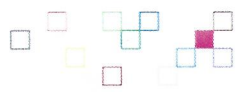
IF: 6,789 Punkty MEiN: 100

Oświadczenie

Oświadczam, że mój udział w pracy:

S. Dudek, D. Kołodyńska, Arsenate removal on the iron oxide ion exchanger modified with neodymium(III) ions, J. Environ. Manage. 307 (2022) 114551

polegał na współtworzeniu jej ogólnej koncepcji, wykonaniu wszystkich eksperymentów, opracowaniu wyników, współudziale w stworzeniu oryginalnego manuskryptu, pełnieniu roli autora korespondencyjnego, współudziale w przygotowywaniu odpowiedzi do recenzentów. Udział ten szacuję na 75%.



OŚWIADCZENIE

Oświadczam, że w pracy:

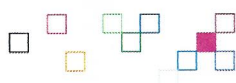
Sebastian Dudek, Dorota Kołodyńska, Arsenate removal on the iron oxide ion exchanger modified with neodymium(III) ions, Journal of Environmental Management, 100, 307 (2022) 114551, IF₂₀₂₂ 6,789, pkt MNiE₂₀₂₂.

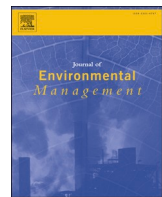
mój wkład merytoryczny w przygotowanie, przeprowadzenie i opracowanie badań oraz przedstawienie pracy w formie publikacji to:

opracowanie koncepcji i założeń, interpretacja i analiza otrzymanych wyników i współudział w redagowaniu odpowiedzi na uwagi recenzentów.

Swój wkład szacuję na 25%.

Jednocześnie wyrażam zgodę na przedłożenie wyżej wymienionej pracy przez Pana mgr Sebastiana Dudka jako część rozprawy doktorskiej w formie spójnego tematycznie cyklu prac opublikowanych w czasopismach naukowych.





Arsenate removal on the iron oxide ion exchanger modified with Neodymium(III) ions

Sebastian Dudek ^{*}, Dorota Kołodyńska

Department of Inorganic Chemistry, Institute of Chemical Sciences, Faculty of Chemistry, Maria Curie-Skłodowska University, Maria Curie-Skłodowska Sq. 2, 20-031, Lublin, Poland



ARTICLE INFO

Keywords:

Arsenic
Adsorption
Neodymium
Iron oxides
Ferrix A33E

ABSTRACT

In this study the iron oxide ion exchanger with the quaternary ammonium groups, Ferrix A33E was modified with neodymium (III) ions in order to obtain the new material Ferrix A33E-Nd(III) characterized by greater sorption efficiency of arsenate(V) ions. A33E-Nd(III) was described by various techniques including scanning electron microscopy SEM, nitrogen adsorption/desorption isotherms, Fourier transform infrared spectroscopy FTIR and X-ray photoelectron spectroscopy XPS. The point of zero charge, pH_{ZC} was also determined. The kinetic and thermodynamic parameters of the arsenate(V) sorption were calculated. The experimental data was fitted to the four isotherm models - Langmuir, Freundlich, Dubinin-Radushkevich and Halsey. Kinetic and equilibrium studies allowed to get to know the behaviour of arsenate(V) ions during the sorption on A33E-Nd (III). The obtained material A33E-Nd(III)- was found to possess a larger maximum sorption capacity than A33E, great stability and the possibility of regeneration at least 3 times without a significant decrease in efficiency. This allows for the complete removal of As(V) ions from a solution with a concentration of 50 mg/dm³ in just 30 min. The Nd(III)-modification improved the sorption properties of the tested ion exchanger.

1. Introduction

Safe drinking water is one of the crucial issues in terms of water supply. Groundwater is the primary source of both useable and drinking water in many parts of the world, and the sole supply of water in the others (Alothman et al., 2020). Various water treatment techniques including nanofiltration, precipitation, coagulation, electrodialysis, reverse osmosis and adsorption are well developed and used in everyday life (Kenawy et al., 2018). Unfortunately, many of these methods have some significant disadvantages. Coagulation/precipitation produces toxic sludge, nanofiltration is high-cost and requires pre-conditioning, reverse osmosis is characterized by high-tech operation and maintenance and electrodialysis produces toxic wastewater (Alka et al., 2021; Zakhar et al., 2018). Though characterized by some disadvantages, adsorption is regarded as one of the most efficient, adaptable, and cost-effective procedures (Alothman, 2012; M. A. Khan et al., 2020; Mittal et al., 2016).

Unfortunately, in many countries around the world, e.g. Bangladesh, China, India, Mexico or USA in natural waters there is an increased amount of pollutants, including arsenic (Adelaju et al., 2021; Shaji et al., 2021). This is due to natural and anthropogenic factors that significantly

reduce the quality of water, often making it impossible to be consumed. The consumption of such water is associated with the risk of diseases such as skin lesions and different types of cancer (skin, bladder, lungs) (Singh et al., 2021). Taking the above into consideration, there is a justified need to develop a method that will contribute to follow the strict World Health Organization (WHO) limit concerning the arsenic content in drinking water (10 µg/dm³) (Mushtaq et al., 2021).

It is worth noting that the most common inorganic forms of arsenic in the groundwater (more toxic than the organic ones) are As(III) and As (V). In the most common groundwater pH range, the dominant forms of As(V) are negatively charged H₂AsO₄⁻ and HAsO₄²⁻, while As(III) exists in the form of neutrally charged H₃AsO₃ (Yu et al., 2018). As a result of As(V) being more readily adsorbed on an electrically charged surface, all forms of arsenic should be oxidized to the +5 oxidation state in order to remove arsenic efficiently.

Recently many sorbents have been developed for this purpose. In turn, this study attempted to improve the already existing sorbent Ferrix A33E (Purolite, USA) by its modification with neodymium (III) ions. Ferrix A33E (A33E in the abbreviated form) is the iron oxide ion exchanger with the structure of polystyrene crosslinked with divinylbenzene. It contains the quaternary ammonium functional groups. There

* Corresponding author.

E-mail address: sebastian.dudek@mail.umcs.pl (S. Dudek).

are papers on the modification of sorbents with rare earth elements for the removal of arsenic from aqueous solutions. However, many of them deal mainly with the modification with lanthanum or cerium ions (Tan et al., 2020; Yang et al., 2019; Yu et al., 2017). So far, the literature has not reported the studies on the modification of the sorbent with neodymium (III) ions in terms of arsenic removal. Therefore, the aim of this paper was to prepare a new A33E-Nd(III) sorbent obtained as a result of A33E modification with neodymium (III) ions. The other objectives were the sorbent characterization and its investigation in terms of arsenate(V) ions removal.

2. Materials and methods

2.1. Materials

The materials and reagents used are as follows: neodymium (III) oxide Nd₂O₃ (Sigma Aldrich, USA), 1M nitric acid HNO₃ (Chempur, Poland), 1M sodium hydroxide NaOH (Chempur, Poland), FerriX A33E (Purolite, USA), 0.01M sodium chloride NaCl (Chempur, Poland), 1M hydrochloric acid HCl (Chempur, Poland), disodium hydrogen arsenate heptahydrate Na₂HAsO₄·7H₂O (Sigma Aldrich, USA).

2.2. Instruments

The instruments that have been used are as follows: laboratory shaker Elpin + type 357 (Elpin Plus, Poland), scanning electron microscope (SEM) Quanta 3D FEG (FEI, USA) with an extended depth of field (EDF) function, volumetric adsorption analyzer at 77 K ASAP 2405 (Micromeritics, USA), pH meter PHM 84 (Radiometer, Denmark) with the glass REF 451 and calomel pHG 201–8 electrodes, Cary 630 FTIR spectrometer (Agilent Technologies, USA), X-ray photoelectron spectroscopy XPS was used (Prevac, Poland), spectrophotometer Cary 60 (Agilent Technologies, USA), inductively coupled plasma optical emission spectrometry (ICP-OES) 720 ES (Varian, USA).

2.2.1. Sorbent modification with Nd(III) ions

The Nd(III) solution of the concentration 1000 mg/dm³ was prepared by dissolving the proper amount of neodymium (III) oxide Nd₂O₃ (Sigma Aldrich, USA) in 1M nitric acid (Chempur, Poland) and then in a concentrated one. In the next step, the solution was diluted to 100 mg/dm³ and the pH value was adjusted to 4 adding the appropriate amount of 1M NaOH (Chempur, Poland). The weighed amounts of 0.5 g of A33E were placed in 500 cm³ conical flasks and 100 cm³ of the previously prepared Nd(III) solution of the concentration of 100 mg/dm³ was added to each of them. The samples were shaken for 6 h at 180 rpm and 295 K. Then the sorbent was separated from the solution by gravity filtration and dried for 24 h at 333 K. In this way there was obtained the modified A33E-Nd(III) sorbent which was further tested for characterization and removal of arsenic(V) ions.

2.2.2. Sorbent characterization

Scanning electron microscopy (SEM) (Quanta 3D FEG, FEI, USA) with an extended depth of field (EDF) function was used to characterize the surface morphology, including surface structures. The SEM A33E and A33E-Nd(III) images were compared. The images of the A33E-Nd(III) surface after the As(V) ion sorption were also obtained.

The morphological properties of A33E, A33E-Nd(III) and A33E-Nd(III)-As(V) were examined by the nitrogen adsorption/desorption isotherms at 77 K (ASAP 2405, Micromeritics, USA) after the prior degassing of the samples at the established temperature. The Brunauer, Emmett and Teller (BET) method was employed to determine the specific surface area. Furthermore, the total pore volumes and average pore diameters were calculated using the Barret-Joyner-Halenda model.

The drift method was used to assess the point of zero charge (pH_{pzc}) of A33E and A33E-Nd(III) (Linh et al., 2019). The pH_{pzc} was determined by changing the pH of 20 mL 0.01 M NaCl in the range from 2 to 11

(pH_i). 0.1 g of A33E or A33E-Nd(III) was placed in the flask and the final pH (pH_f) was measured after 6 h of shaking. The pH_{pzc} value is the point at which pH_i-pH_f = 0. The pH measurements were made using the Radiometer PHM 84 pH meter (Denmark) with the glass REF 451 and calomel pHG 201–8 electrodes.

The spectra of the tested adsorbents were recorded by means of the infrared spectroscopy analysis with the Fourier transformation (FTIR). Before and after the As(V) adsorption, A33E and A33E-Nd(III) were examined by the attenuated total reflection method using the Agilent Cary 630 FTIR spectrometer (USA). Thus it was possible to identify the specified functional groups on the materials surface. The FTIR spectra were recorded in the wavenumber range of 4000–400 cm⁻¹.

In order to study the composition and valence state of the elements contained in A33E and A33E-Nd(III) before and after the arsenate(V) ions uptake, the X-ray photoelectron spectroscopy XPS was used (Prevac, Poland).

2.2.3. Effect of pH

The experiment on pH effect on As(V) adsorption efficiency was conducted in 100 cm³ flasks. The A33E-Nd(III) samples of 0.1 g were put into the flasks containing 20 cm³ of arsenate(V) solution with the concentration equal to 100 mg/dm³. The pH values range was established from 4 to 11 by adding proper amounts of 0.01M NaOH or 0.01M HCl. In the next step, the flasks were shaken using the laboratory shaker Elpin + type 357 (Elpin Plus, Poland) for 360 min. The A33E-Nd(III) was split off the solution by gravity filtration. The concentration of arsenate(V) ions was analyzed by the spectrophotometric method (Cary 60, Agilent Technologies, USA) which consisted in the formation of complexes with ammonium molybdate and the measurement of absorbance at the wavelength 870 nm. The adsorption capacity of As(V) ions was determined using Equation (1) (Ali et al., 2017; Naushad et al., 2019b):

$$q_t = (c_0 - c_t) \times \frac{V}{m} \quad (1)$$

where: q_t is the amount of arsenate(V) adsorbed at time t (mg/g), c_0 is the initial concentration of arsenate(V) in the solution (mg/dm³), c_t is the concentration of arsenate(V) in the solution after time t (mg/dm³), V is the volume of the solution containing arsenate(V) ions (dm³), m is the mass of ion exchanger (g).

Moreover, the sorption percentage was determined from Equation (2):

$$\%S = \frac{(c_0 - c_t)}{c_0} \times 100\% \quad (2)$$

2.2.4. Kinetic studies

The kinetics of arsenate(V) adsorption was studied in batch experiments at the initial As(V) concentrations of 25, 50 and 100 mg/dm³ and pH 6. The 0.1 g weighed amounts of A33E-Nd(III) were prepared in the 100 cm³ conical flasks and 20 cm³ of As(V) solutions was added to be shaken at the established time – from 1 to 360 min (temperature 295 K, shaking speed 180 rpm). The adsorption capacities and the percentages of sorption were calculated from Equations (1) and (2). The adsorption kinetics of arsenate(V) onto A33E-Nd(III) was investigated using the pseudo-first order (PFO), pseudo-second order (PSO), Elovich and intraparticle diffusion (IPD) models. The applicability of the models was evaluated by the error analysis – correlation coefficient (R^2) and the sum of squared errors (SSE).

2.2.5. Adsorption equilibrium and thermodynamic studies

Arsenate(V) solutions of varying initial concentrations (25–1000 mg/dm³) were prepared and their pH was adjusted to 6 before employment. Adsorption tests were carried out at different temperatures: 295 K, 313 K, 333 K and shaking speed 180 rpm. All the experiments were done with a 6-h contact time as well as the same adsorbent dosage and adsorbate volume as in Section 2.3.3. The experimental data

was fitted to the Langmuir, Freundlich, Dubinin-Radushkevich and Halsey isotherms.

2.2.6. Reusability of A33E-Nd(III)

In order to evaluate the reusability of A33E-Nd(III), 0.1 g of the sorbent was placed in three 100 cm³ flasks and 20 cm³ of arsenate(V) solution with a concentration of 100 mg/dm³ and pH 6 was added to each of them. The samples were shaken for 6 h at 295 K and 180 rpm. Then the sorbent was separated from the solution by gravity filtration and dried for 24 h at 333 K. The samples were placed again in the 100 cm³ flasks and 20 cm³ of NaOH solutions at 0.05, 0.2 and 1M concentrations was added to them. The samples were also shaken for 6 h at 295 K and 180 rpm. Subsequently, the sample was separated from the solution by filtration and dried for 24 h at 333 K. The test was repeated twice with 1M NaOH. After each adsorption and desorption, the concentration of arsenate(V) ions in the solution was determined.

3. Results and discussion

3.1. Sorbent characterization

The morphological study of A33E, A33E-Nd(III) and A33E-Nd(III) after the sorption of As(V) (A33E-Nd(III)-As(V)) was carried out using the SEM analysis (Fig. 1). After the sorbent modification with Nd(III)

ions the surface became more heterogeneous. The particles were deposited forming agglomerates. The objects of irregular shapes on the A33E-Nd(III) surface varied in size from about 40 to even 400 nm (Fig. 2a and b). The average size was calculated to be approximately 170 nm. These particles seemed to be bubble-, plate- and grain-like in structure. In other papers spherical objects could be seen on the surface of neodymium (III)-based adsorbents (Ahmadi et al., 2020; M. U. Khan et al., 2020). Numerous pores of varying size would enable the active sites to adsorb As(V) ions. Fig. 2c presents the SEM image of A33E-Nd(III) taken using the backscattered electron detector BSED which locates high atomic number elements (Robinson, 1980). The bright spots correspond to the adsorbed neodymium (III) ions showing the successful incorporation on the surface of A33E. After the As(V) adsorption the A33E-Nd(III) surface became smoother but there were still visible objects (Fig. 1 g, h, i). This can be explained by the pores filling with arsenate(V) ions.

The specific surface areas, pore volumes and average pore diameters of A33E, A33E-Nd(III) and A33E-Nd(III)-As(V) were determined using N₂ adsorption-desorption method. The differences in the specific surfaces of the materials were slight. After the modification, it increased from 53.12 to 54.74 m²/g, and after the sorption of arsenate(V) ions, it reached 60.38 m²/g. The total pore volume and the average pore diameter of A33E were 0.122 cm³/g and 9.18 nm while those of A33E-Nd(III) were 0.128 cm³/g and 9.37 nm, respectively. After the sorption

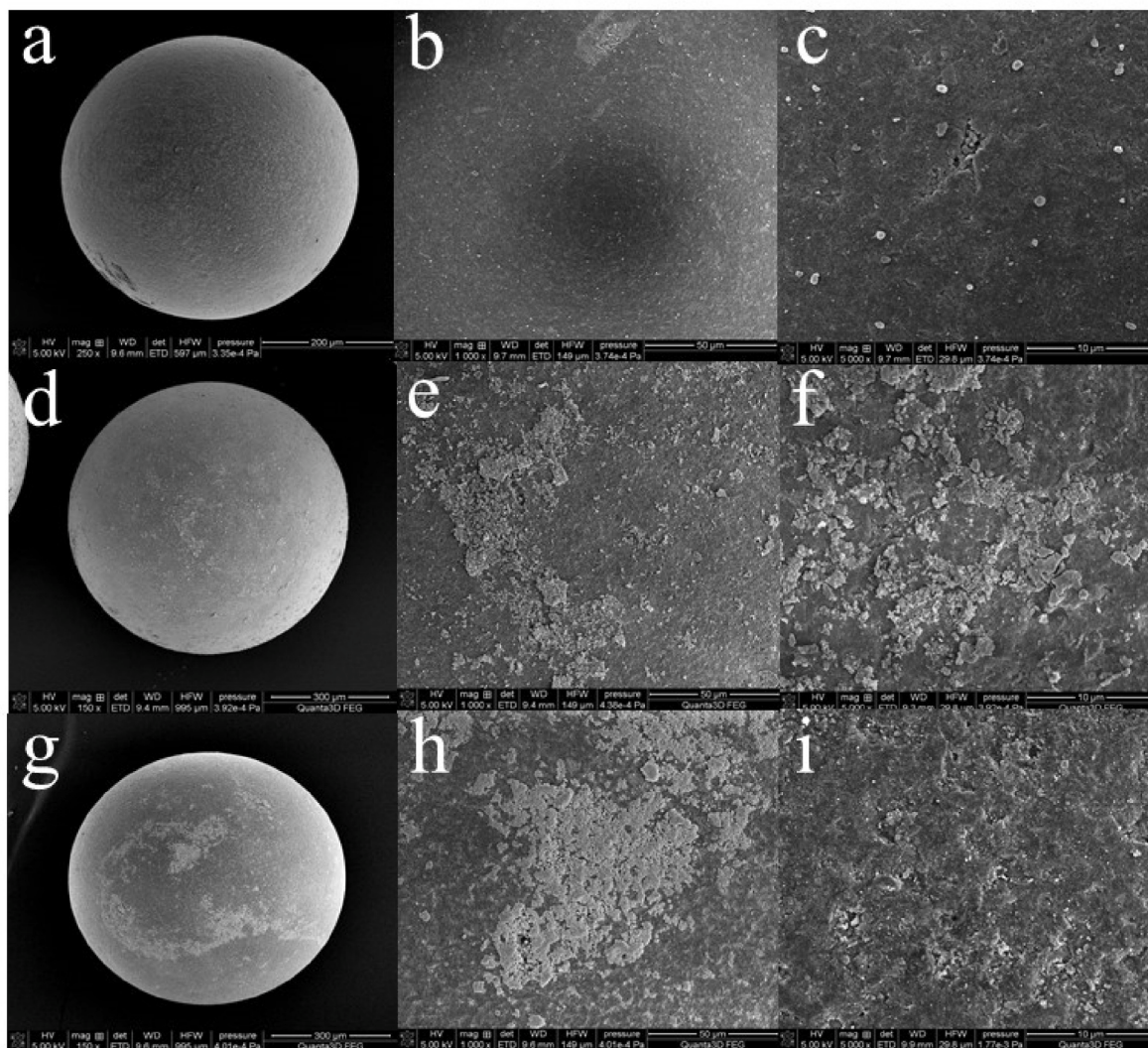


Fig. 1. SEM images of A33E (a–c), A33E-Nd(III) (d–f) and A33E-Nd(III)-As(V) (g–i) at the magnifications 150× (d, g), 250 x (a), 1000 x (b, e, h) and 5000 x (c, f, i).

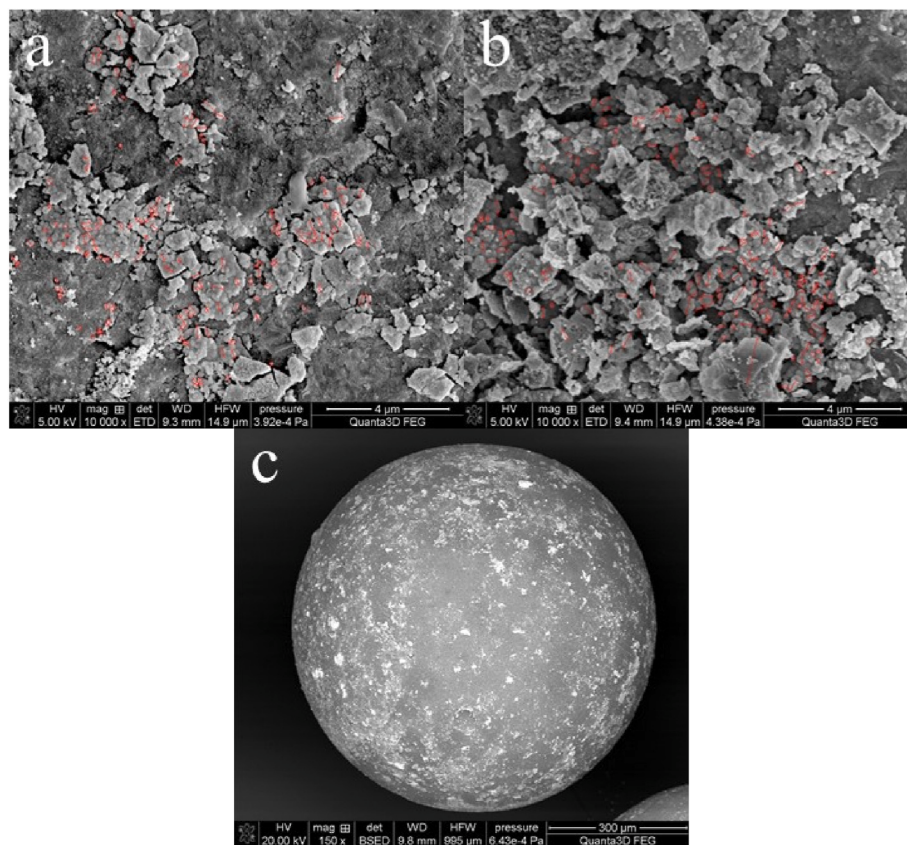


Fig. 2. SEM images of A33E-Nd(III) with the measured objects at the magnification 10000 \times (a, b) and the SEM image of A33E-Nd(III) taken using the BSE detector at the magnification 150 \times (c).

of As(V) ions, the total pore volumes and the average pore diameters increased to 0.143 cm³/g and 9.48 nm, respectively. The all presented isotherms (Fig. 3) are of type IV with the visible hysteresis loops (Sing, 1982). Their shape is practically identical. These facts indicate the mesopores capillary condensation and the limiting adsorption in the range of high p/p_0 . The first part of the isotherm follows the same shape

as type II isotherm suggesting monolayer and multilayer adsorption. The H3 type of hysteresis loop confirms no limiting uptake at high p/p_0 (Brão et al., 2020). The hysteresis loop shape and the SEM images proved the aggregate formation on the adsorbent surface. The deposit of aggregates led to the slit-shaped pores formation.

This is commonly known that pH influences the ionization degree of particles present in the solution and the surface charge of the ion exchanger (Komnitsas et al., 2017). As shown in Fig. 4 the pH_{PZC} for A33E is 8.01 while after the modification it increased and reached a

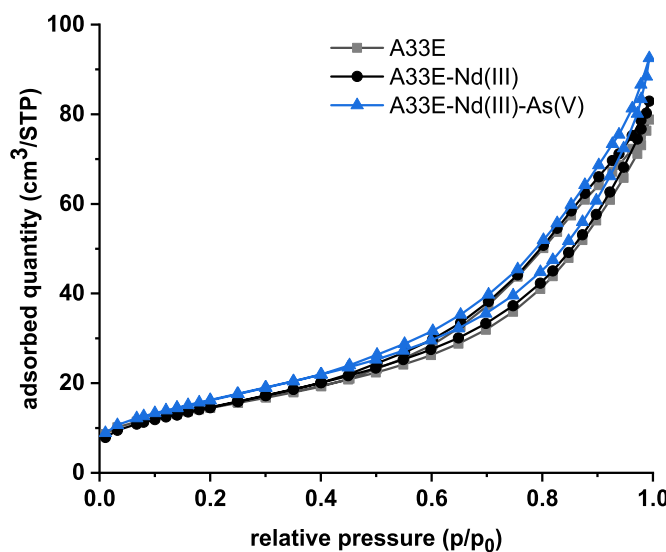


Fig. 3. N₂ adsorption/desorption isotherms of A33E (grey), A33E-Nd(III) (black) and A33E-Nd(III)-As(V) (blue). (For interpretation of the references to colour in this figure legend, the reader is referred to the Web version of this article.)

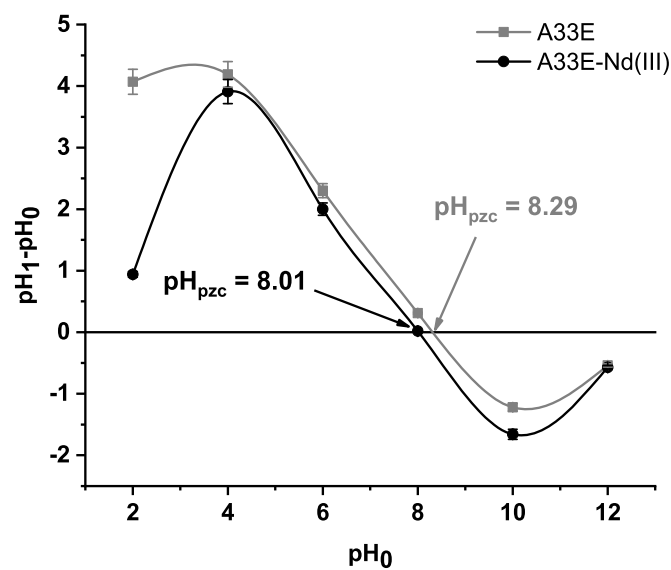


Fig. 4. Points of zero charge of A33E (grey) and A33E-Nd(III) (black).

value of 8.21. This means that at pH below 8.21 the A33E-Nd(III) surface is protonated. At pH of groundwater, i.e. 6.5 to 8.5 (Baba et al., 2020), inorganic As(V) occurs as a deprotonated anionic species (Reid et al., 2020). At pH below 8.21 the positively charged surface of A33E-Nd(III) would be favourable for the As(V) adsorption due to the improvement of mass transfer and increased electrostatic attraction. In contrast, pH above 8.21 would inhibit arsenate(V) adsorption as a result of deprotonated adsorbent surface.

The FTIR analysis was applied to identify functional groups and chemical bonds in A33E and A33E-Nd(III) before and after the As(V) adsorption (Suri et al., 2014). As shown in Fig. 5 a strong wide band in the range of 3600 to 3100 cm⁻¹ can be assigned to the O-H symmetric and asymmetric stretching bond coming from the physisorbed water (Suhailath and Ramesan, 2019). The band at 3030 cm⁻¹ corresponds to the vibration of aromatic C-H stretching originated from polystyrene crosslinked with divinylbenzene (Badruddoza et al., 2013). The double peak at 1637 and 1614 cm⁻¹ originates from H-O-H bending vibrations and the quaternary ammonium group -NR₄⁺, respectively (Suhailath and Ramesan, 2019; Wang et al., 2009). It can be seen that after the modification and the adsorption of As(V) the peaks are getting less intensive. Moreover, the band at 1481 cm⁻¹ also corresponds to the -NR₄⁺ group and becomes less intense due to the Nd(III) and As(V) uptake (Valdés et al., 2018). In the case of A33E-Nd(III)-As(V) the new peak occurs at 445 cm⁻¹. It can be assigned to the Nd-O-As bond, just as the La-O-As vibration band in the lanthanum arsenate (Wang et al., 2020). This is attributed to the Nd-O coordination between the neodymium of active sites and the oxygen atom of arsenate(V). These results indicate formation of inner-sphere surface complexes.

X-ray photoelectron spectroscopy (XPS) was used to assess the chemical and electronic states of the elements after the Nd(III) modification and As(V) adsorption on A33E. The XPS full spectra (Fig. 6a and b) indicated the presence of Fe, O, N, C in all cases. Nitrogen occurs in the form of quaternary ammonium groups while carbon appears mainly in the aromatic C=C, aliphatic C-H and aliphatic C-C bonds coming from polystyrene crosslinked with divinylbenzene. Fig. 6a and b also shows that after the As(V) adsorption new peaks appear at 44.7 and 45.3 eV in the case of A33E and A33E-Nd(III), respectively (Huo et al., 2017; Zhou et al., 2017). This can be assigned to the As3d peak pointing out to successful adsorption of As(V) on the unmodified and modified ion exchanger. Some amounts of As(III) ions on the sorbent surface

appeared due to the partial reduction of As(V) ions by X-ray radiation (Han et al., 2018). Fig. 6b proves also that modification of A33E with neodymium (III) ions took place. The new Nd3d peak occurs at 983.8 eV (M. U. Khan et al., 2020). The XPS spectra of the As3d region of A33E and A33E-Nd(III) after the As(V) adsorption (Fig. 6c and d) indicate shifts in the binding energies. Moreover, in the case of A33E-Nd(III)-As(V) the peaks are more intensive. These facts suggest that the mechanism of As(V) adsorption is different in comparison to the unmodified ion exchanger. The high resolution Nd3d spectra of A33E-Nd(III) before and after the arsenate(V) uptake (Fig. 6e and f) revealed that the adsorbed neodymium (III) was involved in the As(V) sorption. This is evidenced by the shift of the neodymium peaks and the reduction in their intensity. It should be added that the O KLL peaks overlap with the Nd3d peaks.

3.2. Effect of pH

The results of the pH effect on the efficiency of arsenate(V) adsorption on A33E-Nd(III) are presented in Fig. 7. The removal efficiency was studied with respect to the equilibrium pH over the range of pH 4–11 and it can be seen that the solution pH affected the adsorption of As(V). In the given range it can be seen that the sorption capacity differs depending on the pH value.

The sorption efficiency increased constantly in the pH range of 4–6 and then decreased steadily at pH 7–11. At the optimal pH 6 (pH < p_{H_{PZC}}) arsenic(V) ions form negatively charged species which are electrostatically attracted to the protonated surface of A33E-Nd(III) according to Equations (3) and (4) (Deng and Yu, 2012):

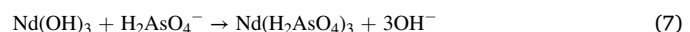


Moreover, positively charged quaternary ammonium groups also enhanced the electrostatic attraction of As(V) species. In the acidic environment neodymium (III) occurs mainly as Nd³⁺ ions (Park and Tavlarides, 2010), therefore formation of insoluble neodymium arsenate also took place on the A33E-Nd(III) surface according to Equations (5) and (6) (Jais et al., 2016):



Interestingly, the FTIR analysis confirmed the formation of the new Nd-O-As bond. This indicates formation of the Nd-O coordination bond between the neodymium active sites and the oxygen atom of arsenate(V) being the evidence of inner-sphere surface complexes formation.

At alkaline pH (pH > p_{H_{PZC}}) the adsorption of As(V) could still proceed but the sorption efficiency was significantly smaller. That was due to the fact that the deprotonated surface of A33E-Nd(III) caused electrostatic repulsion of negatively charged As(V) species. Moreover, under such conditions neodymium (III) took the form of insoluble Nd(OH)₃, therefore the only possible mechanism can assume formation of Nd(H₂AsO₄)₃ or Nd₂(HAsO₄)₃ according to Equations (7) and (8) (Tokunaga et al., 1997):



3.3. Kinetic studies

The time needed to reach the equilibrium state is important in adsorption processes. Therefore, the effect of concentration and contact time on sorption efficiency was studied to find out how fast the process proceeded. It was found that the equilibrium for A33E-Nd(III) was established quickly, i.e. 30 min for the As(V) initial concentrations of 25

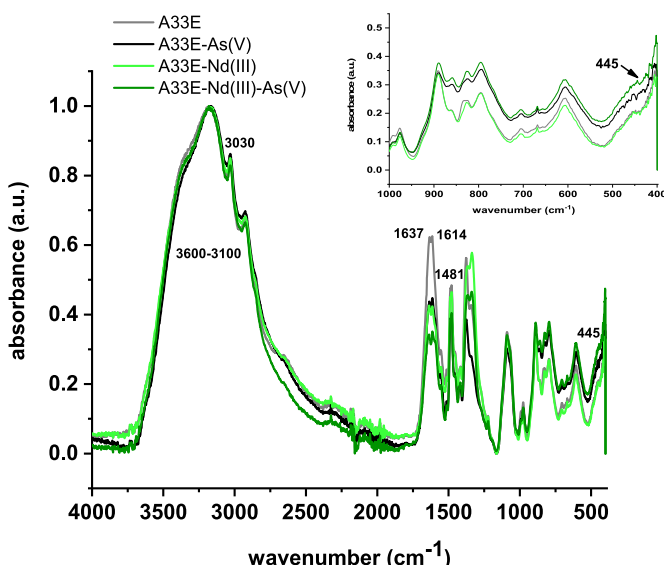


Fig. 5. FTIR spectra of A33E (grey), A33E after the As(V) adsorption (black), A33E-Nd(III) (light green) and A33E-Nd(III) after the As(V) adsorption (dark green). (For interpretation of the references to colour in this figure legend, the reader is referred to the Web version of this article.)

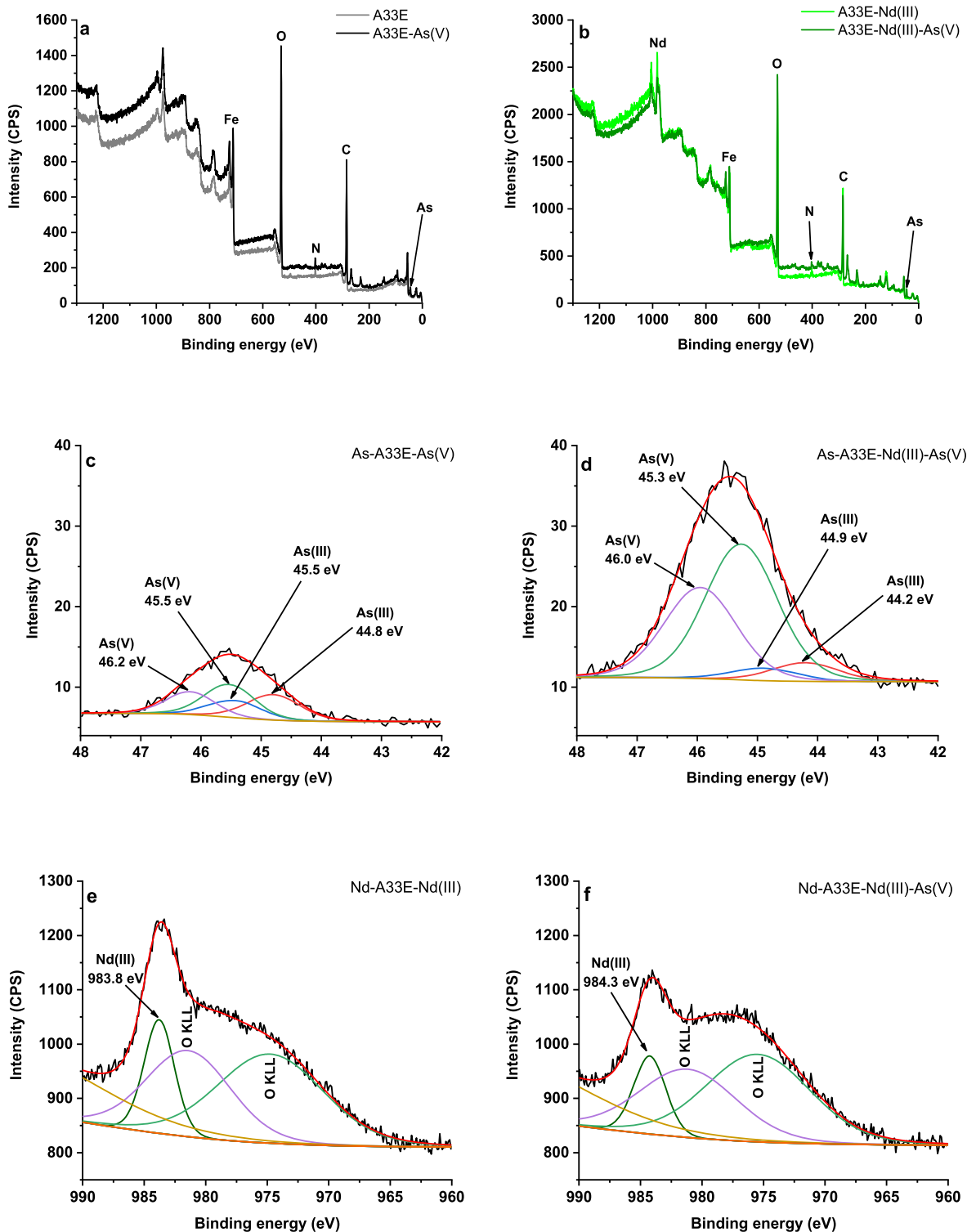


Fig. 6. XPS spectra of A33E, A33E-As(V) (a), A33E-Nd(III), A33E-Nd(III)-As(V) (b), As-A33E-As(V) (c), As-A33E-Nd(III)-As(V) (d), Nd-A33E-Nd(III) (e) and Nd-A33E-Nd(III)-As(V).

and 50 mg/dm³ and about 120 min for 100 mg/dm³ (Fig. 8). Those periods of time were very similar for both sorbents – the modified and unmodified one. This indicates that the equilibrium time of A33E-Nd(III) was not worse than that of A33E. It is worth noting that the As(V) removal percentage of the modified ion exchanger was 100% at the initial concentrations 25 and 50 mg/dm³. At the same concentrations the unmodified ion exchanger exhibited 97 and 88% removal. This leads to the conclusion that owing to the modification it was possible to reach

the WHO limit even in a solution with a concentration as high as 50 mg/dm³ in just 30 min. When removing other impurities from the aqueous solutions at similar initial concentrations, the time ranged from 30 to 120 min (Al-Shaan et al., 2019; Ali et al., 2018a, 2018b, 2019a, 2019b; Alqadami et al., 2018; Naushad et al., 2019a). Therefore, this material can compete successfully with other materials available on the market. At 100 mg/dm³ the removal percentages equalled to 96 and 86% for A33E-Nd(III) and A33E, respectively.

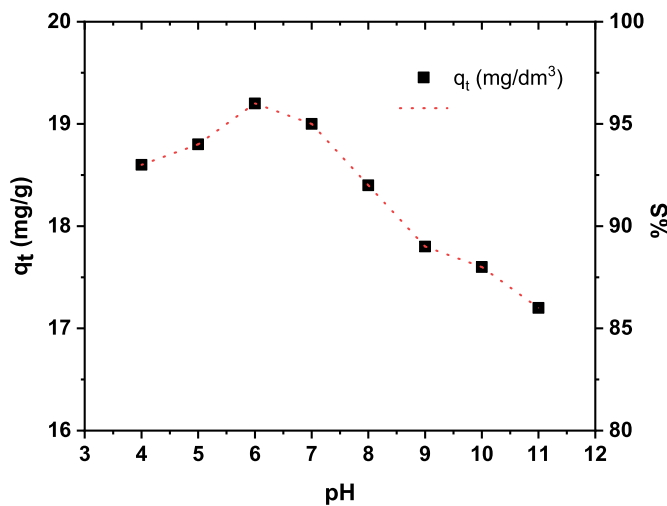


Fig. 7. Effect of pH on the adsorption efficiency of As(V) onto A33E-Nd(III) (initial As(V) concentration c_0 100 mg/dm³, time t 360 min, temperature T 295 K, shaking speed 180 rpm).

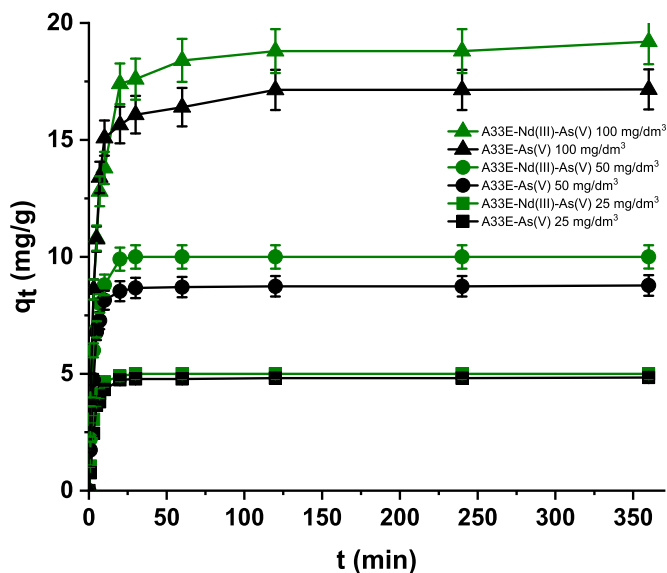


Fig. 8. Effect of As(V) initial concentration and contact time on the adsorption capacities of A33E (black) and A33E-Nd(III) (green) (initial As(V) concentration c_0 25, 50, 100 mg/dm³, time t 1–360 min, temperature T 295 K, pH 6, shaking speed 180 rpm). (For interpretation of the references to colour in this figure legend, the reader is referred to the Web version of this article.)

Kinetic parameters can provide valuable information on the efficiency and mechanism of the adsorption process. Adsorption kinetics is determined by the physical and chemical properties of the adsorbent and adsorbate. Various stages are involved in the adsorption process to transport the pollutant from the aqueous solution to the adsorbent surface. The speed of the entire process can be controlled by a single phase or combination of phases. The experimental kinetic data was fitted to several kinetic models in order to examine the rate or mechanism of As(V) adsorption onto A33E-Nd(III).

The first kinetic model, introduced by Lagergren and refined by Ho for the study of sorption in the liquid-solid systems, is known as the pseudo-first-order (PFO) kinetic model. It is represented by Equation (9) and Equation (10) as the linear form (Guo and Wang, 2019):

$$\frac{dq_t}{dt} = k_1(q_e - q_t) \quad (9)$$

$$\ln(q_e - q_t) = \ln q_e - k_1 t \quad (10)$$

where: q_t is the amount of As(V) adsorbed onto the adsorbent at time t (mg/g), q_e is the equilibrium adsorption capacity (mg/g), k_1 is the PFO rate constant (1/min).

The PSO equation is based on the hypothesis that the rate of adsorption is a quadratic function of the difference between the adsorption capacity at equilibrium and at time t , which is given as (Equation (11)) (Kuśmirek et al., 2021):

$$\frac{dq_t}{dt} = k_2(q_e - q_t)^2 \quad (11)$$

where: k_2 is the PSO rate constant (g/(mg•min)).

The linear form of the equation of PSO model can be written as follows (Equation (12)) (Bujdák, 2020):

$$\frac{t}{q_t} = \frac{1}{k_2 q_e^2} + \frac{t}{q_e} \quad (12)$$

The Elovich model assumes that the solid surface is energetically heterogeneous and that the process is of the chemisorption type. The non-linear and linear forms of the Elovich model can be represented by Equations (13) and (14) (Giri et al., 2021; Xiong et al., 2021):

$$\frac{dq_t}{dt} = \alpha \exp^{-\beta q_t} \quad (13)$$

$$q_t = \frac{1}{\beta} \ln(\alpha\beta) + \frac{1}{\beta} \ln t \quad (14)$$

where: α is the initial adsorption rate (mg/(g•min)) and β is associated with the surface coverage and activation energy of chemisorption (g/mg).

According to the intraparticle diffusion (IPD) model, the plot of q_t versus the square root of time (\sqrt{t}) should be linear if the adsorption process is controlled by the IPD process. Equation (15) shows the linear form of the mentioned model (Ravi and Pandey, 2019):

$$q_t = k_i \sqrt{t} + C \quad (15)$$

where: k_i is the IPD rate constant and C is the boundary layer thickness.

All kinetic parameters and fitting to the models are presented in Table 1 and Fig. 9a, respectively. The regression coefficients R^2 0.4842,

Table 1
Kinetic parameters of As(V) adsorption on A33E-Nd(III).

Model	Parameter	As(V) 25 mg/dm ³	As(V) 50 mg/dm ³	As(V) 100 mg/dm ³
PFO	q_e (mg/g)	5.00	10.00	19.20
	q_1 (mg/g)	0.32	0.59	5.40
	k_1 (1/min)	0.030	0.033	0.014
	R^2	0.4842	0.4823	0.6475
	SSE	195.97	763.44	1834.58
PSO	q_2 (mg/g)	5.03	10.06	19.30
	k_2 (g/mg•min)	0.152	0.067	0.015
	R^2	0.9999	0.9999	0.9999
	SSE	1.62	5.37	1.94
Elovich	α (mg/g•min)	68.93	92.69	39.08
	β (g/mg)	1.87	0.90	0.40
	R^2	0.6594	0.7095	0.8544
IPD	SSE	5.20	17.94	37.67
	k_{i1} (mg/g•min ^{-1/2})	2.261	3.461	4.692
	C_1 (mg/g)	-1.112	-0.814	-0.152
	R^2_1	0.9775	0.9481	0.9649
	k_{i2} (mg/g•min ^{-1/2})	0.368	0.533	0.313
	C_2 (mg/g)	3.307	7.235	15.951
	R^2_2	0.8218	0.8665	0.9870
	k_{i3} (mg/g•min ^{-1/2})	0.000	0.000	0.047
	C_3 (mg/g)	4.997	9.996	18.215
	R^2_3	0.5370	0.5870	0.6817
	SSE	0.14	1.11	2.27

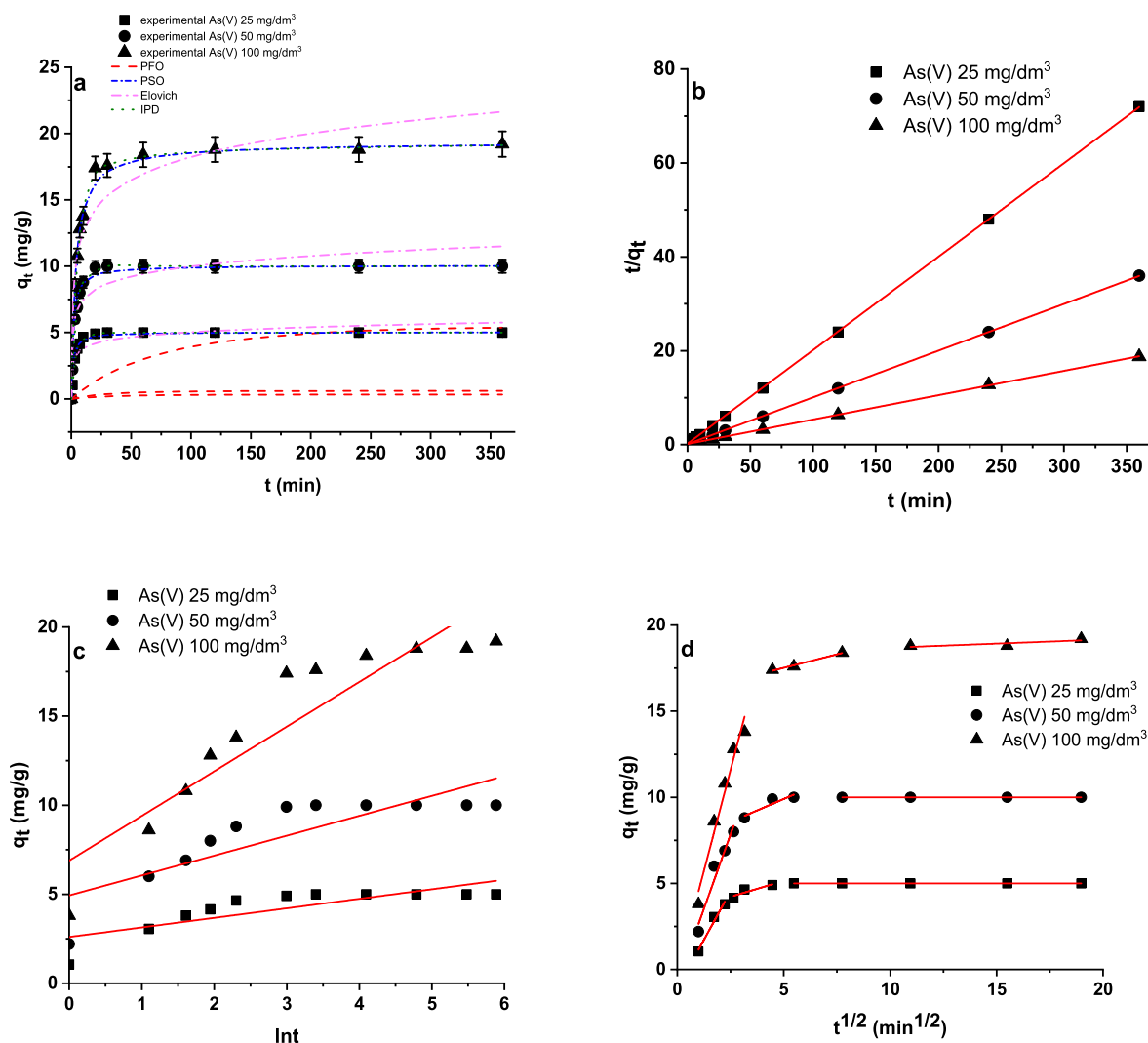


Fig. 9. Kinetics of As(V) adsorption onto A33E-Nd(III) with the fitted models of PFO, PSO, Elovich and IPD ($c_0 = 25, 50$ and 100 mg/dm^3 , pH = 6, shaking speed 180 rpm, temperature 295 K) (a), linear PSO kinetic plots for the As(V) adsorption onto A33E-Nd(III) (b), Elovich kinetic plots for the As(V) adsorption onto A33E-Nd(III) (c), IPD kinetic plots for As(V) adsorption onto A33E-Nd(III) (d).

0.4823 and 0.6475 suggested very poor fitting of the experimental data to the PFO model. All regression R^2 values of the PSO model were equal to 0.9999 indicating that the pseudo-second order describes the adsorption process much better. This was also confirmed by the error analysis using the sum of squared errors SSE proving that the PSO model can be employed to describe the sorption process which is controlled by chemisorption. Linear fitting of PSO model to the experimental data is presented in Fig. 9b. The correlation coefficients R^2 of the Elovich model are relatively small but they increase with the increasing As(V) initial concentration confirming that the process is chemisorption (Berhane et al., 2017). What is more, the constant β (related to the surface coverage) decreases with the increasing initial adsorbate concentration due to the available adsorption surface reduction. Linear fitting of the Elovich model is presented in Fig. 9c. The fit lines in the IPD model do not pass through the origin, showing that intraparticle diffusion is not the only affecting step (Sharma et al., 2019). The multilinear IPD plot for q_t vs $t^{1/2}$ indicates that three diffusion steps are included in the As(V) adsorption on A33E-Nd(III). In the first stage prompt adsorption takes place. In the second stage balanced adsorption occurs controlling the intraparticle diffusion and the final step is achieving equilibrium.

3.4. Adsorption equilibrium and thermodynamic studies

In order to determine adsorption capabilities of A33E-Nd(III) the effect of the initial As(V) concentration was studied. It was noticed that with the increase of the initial concentration, the sorption capacity increased until the equilibrium state was reached. The experimental results were fitted to various isotherm models for better explanation of the adsorptive behaviour of arsenate(V) ions on A33E-Nd(III). The linear regression analysis as well as the sum of squared errors (SSE) and F-Test were used to examine the data fit to the theoretical models. The linear forms of Langmuir (Equation (16)), Freundlich (Equation (17)), Dubinin-Radushkevich (Equations (18)–(20)) and Halsey (Equation (21)) models are presented below (Yetilmezsoy et al., 2020).

$$\frac{c_e}{q_e} = \frac{1}{q_m K_L} + \frac{c_e}{q_m} \quad (16)$$

where: c_e is the equilibrium solute concentration (mg/g), q_e is the sorption capacity at equilibrium (mg/g), q_m (g/mg) and K_L (dm³/mg) are the Langmuir constants, related to the maximum sorption capacity and the sorption energy, which were determined from the slope and intercept of the linear plot c_e/q_e vs c_e .

$$\log q_e = \log K_F + \frac{1}{n} \log c_e \quad (17)$$

where: K_F (mg/g) and $1/n$ (–) are the constants referring to the adsorption capacity and adsorption intensity, respectively. They can be determined from the slope and intercept of the plot $\log q_e$ vs $\log c_e$.

$$\ln q_e = \ln q_{DR} - \beta e^2 \quad (18)$$

$$\varepsilon = RT \ln \left(1 + \frac{1}{c_e} \right) \quad (19)$$

$$E = \frac{1}{\sqrt{2}\beta} \quad (20)$$

where: q_{DR} (mol/g) is the theoretical adsorption capacity, β (mol²/J²) is the activity constant linked to the mean free energy of adsorption, ε is related to the Polanyi potential, R (8.314 J/K/mol) represents the gas constant, T (K) is the temperature, E (J/mol) is associated with the essential energy to transfer a mole of sorbate from the solution to the sorbent surface.

$$\ln q_e = \frac{1}{n_H} \ln K_H - \frac{1}{n_H} \ln \frac{1}{c_e} \quad (21)$$

where: K_H and n_H are the Halsey coefficients which can be determined from the slope and intercept of the plot $\ln q_e$ vs $\ln c_e$.

All isotherm parameters and linear plots of the isotherm models are presented in Table 2 and Fig. 10, respectively.

It was found that all models presented relatively high correlation coefficients ($R^2 > 0.9$). This indicates that the experimental data could be acceptably described by the aforementioned models. The dimensionless R_L factor from the Langmuir model and $1/n$ from the Freundlich model were equal to 0.348 and 0.190 ($n = 5.261$), respectively indicating that arsenate(V) adsorption on A33E-Nd(III) is a favourable and feasible process (Maji et al., 2018). The maximum adsorption capacity on the monomolecular layer of A33E-Nd(III) determined from the Langmuir model was 56.01 mg/g at 295 K. It is worth noting that the maximum sorption capacity for the unmodified A33E is only 34.41

Table 2

Langmuir, Freundlich, Dubinin-Radushkevich and Halsey isotherm parameters with the error analysis (correlation coefficients R^2 , sum of squared errors SSE and F-Test).

Parameters and error analysis	
Langmuir model	
q_m (mg/g)	56.01
K_L (dm ³ /mg)	0.075
R_L	0.348
R^2	0.997
SSE	355.01
F-Test	0.68
Freundlich model	
K_F (mg/g)	16.353
N	5.261
R^2	0.945
SSE	113.92
F-Test	0.89
Dubinin-Radushkevich model	
q_{DR} (mol/g)	$7.975 \cdot 10^{-4}$
β (mol ² /J ²)	$1.461 \cdot 10^{-9}$
E (kJ/mol)	18.50
R^2	0.914
SSE	299.05
F-Test	0.65
Halsey model	
n_H	-5.261
K_H	$4.121 \cdot 10^{-7}$
R^2	0.945
SSE	113.92
F-Test	0.89

mg/g. This is the evidence that the modification with Nd(III) ions increased the maximum sorption capacity over 1.5 times. The comparison of the maximum sorption capacities of various sorbents containing rare earth elements is presented in Table 3. The value of E (18.50 kJ/mol) calculated from the Dubinin-Radushkevich model indicated that the sorption of arsenate(V) ions was essentially chemisorption (Amin et al., 2015). Therefore, the attachment of arsenate(V) ions must have taken place at the active sites on the surface of A33E-Nd(III) with the quaternary ammonium and Nd-OH groups. This confirmed the contribution to the adsorption process by the ion exchange/chemical complexation.

Nevertheless, further error analysis was needed to decide which isotherm gives the best fit. SSE and F-Test indicated that the Freundlich and Halsey models described arsenate(V) sorption on A33E-Nd(III) better. This revealed the possibility of multilayer adsorption on the heterogeneous adsorbent even at a relatively large distance from its surface (Liu and Wang, 2013).

The effect of temperature on the adsorption of As(V) ions on A33E-Nd(III) was also investigated and basic thermodynamic parameters were determined according to Equations (22)–(24) (Pan et al., 2017):

$$K_d = \frac{q_e}{c_e} \quad (22)$$

$$\Delta G^0 = -RT \ln K_d \quad (23)$$

$$\ln K_d = -\frac{\Delta H^0}{RT} + \frac{\Delta S^0}{R} \quad (24)$$

where: K_d (dm³/g) is the distribution coefficient, ΔG^0 (kJ/mol) is the change of Gibbs energy, ΔH^0 (kJ/mol) is the change of enthalpy and ΔS^0 (kJ/mol·K) refers to the entropy.

The effect of temperature on the equilibrium adsorption capacity and the thermodynamic parameters are presented in Fig. 11 and Table 4, respectively. The negative values of ΔG^0 and ΔH^0 indicated that the process was spontaneous, feasible and exothermic (Edet and Ifelebuegu, 2020). Due to the negative value of the enthalpy change ΔH^0 , running the process at high temperatures is not recommended. The positive values of ΔS^0 pointed out to the increase in randomness at the interface during the adsorption of arsenate(V) on A33E-Nd(III).

3.5. Reusability of A33E-Nd(III)

The adsorbent reusability was assessed in 3 cycles of adsorption/desorption. It is commonly believed that NaOH is the best desorbing agent in the case of arsenate(V) ions (He et al., 2012; Jais et al., 2016). In the first cycle three solutions of NaOH at various concentrations of 0.05, 0.2 and 1 mol/dm³ were tested. The desorption efficiencies were equal to 42, 78 and 99%, respectively. Therefore, 1M NaOH was selected for further testing. After 3 consecutive cycles the desorption efficiency decreased from 99 to 94% (Fig. 12). The sorption capacity dropped from 19.20 to 18.00 mg/g. It is worth noting that after 3 cycles A33E-Nd(III) is still characterized by a higher sorption capacity than unmodified A33E before any cycle (17.17 mg/g). The high adsorption efficiency even in the third run proved that A33E-Nd(III) has a potential of regeneration and great stability.

3.6. Cost analysis and the problem of arsenic waste storage

The arsenic(V) removal procedure on the A33E ion exchanger modified with neodymium (III) ions is not costly. The cost of neodymium (III) oxide N₂O₃ used in the sorbent modification is relatively high but it is worth noting that its trace amounts are exploited. This makes the modification itself a reasonably priced process. The maximum sorption capacity of A33E-Nd(III) was over 1.5 times greater than that of A33E, so more arsenic can be adsorbed in the case of the obtained material. Moreover, after 3 sorption/desorption cycles, the desorption efficiency

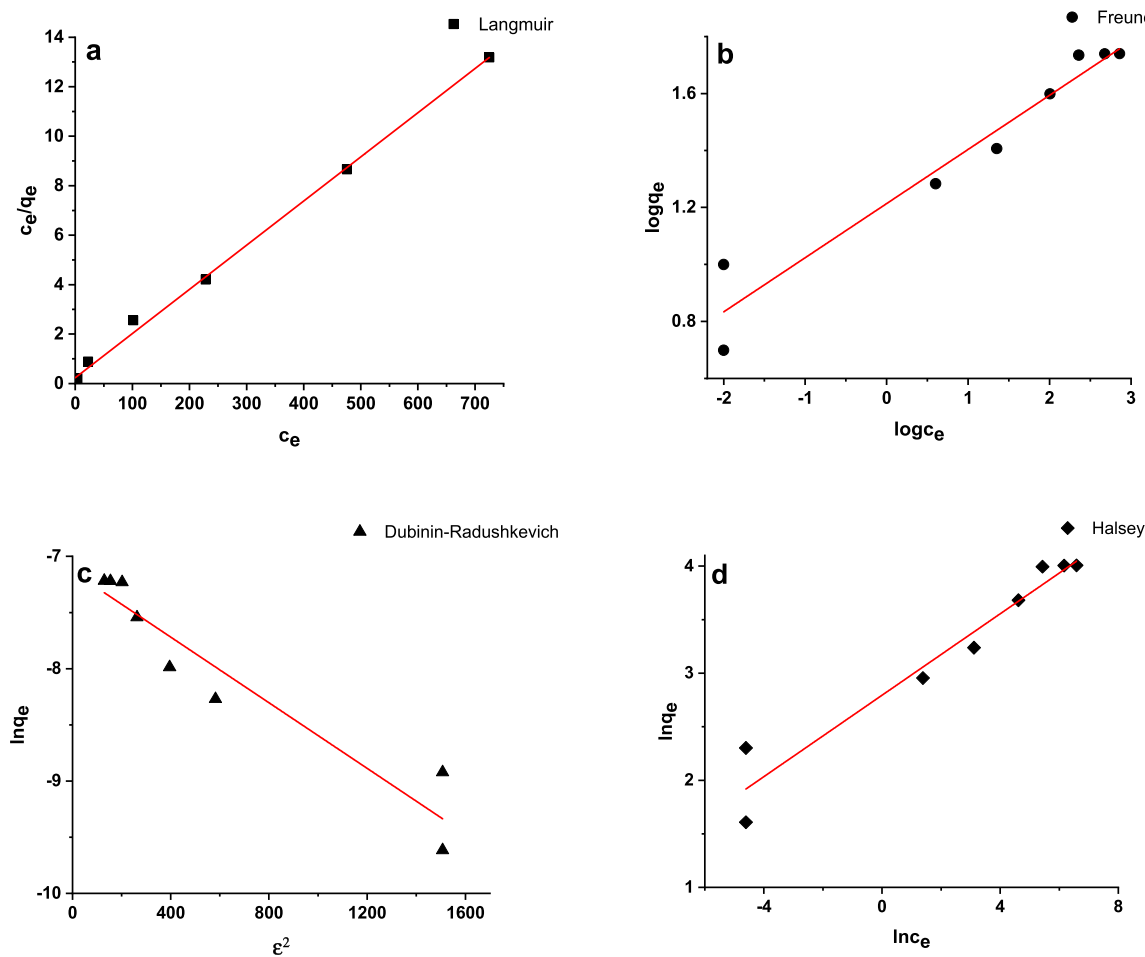


Fig. 10. Linear plots of the Langmuir (a), Freundlich (b), Dubinin-Radushkevich (c) and Halsey (d) isotherm models.

Table 3
Comparison of adsorption capacities of REE sorbents used for the arsenate(V) removal.

Adsorbent	As(V) adsorption capacity (mg/g)	pH	Reference
Cerium oxide modified activated carbon	43.6	5.0	Yu et al. (2017)
Hydroxy cerium oxide-graphene composite	41.31	7.0	Yu et al. (2015)
Ce(III)-loaded Amberlite 200CT resin	53.57	8.7	Shao et al. (2008)
Porous flowered graphene oxide-lanthanum fluoride (GO-LaF)	18.52	6.0	Lingamdinne et al. (2019)
Lanthanum-doped ferric-based layered double hydroxide	47.4	6.0	Jun et al., (2014)
Lanthanum immobilized on electrospun chitosan nanofiber (CSN)	83.6	4.0	Tan et al. (2020)
A33E	34.41	6.0	This study
A33E-Nd(III)	56.01	6.0	This study

decreased slightly and the maximum sorption capacity was greater than that of A33E without any sorption/desorption cycles. It can be seen that the adsorption of a small amount of neodymium ions increases the efficiency of water purification, significantly thus reducing the cost of the entire procedure.

The assessment of proper disposal strategies for the arsenic-bearing wastes generated during the treatment is critical for the effective use of arsenic water treatment systems. Specific guidelines for arsenic waste disposal are either absent or identified as a future study subject, and the

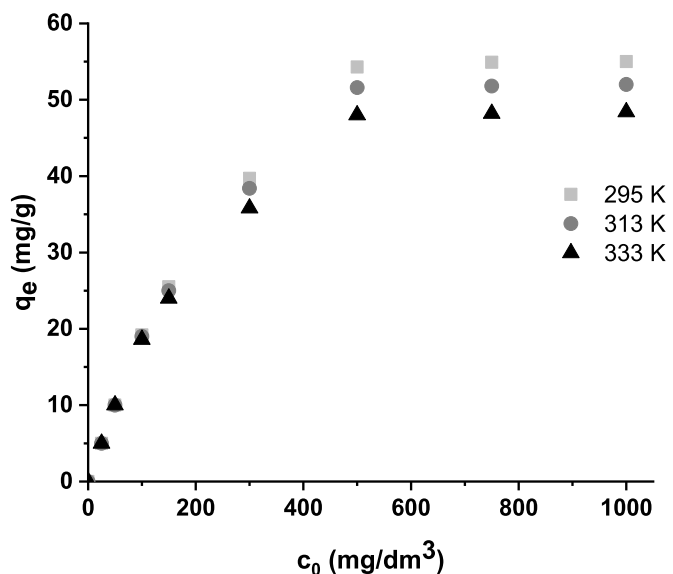


Fig. 11. Effect on the equilibrium adsorption capacity at 295, 313 and 333 K (initial As(V) concentration c_0 25–1000 mg/dm³, time t 360 min, pH 6, shaking speed 180 rpm).

correct disposal and stabilization of arsenic-bearing wastes continues to be a hurdle to the effective adoption of arsenic removal technology. Arsenic-containing wastes should be disposed of in surroundings that

Table 4
Thermodynamic parameters.

T (K)	q_e (mg/ g)	c_e (mg/ g)	K_d (dm ³ /g)	ΔG° (kJ/ mol)	ΔH° (kJ/ mol)	ΔS° (kJ/ mol·K)
295	55.00	725.00	0.076	-10.62	-3.70	0.0235
313	52.00	740.00	0.070	-11.07		
333	48.40	758.00	0.064	-11.51		

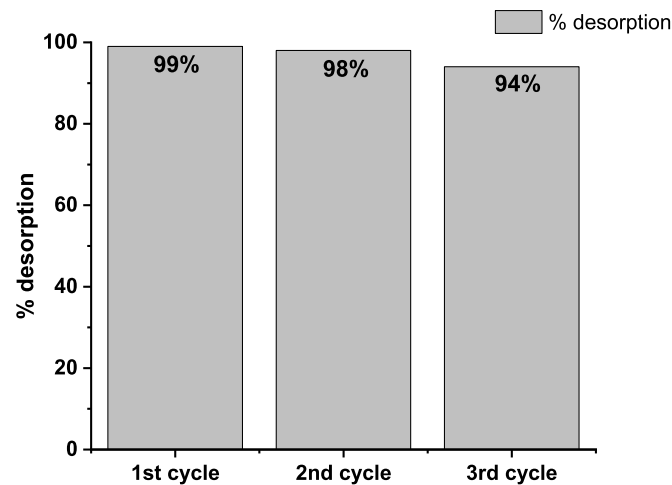


Fig. 12. Reusability of A33E-Nd(III) in the 3 consecutive cycles of sorption and desorption (initial As(V) concentration c_0 100 mg/dm³, sorption time t 360 min, desorption time t 360 min, temperature T 295 K, pH 6, shaking speed 180 rpm).

minimize the danger of arsenic leakage into the environment and pollution of water as well as food supplies (Kasiuliene et al., 2020). Ideal settings are those that are comparable to the circumstances in which arsenic was removed as oxidized arsenic-bearing waste containment in a passive aeration system. Furthermore, given the potential of microbially driven arsenic and iron transformations, wastes should be kept under the small microbial activity conditions. Such a situation might be provided via specific stabilization. Arsenic-containing concrete, on the other hand, should be utilized only in situations where microbiological activity is negligible (Clancy et al., 2013). Future studies should focus on changes of conditions in landfills and other disposal sites across time and space.

4. Conclusions

The iron oxide sorbent with the quaternary ammonium groups was successfully modified with neodymium (III) ions. This is evidenced by the detection of Nd(III) ions by means of the FTIR, XPS and SEM analyses. The obtained A33E-Nd(III) sorbent has excellent sorption properties in relation to the arsenate(V) ions. At optimal pH 6 the main mechanisms of As(V) sorption was formation of inner-sphere complexes and electrostatic attraction by the positively charged sorbent surface enhanced by the presence of quaternary ammonium groups. The additional mechanism of As(V) removal ions in a slightly acidic environment was the precipitation of neodymium arsenate. At the initial As(V) concentration even up to 50 mg/dm³ A33E-Nd(III) could entirely remove arsenate(V) ions after only 30 min. Adding the sorbent to a solution with such a high concentration will meet the stringent requirements of the WHO. Interestingly, the maximum sorption capacity of A33E-Nd(III) (56.01 mg/g) is over 1.5 times greater than that of unmodified A33E (34.41 mg/g). Moreover, after 3 sorption and desorption cycles, A33E-Nd(III) has a better sorption capacity than A33E before the use. The process has also been shown to be exothermic, so it does not need to be carried out at elevated temperatures. It can be concluded that the modification of the sorbent with a small amount of neodymium (III) ions

improves its sorption properties significantly. The process of arsenic removal from the aqueous solutions can become even more efficient and low-cost. The adsorption of a small amount of neodymium ions considerably boosts the effectiveness of water purification, reducing the overall cost of the operation. Moreover, given the potential for microbially driven arsenic and iron transformations, wastes should be stored in small microbial activity settings. Specific stabilization might provide such a condition.

Credit author statement

Sebastian Dudek: Investigation, Writing – original draft, Visualization, **Dorota Kołodyńska:** Supervision, Writing – review & editing.

Declaration of competing interest

The authors declare that they have no known competing financial interests or personal relationships that could have appeared to influence the work reported in this paper.

References

- Adelaju, S.B., Khan, S., Patti, A.F., 2021. Arsenic contamination of groundwater and its implications for drinking water quality and human health in under-developed countries and remote communities—a review. *Appl. Sci.* 11, 1–25. <https://doi.org/10.3390/app11041926>.
- Ahmadi, S., Mohammadi, L., Rahdar, A., Rahdar, S., Dehghani, R., Igwegbe, C.A., Kyazas, G.Z., 2020. Acid dye removal from aqueous solution by using neodymium(III) oxide nanoadsorbents. *Nanomaterials* 10, 1–26. <https://doi.org/10.3390/nano10030556>.
- Al-Shaanah, N.H., Ali, I., ALOthman, Z.A., Al-Wahaibi, L.H., Alabdulmonem, H., 2019. High performance removal and simulation studies of diuron pesticide in water on MWCNTs. *J. Mol. Liq.* 289, 111039. <https://doi.org/10.1016/j.molliq.2019.111039>.
- Ali, I., Alharbi, O.M.L., ALOthman, Z.A., Al-Mohaimeed, A.M., Alwarthan, A., 2019a. Modeling of fenuron pesticide adsorption on CNTs for mechanistic insight and removal in water. *Environ. Res.* 170, 389–397. <https://doi.org/10.1016/j.envres.2018.12.066>.
- Ali, I., Alharbi, O.M.L., ALOthman, Z.A., Alwarthan, A., 2018a. Facile and eco-friendly synthesis of functionalized iron nanoparticles for cyanazine removal in water. *Colloids Surf. B: Biointerfaces* 171, 606–613. <https://doi.org/10.1016/j.colsurfb.2018.07.071>.
- Ali, I., Alharbi, O.M.L., ALOthman, Z.A., Alwarthan, A., Al-Mohaimeed, A.M., 2019b. Preparation of a carboxymethylcellulose-iron composite for uptake of atorvastatin in water. *Int. J. Biol. Macromol.* 132, 244–253. <https://doi.org/10.1016/j.ijbiomac.2019.03.211>.
- Ali, I., Alharbi, O.M.L., ALOthman, Z.A., Alwarthan, A., Al-Mohaimeed, A.M., 2018b. Kinetics, thermodynamics, and modeling of amido black dye photodegradation in water using Co/TiO₂ nanoparticles. *Photochem. Photobiol.* 94, 935–941. <https://doi.org/10.1111/php.12937>.
- Ali, I., ALOthman, Z.A., Alwarthan, A., 2017. Supra molecular mechanism of the removal of 17-β-estradiol endocrine disturbing pollutant from water on functionalized iron nano particles. *J. Mol. Liq.* 241, 123–129. <https://doi.org/10.1016/j.molliq.2017.06.005>.
- Alka, S., Shahir, S., Ibrahim, N., Ndejiko, M.J., Vo, D.V.N., Manan, F.A., 2021. Arsenic removal technologies and future trends: a mini review. *J. Clean. Prod.* 278 <https://doi.org/10.1016/j.jclepro.2020.123805>.
- ALothman, Z.A., 2012. A review: fundamental aspects of silicate mesoporous materials. *Materials* 5, 2874–2902. <https://doi.org/10.3390/ma5122874>.
- ALothman, Z.A., Bahkali, A.H., Khiyami, M.A., Alfadul, S.M., Wabaidur, S.M., Alam, M., Alfarhan, B.Z., 2020. Low cost biosorbents from fungi for heavy metals removal from wastewater. *Separ. Sci. Technol.* 55, 1766–1775. <https://doi.org/10.1080/01496395.2019.1608242>.
- Alqadami, A.A., Khan, M.A., Siddiqui, M.R., ALOthman, Z.A., 2018. Development of citric anhydride anchored mesoporous MOF through post synthesis modification to sequester potentially toxic lead(II) from water. *Microporous Mesoporous Mater.* 261, 198–206. <https://doi.org/10.1016/j.micromeso.2017.11.016>.
- Amin, M.T., Alazba, A.A., Shafiq, M., 2015. Adsorptive removal of reactive black 5 from wastewater using bentonite clay: isotherms, kinetics and thermodynamics. *Sustain. Times* 7, 15302–15318. <https://doi.org/10.3390/su7115302>.
- Baba, M. El, Kayastha, P., Huysmans, M., Smedt, F. De, 2020. Evaluation of the groundwater quality using the water quality index and geostatistical analysis in. *Water* 12, 262.
- Badruddoza, A.Z.M., Shawon, Z.B.Z., Rahman, M.T., Hao, K.W., Hidajat, K., Uddin, M.S., 2013. Ionically modified magnetic nanomaterials for arsenic and chromium removal from water. *Chem. Eng. J.* 225, 607–615. <https://doi.org/10.1016/j.cej.2013.03.114>.
- Berhane, T.M., Levy, J., Krekeler, M.P.S., Danielson, N.D., 2017. Chemosphere Kinetic sorption of contaminants of emerging concern by a palygorskite-montmorillonite

- filter medium. *Chemosphere* 176, 231–242. <https://doi.org/10.1016/j.chemosphere.2017.02.068>.
- Brião, G. de V., Silva, M.G.C. da, Vieira, M.G.A., 2020. Neodymium recovery from aqueous solution through adsorption/desorption onto expanded vermiculite. *Appl. Clay Sci.* 198, 105825. <https://doi.org/10.1016/j.clay.2020.105825>.
- Bujdák, J., 2020. Adsorption kinetics models in clay systems. The critical analysis of pseudo-second order mechanism. *Appl. Clay Sci.* 191, 105630. <https://doi.org/10.1016/j.clay.2020.105630>.
- Clancy, T.M., Hayes, K.F., Raskin, L., 2013. Arsenic waste management: a critical review of testing and disposal of arsenic-bearing solid wastes generated during arsenic removal from drinking water. *Environ. Sci. Technol.* 47, 10799–10812. <https://doi.org/10.1021/es401749b>.
- Deng, H., Yu, X., 2012. Adsorption of fluoride, arsenate and phosphate in aqueous solution by cerium impregnated fibrous protein. *Chem. Eng. J.* 184, 205–212. <https://doi.org/10.1016/j.cej.2012.01.031>.
- Edet, U.A., Ifelebuegu, A.O., 2020. *Wastewater Using Recycled Brick Waste. Processes, vol. 8*.
- Giri, D.D., Jha, J.M., Tiwari, A.K., Srivastava, N., Hashem, A., Alqarawi, A.A., Abd Allah, E.F., Pal, D.B., 2021. Java plum and amaltash seed biomass based bio-adsorbents for synthetic wastewater treatment. *Environ. Pollut.* 280, 116890. <https://doi.org/10.1016/j.envpol.2021.116890>.
- Guo, X., Wang, J., 2019. A general kinetic model for adsorption: theoretical analysis and modeling. *J. Mol. Liq.* 288, 111100. <https://doi.org/10.1016/j.molliq.2019.111100>.
- Han, Y.-S., Jeong, H.Y., Hyun, S.P., Hayes, K.F., Chon, C.-M., IUCr, 2018. Beam-induced redox transformation of arsenic during as K-edge XAS measurements: availability of reducing or oxidizing agents and as speciation. *J. Synchrotron Radiat.* 25, 763–770. <https://doi.org/10.1107/S1600577518002576>.
- He, Z., Tian, S., Ning, P., 2012. Adsorption of arsenate and arsenite from aqueous solutions by cerium-loaded cation exchange resin. *J. Rare Earths* 30, 563–572. [https://doi.org/10.1016/S1002-0721\(12\)60092-1](https://doi.org/10.1016/S1002-0721(12)60092-1).
- Huo, L., Zeng, X., Su, S., Bai, L., Wang, Y., 2017. Enhanced removal of As(V) from aqueous solution using modified hydrous ferric oxide nanoparticles. *Sci. Rep.* 7, 1–12. <https://doi.org/10.1038/srep40765>.
- Jais, F.M., Ibrahim, S., Yoon, Y., Jang, M., 2016. Enhanced arsenate removal by lanthanum and nano-magnetite composite incorporated palm shell waste-based activated carbon. *Separ. Purif. Technol.* 169, 93–102. <https://doi.org/10.1016/j.seppur.2016.05.034>.
- Jun, H., Zhiliang, Z., Hongtao, L., Yanling, Q., 2014. Effect of metal composition in lanthanum-doped ferric-based layered double hydroxides and their calcined products on adsorption of arsenate. *RSC Adv.* 4, 5156–5164. <https://doi.org/10.1039/c3ra46680a>.
- Kasiuliene, A., Carabante, I., Sefidari, H., Öhman, M., Bhattacharya, P., Kumpiene, J., 2020. Leaching of metal(loid)s from ashes of spent sorbent and stabilisation effect of calcium-rich additives. *Environ. Sci. Pollut. Res.* 27, 29248–29256. <https://doi.org/10.1007/s11356-020-09269-z>.
- Kenay, E.R., Ghfar, A.A., Wabaidur, S.M., Khan, M.A., Siddiqui, M.R., Alothman, Z.A., Alqadami, A.A., Hamid, M., 2018. Cetyltrimethylammonium bromide intercalated and branched polyhydroxystyrene functionalized montmorillonite clay to sequester cationic dyes. *J. Environ. Manag.* 219, 285–293. <https://doi.org/10.1016/j.jenvman.2018.04.121>.
- Khan, M.A., Alqadami, A.A., Wabaidur, S.M., Siddiqui, M.R., Jeon, B.H., Alshareef, S.A., Alothman, Z.A., Hamedelniel, A.E., 2020. Oil industry waste based non-magnetic and magnetic hydrochar to sequester potentially toxic post-transition metal ions from water. *J. Hazard Mater.* 400, 123247. <https://doi.org/10.1016/j.jhazmat.2020.123247>.
- Khan, M.U., Rather, R.A., Siddiqui, Z.N., 2020. Design, characterization and catalytic evaluation of halometallic ionic liquid incorporated Nd₂O₃ nanoparticles ([smim][FeCl₄]/Nd₂O₃) for the synthesis of N-aryl indeno pyrrole derivatives. *RSC Adv.* 10, 44892–44902. <https://doi.org/10.1039/d0ra08812a>.
- Komnitsas, K., Zaharaki, D., Bartzas, G., Alevizos, G., 2017. Adsorption of scandium and neodymium on biochar derived after low-temperature pyrolysis of sawdust. *Minerals* 7, 1–18. <https://doi.org/10.3390/min710020>.
- Kuśmierek, K., Świątkowski, A., Kotkowski, T., Cherbański, R., Molga, E., 2021. Adsorption on activated carbons from end-of-life tyre pyrolysis for environmental applications. Part II. Adsorption from aqueous phase. *J. Anal. Appl. Pyrolysis* 158. <https://doi.org/10.1016/j.jaap.2021.105206>.
- Lingamdinne, L.P., Koduru, J.R., Chang, Y.Y., Kang, S.H., Yang, J.K., 2019. Facile synthesis of flowered mesoporous graphene oxide-lanthanum fluoride nanocomposite for adsorptive removal of arsenic. *J. Mol. Liq.* 279, 32–42. <https://doi.org/10.1016/j.molliq.2019.01.103>.
- Linh, N.L.M., Hoang Van, D., Duong, T., Tinh, M.X., Khieu, D.Q., 2019. Adsorption of arsenate from aqueous solution onto modified Vietnamese bentonite. *Adv. Mater. Sci. Eng.* <https://doi.org/10.1155/2019/2710926>.
- Liu, J., Wang, X., 2013. Novel silica-based hybrid adsorbents: lead(II) adsorption isotherms. *Sci. World J.* <https://doi.org/10.1155/2013/897159>.
- Maji, S., Ghosh, Ayan, Gupta, K., Ghosh, Abir, Ghorai, U., Santra, A., Sasikumar, P., Ghosh, U.C., 2018. Efficiency evaluation of arsenic(III) adsorption of novel graphene oxide@iron-aluminium oxide composite for the contaminated water purification. *Separ. Purif. Technol.* 197, 388–400. <https://doi.org/10.1016/j.seppur.2018.01.021>.
- Mittal, A., Naushad, M., Sharma, G., Alothman, Z.A., Wabaidur, S.M., Alam, M., 2016. Fabrication of MWNTs/TiO₂ nanocomposite and its adsorption behavior for the removal of Pb(II) metal from aqueous medium. *Desalination Water Treat.* 57, 21863–21869. <https://doi.org/10.1080/19443994.2015.1125805>.
- Mushtaq, N., Masood, N., Khattak, J.A., Hussain, I., Khan, Q., Farooqi, A., 2021. Health risk assessment and source identification of groundwater arsenic contamination using agglomerative hierarchical cluster analysis in selected sites from upper Eastern parts of Punjab province, Pakistan. *Hum. Ecol. Risk Assess.* 27, 999–1018. <https://doi.org/10.1080/10807039.2020.1794787>.
- Naushad, M., Alqadami, A.A., Alothman, Z.A., Alsohami, I.H., Algarni, M.S., Aldawsari, A.M., 2019a. Adsorption kinetics, isotherm and reusability studies for the removal of cationic dye from aqueous medium using arginine modified activated carbon. *J. Mol. Liq.* 293, 111442. <https://doi.org/10.1016/j.molliq.2019.111442>.
- Naushad, M., Sharma, G., Alothman, Z.A., 2019b. Photodegradation of toxic dye using Gum Arabic-crosslinked-poly(acrylamide)/Ni(OH)₂/FeOOH nanocomposites hydrogel. *J. Clean. Prod.* 241, 118263. <https://doi.org/10.1016/j.jclepro.2019.118263>.
- Pan, M., Lin, X., Xie, J., Huang, X., 2017. Kinetic, equilibrium and thermodynamic studies for phosphate adsorption on aluminum hydroxide modified palygorskite nano-composites. *RSC Adv.* 7, 4492–4500. <https://doi.org/10.1039/C6RA26802A>.
- Park, H.J., Tavlarides, L.L., 2010. Adsorption of neodymium(III) from aqueous solutions using a phosphorus functionalized adsorbent. *Ind. Eng. Chem. Res.* 49, 12567–12575. <https://doi.org/10.1021/ie100403b>.
- Ravi, Pandey, L.M., 2019. Enhanced adsorption capacity of designed bentonite and alginate beads for the effective removal of methylene blue. *Appl. Clay Sci.* 169, 102–111. <https://doi.org/10.1016/j.clay.2018.12.019>.
- Reid, M.S., Hoy, K.S., Schofield, J.R.M., Uppal, J.S., Lin, Y., Lu, X., Peng, H., Le, X.C., 2020. Arsenic speciation analysis: a review with an emphasis on chromatographic separations. *TrAC Trends Anal. Chem.* (Reference Ed.) 123. <https://doi.org/10.1016/j.trac.2019.115770>.
- Robinson, V.N.E., 1980. Imaging with backscattered electrons in a scanning electron microscope. *Scanning* 3, 15–26. <https://doi.org/10.1002/sca.4950030103>.
- Shaji, E., Santosh, M., Sarath, K.V., Prakash, P., Deepchand, V., Divya, B.V., 2021. Arsenic contamination of groundwater: global synopsis with focus on the Indian Peninsula. *Geosci. Front.* 12, 101079. <https://doi.org/10.1016/j.gsf.2020.08.015>.
- Shao, W., Li, X., Cao, Q., Luo, F., Li, J., Du, Y., 2008. Adsorption of arsenate and arsenite anions from aqueous medium by using metal(III)-loaded amberlite resins. *Hydrometallurgy* 91, 138–143. <https://doi.org/10.1016/j.hydromet.2008.01.005>.
- Sharma, M., Singh, J., Hazra, S., Basu, S., 2019. Adsorption of heavy metal ions by mesoporous ZnO and TiO₂@ZnO monoliths. *Adsorp. Kinetic Studies* 145, 105–112. <https://doi.org/10.1016/j.microc.2018.10.026>.
- Sing, K.S.W., 1982. Reporting physisorption data for gas/solid systems. *Pure Appl. Chem.* 54, 2201–2218. <https://doi.org/10.1351/pac198254112201>.
- Singh, R., Gayen, A., Kumar, S., Dewangan, R., 2021. Geo-spatial distribution of arsenic contamination of groundwater resources in intricate crystalline aquifer system of Central India: arsenic toxicity manifestation and health risk assessment. *Hum. Ecol. Risk Assess.* 27, 1588–1612. <https://doi.org/10.1080/10807039.2020.1865787>.
- Suhailath, K., Ramesan, M.T., 2019. Effect of neodymium-doped titanium dioxide nanoparticles on the structural, mechanical, and electrical properties of poly(butyl methacrylate) nanocomposites. *J. Vinyl Addit. Technol.* 25, 9–18. <https://doi.org/10.1002/vnl.21673>.
- Suri, S., Singh, V., Bamzai, K.K., 2014. Effect of neodymium doping on structural, microscopic and electrical properties of barium phosphate system. *J. Adv. Dielectr.* 4, 1450007. <https://doi.org/10.1142/s2010135x14500076>.
- Tan, P., Zheng, Y., Hu, Y., 2020. Efficient removal of arsenate from water by lanthanum immobilized electroporous chitosan nanofiber. *Colloids Surfaces A Physicochem. Eng. Asp.* 589 <https://doi.org/10.1016/j.colsurfa.2020.124417>.
- Tokunaga, S., Wasay, S.A., Park, S.-W., 1997. Removal of arsenic(V) ion from aqueous solutions by lanthanum compounds. *Water Sci. Technol.* 35 [https://doi.org/10.1016/S0273-1223\(97\)00116-9](https://doi.org/10.1016/S0273-1223(97)00116-9).
- Valdés, O., Marican, A., Mirabal-Gallardo, Y., Santos, L.S., 2018. Selective and efficient arsenic recovery from water through quaternary amino-functionalized silica. *Polymers* 10. <https://doi.org/10.3390/polym10060626>.
- Wang, Y., Liu, Y., Guo, T., Liu, H., Li, J., Wang, S., Li, X., Wang, X., Jia, Y., 2020. Lanthanum hydroxide: a highly efficient and selective adsorbent for arsenate removal from aqueous solution. *Environ. Sci. Pollut. Res.* 27, 42868–42880. <https://doi.org/10.1007/s11356-020-10240-1>.
- Wang, Y., Shi, W., Yu, Y., Chen, X., 2009. Synthesis characterization and properties of quaternary ammonium cationic cellulose. In: 2009 3rd International Conference on Bioinformatics and Biomedical Engineering, pp. 1–4. <https://doi.org/10.1109/ICBBE.2009.5163558>.
- Xiong, F., Hwang, B., Jiang, Z., James, D., Lu, H., Moortgat, J., 2021. Kinetic emission of shale gas in saline water: insights from experimental observation of gas shale in canister desorption testing. *Fuel* 300, 121006. <https://doi.org/10.1016/j.fuel.2021.121006>.
- Yang, H., Min, X., Xu, S., Wang, Y., 2019. Lanthanum(III)-Coated ceramics as a promising material in point-of-use water treatment for arsenite and arsenate removal. *ACS Sustain. Chem. Eng.* 7, 9220–9227. <https://doi.org/10.1021/acssuschemeng.8b06878>.
- Yetilmezsoy, K., Özçimen, D., Koçer, A.T., Bahramian, M., Kiyan, E., Akbin, H.M., Gonçalogoğlu, B.I., 2020. Removal of anthraquinone dye via struvite: equilibria, kinetics, thermodynamics, fuzzy logic modeling. *Int. J. Environ. Res.* 14, 541–566. <https://doi.org/10.1007/s41742-020-00275-0>.
- Yu, L., Ma, Y., Ong, C.N., Xie, J., Liu, Y., 2015. Rapid adsorption removal of arsenate by hydrous cerium oxide-graphene composite. *RSC Adv.* 5, 64983–64990. <https://doi.org/10.1039/c5ra08922k>.
- Yu, Y., Yu, L., Shih, K., Chen, J.P., 2018. Yttrium-doped iron oxide magnetic adsorbent for enhancement in arsenic removal and ease in separation after applications. *J. Colloid Interface Sci.* 521, 252–260. <https://doi.org/10.1016/j.jcis.2018.02.046>.
- Yu, Y., Zhang, C., Yang, L., Paul Chen, J., 2017. Cerium oxide modified activated carbon as an efficient and effective adsorbent for rapid uptake of arsenate and arsenite:

- material development and study of performance and mechanisms. Chem. Eng. J. 315, 630–638. <https://doi.org/10.1016/j.cej.2016.09.068>.
- Zakhar, R., Dercó, J., Cácho, F., 2018. An overview of main arsenic removal technologies. Acta Chim. Slovaca 11, 107–113. <https://doi.org/10.2478/acs-2018-0016>.
- Zhou, Z., Liu, Y., guo, Liu, S., bo Liu, H., yu Zeng, G., ming, Tan, X., fei Yang, C., ping Ding, Y., Yan, Z., li Cai, X. xi, 2017. Sorption performance and mechanisms of arsenic (V) removal by magnetic gelatin-modified biochar. Chem. Eng. J. 314, 223–231. <https://doi.org/10.1016/j.cej.2016.12.113>.

D4

S. Dudek, D. Kołodyńska

Arsenate removal on the ion exchanger modified with cerium(III) ions, Physicochem. Probl. Miner. Process., 58 (2022) 147412.

IF: 1,213 Punkty MEiN: 70

Oświadczenie

Oświadczam, że mój udział w pracy:

S. Dudek, D. Kołodyńska, Arsenate removal on the ion exchanger modified with cerium(III) ions,
Physicochem. Probl. Miner. Process. 58 (2022) 147412

polegał na współtworzeniu jej ogólnej koncepcji, wykonaniu wszystkich eksperymentów, opracowaniu wyników, współudziale w stworzeniu oryginalnego manuskryptu, pełnieniu roli autora korespondencyjnego, współudziale w przygotowywaniu odpowiedzi do recenzentów. Udział ten szacuję na 75%.



OŚWIADCZENIE

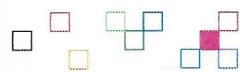
Oświadczam, że w pracy:

Sebastian Dudek, Dorota Kołodyńska, Arsenate removal on the ion exchanger modified with cerium(III) ions, Physicochemical Problems of Mineral Processing, 58 (2022) 147412, IF₂₀₂₂ 1,2133, pkt MNiE₂₀₂₂ 70.

mój wkład merytoryczny w przygotowanie, przeprowadzenie i opracowanie badań oraz przedstawienie pracy w formie publikacji to: opracowanie koncepcji i założeń, interpretacja i analiza otrzymanych wyników.

Swój wkład szacuję na 25%.

Jednocześnie wyrażam zgodę na przedłożenie wyżej wymienionej pracy przez Pana mgr Sebastiana Dudka jako część rozprawy doktorskiej w formie spójnego tematycznie cyklu prac opublikowanych w czasopismach naukowych.



Arsenate removal on the ion exchanger modified with cerium(III) ions

Sebastian Dudek, Dorota Kołodyńska

¹ Department of Inorganic Chemistry, Institute of Chemical Sciences, Faculty of Chemistry, Maria Curie-Skłodowska University, Maria Curie-Skłodowska Sq. 2, 20-031 Lublin, Poland.

Corresponding author: sebastian.dudek@mail.umcs.pl (Sebastian Dudek)

Abstract: The iron oxide ion exchanger Ferrix A33E was successfully modified with cerium(III) ions to obtain Ferrix A33E-Ce(III) providing much better sorption properties in relation to the As(V) species. The new material has been characterized using a number of techniques including scanning electron microscopy SEM, nitrogen adsorption/desorption isotherms, Fourier transform infrared spectroscopy FTIR and X-ray photoelectron spectroscopy XPS. At optimal pH 6 the main mechanism of arsenate adsorption on A33E-Ce(III) was electrostatic attraction and formation of monodentate and bidentate surface complexes. The process was exothermic and spontaneous. Unlike the unmodified ion exchanger, A33E-Ce(III) could completely remove arsenic from the arsenate solution at a concentration of 50 mg/dm³ in 60 minutes. Furthermore, the maximum sorption capacity for As(V) was determined to be 60.41 mg/g which almost doubled after modification with cerium(III) ions. It is also worth noting that even after three cycles of sorption/desorption A33E-Ce(III) exhibited a higher sorption capacity than unmodified A33E before the arsenate adsorption. It can be concluded that modifying the sorbent with a small amount of cerium(III) ions boosts its sorption properties significantly, improves effectiveness of water purification and reduces the overall operation cost.

Keywords: arsenic, adsorption, cerium, iron oxides, Ferrix A33E

1. Introduction

Arsenic contamination in groundwater at elevated concentrations is reported in many countries around the world, e.g. Argentina, Bangladesh, Chile, China, India, Mexico (Hao et al., 2018). The main reasons for this phenomenon include industrial activities, weathering of rocks, geochemical reactions, volcanic emissions and biological activities (Chowdhury and Mulligan, 2011). The arsenic polluted groundwater was used for underdeveloped or developing countries without treatment, which led to various detrimental health effects (including lung cancer, cardiovascular diseases and skin disorders) in the local population (Podgorski et al., 2017). Therefore, the development of an effective method of water purification is of great importance.

Numerous technologies have been elaborated on arsenic removal from aqueous solutions based on various treatment methods (Adelaju et al., 2021). Among these technologies, adsorption seems to demonstrate the greatest potential due to its cost effectiveness, maintenance, versatility and simplicity of operation. Extremely common adsorbents designed to remove arsenic are those based on iron oxides (Siddiqui and Chaudhry, 2017) or also hybrid materials combining iron and other metals including titanium (Gupta and Ghosh, 2009), zirconium (Chaudhry et al., 2017), aluminium (Maji et al., 2018), copper (Zhang et al., 2013). Recently, some papers on the materials containing rare earth elements REE have also been presented (Shi et al., 2015; Yu et al., 2017; Lingamdinne et al., 2019; Dudek and Kołodyńska, 2020; T. Liang et al., 2020; Wang et al., 2020). The metal oxide/hydroxide, metal oxide/hydroxide modified adsorbents, and the metal ion impregnated adsorbents are the most common types of such novel materials. The unusual physicochemical properties of REEs, as well as their exceptional arsenic removal efficiency, have piqued the interest of researchers. It is believed that the multiple-species REE adsorbents exhibit larger arsenic sorption capacity, greater stability and are cheaper compared to the single-species REE materials (Yu et al., 2018). Through ligand exchange, complex formation, and electrostatic interactions, various functional groups on the adsorbent surface

can play a significant role in the adsorption process (Muthu Prabhu et al., 2018). Loading the REE oxides/hydroxides or REE ions onto the porous materials characterized by a large surface area and great porosity may also lead to the increase of adsorption rate (Yu et al., 2018).

As REEs are relatively expensive, it is advantageous to combine them with readily accessible and less expensive metals (e.g., aluminium, iron, manganese) to create a new series of composites as adsorbents that retain the advantages of REEs while reducing overall costs (S. Liang et al., 2020; Muthuselvi et al., 2021). Therefore, in this study the modification of the commercially available iron oxide ion exchanger Ferrix A33E (containing the quaternary ammonium groups) was made using cerium(III) ions. There is no report in the literature about Ce(III)-modification of an iron-based sorbent with the quaternary ammonium groups. The main objectives of the research were (1) modification of Ferrix A33E with Ce(III) ions (2) characterization of the newly obtained material and (3) investigating the arsenate(V) adsorption process and comparing the sorption efficiency on the modified and unmodified ion exchangers.

2. Materials and methods

2.1. Sorbent modification and characterization

The Ce(III) solution of the concentration 1000 mg/dm³ was prepared by dissolving the proper amount of cerium(III) nitrate hexahydrate Ce(NO₃)₃ · 6H₂O (Sigma Aldrich, USA) in distilled water. The solution was then diluted to 100 mg/dm³ and the pH was adjusted to 4 by adding the proper amount of 1M NaOH (Chempur, Poland). The portions of 0.5 g of A33E (Purolite, USA) were inserted in 500 cm³ conical flasks and 100 cm³ of the previously prepared Ce(III) solution of the concentration of 100 mg/dm³ was added to each of them. The samples were then shaken under the following conditions: time 6 hours, shaking speed 180 rpm and temperature 295 K. In the next step, the sorbent was removed from the solution by gravity filtration and dried at 333 K for 24 hours. As a result there was developed the modified A33E-Ce(III) sorbent, which was then examined for characterisation and removal of arsenic(V) ions.

To assess the surface morphology, including surface features, scanning electron microscopy (SEM) (Quanta 3D FEG, FEI, USA) with an extended depth of field (EDF) function was utilized. The pictures of SEM A33E and A33E-Ce(III) were compared. Images of the surface of A33E-Ce(III) following the As(V) ion sorption were also taken.

The nitrogen adsorption/desorption isotherms at 77 K (ASAP 2405, Micromeritics, USA) were used to study the morphological characteristics of A33E, A33E-Ce(III), and A33E-Ce(III)-As(V) following the preliminary degassing of the samples at the specified temperature. To calculate the specific surface area, the Brunauer, Emmett, and Teller (BET) technique was used. The Barret-Joyner-Halenda model was also applied to compute total pore volumes and average pore diameters.

The point of zero charge (pH_{pzc}) of A33E and A33E-Ce(III) was determined using the drift technique (Jiao et al., 2017). The pH_{pzc} was calculated by varying the pH of 20 cm³ 0.01 M NaCl from 2 to 11 (pH_i). 0.1 g of A33E or A33E-Ce(III) was added into the flask, shaken for 6 hours and then the final pH_f was determined. The pH_{pzc} value is the point at which pH_i-pH_f = 0. The pH was measured with a Radiometer PHM 84 pH meter (Denmark) with glass REF 451 and calomel pHG 201-8 electrodes.

The spectra of the studied adsorbents were acquired using infrared spectroscopy with the Fourier transformation (FTIR). The attenuated total reflection technique was used to evaluate A33E and A33E-Ce(III) before and after the As(V) adsorption using the Nicolet 8700A spectrometer (Thermo Scientific, USA). As a result, the specified functional groups on the material surface could be identified. The FTIR spectra were collected in the wavenumber range of 4000–400 cm⁻¹.

The X-ray photoelectron spectroscopy XPS was used to investigate the composition and valence state of the elements included in A33E and A33E-Ce(III) before and after the arsenate(V) ion uptake (Prevac, Poland).

2.2. Batch experiments

To determine the pH effect on As(V) adsorption efficiency on experiment was conducted in 100 cm³ flasks. The A33E-Ce(III) samples weighing 0.1 g were placed in the flasks containing 20 cm³ of arsenate(V) solution at the concentration of 100 mg/dm³. The pH range was set from 4 to 11 by adding

the appropriate amounts of 0.01M NaOH or 0.01M HCl. The flasks were then shaken for 360 minutes with the laboratory shaker Elpin+ type 357 (Elpin Plus, Poland). The gravity filtration was used to separate A33E-Ce(III) from the solution. The concentration of arsenate(V) ions was determined using the spectrophotometric method (Cary 60, Agilent Technologies, USA), which involved the formation of complexes with ammonium molybdate and the absorbance measurement at 870 nm. Eq. 1 was used to calculate the adsorption capacity of As(V) ions (Badruddoza et al., 2013):

$$q_t = (c_0 - c_t) \times \frac{V}{m} \quad (1)$$

where: q_t is the amount of As(V) adsorbed at time t (mg/g), c_0 denotes the initial concentration of As(V) in the solution (mg/dm³), c_t represents the concentration of As(V) in the solution after time t (mg/dm³), V is the volume of the solution containing As(V) ions (dm³) and m symbolizes the mass of ion exchanger (g).

Additionally, the sorption percentage was calculated using Eq. 2 (Yetilmezsoy et al., 2020):

$$\%S = \frac{(c_0 - c_t)}{c_0} \times 100\% \quad (2)$$

Batch experiments were also conducted to investigate the kinetics of arsenate(V) adsorption at the initial As(V) concentrations of 25, 50, and 100 mg/dm³ and pH 6. A33E-Ce(III) samples weighing 0.1 g were prepared in 100 cm³ conical flasks and 20 cm³ As(V) solutions were added to be shaken for the specified time – between 1 and 360 minutes (temperature 295 K, shaking speed 180 rpm). Eqs. 1 and 2 were used to calculate the adsorption capacities and sorption percentages. The kinetics of arsenate(V) adsorption onto A33E-Ce(III) was studied using the pseudo-first order (PFO), pseudo-second order (PSO), Elovich, and intraparticle diffusion (IPD) models. The models applicability was assessed using the error analysis – determination coefficient (R^2), the sum of squared errors (SSE) and F-test. The pseudo-first-order (PFO) kinetic model was developed by Lagergren and Ho to explore sorption in the liquid-solid systems. It is described by Eqs. 3 and 4 presenting the linear form (Xiong et al., 2021):

$$\frac{dq_t}{dt} = k_1(q_e - q_t) \quad (3)$$

$$\ln(q_e - q_t) = \ln q_e - k_1 t \quad (4)$$

where: q_t represents the quantity of As(V) adsorbed onto the adsorbent at time t (mg/g), q_e denotes the equilibrium adsorption capacity (mg/g), k_1 is the PFO rate constant (1/min).

The PSO Eq. is built on the concept that the rate of adsorption is a quadratic function of the difference between the equilibrium adsorption capacity and the adsorption capacity after time t . Eqs. 5 and 6 represent the non-linear and linear forms of PSO model, respectively (Guo and Wang, 2019):

$$\frac{dq_t}{dt} = k_2(q_e - q_t)^2 \quad (5)$$

$$\frac{t}{q_t} = \frac{1}{k_2 q_e^2} + \frac{t}{q_e} \quad (6)$$

where: k_2 indicates the PSO rate constant (g/(mg·min)).

The Elovich model presupposes an energetically heterogeneous solid surface and a chemisorption process. Eqs. 7 and 8 reflect the non-linear and linear variants of the Elovich model, respectively (Ali et al., 2019):

$$\frac{dq_t}{dt} = \alpha \exp^{-\beta q_t} \quad (7)$$

$$q_t = \frac{1}{\beta} \ln(\alpha\beta) + \frac{1}{\beta} \ln t \quad (8)$$

where: α represents the initial adsorption rate (mg/(g·min)) and β is related to the surface coverage and chemisorption activation energy (g/mg).

If the adsorption process is regulated by intraparticle diffusion, the plot of q_t versus the square root of time (\sqrt{t}) should be linear according to the intraparticle diffusion IPD model represented by Eq. 9 (Ravi and Pandey, 2019):

$$q_t = k_i \sqrt{t} + C \quad (9)$$

where: k_i signifies the IPD rate constant and C is the boundary layer thickness.

In the case of equilibrium and thermodynamic studies As(V) solutions with different initial concentrations (25 – 1000 mg/dm³) were made and their pH was adjusted to 6 before the use. Adsorption experiments were performed at various temperatures: 295 K, 313 K, 333 K and a shaking

speed of 180 rpm. All tests were carried out with the established parameters, i.e. 6-hour contact time, the same adsorbent dosage and adsorbate volume as for the study of pH effect on the adsorption efficiency and kinetics. In order to fit the experimental data four isotherm models were used. The Langmuir (Eq. 10), Freundlich (Eq. 11), Dubinin-Radushkevich (Eqs. 12, 13, 14) and Redlich-Peterson (Eq. 15) models non-linear forms are shown below (Bergmann and Machado, 2015; Zhang and Leiviskä, 2020):

$$q_e = \frac{q_m K_L c_e}{1 + K_L c_e} \quad (10)$$

where: q_e represents the sorption capacity at equilibrium (mg/g), c_e indicates the equilibrium solute concentration (mg/dm³), q_m (g/mg) and K_L (dm³/mg) denotes the Langmuir constants related to the maximum sorption capacity and the sorption energy, which were calculated from the slope and intercept of the linear plot c_e/q_e vs c_e ;

$$q_e = K_F c_e^n \quad (11)$$

where: K_F (mg/g) and n (-) denote the constants related to the adsorption capacity and adsorption intensity, respectively. They can be obtained from the slope and intercept of the plot $\log q_e$ vs $\log c_e$:

$$q_e = q_{DR} e^{-K_{DR} \varepsilon^2} \quad (12)$$

$$\varepsilon = RT \ln \left(1 + \frac{1}{c_e} \right) \quad (13)$$

$$E = \frac{1}{\sqrt{2\beta}} \quad (14)$$

where: q_{DR} (mol/g) signifies the theoretical adsorption capacity, β (mol²/J²) represents the activity constant related to the mean free energy of adsorption, ε corresponds to the Polanyi potential, R (8.314 J/K/mol) represents the gas constant, T (K) denotes the temperature, E (J/mol) is related to the required energy to transfer a mole of sorbate from the solution to the sorbent surface.

$$q_e = \frac{K_{RP} c_e}{1 + a_{RP} c_e^g} \quad (15)$$

where: K_{RP} (dm³/g) and a_{RP} (dm³/mg)^g denote the Redlich-Peterson constants; g represents an exponent whose value must be between 0 and 1.

Temperature effects on the As(V) ion adsorption on A33E-Ce(III) were also examined, and major thermodynamic parameters were calculated using Eqs. 16, 17 and 18 (Hu et al., 2015):

$$K_d = \frac{q_e}{c_e} \quad (16)$$

$$\Delta G^0 = -RT \ln K_d \quad (17)$$

$$\ln K_d = -\frac{\Delta H^0}{RT} + \frac{\Delta S^0}{R} \quad (18)$$

where: K_d (dm³/g) represents the distribution coefficient, ΔG^0 (kJ/mol) denotes the change of Gibbs energy, ΔH^0 (kJ/mol) signifies the change of enthalpy and ΔS^0 (kJ/mol·K) is related to the entropy.

To assess the reusability of A33E-Ce(III), 0.1 g of the ion exchanger was put into three 100 cm³ flasks, and 20 cm³ of As(V) solution of 100 mg/dm³ and pH 6 was added to each of them. The samples were shaken for 6 hours at the temperature 295 K and the shaking speed 180 rpm. In the next step, the sorbent was removed from the solution by gravity filtration and dried at 333 K for 24 hours. The dry samples were re-placed in the 100 cm³ flasks and 20 cm³ of NaOH solutions at 0.05, 0.2, and 1M concentrations was added to them. The samples were also shaken for 6 hours (temperature 295 K, shaking speed 180 rpm). Following that, the adsorbent was removed from the solution by filtration and dried at 333 K for 24 hours. The experiment was conducted twice more with 1M NaOH. The concentration of As(V) ions in the solution was measured after each adsorption and desorption step.

3. Results and discussion

3.1. Sorbent characterization

SEM was utilized to analyse the morphological properties of A33E, A33E-Ce(III) and A33E-Ce(III)-As(V) (A33E-Ce(III)) after the arsenate adsorption. The all images are presented in Fig. 1. Zhang et al. presented three forms of cerium oxide morphologies, i.e. nanorods (Ce-R), nanoparticles (Ce-P) and nanoflakes (Ce-F) (Zhang et al., 2016). Each morphology can be obtained using a different method of material preparation. In this study, modification with Ce(III) ions resulted in the increased

heterogeneity and the formation of nanoflakes (Ce-F) on the A33E surface. Numerous pores of varied sizes could facilitate the adsorption of As(V) ions at the active sites. Furthermore, backscattered electron (BSE) imaging was employed to detect particles containing heavier elements, such as REEs, that appeared brighter in the SEM-BSE images (Xu et al., 2019). The bright spots in Fig. 2 are related to the adsorbed cerium(III) ions, indicating that A33E was successfully modified. The arsenate adsorption on A33E-Ce(III) resulted in pores filling with As(V) ions and reduction of the surface heterogeneity (Fig. 1 g, h, i).

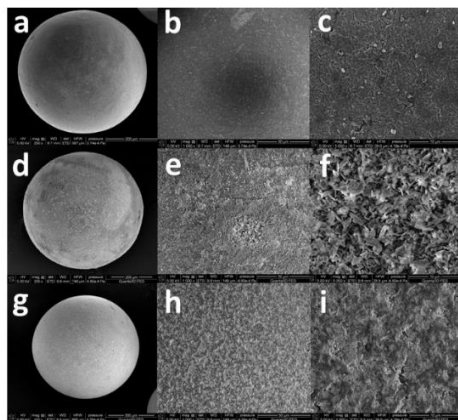


Fig. 1. SEM images of A33E (a-c), A33E-Ce(III) (d-f) and A33E-Ce(III)-As(V) (g-i) at the magnifications 150 x (g), 200 x (d), 250 x (a), 1000 x (b, e, h) and 5000 x (c, f, i)

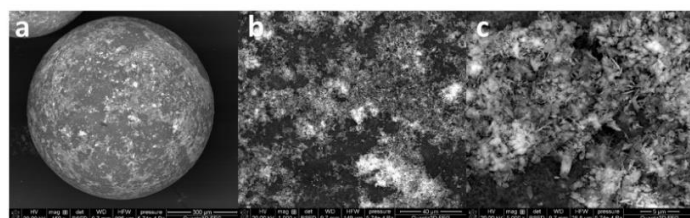


Fig. 2. SEM images of A33E-Ce(III) taken using the BSE detector at the magnifications 150 x (a), 1000 x (b) and 5000 x (c)

Using the N₂ adsorption-desorption technique, the specific surface areas, pore volumes, and average pore diameters of A33E, A33E-Ce(III), and A33E-Ce(III)-As(V) were determined. The variations in the materials specific surfaces were minor. They increased from 53.12 (Dudek and Kołodyńska, 2021) to 56.72 m²/g after modification, and reached 60.71 m²/g following the As(V) sorption. The total pore volume also increased in the order of A33E, A33E-Ce(III), A33E-Ce(III) -As(V) and was equal to 0.122, 0.125 and 0.140 cm³/g, respectively. According to the IUPAC classification all the presented isotherms (Fig. 3) are of type IV and include the H3 hysteresis loops which suggests that the mesoporous structure is formed by the slit-like mesopores (Alothman, 2012; Xiao et al., 2018). The mesoporous nature of the tested materials was also proved by the presented pore distribution (Fig. 3). It can be noticed that the size of pores exhibits a strong peak between 2.0 nm and 50 nm. There were no significant changes in the average pore diameter. After the modification with cerium(III) ions, there was a decrease from 9.18 to 8.80 nm, and after the adsorption of As(V), it increased to 9.22 nm.

It is well known that solution pH affects the surface charge of adsorbents, the dissociation of functional groups on the adsorbent active sites and the degree of ions ionization in the solution (Komnitsas et al., 2017). Inorganic arsenic(V) acid creates deprotonated anionic species in municipal waters with a pH of 6.5-8.5 (Reid et al., 2020; Bhandari et al., 2021). The previous study revealed that the pH_{PZC} for A33E is 8.29 (Dudek and Kołodyńska, 2021), however, the value for A33E-Ce(III) is smaller and approaches 8.12 (Fig. 4). Given that the pH_{PZC} of the A33E-Ce(III) surface is 8.12, it is clear that a negative charge occurs on its surface at pH above pH_{PZC} and a positive charge forms at pH below that value (Dutta et al., 2004). As a result, adsorption of arsenate anions on the surface of A33E-Ce(III) is

expected to be preferred for the solution pH values smaller than 8.12 where greater electrostatic attraction may occur.

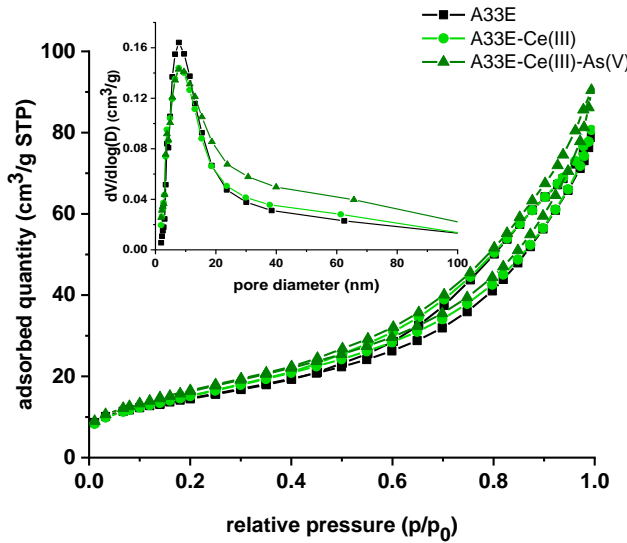


Fig. 3. N_2 adsorption/desorption isotherms of A33E (black), A33E-Ce(III) (light green) and A33E-Ce(III)-As(V) (dark green). The inset image shows the pore distribution of the tested materials

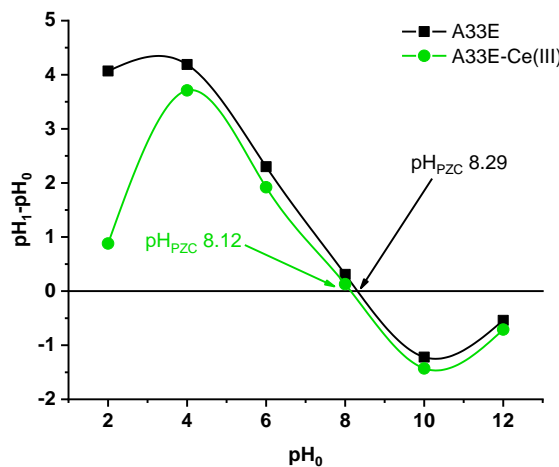


Fig. 4. Points of zero charge of A33E (black) and A33E-Ce(III) (green)

The FTIR analysis was used to determine changes in the functional groups and chemical bonds in A33E and A33E-Ce(III) before and after the As(V) adsorption (Fig. 5). The broad band observed between 3650 and 3100 cm^{-1} centered around 3200 cm^{-1} is attributed to the O-H stretching vibrations derived from the physisorbed water (Mino et al., 2020). The bands at 3030 cm^{-1} and 2920 cm^{-1} relate to polystyrene crosslinked with divinylbenzene and correspond to the vibrations of aromatic C-H and aliphatic C-H, respectively (Shin et al., 2015). The quaternary ammonium group $-\text{NR}_4^+$ and H-O-H bending vibrations can be attributed to the double peak at 1636 and 1613 cm^{-1} (Wang et al., 2009; Mino et al., 2020). Additionally, the band at 1480 cm^{-1} also belongs to the $-\text{NR}_4^+$ group and becomes less intense as a result of the Ce(III) and As(V) adsorption (Valdés et al., 2018). The spectra after the As(V) adsorption revealed the appearance of a new peak at 865 cm^{-1} that was not present before adsorption. Most likely this peak indicates the formation of an As-O bond, which is consistent with the previous research results (T. Liang et al., 2020). Moreover, the peak for A33E-Ce(III)-As(V) is more intense than that of A33E-As(V) suggesting that the mechanism of arsenate adsorption could be different. In the case of A33E-Ce(III)-As(V) a new peak is observed at 448 cm^{-1} . It can be attributed to the Ce-O-As bond, just as the La-O-As vibration band at 445 cm^{-1} in the lanthanum arsenate (Wang et al., 2020). This is due to the bonding formation between the cerium active sites and the oxygen atoms of arsenate(V). These findings point out to the formation of inner-sphere surface complexes.

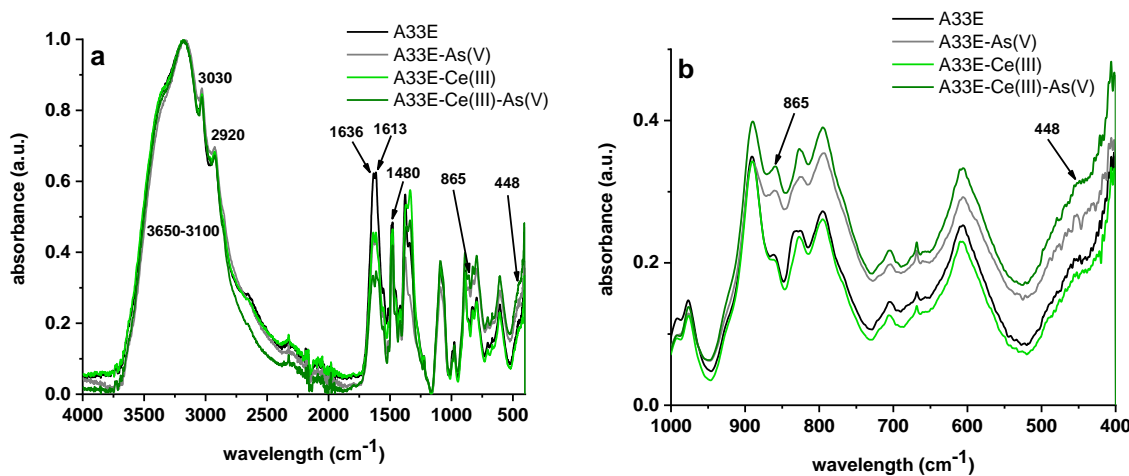


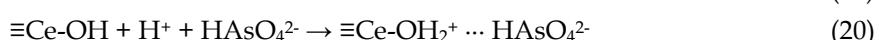
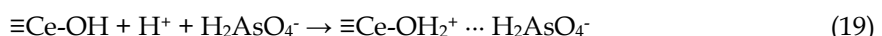
Fig. 5. FTIR spectra of A33E (black), A33E after the As(V) adsorption (grey), A33E-Ce(III) (light green) and A33E-Ce(III) after the As(V) adsorption (dark green) in the range of 4000–400 cm⁻¹ (a) and 1000–400 cm⁻¹ (b).

The surface elemental composition and the oxidation states of the elements were analysed by X-ray photoelectron spectroscopy. The survey spectra of A33E and A33E-Ce(III) before and after the As(V) adsorption are presented in Fig. 6a which reveals the presence of Fe, O, N and C in all samples. The main forms of iron and oxygen are iron(II,III) oxides Fe_xO_y. Nitrogen occurs mainly as the quaternary ammonium groups while carbon results from the presence of the aliphatic C-H, aliphatic C-C and aromatic C=C bonds derived from polystyrene crosslinked with divinylbenzene. In the survey spectrum of A33E-Ce(III) the Ce peak appears which proves successful adsorption with the cerium(III) ions. Moreover, the As peaks indicate that the arsenate adsorption could proceed on both modified and unmodified ion exchangers. Fig. 6b and 6c presents the As3d region in the range of 48–42 eV. It can be seen that in the case of A33E-Ce(III) the As peaks are shifted and have different intensities compared to A33E. This suggests various mechanisms of arsenate adsorption on the tested materials. Interestingly, in the As3d region the peaks originating from As(III) appear. This can be explained by the susceptibility of As(V) ions to the reduction induced by X-rays during the XPS analysis. For instance, Viltres et al. proved that As₂O₅ is degraded due to the XPS measurements and this damage involves the reduction of As(V) to As(III) species along with oxygen losses from the oxide surface (Viltres et al., 2020). In the case of the Ce3d region (Fig. 6d and 6e), the cerium peaks were also shifted and their intensity decreased after the adsorption of As(V) ions. This suggested that cerium was involved in the process of arsenate adsorption. It is worth noting that after the adsorption of cerium(III) ions on A33E, they were partially oxidized to cerium(IV) ions. This phenomenon can be explained by converting Ce(III) into Ce(IV) ions under the influence of oxidants such as oxygen during the preparation process of the Ce-modified material (He et al., 2012).

3.2. Effect of pH

The influence of solution pH on the arsenate adsorption was investigated over a pH range of 4–11. As illustrated in Fig. 7, when the solution pH increases from 4 to 6, the adsorption of arsenate on A33E-Ce(III) is slightly boosted, and the maximum adsorption capacity of 19.6 mg/g is achieved at pH 6. The arsenate adsorption onto A33E-Ce(III) decreases as the solution pH rises.

Based on the arsenic speciation diagram presented by Issa et al., the main arsenate species in the pH range of 4 to 11 are H₂AsO₄⁻ and HAsO₄²⁻ (Issa et al., 2011). Electrostatic interactions between the adsorbent active sites and arsenate may be critical in the adsorption process. Due to the fact that the pH_{PZC} of the adsorbent is 8.12, stronger protonation of the functional groups on its surface can be achieved at the pH values less than 8.12, resulting in the enhanced electrostatic attraction between the adsorbent positively charged active sites and the negatively charged arsenate (Li et al., 2011), as shown in Eqs. 19 and 20.



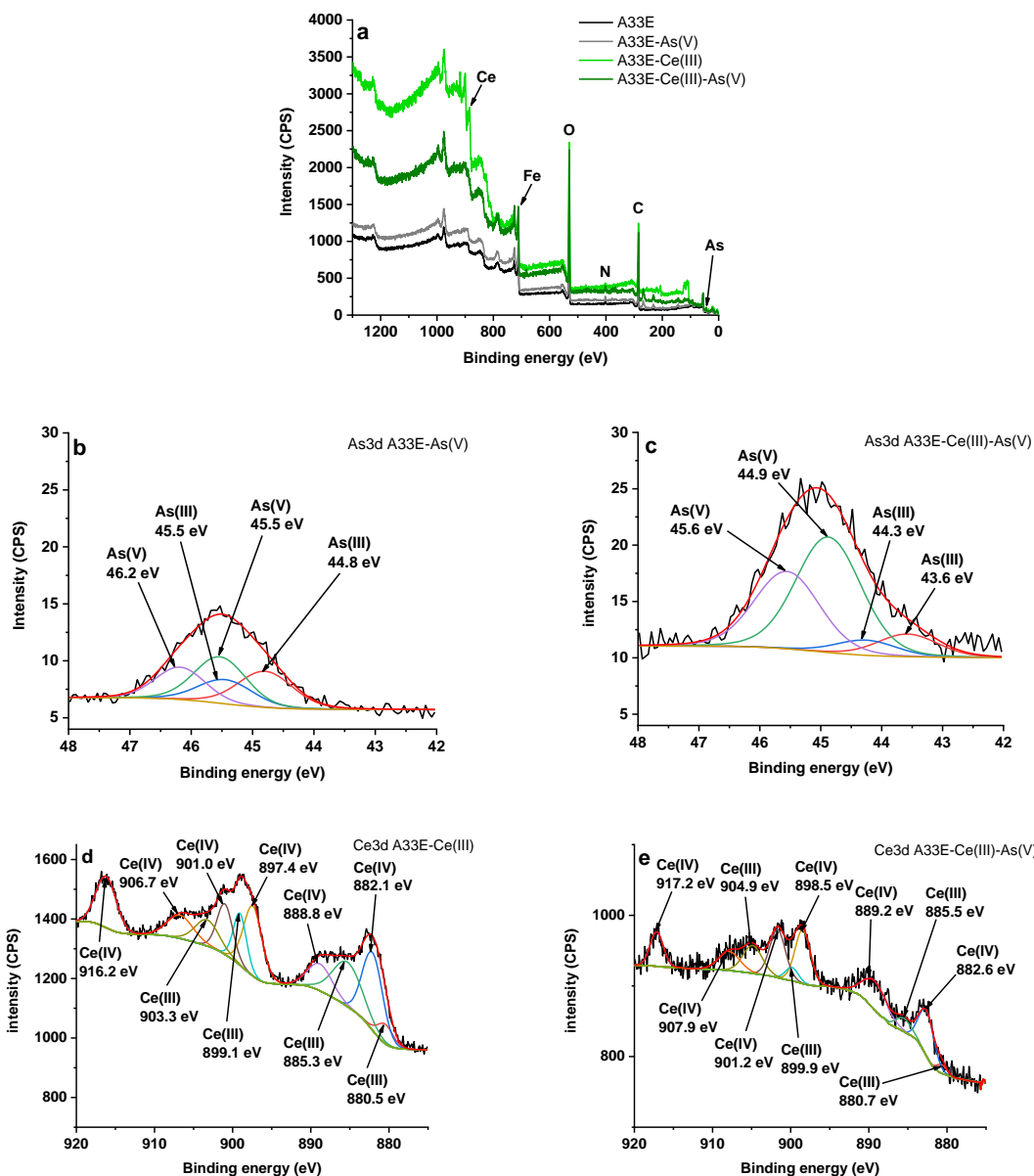


Fig. 6. XPS survey spectra of A33E, A33E-As(V), A33E-Ce(III), A33E-Ce(III)-As(V) (a), As3d region of A33E-As(V) (b), As3d region of A33E-Ce(III)-As(V) (c), Ce3d region of A33E-Ce(III) (d) and Ce3d region of A33E-Ce(III)-As(V) (e)

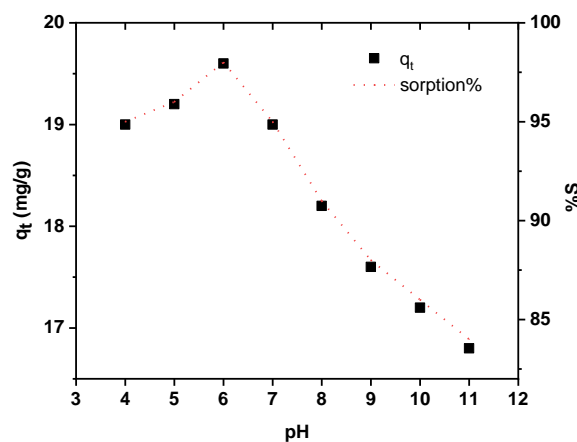


Fig. 7. Influence of pH on the adsorption efficiency of As(V) on A33E-Ce(III) (initial As(V) concentration c_0 100 mg/dm³, time t 360 minutes, shaking speed 180 rpm, temperature T 295 K)

Moreover, the FTIR analysis revealed the formation of a new Ce-O-As bond. This indicates formation of the monodentate and bidentate surface complexes (Peng et al., 2005) which is presented in Fig. 8.

Though adsorption of As(V) was still possible at alkaline pH, the sorption efficiency was significantly reduced. When the pH of the adsorbent exceeds 8.12, the electrostatic repulsion effect limits considerably arsenate adsorption (Nabi et al., 2009).

It should be noted that the batch adsorption studies were carried out with the model solutions containing only arsenate(V) ions. When removing arsenic from natural waters, the influence of accompanying ions should be taken into account. Largely present Cl⁻, SO₄²⁻, Na⁺ and K⁺ ions do not show any significant effect on the arsenate(V) adsorption. Ca²⁺ and Mg²⁺ ions exhibit even promoting effects on the arsenic removal. However, both phosphate PO₄³⁻ and hydrogen carbonate HCO₃⁻ can have a negative impact on the process. The PO₄³⁻ and HCO₃⁻ inhibitory effects are related to competing adsorption mechanisms. Boosting action of Ca²⁺ and Mg²⁺ ions may be a consequence of electrostatic attraction, co-precipitation, and surface complexation on the porous iron-based material in aqueous solutions (Yang et al., 2015).

3.3. Kinetic studies

Fig. 9 shows the rate of adsorption of As(V) on A33E-Ce(III) and A33E at the initial concentrations of 25, 50 and 100 mg/dm³. As follows from this Fig. the adsorption capacities increased very fast during the first 30 minutes with the increasing contact time. Equilibrium was attained after about 30, 60 and 120 minutes for the initial concentrations of 25, 50 and 100 mg/dm³, respectively. It is worth noting that the time needed to achieve equilibrium did not deteriorate after the modification. Moreover, at each tested concentration, A33E-Ce(III) showed better sorption percentage than A33E. In contrast with the unmodified ion exchanger (Dudek and Kołodyńska, 2022), it could remove arsenic even completely in 60 minutes from an arsenate solution at such a high concentration as 50 mg/dm³.

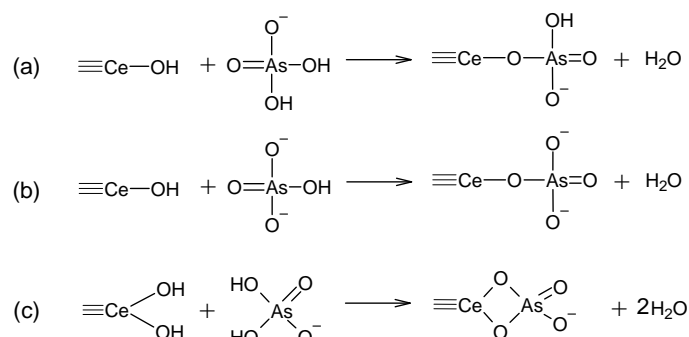


Fig. 8. Formation of monodentate (a, b) and bidentate complexes (c) by arsenate species

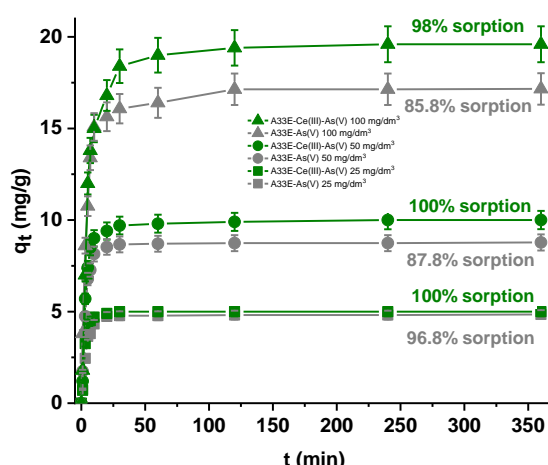


Fig. 9. Influence of As(V) initial concentration and contact time on the adsorption capacities of A33E (grey) and A33E-Ce(III) (green) (initial As(V) concentration c_0 25, 50, 100 mg/dm³, pH 6, time t 1-360 minutes, temperature T 295 K, shaking speed 180 rpm)

During the investigations the pseudo-first order PFO, pseudo-second order, Elovich and intraparticle diffusion models were tested for explaining the adsorption behaviour of arsenate ions on A33E-Ce(III). All kinetic parameters are presented in Table 1. Figs. 10 and S1 show the non-linear and linear fitting of the tested kinetic models in turn.

The PFO and PSO models are the most often used in the environmental kinetic studies (Guo and Wang, 2019). According to the kinetic parameters presented in Table 1 for the sorption of arsenate ions on A33E-Ce(III), the PSO model with the correlation coefficients close to one provides the best fit to the data expected from the experimental values. This is also confirmed by the SSE error analysis and indicates the chemical adsorption process (Khan et al., 2020). Moreover, the equilibrium adsorption capacities q_e obtained from the PSO model are close to the experimental data. The applicability of the PSO model was also compared with that of the Elovich model. It was noticed that the Elovich model was not well suited to fit the arsenate adsorption kinetics owing to its low R^2 and relatively high SSE values. However, the attention should be paid to the fact that numerous studies proved that adsorption behaviour that closely matches the PSO model can often be explained by the diffusion-based processes (Hubbe et al., 2019; Simonin, 2016). It has been shown that the hypothetical data obtained from the premise of pseudo-first-order rate behavior fit the PSO model quite well. According to published research, the adsorption kinetics of various materials are likely to be dominated by the diffusion-limited processes, as influenced by the heterogeneous pore size distributions and continuous partitioning of solute species between their dissolved and fixed states of adsorption.

Since the PSO model does not explain the process of adsorption diffusion, the intraparticle diffusion model (IPD) can be used to determine the rate controlling stages. The multilinear IPD plot for q_t vs $t_{1/2}$ (Fig. 10 c) indicates that three diffusion steps are involved in the As(V) adsorption on A33E-Ce(III) (Sharma et al., 2019). The first stage involves the diffusion of arsenate ions through the solution to the surface of A33E-Ce(III). The adsorption process is rapid in this stage, and the curve is steeply sloped. The intraparticle diffusion limits the reaction rate in the second stage, resulting in curve flattening. Due to reaching equilibrium and the decrease in arsenate ions concentration in the solution,

Table 1. Kinetic parameters of As(V) adsorption on A33E-Ce(III)

Model	Parameter	As(V)	As(V)	As(V)
		25 mg/dm ³	50 mg/dm ³	100 mg/dm ³
PFO	q_e (mg/g)	5.00	10.00	19.60
	q_1 (mg/g)	0.26	2.20	8.00
	k_1 (1/min)	0.029	0.030	0.035
	R^2	0.4798	0.8974	0.9631
PSO	SSE	207.43	605.85	1346.07
	q_2 (mg/g)	5.03	10.08	19.89
	k_2 (g/mg·min)	0.144	0.043	0.012
	R^2	0.9998	0.9998	0.9997
Elovich	SSE	2.45	5.42	11.28
	α (mg/g·min)	97.39	63.98	25.45
	β (g/mg)	1.92	0.86	0.36
	R^2	0.5567	0.6626	0.8134
IPD	SSE	7.56	24.37	63.55
	k_{i1} (mg/g·min ^{-1/2})	2.991	4.451	6.416
	C_1 (mg/g)	2.187	2.773	3.907
	R^2_1	0.9858	0.9641	0.9547
	k_{i2} (mg/g·min ^{-1/2})	0.206	0.303	0.603
	C_2 (mg/g)	3.994	8.044	14.511
	R^2_2	0.9408	1.0000	0.7901
	k_{i3} (mg/g·min ^{-1/2})	0.000	0.018	0.026
	C_3 (mg/g)	4.997	9.682	19.141
	R^2_3	0.5370	0.8978	0.8193
	SSE	0.10	1.12	5.97

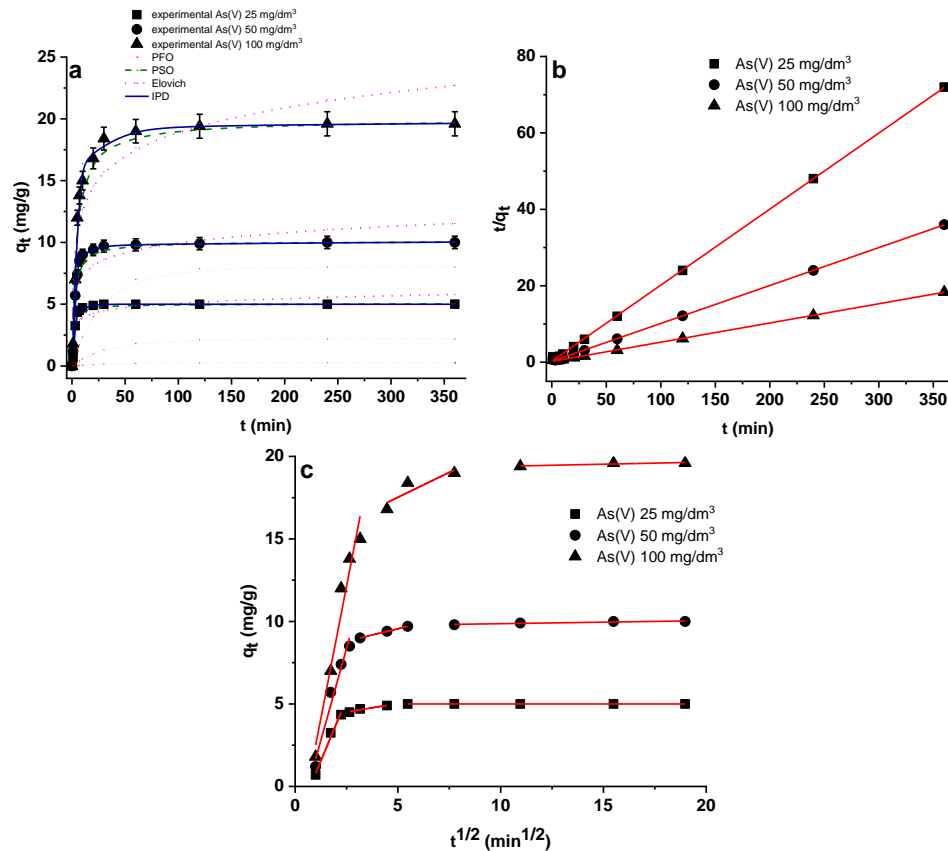


Fig. 10. Non-linear fitting of PFO, PSO, Elovich and IPD models (a) as well as linear fitting of PSO (b) and IPD (c) kinetic models related to As(V) adsorption on A33E-Ce(III) ($c_0 = 25, 50$ and 100 mg/dm^3 , pH = 6, shaking speed 180 rpm, temperature 295 K)

the diffusion process is inhibited (the third step). Based on the obtained values of the intraparticle diffusion rate constant, it can be deduced that these parameters decrease in the series $k_{i1} > k_{i2} > k_{i3}$. The surface gets saturated and the adsorption rate drops once the external surface is filled with arsenate ions.

3.4. Equilibrium and thermodynamic studies

The experimental data were analysed using four isotherm Eqs. (Langmuir, Freundlich, Dubinin-Radushkevich and Redlich-Peterson) to have an insight into the adsorption behaviour of arsenate ions on A33E-Ce(III) and to get the best fitting of the theoretical model. All isotherm parameters and non-linear fitting to the experimental data are presented in Table 2 and Fig. 11, respectively.

Each model is characterized by high determination coefficients ($R^2 > 0.92$), which proves their possible application in the description of the sorption process of arsenate ions on the tested ion exchanger. Based on the Langmuir model the maximum adsorption capacity for As(V) was found to be 60.41 mg/g. This indicates that the maximum sorption capacity almost doubled after the modification with cerium(III) ions. Table 3 shows the comparison of the maximum sorption capacities of various sorbents applied in the arsenic removal. It is worth noting that A33E-Ce(III) can compete successfully with other materials available on the market. The Langmuir and Freundlich models revealed that the arsenate ion adsorption on A33E-Ce(III) is a favourable and feasible process. This is evidenced by the R_L and $1/n$ factors obtained from the above-mentioned Eqs. and they were equal to 0.341 and 0.197 ($n = 5.080$), respectively.

The average sorption energies indicate whether the sorption is physical or chemical. Physical sorption occurs when the value is less than 8 kJ/mol while chemical adsorption occurs when the value is more than 8 kJ/mol (Ali et al., 2019). Based on the Dubinin-Radushkevich model the energy was equal to 18.12 kJ/mol. This confirms one of the conclusions drawn from the kinetic, XPS and FTIR studies that the process is chemical in nature.

Table 2. Langmuir, Freundlich, Dubinin-Radushkevich and Redlich-Peterson isotherm parameters with the error analysis (determination coefficients R^2 , sum of squared errors SSE and F-Test)

Parameters and error analysis	
Langmuir model	
q_m (mg/g)	60.41
K_L (dm ³ /mg)	0.077
R_L	0.341
R^2	0.997
SSE	480.89
F-Test	0.64
Freundlich model	
K_F (mg/g)	17.190
n	5.080
R^2	0.951
SSE	109.74
F-Test	0.93
Dubinin-Radushkevich model	
q_{DR} (mol/g)	$8.790 \cdot 10^{-4}$
β (mol ² /J ²)	$1.523 \cdot 10^{-9}$
E (kJ/mol)	18.12
R^2	0.928
SSE	286.85
F-Test	0.69
Redlich-Peterson model	
K_{RP} (dm ³ /g)	$9.424 \cdot 10^6$
a_{RP} (dm ³ /mg) ^g	$5.520 \cdot 10^5$
g	0.800
R^2	0.970
SSE	107.27
F-Test	0.98

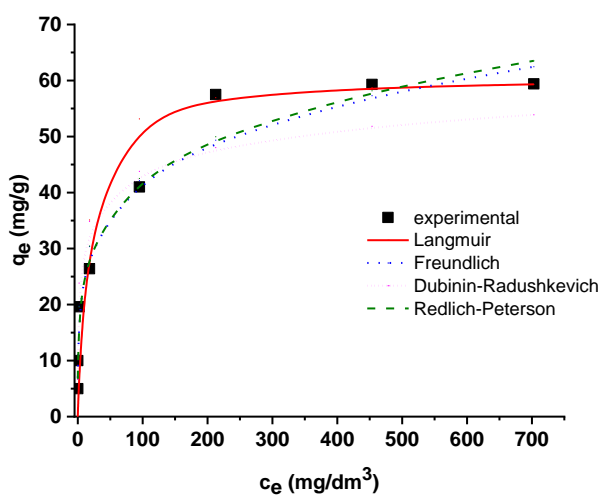


Fig. 11. Non-linear plots of the Langmuir (a), Freundlich (b), Dubinin-Radushkevich (c) and Redlich-Peterson (d) isotherm models.

Due to the fact that all determination coefficients R^2 are relatively high, a further error analysis had to be performed in order to select the best isotherm model. The sum of squared errors (SSE) and F-test revealed that the experimental data fitted best the Redlich-Peterson model which is a combination of the Langmuir and Freundlich isotherms. Due to its versatility, it describes adsorption equilibrium over

a wide range of adsorbate concentrations and is applicable to both homogeneous and heterogeneous systems. As a consequence, it was found that the As(V) adsorption on A33E-Ce(III) did not follow the ideal monolayer adsorption (Ayawei et al., 2017).

Temperature is one of the factors that impact arsenate adsorption capacity in the liquid-solid system. The temperature effect was investigated in this research at 295, 313 and 333 K. All thermodynamic parameters are given in Table 4. The negative value of the enthalpy change ($\Delta H^\circ = -3.74 \text{ kJ/mol}$) indicated the exothermic process of arsenate adsorption on A33E-Ce(III). This revealed a decrease in the As(V) removal efficiency at higher temperatures (Khan et al., 2020). The findings demonstrated that the values of Gibbs free energy change (G°) were all negative at all tested temperatures. This confirmed that the adsorption process proceeded spontaneously and in a thermodynamically satisfactory manner (Dehghani et al., 2020). The positive value of the entropy change ($\Delta S^\circ = 0.0241 \text{ kJ/mol/K}$) observed in this study may be attributed to the increased degree of disorderliness at the adsorbent-solution interface during the As(V) adsorption on A33E-Ce(III) (Yetilmezsoy et al., 2020). Taking into account the thermodynamic studies, it is not advisable to conduct the process at elevated temperature.

Table 3. Comparison of adsorption capacities of various sorbents used for the As(V) removal

Adsorbent	As(V) adsorption capacity (mg/g)	pH	Reference
Chitosan/Cu(OH) ₂ sorbent	39.1	4.0	(Elwakeel and Guibal, 2015)
Magnate gelatin modified chestnut shell biochar	45.8	3.0-4.0	(Zhou et al., 2017)
Al-bentonite	35.71	4.0	(My Linh et al., 2019)
Hybrid anion exchange resin impregnated with hydrous zirconium oxide nanoparticles (HAIX-Zr)	20.00	7.0	(Padungthon et al., 2015)
Polymeric Al/Fe-modified montmorillonite	21.23	4.0	(Ramesh et al., 2007)
Iron-containing magnetic nanoparticles (iMNP)	12.74	6.6	(Zeng et al., 2020)
Ion exchanger based on iron oxide A33E	34.41	6.0	(Dudek and Kołodyńska, 2021)
Ion exchanger based on iron oxide modified with cerium(III) ions A33E-Ce(III)	60.41	6.0	This study

Table 4. Thermodynamic parameters

T (K)	q_e (mg/g)	c_e (mg/dm ³)	K_d (dm ³ /g)	ΔG° (kJ/mol)	ΔH° (kJ/mol)	ΔS° (kJ/mol·K)
295	59.40	703.00	0.084	-10.88	-3.74	0.0241
313	55.00	725.00	0.076	-11.27		
333	52.40	738.00	0.071	-11.80		

3.5. Reusability of A33E-Ce(III)

To evaluate the reusability of the utilized A33E-Ce(III), the regeneration with the NaOH solution and the re-adsorption of As(V) ions were examined (Zhang et al., 2014). These adsorption-regeneration cycles were repeated up to three times with the results shown in Fig. 12. After the first sorption cycle, 1M was selected as the optimal concentration of the desorbing agent. The As(V) adsorption capacity of A33E-Ce(III) reduced gradually with the increasing regeneration cycle. This decline was not so significant and after three desorptions around 92.5% of the initial adsorption capacity was still maintained. These results show that the As(V) adsorption on A33E-Ce(III) is reversible and that the exhausted ion exchanger can be successfully regenerated using NaOH. It is also worth noting that after the third desorption, A33E-Ce(III) still demonstrates greater sorption capacity than unmodified A33E before the first adsorption of arsenate ions. It should be mentioned that during the modification, the

sorption capacity for Ce(III) ions was equal to 19.74 mg/g (the initial concentration of Ce(III) solution was 100 mg/dm³). The content of cerium ions in the solution after sorption and desorption of arsenate(V) ions was checked. There was no presence of cerium, which proves the stability of loaded REE onto the sorbent during the sorption and desorption cycles.

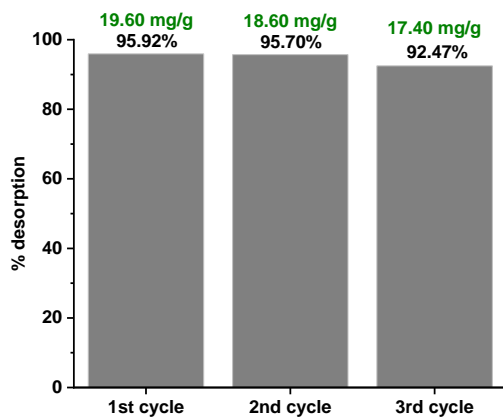


Fig. 12. Reusability of A33E-Ce(III) in the 3 consecutive cycles of sorption and desorption (initial As(V) concentration c_0 100 mg/dm³, sorption time t 360 minutes, desorbing agent 1M NaOH, desorption time t 360 minutes, pH 6, temperature T 295 K, shaking speed 180 rpm). The sorption capacities for As(V) in each cycle are marked in green

4. Conclusions

In this study the modification of the commercially available iron oxide ion exchanger Ferrix A33E (containing the quaternary ammonium groups) was successfully performed with the cerium(III) ions. This was confirmed by the SEM, FTIR and XPS analyses. In the SEM images formation of nanoflakes took place on the surface of A33E-Ce(III). The FTIR spectra revealed a new band at 448 cm⁻¹ and the XPS study found new peaks in the range of 920 and 880 eV. Compared to unmodified A33E all these changes were attributed to the presence of cerium on the sorbent surface.

The research also confirmed that the obtained material had a great affinity for the arsenate ions. According to the kinetic and isotherm models the As(V) removal process was chemisorption and it did not follow the ideal monolayer adsorption. The optimal pH for the removal of As(V) was found to be 6. Then the enhanced electrostatic attraction between the adsorbent positively charged active sites and the negatively charged arsenic species occurred. Moreover, formation of the monodentate and bidentate surface complexes took place on A33E-Ce(III). The process was exothermic, spontaneous and thermodynamically effective.

A33E-Ce(III) was characterized by much better sorption properties in relation to As(V) than A33E. In contrast with the unmodified ion exchanger, it could remove arsenic from the arsenate solution entirely at the concentration of 50 mg/dm³ in 60 minutes. Moreover, the maximum adsorption capacity for As(V) was found to be 60.41 mg/g, so it was almost doubled after the modification with cerium(III) ions. It is also worth mentioning that even after three cycles of sorption/desorption, A33E-Ce(III) still had a greater sorption capacity than unmodified A33E prior to any arsenate adsorption. It can be stated that modifying the sorbent with a small dose of cerium(III) ions increases its sorption capabilities considerably. The removal of arsenic from the aqueous solutions can be made even more effectively and low-cost. The adsorption of a small amount of cerium ions improves the efficacy of water purification significantly while reducing the total cost of the operation.

Acknowledgments

This research received no external funding.

References

- ADELOJU, S.B., KHAN, S., PATTI, A.F., 2021. *Arsenic contamination of groundwater and its implications for drinking water quality and human health in under-developed countries and remote communities – a review*. Appl. Sci. 11, 1–25.

- ALI, I., ALHARBI, O.M.L., ALOTHMAN, Z.A., ALWARTHAN, A., AL-MOHAIMEED, A.M., 2019. Preparation of a carboxymethylcellulose-iron composite for uptake of atorvastatin in water. *Int. J. Biol. Macromol.* 132, 244–253.
- ALOTHMAN, Z.A., 2012. A review: Fundamental aspects of silicate mesoporous materials. *Materials*. 5, 2874–2902.
- AYAWEI, N., EBELEGI, A.N., WANKASI, D., 2017. Modelling and Interpretation of Adsorption Isotherms. *J. Chem.* 2017, 3039817.
- BADRUDDOZA, A.Z.M., SHAWON, Z.B.Z., RAHMAN, M.T., HAO, K.W., HIDAJAT, K., UDDIN, M.S., 2013. Ionically modified magnetic nanomaterials for arsenic and chromium removal from water. *Chem. Eng. J.* 225, 607–615.
- BERGMANN, C.P., MACHADO, F.M., 2015. Carbon nanomaterials as adsorbents for environmental and biological applications. Springer International Publishing, Switzerland.
- BHANDARI, P., BANJARA, M.R., SINGH, A., KANDEL, S., RAWAL, D.S., PANT, B.R., 2021. Water quality status of groundwater and municipal water supply (tap water) from bagmati river basin in Kathmandu valley, Nepal. *J. Water Sanit. Hyg. Dev.* 11, 102–111.
- CHAUDHRY, S.A., ZAIDI, Z., SIDDIQUI, S.I., 2017. Isotherm, kinetic and thermodynamics of arsenic adsorption onto iron-zirconium binary oxide-coated sand (IZBOCS): Modelling and process optimization. *J. Mol. Liq.* 229, 230–240.
- CHOWDHURY, M.R.I., MULLIGAN, C.N., 2011. Biosorption of arsenic from contaminated water by anaerobic biomass. *J. Hazard. Mater.* 190, 486–492.
- DEHGHANI, M.H., YETILMEZSOY, K., SALARI, M., HEIDARINEJAD, Z., YOUSEFI, M., SILLANPÄÄ, M., 2020. Adsorptive removal of cobalt(II) from aqueous solutions using multi-walled carbon nanotubes and γ -alumina as novel adsorbents: Modelling and optimization based on response surface methodology and artificial neural network. *J. Mol. Liq.* 299, 112154.
- DUDEK, S., KOŁODYŃSKA, D., 2022. Arsenate removal on the iron oxide ion exchanger modified with neodymium(III) ions. *J. Environ. Manage.* 307, 114551.
- DUDEK, S., KOŁODYŃSKA, D., 2021. Arsenic(V) removal on the lanthanum-modified ion exchanger with quaternary ammonium groups based on iron oxide. *J. Mol. Liq.* 347, 117985.
- DUDEK, S., KOŁODYŃSKA, D., 2020. Enhanced arsenic(V) removal on an iron-based sorbent modified by lanthanum(III). *Materials*. 13, 2553.
- DUTTA, P.K., RAY, A.K., SHARMA, V.K., MILLERO, F.J., 2004. Adsorption of arsenate and arsenite on titanium dioxide suspensions. *J. Colloid Interface Sci.* 278, 270–275.
- ELWAKEEL, K.Z., GUIBAL, E., 2015. Arsenic(V) sorption using chitosan/Cu(OH)₂ and chitosan/CuO composite sorbents. *Carbohydr. Polym.* 134, 190–204.
- GUO, X., WANG, J., 2019. A general kinetic model for adsorption: theoretical analysis and modeling. *J. Mol. Liq.* 288, 111100.
- GUPTA, K., GHOSH, U.C., 2009. Arsenic removal using hydrous nanostructure iron(III)-titanium(IV) binary mixed oxide from aqueous solution. *J. Hazard. Mater.* 161, 884–892.
- HAO, L., LIU, M., WANG, N., LI, G., 2018. A critical review on arsenic removal from water using iron-based adsorbents. *RSC Adv.* 8, 39545–39560.
- HE, Z., TIAN, S., NING, P., 2012. Adsorption of arsenate and arsenite from aqueous solutions by cerium-loaded cation exchange resin. *J. Rare Earths* 30, 563–572.
- HU, Q., CHEN, N., FENG, C., HU, W.W., 2015. Nitrate adsorption from aqueous solution using granular chitosan-Fe³⁺ complex. *Appl. Surf. Sci.* 347, 1–9.
- HUBBE, M.A., AZIZIAN, S., DOUVEN, S., 2019. Implications of apparent pseudo-second-order adsorption kinetics onto cellulosic materials: A review. *BioRes.* 14, 7582–7626.
- ISSA, N.B., RAJAKOVIĆ-OGNjanović, V.N., MARINKOVIĆ, A.D., RAJAKOVIĆ, L. V., 2011. Separation and determination of arsenic species in water by selective exchange and hybrid resins. *Anal. Chim. Acta* 706, 191–198.
- JIAO, Y., HAN, D., LU, Y., RONG, Y., FANG, L., LIU, Y., HAN, R., 2017. Characterization of pine-sawdust pyrolytic char activated by phosphoric acid through microwave irradiation and adsorption property toward CDNB in batch mode. *Desalin. Water Treat.* 77, 247–255.
- KHAN, M.A., ALQADAMI, A.A., WABAIDUR, S.M., SIDDIQUI, M.R., JEON, B.H., ALSHAREEF, S.A., ALOTHMAN, Z.A., HAMEDELNIEL, A.E., 2020. Oil industry waste based non-magnetic and magnetic hydrochar to sequester potentially toxic post-transition metal ions from water. *J. Hazard. Mater.* 400, 123247.
- KOMNITSAS, K., ZAHARAKI, D., BARTZAS, G., ALEVIZOS, G., 2017. Adsorption of scandium and neodymium on biochar derived after low-temperature pyrolysis of sawdust. *Minerals* 7, 1–18.
- LI, Z., QU, J., LI, H., LIM, T.C., LIU, C., 2011. Effect of cerium valence on As(V) adsorption by cerium-doped titanium dioxide adsorbents. *Chem. Eng. J.* 175, 207–212.

- LIANG, S., WANG, H., LI, Y., QIN, H., LUO, Z., HUANG, B., ZHAO, X., ZHAO, C., CHEN, L., 2020. *Rare-earth based nanomaterials and their composites as electrode materials for high performance supercapacitors: A review*. Sustain. Energy Fuels 4, 3825–3847.
- LIANG, T., LI, L., ZHU, C., LIU, X., LI, H., SU, Q., YE, J., GENG, B., TIAN, Y., SARDAR, M.F., HUANG, X., LI, F., 2020. *Adsorption of As(V) by the novel and efficient adsorbent cerium-manganese modified biochar*. Water 12, 2720.
- LINGAMDINNE, L.P., KODURU, J.R., CHANG, Y.Y., KANG, S.H., YANG, J.K., 2019. *Facile synthesis of flowered mesoporous graphene oxide-lanthanum fluoride nanocomposite for adsorptive removal of arsenic*. J. Mol. Liq. 279, 32–42.
- LINH, N.L.M., HOANG VAN, D., DUONG, T., TINH, M.X., KHIEU, D.Q., 2019. *Adsorption of arsenate from aqueous solution onto modified Vietnamese bentonite*. Adv. Mater. Sci. Eng. 2019, 2710926.
- MAJI, S., GHOSH, AYAN, GUPTA, K., GHOSH, ABIR, GHORAI, U., SANTRA, A., SASIKUMAR, P., GHOSH, U.C., 2018. *Efficiency evaluation of arsenic(III) adsorption of novel graphene oxide@iron-aluminium oxide composite for the contaminated water purification*. Sep. Purif. Technol. 197, 388–400.
- MINO, L., NEGRI, C., SANTALUCIA, R., CERRATO, G., SPOTO, G., MARTRA, G., 2020. *Morphology, surface structure and water adsorption properties of TiO₂ nanoparticles: A comparison of different commercial samples*. Molecules 25, 4605.
- MUTHU PRABHU, S., CHUAICHAM, C., SASAKI, K., 2018. *A mechanistic approach for the synthesis of carboxylate-rich carbonaceous biomass-doped lanthanum-oxalate nanocomplex for arsenate adsorption*. ACS Sustain. Chem. Eng. 6, 6052–6063.
- MUTHUSELVI, M., JEYASUBRAMANIAN, K., HIKKU, G.S., MUTHUSELVARAN, M., ESWARAN, M., SENTHIL KUMAR, N., PONNUSAMY, V.K., 2021. *Rare earth metal oxide-doped reduced graphene-oxide nanocomposite as binder-free hybrid electrode material for supercapacitor application*. Int. J. Energy Res. 45, 8255–8266.
- NABI, D., ASLAM, I., QAZI, I.A., 2009. *Evaluation of the adsorption potential of titanium dioxide nanoparticles for arsenic removal*. J. Environ. Sci. 21, 402–408.
- PADUNGTHON, S., GERMAN, M., WIRIYATHAMCHAROEN, S., SENGUPTA, A.K., 2015. *Polymeric anion exchanger supported hydrated Zr(IV) oxide nanoparticles: A reusable hybrid sorbent for selective trace arsenic removal*. React. Funct. Polym. 93, 84–94.
- PENG, X., LUAN, Z., DING, J., DI, Z., LI, Y., TIAN, B., 2005. *Ceria nanoparticles supported on carbon nanotubes for the removal of arsenate from water*. Mater. Lett. 59, 399–403.
- PODGORSKI, J.E., EQANI, S.A.M.A.S., KHANAM, T., ULLAH, R., SHEN, H., BERG, M., 2017. *Extensive arsenic contamination in high-pH unconfined aquifers in the Indus Valley*. Sci. Adv. 3, 1700935.
- RAMESH, A., HASEGAWA, H., MAKI, T., UEDA, K., 2007. *Adsorption of inorganic and organic arsenic from aqueous solutions by polymeric Al/Fe modified montmorillonite*. Sep. Purif. Technol. 56, 90–100.
- RAVI, PANDEY, L.M., 2019. *Enhanced adsorption capacity of designed bentonite and alginate beads for the effective removal of methylene blue*. Appl. Clay Sci. 169, 102–111.
- REID, M.S., HOY, K.S., SCHOFIELD, J.R.M., UPPAL, J.S., LIN, Y., LU, X., PENG, H., LE, X.C., 2020. *Arsenic speciation analysis: A review with an emphasis on chromatographic separations*. TrAC - Trends Anal. Chem. 123, 115770.
- SHARMA, M., SINGH, J., HAZRA, S., BASU, S., 2019. *Adsorption of heavy metal ions by mesoporous ZnO and TiO₂@ZnO monoliths: Adsorption and kinetic studies*. 145, 105–112.
- SHI, Q., YAN, L., CHAN, T., JING, C., 2015. *Arsenic adsorption on lanthanum-impregnated activated alumina: spectroscopic and DFT study*. ACS Appl. Mater. Interfaces 7, 26735–26741.
- SHIN, S.M., PARK, J.K., JUNG, S.M., 2015. *Changes of aromatic CH and aliphatic CH in in-situ FT-IR spectra of bituminous coals in the thermoplastic range*. ISIJ Int. 55, 1591–1598.
- SIDDQUI, S.I., CHAUDHRY, S.A., 2017. *Iron oxide and its modified forms as an adsorbent for arsenic removal: A comprehensive recent advancement*. Process Saf. Environ. Prot. 111, 592–626.
- SIMONIN, J.P., 2016. *On the comparison of pseudo-first order and pseudo-second order rate laws in the modeling of adsorption kinetics*. Chem. Eng. J. 300, 254–263.
- VALDÉS, O., MARICAN, A., MIRABAL-GALLARDO, Y., SANTOS, L.S., 2018. *Selective and efficient arsenic recovery from water through quaternary amino-functionalized silica*. Polymers. 10, 626.
- VILTRES, H., ODIO, O.F., LARTUNDO-ROJAS, L., REGUERA, E., 2020. *Degradation study of arsenic oxides under XPS measurements*. Appl. Surf. Sci. 511, 145606.
- WANG, Y., LIU, Y., GUO, T., LIU, H., LI, J., WANG, S., LI, X., WANG, X., JIA, Y., 2020. *Lanthanum hydroxide: a highly efficient and selective adsorbent for arsenate removal from aqueous solution*. Environ. Sci. Pollut. Res. 27, 42868–42880.
- WANG, Y., SHI, W., YU, Y., CHEN, X., 2009. *Synthesization characterization and properties of quaternary ammonium cationic cellulose*. 3rd International Conference on Bioinformatics and Biomedical Engineering. 1–4.

- XIAO, X., PENG, B., CAI, L., ZHANG, X., LIU, S., WANG, Y., 2018. *The high efficient catalytic properties for thermal decomposition of ammonium perchlorate using mesoporous ZnCo₂O₄ rods synthesized by oxalate co-precipitation method.* Sci. Rep. 8, 1–13.
- XIONG, F., HWANG, B., JIANG, Z., JAMES, D., LU, H., MOORTGAT, J., 2021. *Kinetic emission of shale gas in saline water: Insights from experimental observation of gas shale in canister desorption testing.* Fuel 300, 121006.
- XU, N., RATE, A.W., MORGAN, B., SAUNDERS, M., 2019. *Micro- and nanoscale identification of rare earth element-mineral associations in an acidified dredge spoil and adjacent reduced sediments.* ACS Earth Sp. Chem. 3, 51–61.
- YANG, G., LIU, Y., SONG, S., 2015. *Competitive adsorption of As(V) with co-existing ions on porous hematite in aqueous solutions.* J. Environ. Chem. Eng. 3, 1497–1503.
- YETİLMEZSOY, K., ÖZÇİMEN, D., KOÇER, A.T., BAHRAMIAN, M., KIYAN, E., AKBIN, H.M., GONCALOĞLU, B.İ., 2020. *Removal of anthraquinone dye via struvite: equilibria, kinetics, thermodynamics, fuzzy logic modeling.* Int. J. Environ. Res. 14, 541–566.
- YU, Y., YU, L., KOH, K.Y., WANG, C., CHEN, J.P., 2018. *Rare-earth metal based adsorbents for effective removal of arsenic from water: A critical review.* Crit. Rev. Environ. Sci. Technol. 48, 1127–1164.
- YU, Y., ZHANG, C., YANG, L., PAUL CHEN, J., 2017. *Cerium oxide modified activated carbon as an efficient and effective adsorbent for rapid uptake of arsenate and arsenite: material development and study of performance and mechanisms.* Chem. Eng. J. 315, 630–638.
- ZENG, H., ZHAI, L., QIAO, T., YU, Y., ZHANG, J., LI, D., 2020. *Efficient removal of As(V) from aqueous media by magnetic nanoparticles prepared with Iron-containing water treatment residuals.* Sci. Rep. 10, 1–12.
- ZHANG, G., REN, Z., ZHANG, X., CHEN, J., 2013. *Nanostructured iron(III)-copper(II) binary oxide: A novel adsorbent for enhanced arsenic removal from aqueous solutions.* Water Res. 47, 4022–4031.
- ZHANG, R., LEIVISKÄ, T., 2020. *Surface modification of pine bark with quaternary ammonium groups and its use for vanadium removal.* Chem. Eng. J. 385, 123967.
- ZHANG, W., FU, J., ZHANG, G., ZHANG, X., 2014. *Enhanced arsenate removal by novel Fe-La composite (hydr)oxides synthesized via coprecipitation.* Chem. Eng. J. 251, 69–79.
- ZHANG, W., NIU, X., CHEN, L., YUAN, F., ZHU, Y., 2016. *Soot combustion over nanostructured ceria with different morphologies.* Sci. Rep. 6, 1–10.
- ZHOU, Z., LIU, Y., LIU, S., LIU, H., ZENG, G., TAN, X., YANG, C., DING, Y., YAN, Z., LI, CAI, X., 2017. *Sorption performance and mechanisms of arsenic(V) removal by magnetic gelatin-modified biochar.* Chem. Eng. J. 314, 223–231.